UNIVERSITÉ DE LORRAINE | BIBLIOTHÈQUES UNIVERSITAIRES

AVERTISSEMENT

Ce document est le fruit d'un long travail approuvé par le jury de soutenance et mis à disposition de l'ensemble de la communauté universitaire élargie.

Il est soumis à la propriété intellectuelle de l'auteur. Ceci implique une obligation de citation et de référencement lors de l'utilisation de ce document.

D'autre part, toute contrefaçon, plagiat, reproduction illicite encourt une poursuite pénale.

Contact bibliothèque : ddoc-theses-contact@univ-lorraine.fr
(Cette adresse ne permet pas de contacter les auteurs)

LIENS

Code de la Propriété Intellectuelle. articles L 122. 4
Code de la Propriété Intellectuelle. articles L 335.2- L 335.10
http://www.cfcopies.com/V2/leg/leg_droi.php
http://www.culture.gouv.fr/culture/infos-pratiques/droits/protection.htm

Ecole Doctorale BioSE (Biologie-Santé-Environnement)

Thèse

Présentée et soutenue publiquement pour l'obtention du titre de

DOCTEUR DE l'UNIVERSITE DE LORRAINE

Mention : « Sciences de la Vie et de la Santé »

par **Razan ALSOHAIBANI**

Biochemical characterization of the promiscuous activities of rhodanese family enzymes

14 March 2024

Membres du jury :

Rapporteurs :	**Pr. Fernando RODRIGUES LIMA**	**Professeur, Université Paris Cité, Paris Président de jury**
	Dr. Virginie LATTARD	**Directrice de Recherche, INRAE, Lyon**
Examinateurs :	**Dr. Nicolas SOLER**	**Maître de Conférences, Université de Lorraine, Nancy**
	Dr. Magali BLAUD	**Maître de Conférences, Université Paris Cité**
	Pr. Sandrine BOSCHI- MULLER	**Professeur, Université de Lorraine, Nancy, Directrice de thèse**
	Pr. François TALFOURNIER	**Professeur, Université de Lorraine, Nancy, Co-directeur de thèse**

UMR 7365 – CNRS-Université de Lorraine –
Laboratoire IMoPA Ingénierie Moléculaire, Cellulaire et Physiopathologie
Campus Biologie-Santé, Faculté de Médecine, Bâtiment Biopôle,
9 avenue de la forêt de Haye, 54505, Vandoeuvre-lès-Nancy

This thesis is dedicated to my beloved parents & my family for their endless love, support and prayers.

Acknowledgment

I am immensely grateful to my beloved country, Saudi Arabia, for providing me with the exceptional opportunity to pursue higher education abroad. The generous financial support I have received from my government has been instrumental in making this dream a reality. I am deeply thankful for this support, without which my journey of academic excellence would have been significantly hindered. I am particularly indebted to my esteemed supervisor, Dr. Jamal ALSHEBANI, for his invaluable guidance and belief in my abilities. His mentorship has been instrumental in shaping my research and personal growth.

I would like to thank Pr. Jean Yves JOUZEAU, director of the IMoPA laboratory & Pr.Bruno CHARPENTIER Deputy director of the IMoPA laboratory, for allowing me to carry out my doctorate in this laboratory and for enabling me to work under optimal conditions. I also extend my gratitude to Pr. Sophie RAHUEL-CLERMONT, the director of the BIOSE doctorate school, for her support.

I would like to express my sincere thanks to Dr, Virginie LATTARD and Dr. Magali BLAUD for accepting to be on the jury.

The successful completion of this doctoral thesis would have remained an unattainable feat if it weren't for the support and guidance generously bestowed upon me by my esteemed supervisors, Pr. Sandrine BOSCHI-MULLER and Pr. François TALFOURNIER. I am immensely grateful for the exceptional research environment they have cultivated, which has not only facilitated my academic growth but also equipped me with invaluable mentorship, endless patience, constructive criticism, and care. Having them as my supervisors is an immense honor that I hold in the highest regard.

I am deeply grateful to Prof, Fernando RODRIGUES LIMA and Dr. Nicolas SOLER, esteemed members of my community and jury, who generously devoted their time to assist me with my research work and offered me invaluable guidance.

I am extremely grateful to Dr. Benjamin SELLES for all the assistance and guidance provided during our collaborative efforts in the experimental work related to MOCS3. Additionally, their expertise in enzyme engineering and their contribution to the review paper have been invaluable. The genuine and limitless enthusiasm for science exhibited by Dr. SELLES is both contagious and inspiring.

To Dr. Alexandre KRIZNIK, I want to express my sincere gratitude for your empathy and constant availability to lend an ear. The supportive learning environment you have fostered has made a profound impact on my academic journey. Your mentorship has been invaluable, and I will forever be grateful for your guidance. I would also like to extend my appreciation to Dr. Hortense MAZON for conducting the mass spectrometry analyses. The contribution of the entire redox group has been instrumental, and I am thankful for their continuous assistance and support.

In my day-to-day job, I am incredibly fortunate to be surrounded by a supportive and cheerful group of colleagues in the lab. I want to express my deepest gratitude to Anne-Lise and Julie for being such amazing collaborators. Working alongside each of you has been an absolute

delight. I am particularly thankful for your friendship, your ability to listen patiently, and your invaluable French translation skills.

My colleagues and friends have been incredibly supportive, especially during the latter stages of my PhD. Rim's presence in the laboratory added a warm and welcoming atmosphere, making me feel at home. Jade's encouragement and support, especially on those days when I felt completely overwhelmed, were invaluable.

Big thanks to all my cherished friends in Paris and Nancy, especially Hala & Riyad, I extend my heartfelt gratitude for your support and friendship. You have been a beacon of light during my journey abroad, from the early days at the French Language Institute to my current doctoral studies. You are the most precious gift of my time abroad.

Thanks for all my friends in Saudi Arabia, especially Roaa, I extend my deepest gratitude for your support and friendship over the past 13 years. Thank you for being my constant companion, my confidant, and the pillar of strength that have held me up throughout my life.

My deepest gratitude goes to my dearest family, my parents, and my sisters (Atheer, Lojain, &Layan) and my brother (Mohanad), this thesis is an embodiment of your love, support and prayers that have been the guiding lights throughout my journey. Your love has been the bedrock upon which I have built my dreams, your support has been the anchor that has kept me afloat amidst challenges, and your prayers have been the celestial tapestry that has woven hope into my aspirations. Even though we are physically apart, your presence has always been felt in my heart. I am eternally grateful for your sacrifices and your unfailing support. This accomplishment would not have been possible without you.

The person who deserves great acknowledgment and thanks is my husband (Muaath), you are the driving force behind my dreams. Your support and unconditional love have been the bedrock of my success, providing me with the strength and resilience to persevere through life's challenges.Thank you for believing in me unconditionally, even when I doubted myself. Without your love and support, this accomplishment would not have been possible. I dedicate this work to you. And a heartfelt thank you to my family in Law for their support and love.I am forever grateful for your presence in my life

"My son Khaled, I dream of the day when you will be able to say, 'My mom was a strong pillar of support in my life. She instilled in me the strength and resilience to overcome any challenge. She never gave up on me, even when times were tough. She sacrificed everything for my well-being and happiness. "Khaled, my entire life and my future belong to you. Your smile is my source of strength and motivation. I love you Habibi Khaled more than words can express.

This project was done,
with many challenges, passion and tears.
I hope reading it brings you enjoyment.
Razan

TABLE OF CONTENTS

Introduction

I. **Promiscuous enzymes**.....1

A. General 1
B. What does promiscuous enzyme mean? 4
C. Mechanisms of enzyme promiscuity.....6
D. Enzyme promiscuity and evolution 9
E. Functions of promiscuous.....10
F. Applications and examples of promiscuous enzymes 11

II. **The rhodanese-containing proteins**.....12

A. History of the rhodanese domain 12
B. Reactions catalysed by Rhodanese-containing enzymes 13
C. The classification of Rhodanese-containing enzymes 15

III. **Sulfurtransferases** 16

A. Rhodanese, a class 2 TST.....17
B. TST from class 1.....23
C. 3MSTs.....25
D. MOCS3.....31

IV. **TrhO**.....34

V. **CDC25 phosphatases** 36

VI. **Arsenate reductases** 39

Objectives of the thesis..... 41

Materials and methods

1. Biological materials.....45
2. Genetic engineering techniques.....48
   2.1. Site-directed mutagenesis.....48
   2.2 DNA sub -cloning 49
   2.3 Agarose gel electrophoresis 50
3. Production and purification of recombinant enzymes.....51
   3.1Transformation of competent bacteria 51

3.2Production and purification TSTD1……..51
3.3Production and purification TSTD1+Ser……52
3.4Production and purification Ex-MUT-TSTD1……52
3.5Production and purification of CRD-CDC25B$_{cd}$……..53
3.6Production and purification of His-CDC25B$_{cd}$……54
3.7Production and purification of His-CDC25B$_{cd}$ΔSer……55
3.8Production and purification of EX-MUT-CDC25B$_{cd}$……56
3.9Production and purification of ArsC……57
3.10 Production and purification ofMOCS3 303……57
3.11 Production and purification ofMOCS3 303……58

4. Biochemical characterization of recombinant enzymes……..59
4.1 Polyacrylamide Gel Electrophoresis under denaturing Conditions(SDSPAGE)……59
4.2 Determination of protein concentrations……..59
4.3 Determination of the molecular mass of recombinant proteins by mass spectrometry ……59
5. Enzymatic properties of recombinant enzymes……..60
5.1 Sulfurtransferase activity……60
5.2 Phosphatase activity……..61
a) With pNPP substrate……61
b) With 4-MUPsubstrate……61
5.3 Arsenate reductase activity……..61
5.4 Kinetic data fitting……62

Results

Axis1……63

A) Production and purification of TSTD1 and its variants……..64
1- TSTD1……..64
2- TSTD1+Ser……64
3- EX-MUT-TSTD1……65
4- Preliminary quality controls……68

B) Production and purification of CDC25B$_{cd}$ and its variants……..69
1- CRD-CDC25B$_{cd}$……..69
2- His-CDC25B$_{cd}$……70
3- His-CDC25BcdΔSer……..…..72
4- Ex-MUT-CDC25B$_{cd}$……..75

5- Storage concerns for wild-type and mutated CDC25B$_{cd}$s…….. 78

C) Characterization of the catalytic properties……..79
1- Sulfurtransferase activity……..79
1.1 Wild-type and mutated TSTD1s……80
1.2 Wild-type and mutated CDC25B$_{cd}$s……82
2- Phosphatase activity
2.1Wild-type and mutated CDC25B$_{cd}$s……85
2.2Wild-type and mutated TSTD1s……88
3- Arsenate reductase……89
3.1 Production and purification of ArsC……89
3.2 Kinetics with ArsC……91
3.3 Kinetics with wild- type and mutated CDC25B$_{cd}$s...91
3.4 Kinetics with wild- type and mutated TSTD1s……93

Axis2……94
1- Construction of the expression vectors……95
2- Tests production of MOCS3 303 and MOCS3 335……95
3- Production and purfication of MOCS3 303……97
4- Production and purfication of MOCS3 335……97

Discussion. 99

References 111

Annexe.....135

Abbreviations

3MP	3-mercaptopyruvate
3MST	3-mercaptopyruvate sulfurtransferase
ATP	Adenosine triphosphate
CDC25	Cell Division Cycle 25
CDK	Cyclin Dependent Kinase
CRD	Carbohydrate Recognition Domain
CSE	Cystathionine-γ-lyase
CysSSH	Cysteine persulfide
DHLA	Dihydrolipoic acid
DTT	Dithiothreitol
E. coli	*Escherichia coli*
EDTA	Ethylenediaminetetraacetic acid
ESI-MS	Electrospray ionisation mass spectrometry
ETHE1	Persulfide dioxygenase
GlpE	Bacterial TST (Glycerol-3-phosphate *E. coli*)
Grx	Glutaredoxine
GSH	Glutathione
GSSG	Oxidized Glutathione
H_2S	Hydrogen sulfide
IPTG	Isopropyl-β-D-1-thiogalactopyranoside
K	Affinity constant
KAT	Gene for human TSTD1
k_{cat}	Catalytic rate constant
k_{cat}/K_M	Catalytic efficiency
K_M	Michaelis constant
k_{max}	Maximal rate constant
k_{obs}	Observed rate constant
LB	«Luria Bertani »

LBNB	Luria Bertani, NaCl, betaine
MoCo	Molybdenum cofactor
MPST	Gene encoding human 3-MST
PAGE	Polyacrylamide gel electrophoresis
PCR	Polymerase Chain Reaction
PDO	Persulfide dioxygenase
PON1	Serum paraoxonase and arylesterase 1
Rhd	Rhodanese
SOU	Sulfide oxidation unit
tRNA	Transfer RNA
Trx	Thioredoxin
TST	Thiosulfate:cyanide sulfurtransferase
TSTD1	Thiosulfate Sulfurtransferase Like Domain Containing 1

INTRODUCTION

The main axis of my PhD project focused on the identification of the molecular basis responsible for the promiscuous activities of rhodanese-fold enzymes with particular emphasis on the relation between the length and the sequence of the catalytic loop and the catalytic properties (sulfurtransferase, phosphatase and arsenate reductase). Therefore, the two parts of the introduction will be devoted successively to promiscuous enzymes and the rhodanese-fold containing enzymes.

I. Promiscuous enzymes

A. General

Life is orchestrated by an intricate network of chemical reactions, and enzymes play a pivotal role in accelerating these reactions under the conditions that prevail in living organisms. In the absence of enzymes, these chemical reactions would proceed at an extremely slow rate or would not occur at all due to their unfavorable thermodynamic and/or kinetic properties.

Enzymes are often presented as efficient catalysts with highly specific substrate and reaction preferences. However, these attributes are often associated with a lack of adaptability and an inability to acquire new functions. This perception stands in contrast to the well-established concept of rapid enzyme evolution. According to the so-called patchwork theory, enzymes can catalyze secondary reactions in addition to their primary functions (Jensen, 1976). Indeed, in his theory of pathway evolution Jensen proposed that ancestral enzymes exhibited broad specificities, compared to modern enzymes that are more specialized towards a single substrateand reaction. This suggested that a limited number of rudimentary enzymes with extended catalytic activities could have supported a broader range of metabolic capabilities (Figure 2).

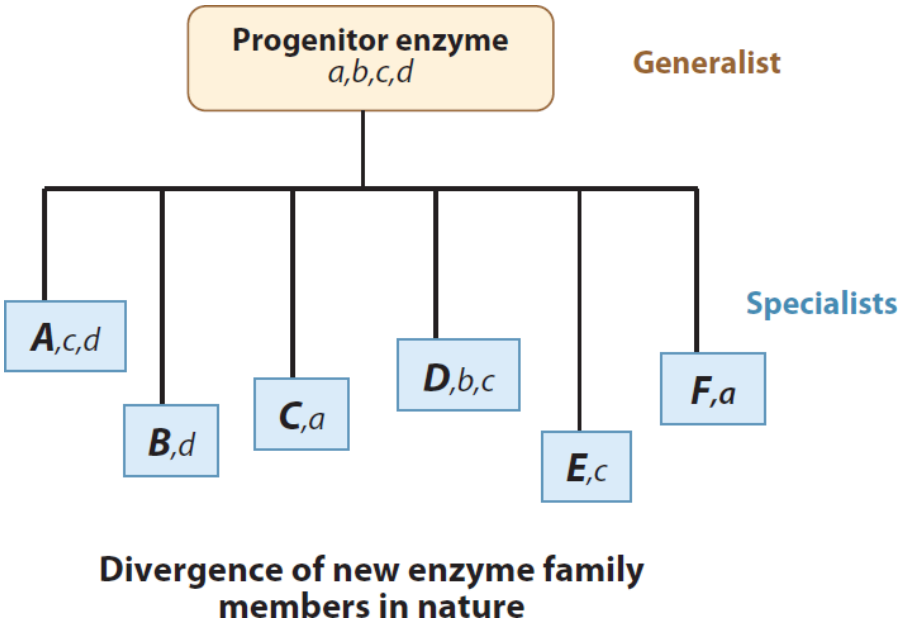

Figure 1: Divergence of a generalist progenitor enzyme to a family of specialist enzymes (Khersonsky & Tawfik, 2010).
Jensen's hypothesis (Jensen, 1976) surmises that, in nature, an ancestor protein displaying a low level of a range of activities (denoted as a, b, c, d) has been subjected to selection pressures for those activities, thus duplicating and diverging into a familyof potent and highly specialized enzymes of the kind seen today (denoted A, B, etc.). In the course of divergence, new activities that were not present in the progenitor may also emerge(denoted as E and F). Today's specialists may still retain some of the functions of the common ancestor (denoted in lower case letters) as low levels of promiscuous activities. Indeed, several reports indicate a low level of shared activities within a family and, in particular, that the nativeactivity of one member is the promiscuous activity of another, and vice versa.

In line with this hypothesis, more recent in silico studies focused on comparison between enzyme promiscuity (see below) and phylogenetic diversity of species (Carbonell *et al.*, 2011, Figure 2), pointed out the fact that reactions catalysed by less specific enzymes are likely to be widespread across species in the tree of life, in contrast to the reactions catalysed by highly specific enzymes that are shared by less divergent organisms.

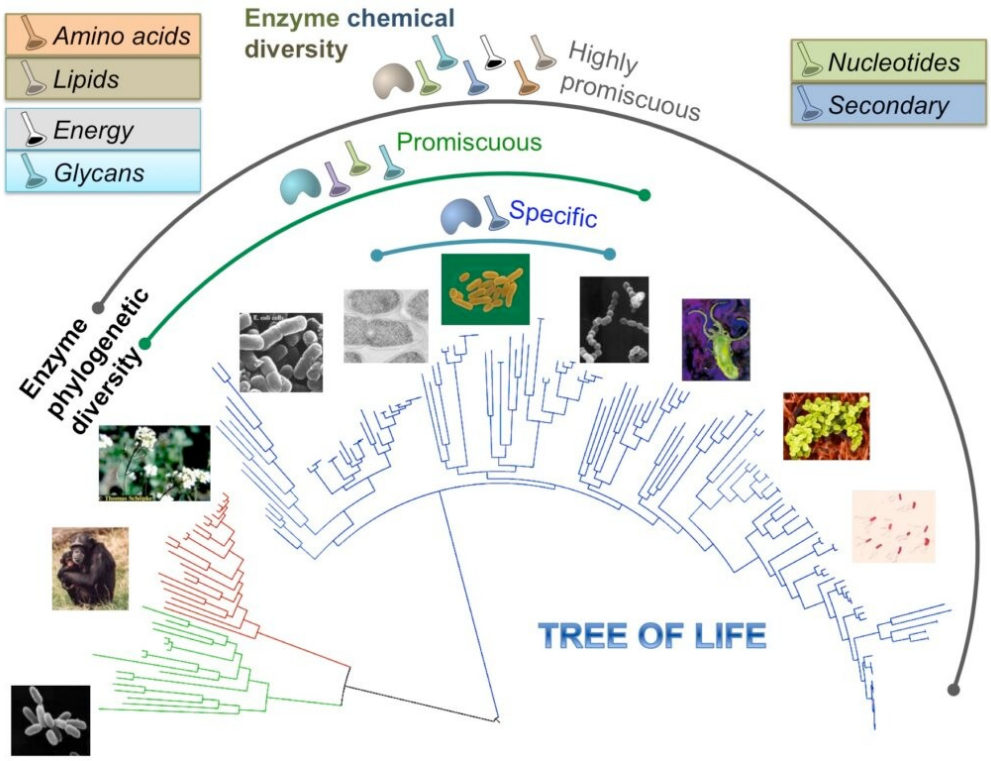

Figure 2: Origins of specificity and promiscuity in metabolic networks (Carbonell *et al.*, 2011; https://jfaulon.com/origins-of-specificity-and-promiscuity-in-metabolic-networks/).
Chemical diversity present in a large unbiased dataset of catalytic reactions processed by modern enzymes was explored across the tree of life. As a result, enzymes involved in amino acid and lipid metabolisms appear to be more promiscuous and this might be linked to the earliest form of biochemical reactions.

Thus, enzyme promiscuity, the ability of enzymes to catalyze multiple reactions, highlights the versatility of these biological catalysts and underscores their adaptability in fulfilling the metabolic demands of living organisms (O'Brien &Herschlag, 1999; Bornscheuer & Kazlauskas, 2004). Although enzymes are known for their specificity, many enzymes have been reported to be promiscuous in nature (Gupta, 2016). As Hult and Burglund (Hult & Berglund, 2007) aptly point out, the discovery of pyruvate decarboxylase's promiscuous catalysis of C-C bond synthesis dates back to 1921 and underpins an ongoing commercial procedure. Even older examples meet the definition in the literature as promiscuity was observed in the reversal of hydrolytic enzyme activity for maltase 1898 (Hill, 1898) and for pancreatic lipase in 1900 (Kastle & Loevenhart, 1900). Other classical examples of promiscuity include carbonic

anhydrase (Pocker & Stone, 1965), pepsin (Reid & Fahrney, 1967), chymotrypsin (Nakagawa & Bender, 1969), and L-asparaginase (Jackson & Handschumacher, 1970).

Interestingly, increasing number of enzymes not only exhibit secondary activities but can also perform these reactions with remarkable efficiency, thus challenging the notion “one enzyme-one reaction” or that proficient catalysis requires specificity (Gatti-Lafranconi & Hollfelder, 2013).

B. What does promiscuous enzyme mean?

Nothing propels scientific progress quite like the introduction of novel terminology. Nanotechnology, synthetic biology, and system biology serve as prime examples. Another notable example is enzyme promiscuity which usually means the ability of an enzyme to catalyze a reaction that is not its specialized one. The initial perception of enzyme promiscuity was largely associated with undesirable side effects, suboptimal catalytic properties, and malfunctions in biological processes (Nobeli *et al.,* 2009). However, it is now widely recognized as ahighly beneficial phenomenon that can significantly enhance the utilization of biocatalysis in biotechnology.

In the scientific literature, there's a distinction between two different interpretations of the term "promiscuity" as applied to enzymes. Some researchers use the term to describe enzymeswith broad substrate specificity, while others prefer to limit it to secondary activities that holdlittle physiological significance (Khersonsky &Tawfik, 2010; Copley, 2003). Making this distinction is crucial, however, as broad specificity can be an advantageous trait from an evolutionary standpoint, especially for enzymes like glutathione S-transferases found in the liver of mammals, which play a critical role in detoxifying endogenous and exogenous electrophilic substances (Figure 2).

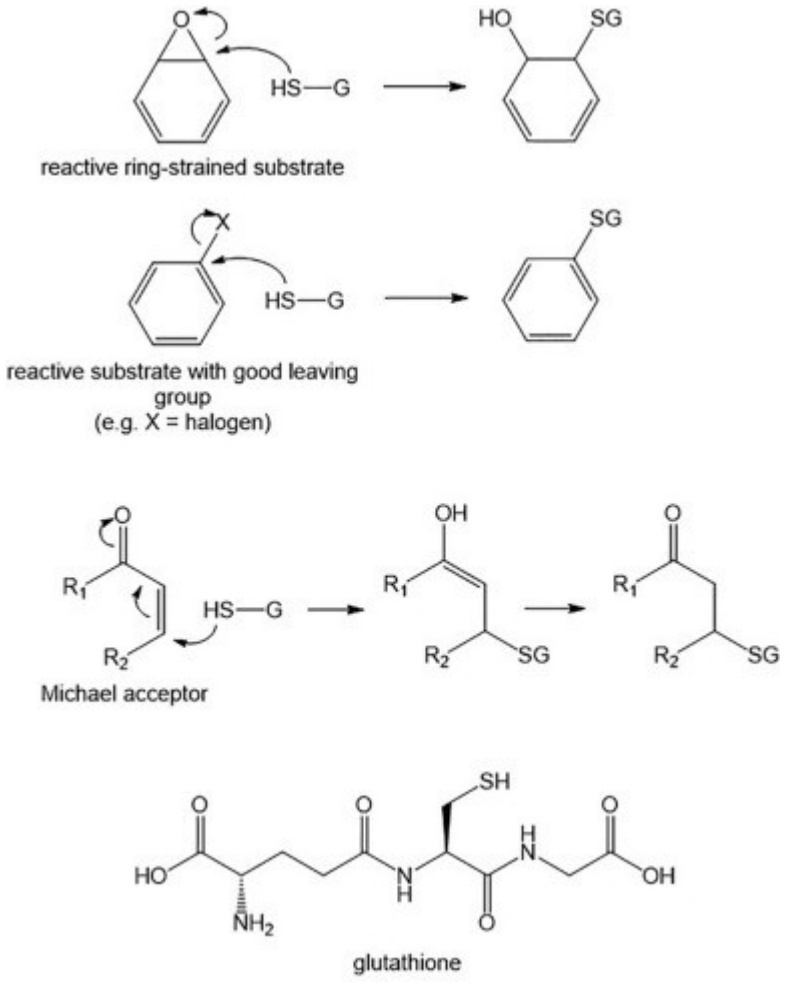

Figure 3: Simplified GST reaction mechanism. The thiol (under the thiolate form i.e. deprotonated) of the cysteine in glutathione acts as a nucleophile to attack various electrophiliccenters of xenobiotic compounds (e.g., aryl halides and Michael acceptors) and reactive metabolites (e.g., epoxides) (adapted from Obach & Isoherranen,2022).

Similarly, the relatively low specificity of cytochrome P450s (P450s) could be considered as a general defense system against the detrimental effects of natural products, drugs and other synthetic chemicals. (Figure 4). Clearly, the picture clearly differs for an enzyme exhibiting numerous, inefficient secondary actions that contribute little to the organism's fitness (Copley,2017).

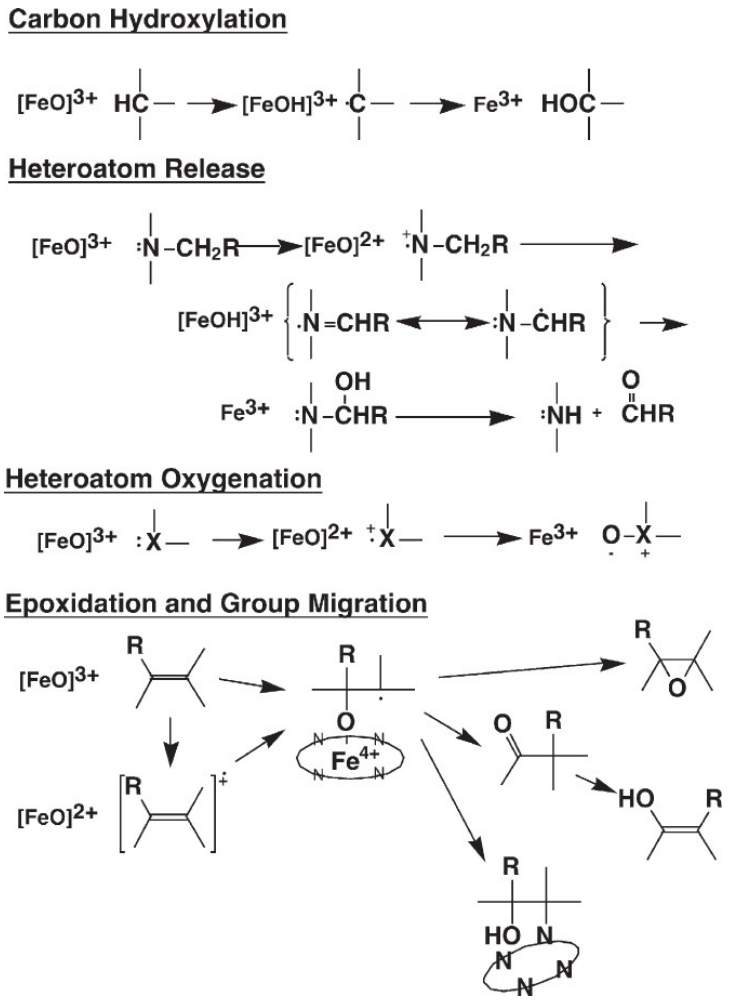

Figure 4: Mechanisms of major reactions in P450 catalysis
The basic P450 reactions include C-hydroxylation, heteroatom oxygenation, heteroatomrelease (dealkylation), epoxide formation, and 1,2-migration.

C. Mechanisms of enzyme promiscuity

The promiscuous nature of enzymes has sparked numerous inquiries, including: "What rendersan enzyme promiscuous?" and "How can the active site of an enzyme accommodate a substratethat deviates from its physiological counterpart?"

Numerous studies have demonstrated that the mechanism of catalysis for promiscuous substrates differs from the physiological reaction mechanism. The mechanisms underlying enzyme promiscuity are grounded in the conformational diversity of the enzyme's active site, substrate ambiguity, varying protonation states, distinct subsites within the same active sites, and cofactor ambiguity (Khersonsky & Tawfik, 2010; Copley, 2014). Based on the diverse factors responsible for enzyme promiscuity, they can be categorized into three primary groups: (1) substrate promiscuity, (2) catalytic promiscuity and (3) conditional promiscuity (Figure 5).

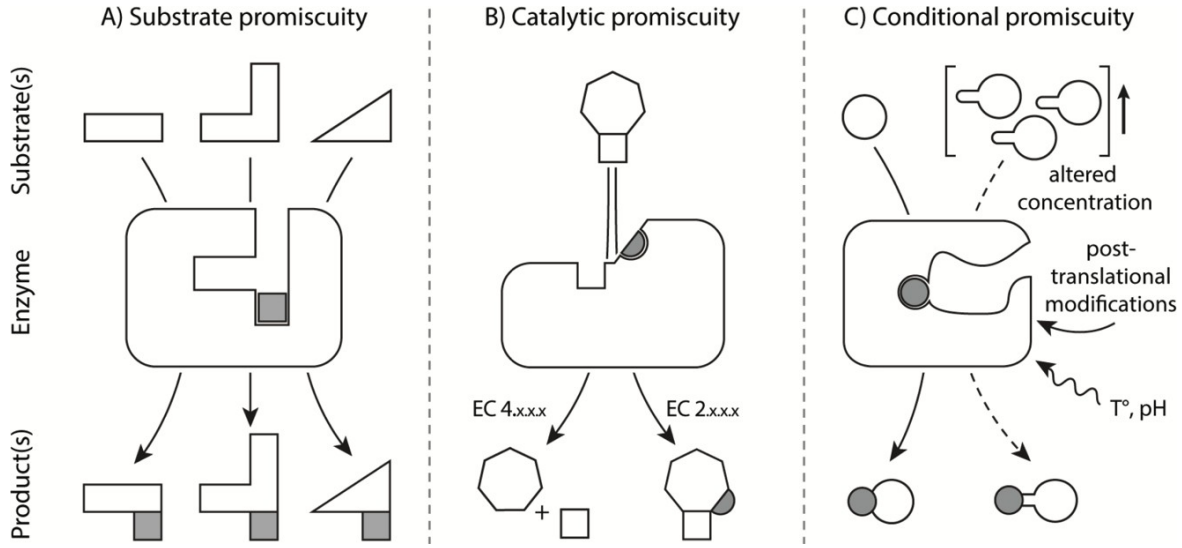

Figure 5: Mechanism-based classification of enzyme promiscuity (adapted from **Piedrafita *et al.,* 2015).** (A) Substrate promiscuity or multispecificity. An enzyme can perform the same catalytic reaction with a range of substrates that are structurally related but not identical, exhibiting a broader substrate specificity than initially perceived. (B) Catalytic promiscuity: Anenzyme can catalyze multiple chemically distinct reactions, expanding its functional repertoire and enabling it to participate in a wider range of metabolic processes. (C) Conditional promiscuity: An enzyme's latent secondary activities can be induced or activated under specific environmental conditions, such as increased concentrations of alternative substrates with lower affinity for the enzyme or post-translational modifications that trigger conformational changes.

Substrate promiscuity describes an enzyme's ability to accept and catalyze reactions with a diverse range of substrates as above-mentioned for GSTs and P450s. Bacterial alkaline phosphatase, is another significant example as it can hydrolyze phosphodiesters, phosphamides, sulfate esters, thiophosphates, and phosphite, showcasing its broad substrate specificity. This promiscuous enzyme also exhibits excellent phosphate monoesterase activity (O'Brien & Herschlag, 2001*;* Yang & Metcalf, *2004*). Methane monooxygenase, capable of hydroxylating methane and over 150 other substrates, represents a remarkable example of substrate promiscuity (Copley, 2003).

Catalytic promiscuity refers to an enzyme's ability to catalyze different reactions with different transition states or multiple reaction types with a single substrate, leading to the formation of diverse product pathways. Enzyme catalytic promiscuity can be either: (i) accidental – a side reaction catalyzed by the wild-type enzyme; (ii) induced – a new reaction established by one orseveral mutations rerouting the reaction catalyzed by the wild-type enzyme. These enzymes often possess substrate promiscuity as well. A good example is the

use of pyruvate decarboxylase to form carbon–carbon bonds; this was first studied in 1921 (Neuberg & Hirsch, 1921), and is, today, an industrial activity. Mammalian serum paraoxonase (PON1), for instance, functions as an esterase, phosphotriesterase, and lactonase (Khersonsky & Tawfik, 2006). While the first two of these catalytic activities are mediated by a histidine dyad, distinct sets of catalytic residues are employed for the third (Figure 6).

Conditional promiscuity is characterized by the ability of an enzyme to perform non-native reactions in response to environmental changes, e.g., due to a change in cofactor, to an increase in the concentration of substrate analogs with lower affinity for the enzyme, or by post-translational modifications (Hult & Berglund, 2007). This was explored by Rona *et al*. in the early 1930s in a series of experiments using pig liver lipase and pancreatic lipase in organic solvents for resolution of chiral alcohols and esters (Rona *et al*., 1931). Regarding the impact of metal exchange, substitution of the native Zn^{2+} by Mn^{2+} in carbonic anhydrase permitted the styrene epoxidation to be catalyzed (Fernández-Gacio *et al.,* 2006).

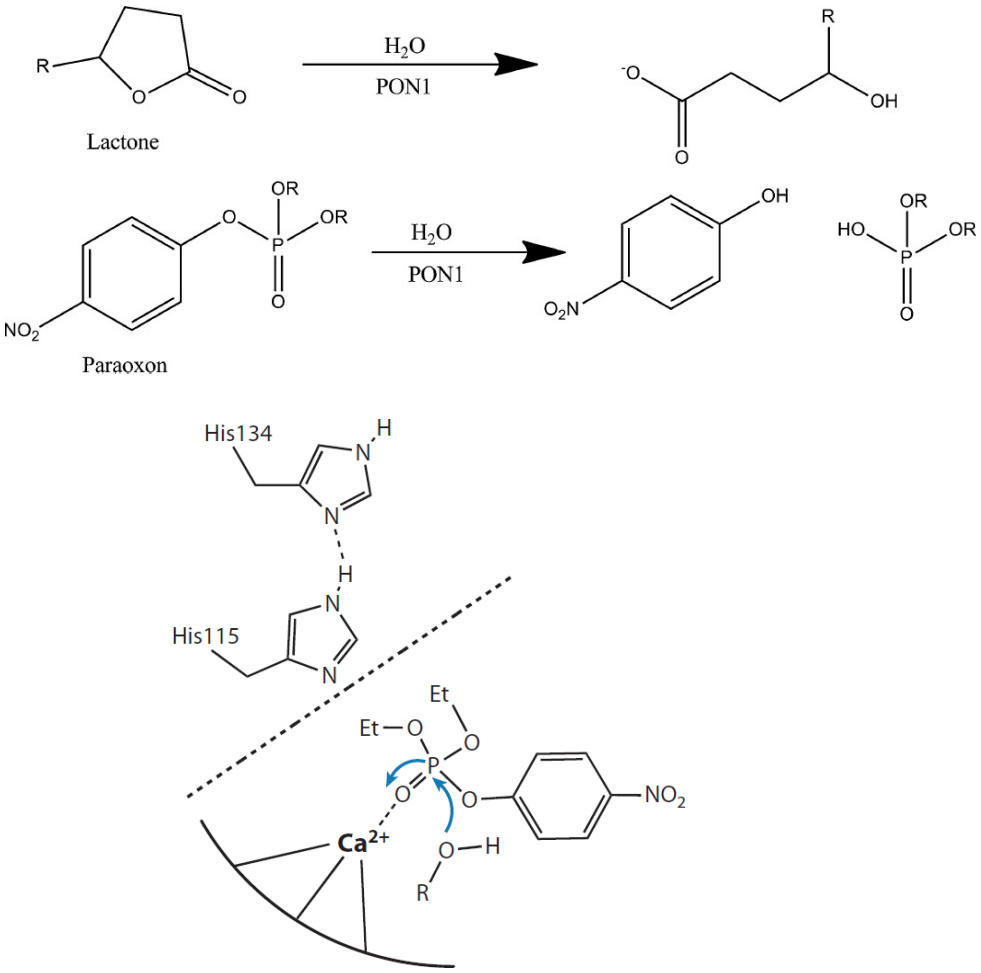

Figure 6: Different subsites within the same active site (adapted from Khersonsky & Tawfik, 2010). The main active-site feature of the serum paraoxonase (PON1) is the catalytic calcium ion, which lies at the bottom of a deep and hydrophobic active site and is thought to act as the"oxyanion hole" of PONs. PONs exhibit native lactonase with promiscuous phosphotriesterase activity where hydrolysis of lactone is mediated by a His115-His134 dyad, which deprotonates awater molecule to generate the attacking hydroxide, while phosphotriesterase activity (shown forparaoxon as substrate) is mediated by another set of residues in the same active site groove.

D. Enzyme promiscuity and evolution

To conclusively attribute enzyme promiscuity to the emergence of new enzymatic functions, it is essential to assume that the enhancement of a latent promiscuous activity by a small numberof mutations could confer a clear selective advantage once that activity becomes crucial. Directed laboratory evolution has provided ample evidence supporting this hypothesis. Rarely does a scenario arise where an entirely new substrate and activity are added to an existing enzyme, seemingly out of nowhere. Instead, such transitions require substantial sequence modifications, including the simultaneous removal and insertion of a small number of active site loops (Park *et al.*, 2006).

Furthermore, by accumulating a few advantageous mutations or neutral mutations, the weaker promiscuous behaviors can gradually enhance (Amitai *et al.,* 2007; Gupta & Tawfik, 2008). New functions can emerge in existing protein folds because of minor changes in the active site. For evidence, the fact that 6-pyruvoyltetrahydropterin synthase homologs from bacteria and mammals catalyze different reactions with the identical substrate (7, 8-dihydroneopterin triphosphate) indicates that small variation in active site can lead to the emergence of new enzyme (Miles *et al.,* 2014). There is lots of evidence supporting the role of promiscuity in the evolution of novel activities from studies of enzyme families and superfamilies. In particular, the discovery of promiscuous activities, or cross-reactivities, between various members of the same enzyme family or superfamily, and the capacity to evolve these promiscuous activities in the lab offer crucial hints regarding evolutionary, structural, and mechanistic relationships within enzyme superfamilies (Khersonsky *et al.,* 2006).

E. Functions of promiscuous enzymes

Promiscuous activities may not be essential for the organism's survival or fitness, but they provide a reservoir of catalytic potential that can be exploited when a new enzyme is needed to enhance fitness. The functions of promiscuous enzymes can vary widely, from metabolic pathways to detoxification processes, and they can be recruited to serve new functions when a genetic or environmental change makes catalysis of a novel reaction important for fitness or survival (Copley, 2023).

Promiscuous activities are significant because they provide the groundwork for the emergenceof new enzymes. Promiscuous activities can accelerate reactions by factors of up to 10^{26}, despite often being less efficient than their primary activities (Edwards *et al*., 2012). When an environmental change makes a promiscuous activity beneficial for fitness, gene duplication and divergence can allow for the evolution of a new enzyme while still maintaining the originalactivity (Hughes, 1994; Bergthorsson *et al.,* 2007). Promiscuous activities can offer useful starting points for the development of new enzymes in pathways that synthesize important compounds and medications (Bornscheuer & Kazlauskas, 2004). In rare cases, a single mutation can increase promiscuous behavior by a factor of 100 or more (Khanal *et al.,* 2015; Rahmi *et al.,* 2016). One notable example is the mutation of Glu323 to Gly in muconate

lactonizing enzyme II, which resulted in a 10^6-fold increase in promiscuous o-succinylbenzoate synthase activity (Schmidt *et al*., 2003). However, the evolutionary potential of promiscuous enzymes extends beyond their role as building blocks for unique new enzymes. It is possible to assemble several promiscuous activities to create novel metabolic pathways, both in the lab and in nature. Examples include novel routes for the synthesis of vanillin (Hansen *et al*., 2009), pyridoxal 5'-phosphate (Kim *et al*., 2010), (R)-hydroxybutyrate and (S)-3-hydroxybutyrate (Tseng *et al*., 2009), and the degradation of anthropogenic contaminants (Copley, 2009).

Many enzymes have recently evolved for the degradation of xenobiotic compounds such as (pesticides,explosives) (Ramos *et al.,* 2005; Afriat *et al.,* 2006; Copley, 2009 ; Wackett, 2009) and antibiotics (Bebrone, 2007; Lozovsky *et al.*, 2009). The functional expansion in these and other superfamilies is still ongoing.

F. Applications and examples of promiscuous enzymes

The promiscuity of enzymes can serve as a starting point for divergent evolution, as we have already explained. By accumulating just one or more advantageous mutations that help the organism's survival, the enzyme's low promiscuous activity toward a physiologically irrelevant substrate may be transformed into a considerably more effective catalyst. Furthermore, by using directed laboratory evolution or rational, semi-rational protein engineering techniques, apromiscuous function can serve as the basis for the development of a novel enzyme activity (Renata *et al.,* 2015 ;Colin *et al.,* 2015). Below are several recent studies that have demonstrated notable advancements in promiscuous behavior and/or changes in substrate specificity.

Many examples of promiscuous enzymes exist in nature or in laboratories, and industy. For example, in industrial Enzymes that degrade synthetic chemicals introduced to the biosystem during the last decades paraoxonase which degrades the paraoxon (Organophosphates used asinsecticides and herbicides) and enzymes associated with drug resistance (β-lactamases) and in nature pyruvate decarboxylase (Hult & Berglund, 2007), carbonic anhydrase (Pocker & Stone, 1965), pepsin (Reid & Fahrney, 1967), chymotrypsin (Nakagawa & Bender, 1969), and L-asparaginase (Jackson & Handschumacher, 1970). Finally, in terms of fundamental knowledge, rhodanese family enzymes are also depicted to be promiscuous and this is the topic of the second part of the introduction.

II. The rhodanese-containing proteins

A. History of the rhodanese domain

Lang's groundbreaking 1933 research identified an enzyme in mammalian tissues capable of catalyzing the conversion of thiosulfate and cyanide into thiocyanate and sulfite (Lang, 1993). This discovery led to the coining of the enzyme's name, "rhodanese," derived from the German term "rhodanid," meaning thiocyanate, with the suffix "-ase" indicating its enzymatic nature. While term rhodanese remains widely used, the formal nomenclature for the enzyme, based on its in vitro reaction, is thiosulfate:cyanide sulfurtransferase (TST, EC 2.8.1.1) (Cipollone, 2007).

Rhodanese (Rhd) domains are common structural modules found in all three major phyla of evolution. The Rhd domain is made up of approximately 100 amino acid residues with a central β-sheet of three parallel strands, flanked by 4 to 5 alpha helices (Selles *et al*., 2019). Morethan 500 sequences have been found to possibly encode proteins with at least one Rhd domain after the genomes of more than 80 species were analyzed using various techniques (Hofmann *et al*., 1998). Multiple Rhd domain proteins are frequently encoded by the same genome. For instance, the human genome contains 47 distinct proteins, and *Escherichia coli* has 7 known proteins.

As we will explore throughout this chapter, rhodanese exhibits a diversity that far surpasses its commonalities. This diversity is precisely what makes this protein module so intriguing, as it is not confined to a single function but participates in a wide array of physiological pathways.

Some Rhd domains exhibit enzymatic activity linked to the presence of a cysteine residue in a catalytic loop (Forlani *et al*., 2003; Bhattacharjee *et al*., 2010). Furthermore, the presence or lack of the catalytic loop can be utilized for differentiation between two primary types of Rhd domains (Bordo & Bork, 2002). The inclusion of a cysteine residue in a CX4R or CX5R motif, which supports various types of chemical processes catalyzed by these domains(Figure 7), identifies this loop as catalytic (Forlani *et al*., 2003). The domains are catalytically inert without the cysteine residue and are instead viewed as protein/protein interaction mediators (Avvakumov *et al*., 2006).

Recent studies have revealed that Rhd-containing proteins play a crucial role in the maturation of molybdenum cofactor (MoCo), a vital prosthetic group essential for the function of key enzymes, including sulfite oxidase (SO), xanthine oxidoreductase (XOR), and

aldehyde oxidase (AO). Additionally, these proteins are involved in tRNA thiolation, a post-transcriptional modification that stabilizes tRNA tertiary structure and facilitates precise decoding processes (Bimai *et al.*, 2020).

Despite a conserved 3D structure, the sequences of Rhd domain proteins are highly variable, making alignment between functionally or evolutionarily distant proteins difficult. At the same time, the growing number of 3D structures of different Rhd domains available (259 entries in the RCSB database, https://www.rcsb.org) has enabled structural motifs to be identified. Thus, for example, authors have identified two highly conserved structural motifs in activity-bearing domains: a DXR motif of unknown function at the end of the β2 strand, and between the β4 strand and the α4 helix the catalytic loop with the conserved CX_4R or CX_5R motif (Bordo & Bork, 2002; Selles *et al.,* 2019).

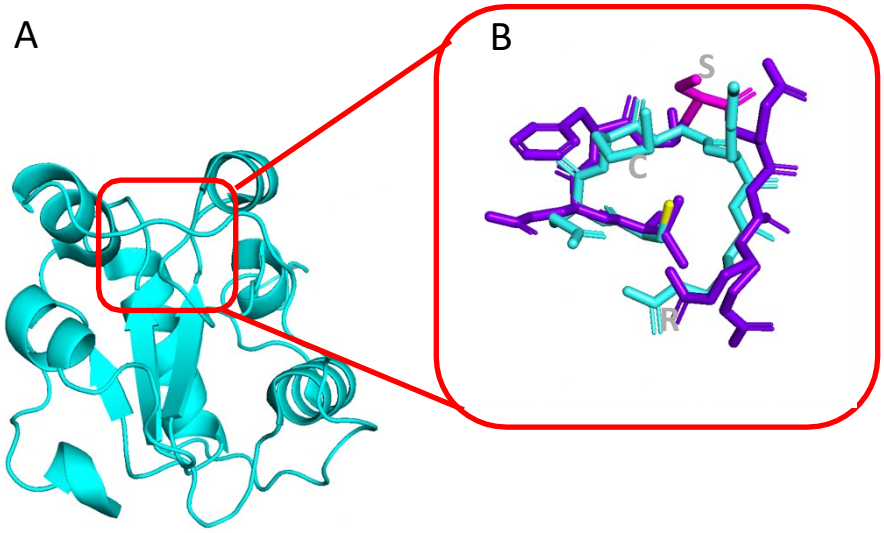

Figure 7. Representation of the Rhd domain (A) and of different catalytic loops (B).
(A) Representation of the Rhd domain of TSTD1, a human thioltransferase (PDB code: 6BEV) in "ribbons and arrows" mode with Pymol software version 2.0.1. (B) The catalytic loops of two enzymes possessing a Rhd domain are represented in "stick" mode with the Pymol software version 2.0.1. In blue, is represented that of TSTD1 with a CX_4R type loop. In purple, is represented that of CDC25B, a human phosphatase (PDB code: 1cwt) containing a CX_5R-type loop.

B. Reactions catalysed by Rhd-containing enzymes.

Currently, Rhd-domain enzymes have been described as catalysing three main types of chemical processes, i.e. the transfer of sulfur or phosphate groups and the reduction of arsenate (Figure 8)(Forlani *et al.*, 2003; Bhattacharjee *et al.*, 2010).

The transfer of a sulfur atom from a donor substrate to an acceptor substrate is catalysed by sulfurtransferase enzymes. Depending on the enzyme, several substrates are described in theliterature: small sulfurated molecules (thiosulfate or 3-mercaptopyruvate (3MP) or proteins in persulfide form as donor, and chemical (DTT) or protein (thioredoxin) reducers as acceptor. Concerning small chemicals as donor substrate, sulfurtransferases can also be classified into 2groups according to their preferred donor substrate: thiosulfate for thiosulfatesulfurtransferases (TST), and 3MP for 3-mercaptopyruvate sulfurtransferases (3MST) (Cipollone *et al.,* 2007).

The dephosphorylation and arsenate reduction reactions described are catalysed by a specificfamily of CDC25-type enzymes. In humans, CDC25 (encoded by the "Cell Division Cycle 25" genes) are phosphatases that catalyse the dephosphorylation of tyrosine, serine and threonineresidues of CDKs ("Cyclin Dependent Kinase") and in addition to their phosphatase activity, CDC25B and CDC25C also reduce *in vitro* arsenate to arsenite (Bhattacharjee *et al.,* 2010) (Figure 8).

Recently, a new activity, i.e. a uridine 34 hydroxylation activity of certain tRNAs, was proposedfor TrhO from *E. coli* (Sakai *et al*., 2019).

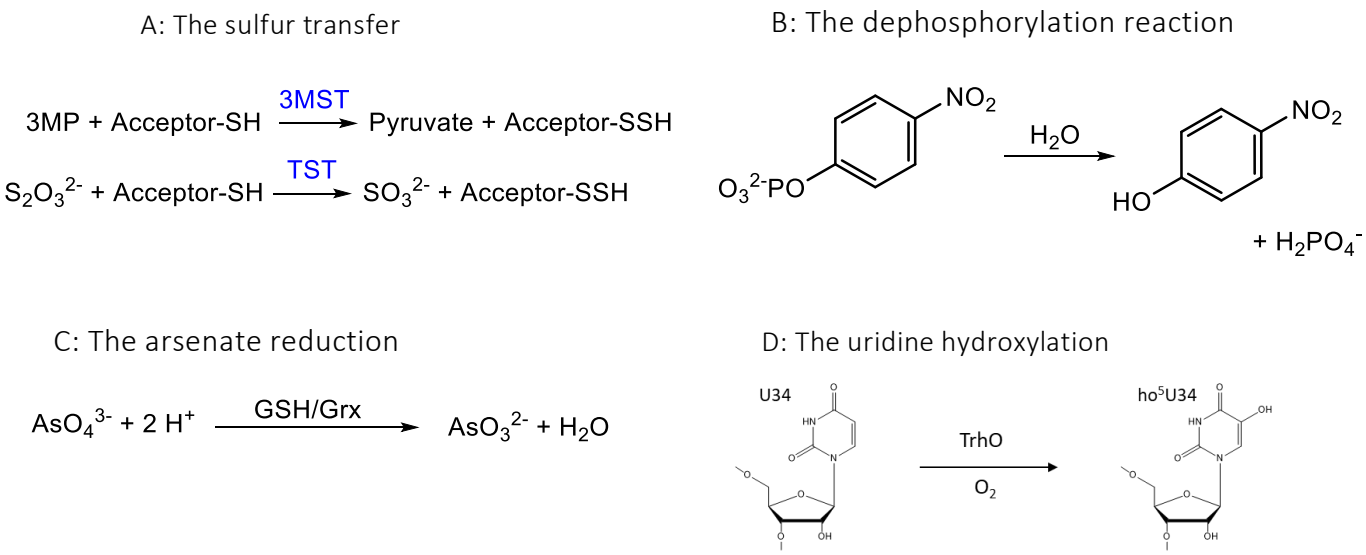

Figure 8: Reactions catalyzed by Rhd-containing enzymes.
(A) Sulfur transfer from 3mercaptopyruvate (3MP) or thiosulfate, (B) phosphate transfer from p-nitrophenylphosphate as artificial substrate, (C) arsenate reduction in the presence of glutathione (GSH) and glutaredoxine (Grx) and (D) uridine hydroxylation on tRNA uridine at position 34 (U34).

C. The classification of Rhd-containing enzymes.

Rhd-containing enzymes are sufficiently different to form a superfamily. Variability can be found in several areas, such as domain organization, essential catalytic Cys residue presence, active site loop length, and presence of other structural domain (Cipollone *et al.,* 2007). Based on the previously established criteria, four families of enzymes can be identified (Figure 9).

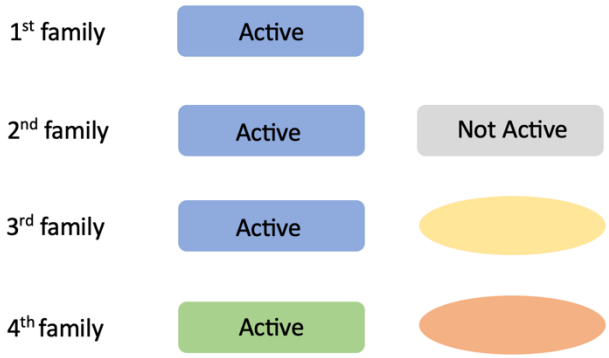

Figure 9: A classification of Rhd-containing enzymes into four families or class has been proposed based on the number of Rhd domains and the presence or absence of additional domains. (Bordo & Bork, 2002; Cipollone *et al.,* 2007)
The first family is composed of enzymes with only one Rhd domain, such as TSTD1. The second family is composed of enzymes with two Rhd domains but only one is active, like human 3MST. The third family is composed of Rhd domains associated with an additional domain (possessing catalytic activity or not, such as 3MST from *L. major*). The fourth family includes enzymes with aconserved catalytic loop of seven residues, such as human CDC25B.

The first family is composed of a single Rhd domain, and is mainly made up of TSTs, like GlpE of *E. coli* or human TSTD1. These enzymes are associated with stress response mechanisms (Adams *et al*., 2002), or in the process of leaf senescence in plants (Azumi & Watanabe, 1991).There are also proteins in this family which are inactive, which do not have a catalytic cysteine, although they are relatively rare (Fauman *et al.,* 1998).

The second family is composed of enzymes comprising an active Rhd domain and another inactive one, for which the catalytic cysteine is generally replaced by an aspartic acid or a glycine. The active domain is always the one located in the C-terminal position. This family is very widespread and includes TSTs as well as 3MSTs, which are both involved in the metabolism of hydrogen sulfide (H_2S), in its catabolism and anabolism, respectively.

The third family is composed of enzymes comprising one or two Rhd domain(s) and another domain having a different activity or no activity. The enzymes of this family are mainly involved in the metabolism of sulfur biomolecules, such as thiamine for proteins of the ThiF

family, molybdopterin for proteins of the ThiI/MoeB family (Cortese *et al.*, 2002). This family is also involved in the formation of 4-thiouridine at position 8 of bacterial tRNA, an important modification for the recognition of certain codons (Yokoyama *et al*., 1985).

The fourth family is composed of enzymes having a catalytic loop of seven residues. This family is mainly represented by CDC25 phosphatases, involved in the regulation of the cell cycle (Bordo & Bork, 2002).

III. Sulfurtransferases

Sulfurtransferases harboring a Rhd domain are involved in a variety of physiological processes, from metabolic pathways and signaling to protein posttranslational modifications, participating in sulfur atom trafficking. In particular, they are now recognized askey players in the emerging gasotransmitter hydrogen sulfide (H_2S) homeostasis.

Among the different active Rhd-containing enzymes, four enzymes catalyze a sulfur transfer reaction: two TSTs from class 1 and class2, and two 3MST-like. All these sulfurtransferases share the same two-step chemical mechanism involving first the nucleophilic attack of the catalytic cysteine in thiolate form on the sulfur atom of the substrate, leading to the formation of a persulfide intermediate and a first product, which is released. Then, the distal sulfur atom is transferred from this intermediate to an acceptor to form the second product and regeneratethe cysteine under thiolate form (Figure 10).

MSTs and TSTs have very low sequence identity (<10%). Moreover, unlike 3-MSTs, TSTs exhibitalso low sequence identity (~40% for 3-MSTs vs. <10% for TSTs), so few residues are conserved between the different known protein sequences, making it difficult to determine common signature sequences. Nevertheless, the catalytic cysteine is obviously conserved in all protein sequences, making it possible to identify the catalytic loop region. Thecatalytic cysteine of 3-MST is present in the conserved sequence C-G-[S/T]-G-[V/I]-T-A (Spallarossa *et al*., 2004) and the signature sequence of this catalytic loop is as follows for all TSTs: C-X(2)-[G/H]-X(2).

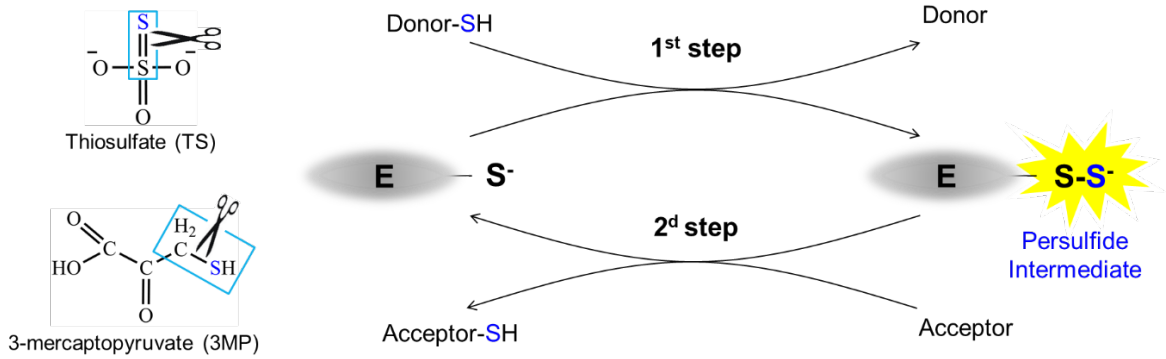

Figure 10: Schematic representation of the sulfurtransferase reaction.
The sulfur atom is first transferred from donor substrate to the thiol of the enzyme (E-S$^-$) (1st step) leading to formation of a persulfide intermediate (E-S-S$^-$), then from E-S-S$^-$ to an acceptor substrate (2nd step). In the absence of acceptor substrate, the persulfide intermediate accumulates.

A. Rhodanese, a class 2 TST

Rhodanese was the first sulfurtransferase to be isolated and characterized, in 1933, from bovine liver, and this TST (EC: 2.8.1.1) is ubiquitously found in both prokaryotes and eukaryotes (Lang ,1933; Tabita *et al.,* 1969; Westley, 1973). Lang's research revealed the presence of an enzyme in rat liver that, in the presence of thiosulfate, catalyzes the conversion of cyanide to thiocyanate (SCN^-).

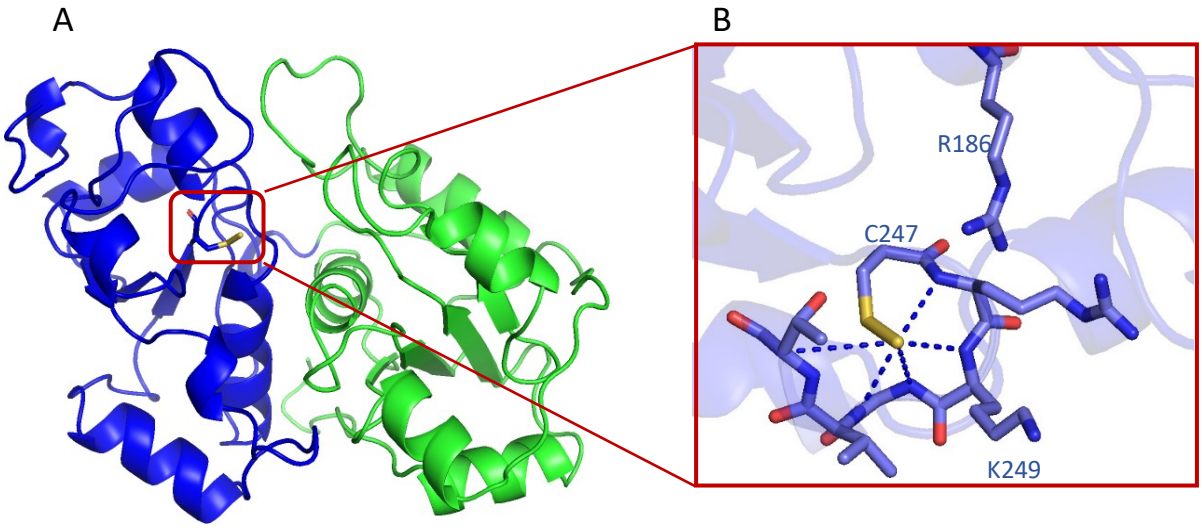

Figure 11. Cartoon representation of bovine Rhodanese monomer (A) and its active site (B) (PBD code: 1RHD).
The monomer is represented in "ribbons and arrows" mode with the active Rhd domain inblue and the inactive one in green (A), and the residues of the active site as sticks (B). The sulfuratom(s) of the catalytic Cys are shown in yellow and the figures were generated using the Pymol software version 4.6.0.

To date, two three-dimensional TST structures with two Rhd domains are known: Rhobov from *Bos taurus* (1RHD) (Ploegman *et al*., 1978) and RhdA from *Azobacter vinelandii* (1E0C) (Bordo *et al*., 2000). The active site, situated between the two domains, consists of a six-residue loop containing the catalytic Cys, which, in its persulfide state, finds stabilization through multiple hydrogen bonds formed with the active site amino acids (Ploegman *et al.,* 1978) (Figure 11).

Rhodaneses use thiosulfate ($S_2O_3^{2-}$) or organic thiosulfonate anions (RSO_2S^{2-}) as donor substrates, but they also exhibit activity with 3MP, which is described to be of the order of 1/100th that determined in the presence of thiosulfate (Ray *et al*., 2000). Bovine Rhodanese is also reported to be able to use thiocystin as a sulfur-donor substrate, as demonstrated by 35S labelling of thiocystin (Abdolrasulnia & Wood, 1980). More recently, it has been shown that human Rhodanese exhibits a thousand-fold higher catalytic efficiency in the presence of glutathione in persulfide form (GSSH) compared to thiosulfate (Libiad *et al*., 2014). Various sulfur-acceptor substrates have also been identified in vitro: as a non-physiological example, DTT is a potential TST acceptor (Pecci *et al*., 1976). The first acceptor substrate to be identified was cyanide, thanks to the study of bovine Rhodanese, that shows a low apparent affinity for cyanide, with K_M exceeding one millimolar (Westley, 1981). The use of a coupled Trx reductase/NADPH system showed that, among potential dithiols, reduced Trx would be the best acceptor for bovine Rhodanese, with apparent affinity constants K_M in the micromolar range, compared with K_M close to the millimolar range for other dithiols such as DTT and DHLA. On the other hand, the use of such substrates by bovine Rhodanese would lead to the production of labile sulfur (Nandi & Westley, 1998).

More recent work shows that sulfite is a good sulfur acceptor substrate for Rhodanese, leading to the formation of thiosulfate, the K_M determined for sulfite being of the order of a hundred micromolar. In the same publication, GSH and L-cysteine were also used as acceptor substrates for the reaction, but the K_M values exceed the millimolar by a wide margin, ruling out the possibility that they are physiological acceptors for this enzyme (Libiad *et al*., 2014).

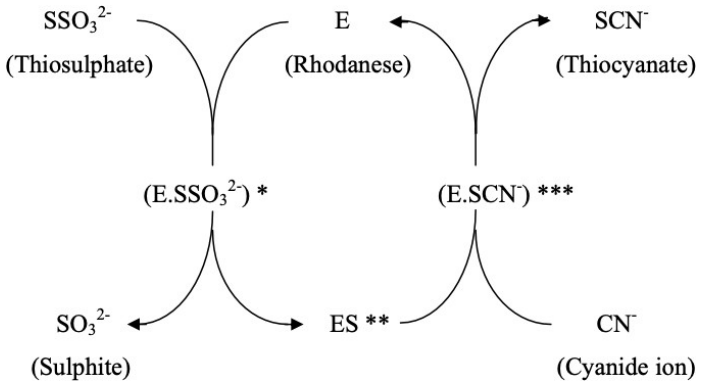

Figure 12: Mechanism of action of Rhodanese. * Rhodanese thiosulphate complex, ** Rhodanese persulfure, * Rhodanese thiocyanate complex.**

Currently, the molecular mechanism of sulfur-sulfur bond cleavage catalyzed by Rhodanese is not elucidate. Due to the electronic nature of the thiosulfate substrate, the nucleophilic cleavage of S=S bond must be electrophilically mediated to decrease the electron density resulting from the Π orbital participation (Chauncey & Westley, 1983; Mintel & Westley, 1966). The reaction could also be enhanced by electrons attraction on the sulfonyl sulfur atom which favors nucleophilic attack and renders the sulfonyl sulfur a better leaving group (Green & Westley, 1961). Based on site-directed mutagenesis and steady-state characterization of bovine and *Azotobacter vinelandii* Rhodaneses, it was proposed that an Arginine residue (R186) is implicated in thiosulfate binding (Weng *et al.,*1978; Nagahara *et al.,* 1995). Moreover,the catalytic cysteine belonging to a six amino acid loop lies in a strongly positive electrostatic field provided by neighboring peptidic NH groups (Spallarossa *et al.,* 2004a; Libiad *et al.,* 2014).

In addition, residues on the active-site loop are predicted to confer substrate specificity. The positive charges at the proximal arginine and lysine residues in the CRKGVT motif are predictedto interact with the negative charges on the substrate (e.g. oxygen atoms in the case of thiosulfate). In fact, the dual replacement of Arg248 and Lys249 with Gly and Ser, respectively, increased the K_M value for thiosulfate (17-fold) and decreased the k_{cat} for rhodanese 6-fold (Nagahara *et al.,* 1995). As well as activity assays on *S. cerevisiae* RDL2 indicate that the Arg111 of the active-site loop is critical for the sulfane sulfur transfer (Wang *et al.,* 2021). Forlani *et al*. study showed that RhdA, a TSTfrom *Azotobacter vinelandii* belonging to the second group, exhibits sulfurtransferase activity in the presence of thiosulfate or 3-mercaptopyruvate as donor substrate and DTT as acceptorsubstrate but no phosphatase activity with an artificial substrate (3-O-methylfluoresceine phosphate) (Forlani *et al.,* 2003).

Moreover, insertion of an Ala/Ser in the CX_4R loop leads to appearance of phosphatase activity and to a decreased sulfurtransferase activity, suggesting that the length of the catalytic loop plays a key role in discriminating sulfur- and phosphate-containing substrates (Forlani *et al*., 2003).

The human rhodanese is coded by the *tst* gene, located on chromosome 22q12.3 (Aita *et al.,* 1997). TST/rhodanese is exclusively localized within the mitochondria of mammals (Sorbo, 1951; Himwich &Saunders, 1948). In point of fact, Rhodanese is in the cytoplasm in inactive form and is transported to the mitochondria when 5S RNA is imported into this organelle. Once in the mitochondria, the enzyme separates from the 5S RNA and its conformation changes thus leading to the active form (Smirnov *et al*., 2010 & Smirnov *et al*., 2011). This explains the mitochondrial localization of Rhodanese, even though its sequence has no mitochondrial addressing signal (Sylvester & Sander, 1990), the interaction of this protein in its unstructured form with 5S RNA provides it with the ability to translocate into mitochondria (Figure 13).

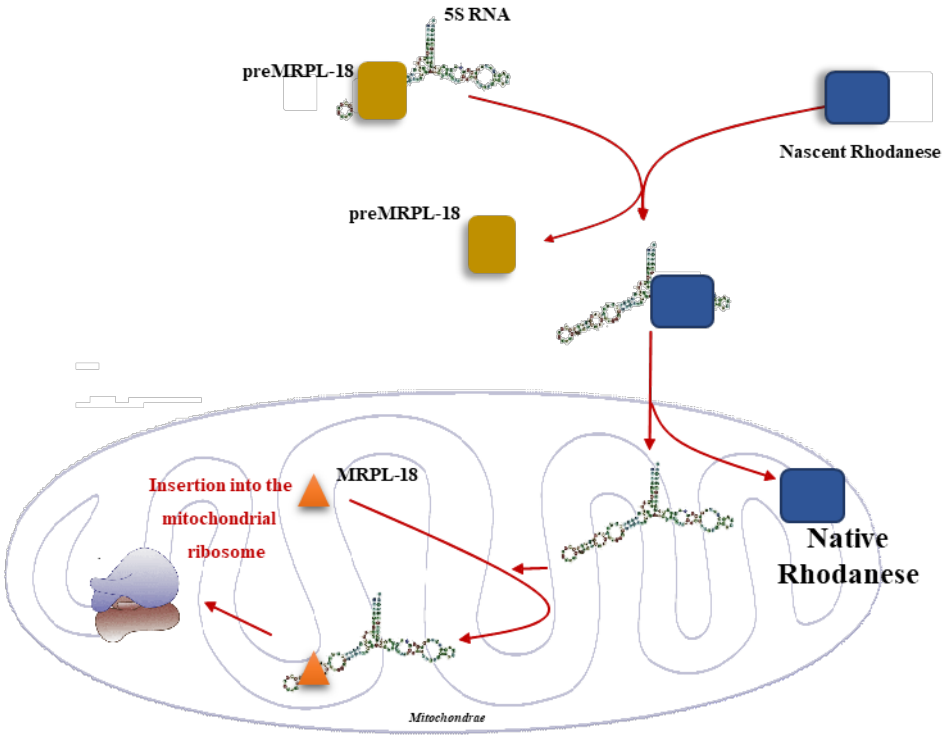

Figure 13: Proposed mechanism of intracellular trafficking of 5S RNA (Adapted from Smirnov *et al*., 2011).

5S RNA, once transcribed, is imported into the mitochondria. The L-18 pre-MRP binds to the α-subunit of the 5S RNA which leads to a change in its conformation. Rhodanese can thus bind to the γ-domain of 5S RNA and there is co-translocation of the two partners of the complex at the mitochondrial level. Rhodanese dissociates from the 5S RNA and folds back to its native conformation while the 5S RNA inserts into the ribosome after binding of the native L-18 MRP protein. The L-18 MRP protein dissociates upon incorporation of the 5S RNA into the ribosome.

Human Rhodanese has been proposed to participate in mitochondrial H_2S catabolism. Indeed,H_2S oxidation is thought to be carried out by the SOU complex, a multienzyme complex composed of three proteins: SQOR, ETHE1 and a human TST that may be Rhodanese or TSTD1 according to the respective hypotheses of Dr. Banerjee and Dr. Jorns (Libiad *et al.,* 2014; Melideo *et al.,* 2014). According to Dr. Banerjee's hypothesis (Figure 14), Rhodanese would produce thiosulfate from sulfite, which would be the elimination form of H_2S (Libiad *et al.,* 2014; Kabil & Banerjee, 2012).

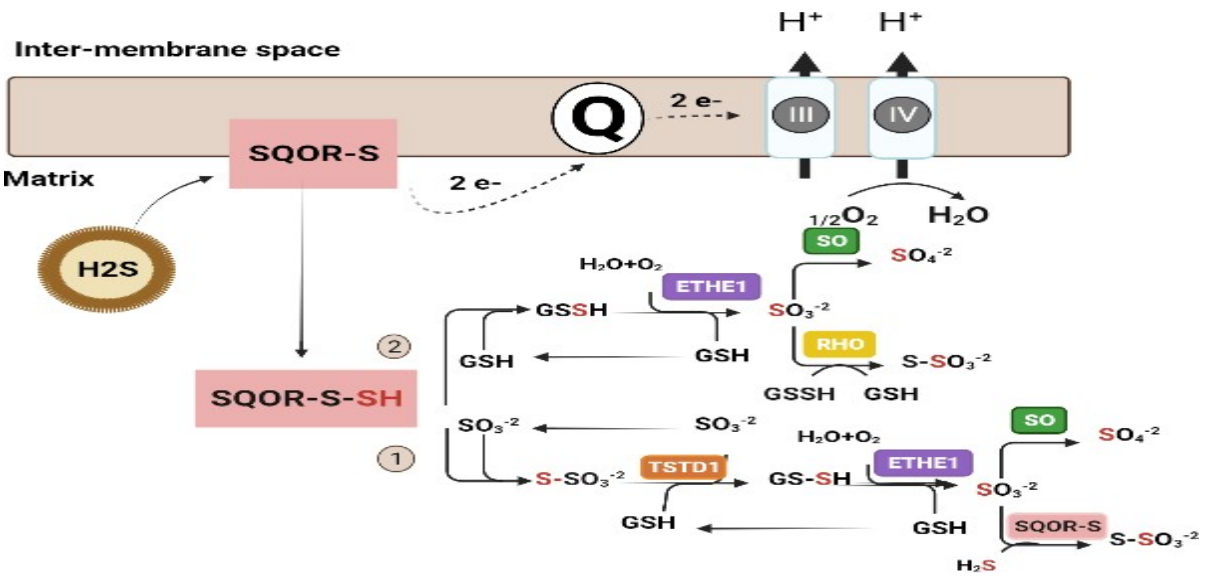

Figure 14: The oxidation of H_2S by the SOU complex (adapted from Melaku & Mossie, 2017). H_2S is initially fixed by a membrane-bound sulfide quinone oxidoreductase (SQOR). The electrons extracted from H_2S enter the respiratory chain at the level of the quinone, are then transferred to complex III, and are finally fixed by cytochrome *c* oxidase (complex IV) to molecular oxygen with the formation of water. Thus, SQOR allows coupling the oxidation of H_2S to electron transfer, H+ pumping, and ultimately ATP synthesis.
Oxidation of H_2S by SQOR produces SQOR persulfide intermediate. The sulfane sulfur is then transferred to a mobile sulfide carrier either sulfite (SO_3^{2-}, pathway 1) or glutathion (GSH, pathway 2) producing thiosulfate ($S\text{-}SO_3^{2-}$) or glutathione persulfide (GSSH), respectively.
In pathway 1, the sulfur is transferred to GSH by TSTD1 forming GSSH, and the sulfur then sequentially oxidized by the mitochondrial ETHE1 to SO_3^{2-} and by sulfide oxidase (SO) to sulfate (SO_4^{2-}). Thiosulfate can also be formed from SO_3^{2-} and H_2S by SQOR.
In pathway 2, ETHE1 oxidizes GSSH to SO_3^{2-}, regenerating GSH. SO_3^{2-} can then be oxidized to SO_4^{2-} by SO, or thiosulfate regenerated by Rhodanese (RHO) transferring a sulfur from GSSH to SO_3^{2-}.
SQOR: sulfide quinone oxidoreductase; SQOR-SH: SQOR persulfide; TSTD1, Thiosulfate sulfurtransferase; RHO: Rhodanese; ETHE1: persulfide dioxygenase; SO: sulfite oxidase; GSH: glutathione; GSSH: glutathione persulfide; Q: quinone.

H_2S distribution throughout the tissues exhibits tissue-specificity, with the liver holding the highest concentration and the kidneys, adrenal glands, and thyroid glands possessing significant levels (Hatzfeld & Saito, 2000; Green & Westley, 1961). Notably, human kidneys exhibit twice the amount of rhodanese activity compared to the liver, followed by the lungs, brain, stomach, and muscles. A multitude of additional disorders characterized by mitochondrial dysfunction and/or imbalances in redox status or H_2S metabolism mitochondrial dysfunction and/or imbalances in redox status or H_2S metabolism showcase the influence of altered rhodanese expression and activity. These conditions encompass colonic aliments and, as per ongoing research, obesity-associated type 2 diabetes mellitus (Figure 15) (Buonvino *et al*., 2022).

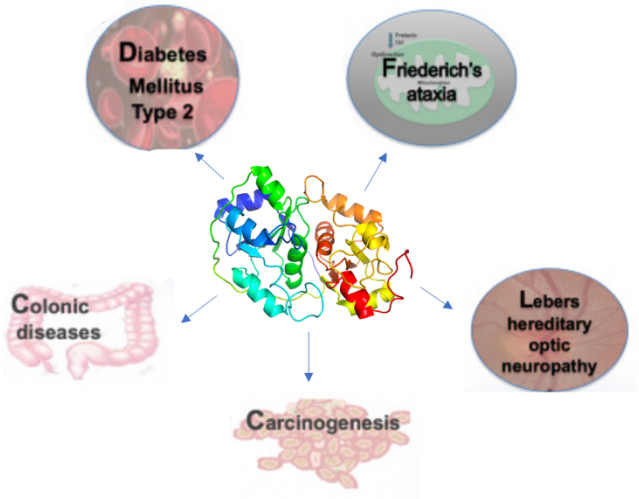

Figure 15: Schematic description of the diseases where Rhodanese expression and activity were suggested to play a relevant role (Buonvino *et al*., 2022).
For example, the autosomal-recessive neurodegenerative illness known as Friederich's ataxia is associated with the suppression of frataxin expression, a protein involved in the formation of iron-sulfur clusters, and is characterized by cardiomyopathy and progressive ataxia. In the neural NT2 cell line, where the expression of frataxin was suppressed, as well as in the fibroblasts and lymphoblast cells from the FRDA patients, there was a down-regulation of both serine hydroxymethyltransferase and rhodanese.
Lebers hereditary optic neuropathy is the first known illness associated with a change in TST/rhodanese expression (LHON). A rare neurological condition called LHON can cause severe vision loss or perhaps complete blindness. Within a year of the disease's inception, retinal ganglion cells (RGCs) selectively degenerate and optic atrophy results. This disease primarily affects young males. Point mutations in the mitochondrial DNA are the cause of LHON. TST activity was significantly reduced in liver biopsies from Leber patients, indicating a potential function for TST in this illness. Furthermore, cyanide detoxification pathway impairment contributes to the advancement of the illness.

B. TSTs from class 1

These enzymes are wildly distributed in all three kingdoms of life and are involved in multiple bioprocesses. For instance, the *Saccharomyces cerevisiae* RDL1 is critical for thiosulfate assimilation through converting thiosulfate to glutathione persulfide (GSSH) (Chen *et al.,* 2018). In vitro research has been done on the sulfurtransferase activity of human TSTD1 using thiosulfate as donor and glutathione as acceptor (Melido *et al*., 2014; Libiad *et al.,* 2014). Additionally, kinetic studies with a combination of sulfur donors and acceptors reveal that TSTD1 exhibits a low K_M for thioredoxin as a sulfane sulfur acceptor and that it utilizes thiosulfate inefficiently as a sulfur donor (Libiad *et al.,* 2018). Furthermore, a possible molecular interaction between TSTD1 and aprotein exhibiting Persulfide Dioxygenase (PDO) activity has been shown by Melideo and colleagues. In fact, by consuming the TSTD1 reaction product (GSSH), they showed how the presence of PDO enhanced the TSTD1 catalysis toward thiosulfate. In addition, the existence of fusions between the PDO and Rhd domain suggests that the TSTD1 protein could be a component of the SOU complex (Shen *et al.,* 2015), which is the main channel of H_2S detoxication in mammalian cells. Recently, STR16 from *Arabidopsis thaliana* has been shown to catalyze the oxidation of roGFP2 *via* trans-persulfidation in the presence of thiosulfate (Selles *et al.,* 2022).

In *E. coli*, there are also several TSTs that preferentially use Thiosulfate as a sulfur-donor substrate (Kawano *et al*., 2017). One of the first to be characterized is GlpE, a monodomain enzyme whose structure is known (PBD code: 1GMX) (Spallarossa *et al.,* 2001). Thioredoxin is also reported to be an efficient acceptor (K_M 34 µM) for the *E. coli* GlpE in the presence of thiosulfate as the sulfur donor (Ray *et al.,* 2000). However, its physiological role is still unknown. PspE is also a monodomain TST with a known structure (PBD code: 2JTQ) (Adams *et al*., 2002). It would allow the transfer of sulfur atoms to other proteins and the formation of membrane disulfide bridges, but this has not yet been proven (Chng *et al*., 2012). Another known protein is YgaP, a single-domain enzyme with a known structure (PBD code: 2MRM) that can catalyze a sulfur transfer reaction using Thiosulfate as the preferred substrate, but its physiological role is unknown.

Six three-dimensional class 1 TST structures have been obtained to date, including *E. coli* PspE(2JTQ) (Li *et al*., 2008), *E. coli* GlpE (1GMX) (Spallarossa *et al*., 2001), *Arabidopsis*

thaliana TST (1TQ1) (Cornilescu *et al*., 2006), *Saccharomyces cerevisiae* RDL1 (3D1P) and RDL2 (6K6R)(Wang *et al*., 2021) and human TSTD1 (6BEV) (Libiad *et al*., 2018). The active site consists of a six-residue loop containing the catalytic Cys, generally in persulfide form (-SSH)(Figure 16). In thestructure of *E. coli* GlpE, the catalytic cysteine adopts two conformations: one corresponding to the persulfide and the other to the thiol form (Spallarossa *et al.,* 2001).

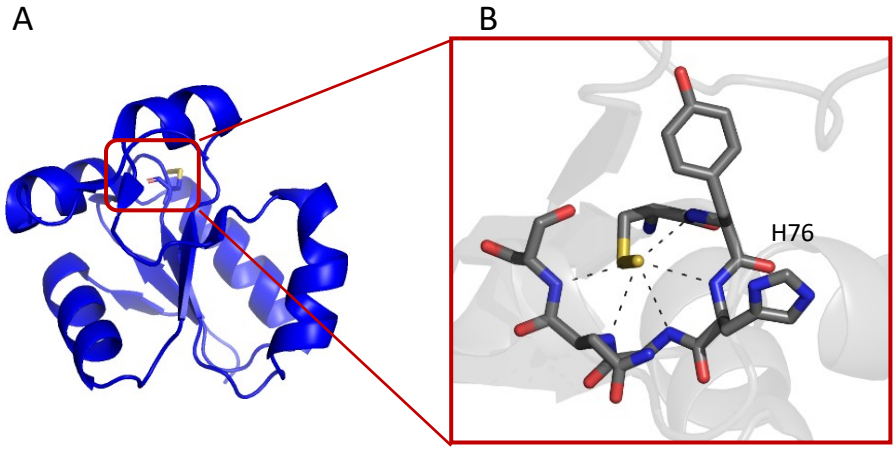

Figure 16. Cartoon representation of *E. coli* GlpE (A) and its active site (B) (PBD code 1GMX).
The monomer is represented in "ribbons and arrows"mode in blue (A), and the residues of the active site as sticks (B). The sulfur atoms of the catalytic Cys are shown in yellow and the figures were generated using the Pymol software version 4.6.0.

In human, TSTD1 is expressed from the *KAT* gene (Melido *et al*., 2014). Four exons and three introns make up its 1.6 kilobases in length. As a result of alternative splicing, three mRNAs aredetected in the RT-PCR analysis results for this gene. Three different isoforms of these transcripts are produced *via* translation (Wenzel *et al.,* 2003). With four exons and 115 residues, the TSTD1-1 isoform (12,530 Da) is derived from the longest transcript. When compared to TSTD1-1, the abbreviated TSTD1-2 isoform (74 residues and 8274 Da) at its N-terminus corresponds to the shortest transcript and omits exon 2. The medium transcript, which lacks exon 4 and has intron 3, yields the TSTD1-3 isoform (109 residues and 11,750 Da), which has a shortened C-terminal end and a decapeptide not found in TSTD1-1 and 1-2 (decapeptide encoded by intron 3) (Figure 17).

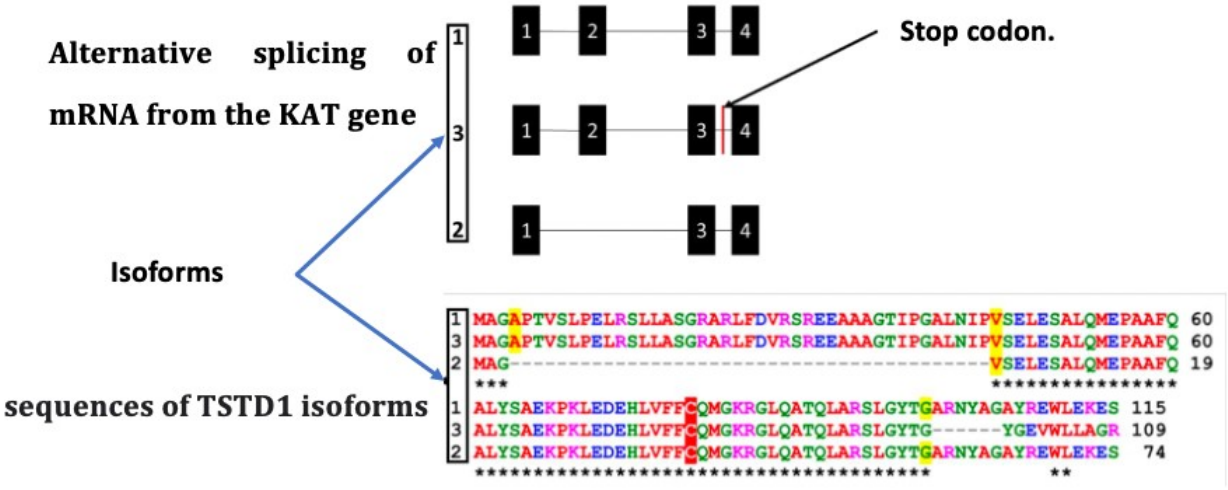

Figure 17: Description of the 3 isoforms of TSTD1.
Representation of alternative splicing of mRNA from the KAT gene leading to the translationof TSTD1 isoforms. For isoform 1, the four exons are conserved (represented by black rectangles). For isoform 2, only exons 1, 3 and 4 are conserved. For isoform 3, a splicing error leads to the conservation in the final mRNA of part of the third intron, which leads to the translation of an additional decapeptide. Alignment of the amino acid sequences of the 3 isoforms of TSTD1. The catalytic cysteine isconserved for all three proteins (shown highlighted in red).

Human TSTD1 transcripts are shown to accumulate in a variety of tissues, including the colon,kidney, liver, skeletal muscle, heart, spleen, thymus, placenta, and lung (Wenzel *et al.,* 2003). Furthermore, multiple cancer-derived cell lines have an accumulation of TSTD1 proteins (Wenzel *et al.,* 2003). Libiad and colleagues have examined the localization of the TSTD1 protein in the human colon, which is exposed to elevated levels of thiosulfate due to gut microbial activity (Libiad *et al.,* 2018: Furne *et al.,* 2001). They showed that the colon's luminal face, which is thought to be a key area of contact between the microbiota and human cells, is where TSTD1 accumulates.

C. 3MSTs

3MST (also annotated MPST or TUM1 in human) is a class 2 enzyme which catalyzes the desulfuration of 3-mercaptopyruvate (3MP) to generate an enzyme-bound persulfide. Subsequently, 3MST transfers the persulfide's distal sulfur atom to proteins or small molecule acceptors. Initially, 3MST activity was discovered as responsible for 3-mercaptolactate accumulation in urine of patients with cystinuria (Hannestad *et al.,* 1981; Meister, 1954;Shih *et al.,* 1977). Despite this difference in substrate specificity, 3MST shares a striking structural

resemblance with Rhodanese, leading to historical confusion between the two enzymes (Spallarossa *et al.,* 2004; Nagahara & Nishino, 1996). Interest in 3MST has increased in recent years since 3MST was recognized as involved in the generation of hydrogen sulfide (H_2S), a physiologically relevant signal transmitter (Shibuya *et al.,* 2009; Wang, 2012).

Presently, four three-dimensional structures of 3MST have been resolved by X-ray diffraction: the 3MST of *E. coli* (Spallarossa *et al*., 2004), that of *Leishmania major* (Alphey *et al*., 2003), and the human enzyme in free form and as a complex with pyruvate (Yadav *et al*., 2013). As previously explained, 3MST folding consists of two Rhd domains, of which only the C-terminal domain is catalytically active. The active site of 3MST is located at the interface of the two Rhd domains and consists of two loops: one, called the catalytic loop, is made up of the 6 residues including the catalytic cysteine, and the second is made up of six residues. The catalytic cysteine is in persulfide form in the 3MST structures of *E. coli* (1URH), *L. major* (1OKG) and human in complex with pyruvate (4JGT), whereas it is reduced in the structure of the human enzyme in free form (3OLH) (Figure 18).

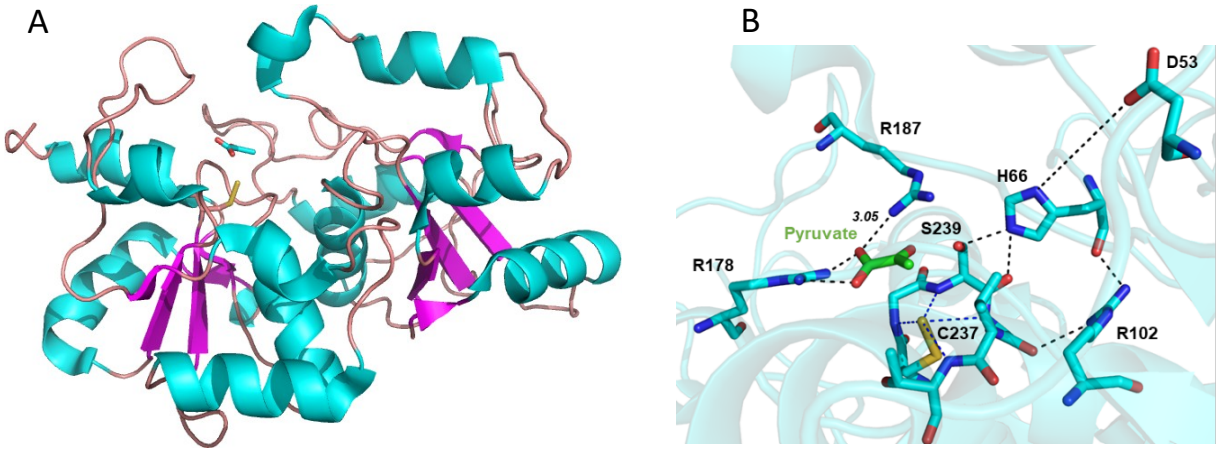

Figure 18. Cartoon representation of human 3MST in complex with pyruvate (A) and its active site (B) (PBD code: 3OLH).
The enzyme is represented in "ribbons and arrows"mode in blue (A), and the pyruvate andresidues of the active site as sticks (B). The sulfur atoms of the catalytic Cys are shown in yellow and the figures were generated using the Pymol software version 4.6.0.

The prevailing 3MST mechanism follows a classical two-step process (Figure 5). When the sulfur acceptor is a compound with a thiol group, the enzyme-independent decomposition of the persulfide acceptor leads to the formation of H_2S. *In vitro*, 3MST can use different donors such as 3MP or thiosulfate, and different acceptors such as cyanide and dithiols like DTT, Trx or dihydrolipoic acid (DHLA) (Mikami *et al.,* 2011). 3MST preferentially uses 3MP as a sulfur donor. Indeed, determination of the steady-state kinetic parameters of 3MST from *L. major* and *T. vaginalis* showed that 3MST exhibits specificity for 3MP over thiosulfate (k_{cat}/K_M ratio 100-fold higher) in the presence of Trx as acceptor (Westrop *et al.,* 2009). Comparable results were obtained for *E. coli* 3MST in the presence of cyanide acceptor (Colnaghi *et al.,* 2001). In addition, steady-state kinetic studies on the human enzyme, using 3MP as sulfur donor and various acceptors, reveal specificity for Trx, with a k_{cat}/K_M ratio 52,000 times higher than that obtained for other dithiols such as DTT and DHLA (Williams *et al.,* 2003).

The structure of the human enzyme with pyruvate suggests enzyme-substrate interactions (Yadav *et al.,* 2013). In particular, two conserved arginines could position the substrate by forming hydrogen bonds with the carboxylate and carbonyl groups of 3MP. More recently, kinetic approaches were developed for studying the reaction catalyzed by the human and *E. coli* enzymes and the role of several conserved residues was also investigated. (Lec *et al.,* 2018). The first step of sulfur transfer that leads to pyruvate release and formation of the persulfide intermediate was shown to be very efficient for both enzymes. It critically depends on the electrostatic contribution provided by the CGSGVT catalytic loop. Furthermore, solvent kinetic isotopic effect and proton inventory studies revealed a concerted mechanism in which the water-mediated protonation of the pyruvate enolate and the S^0 transfer from the deprotonated 3MP to the thiolate form of the catalytic cysteine occurs concomitantly (Figure 19).

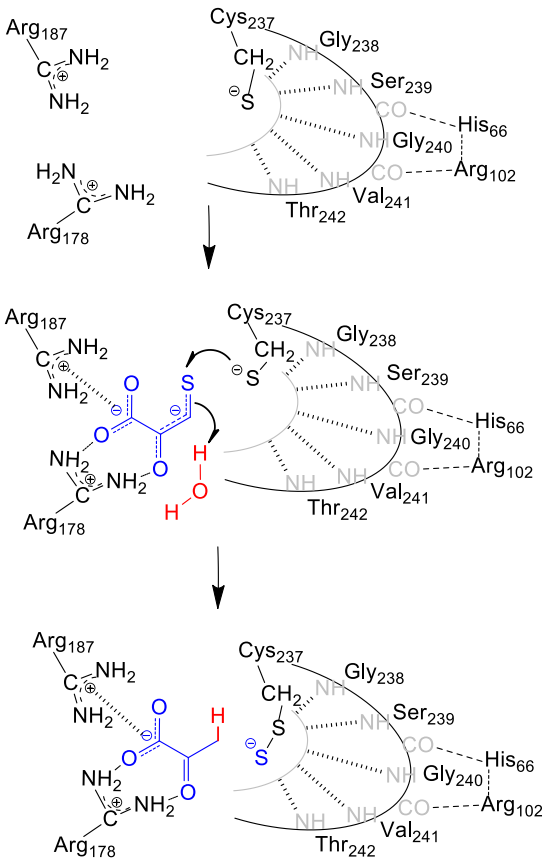

Figure 19: Proposed catalytic mechanism of persulfide 3MST formation (from Lec *et al.*, 2018). Conserved residue R178 is involved in positioning the 3MP in the active site, enabling nucleophilic attack on the thiol group of the catalytic cysteine (residue C237). Pyruvate is then protonated by a water molecule and released from the active site.

In human, 3MST is encoded by the *MPST* gene, which resides on chromosome 22. This enzyme exists as two isoforms, arising from alternative transcription initiation sites. The shorter isoform harbors a mitochondrial addressing signal, leading to its localization within this organelle. Whether this peptide is cleaved after enzyme import remains unclear (Miyamoto *et al.*, 2014). The longer isoform possesses an additional 20-amino acid peptide at its N-terminus, effectively masking the mitochondrial addressing signal. Hence, this isoform is localized in the cytosol (Fräsdorf *et al.*, 2014) (Figure 20).

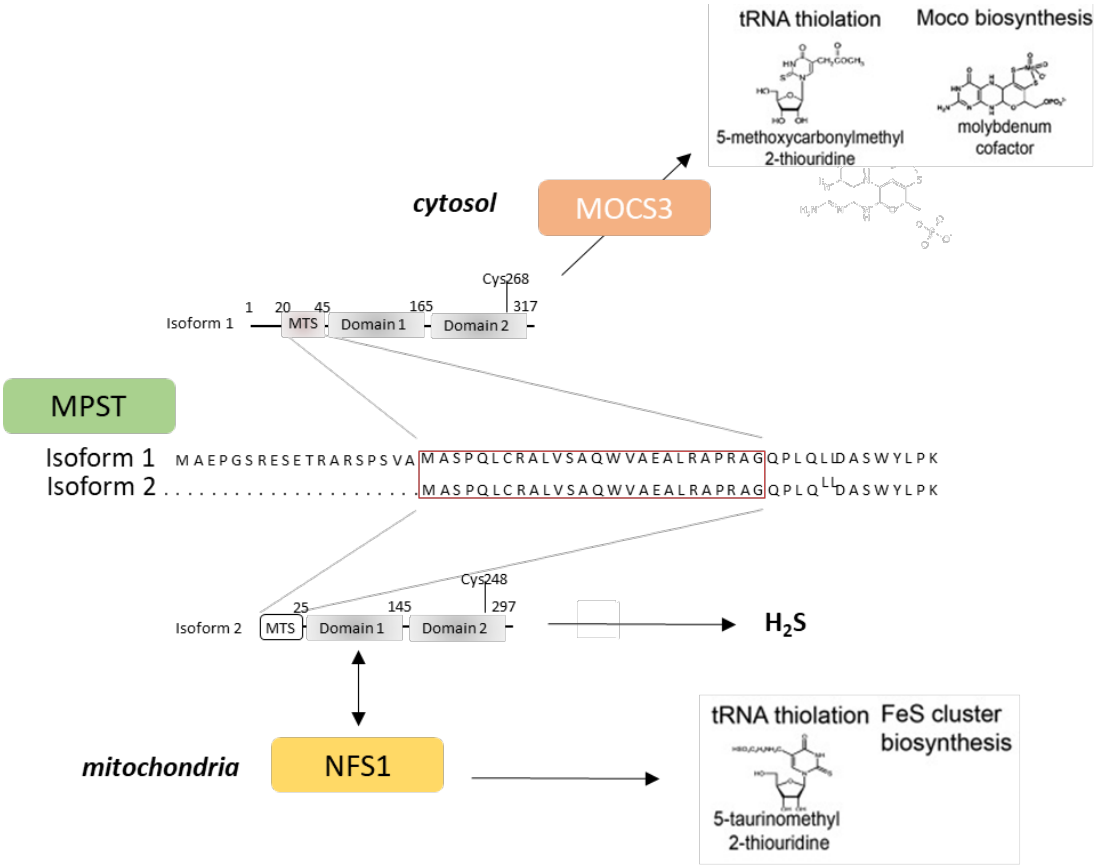

Figure 20: Mechanism of subcellular compartmentalisation of human 3MST and the two proposed roles depending on the localisation of the enzyme (Adapted from Fräsdorf *et al.*, 2014).
Alternative splicing of the gene encoding *MPST* leads after translation to two isoforms of the enzyme. Isoform 1 contains a 20-residue peptide sequence that masks the mitochondrial addressing sequence (MTS) and therefore isoform 1 is present only at the cytosolic level. Isoform 2, on the other hand, does not contain this masking sequence, so the addressing sequence is exposed, allowing for its mitochondrial import.
This dual subcellular localisation and the difference in specificity of interaction between the two isoforms with the MOCS3 and NFS1 proteins leads to the existence of two distinct potential ^physiological roles. The mitochondrial isoform 2 of *MPST* interacts with NFS1 allowing a priori the thiolation of mitochondrial tRNAs and FeS cluster biosynthesis, while cytosolic isoform 1 interacts with MOCS3, which would allow the biosynthesis of proteins with molybdenum cofactors.

3MST is involved in H_2S production in the brain, kidney and liver at the mitochondrial level (Nagahara *et al.*, 2018). This H_2S production is enabled by the use of 3MP as a sulfur donor and the action of a cellular reductant such as thioredoxins then allows the formation of H_2S. Surface plasmon resonance experiments on human proteins coupled with Bimolecular Fluorescence Complementation assays (split-EGFP) performed on human HEK293 cells and HeLa cells showed that: (1) the cytosolic isoform of MPST is able to interact with the cytosolic form of the NFS1 cysteine desulfurase and MOCS3 proteins; (2) the second isoform present in both compartments interacts with MOCS3 at the cytoplasmic level and NFS1 at

the mitochondrial level. These results suggest different roles for 3MST depending on its subcellular location. At the mitochondrial level, the interaction between 3MST and NFS1 allows the thiolation of mitochondrial tRNAs, whereas at the cytosolic level, the 3MST / MOCS3 interaction allows the biosynthesis of molybdenum cofactors (Fräsdorf *et al.,* 2014) (Figure 20).

While some studies briefly touch upon 3MST's involvement in conditions such as obesity, kidney injury, and adipogenesis, most of the existing research on 3MST focuses on its role in cardiovascular function (particularly hypertension, angiogenesis, and myocardial injury), cancer (notably neuroblastoma, colon cancer, and carcinoma), neurology (primarily ischemia and hypoxia), liver function, and cyanide toxicity prevention. Although a small number of studies posit that elevated expression of 3MST underlies multiple disorders, including malignancies like bladder and prostate cancer. Despite extensive research conducted both in vivo and in vitro, the precise mechanisms by which 3MST-mediated H_2S emission influences various disease states remain largely elusive. While some studies advocate for inhibiting the 3MST pathway as a therapeutic approach, others propose augmenting 3MST expression to halt disease progression. Consequently, in-depth investigation of the intricate biochemical pathways, particularly emphasizing the distinctive role of the 3MST/H_2S pathway in disease pathophysiology (Figure 21) (Rao *et al.,* 2023).

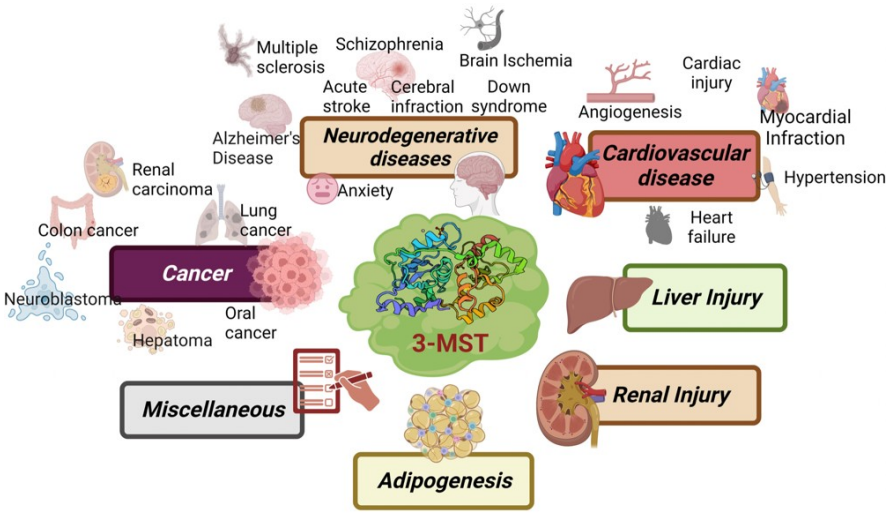

Figure 21: Summaries the physiological effect of 3MST (Rao *et al.,* 2023)

D. MOCS3

MOCS3 is a peculiar TST from class 3 composed of an adenylase domain connected to a Rhd domain at the C-terminal location (Figure 22). In human, the *MOCS3* gene, which is found on chromosome 20 (20q13.13), is made up of a single, 1383 bp long exon that codes for the human MOCS3 protein. MOCS3 is a 49 kDa protein of 461 residues that is composed of the two structural domains (Matthies *et al.,* 2004). The N-terminal domain is homologous to the bacterial ThiF/MoeB/HesA family, according to sequence alignments, and the C-terminal region to Rhd (Mendel & Schwarz, 2002).

Proteins with sequence similarity to *E. coli* MoeB are widely distributed among living organisms. The major characteristic of all eukaryotic homologs is that they contain the C-terminal TST domain. The bacterial homologs are much more divergent, with both types of MoeB homologs (with and without the C-terminal domain), whereas in contrast, archaeal homologs possess only MoeB homologs lacking the C-terminal domain (Krepinsky & Leimkühler, 2007). An aspartate at the last position of the six amino acid active site loop is present in all MoeB homologs in animals and plants, whereas it is a polar amino acid like asparagine and threonine in unicellular eukaryotes. Intriguingly, all known bacterial MOCS3 homologs possess an arginine at the last position of the active site loop.

Regarding the 3D architecture of MOCS3, not much is known. Only one structure of the Rhd domain of human MOCS3 is known (3I2V). Additionally, an Alphafold prediction can be found at https://alphafold.ebi.ac. uk/entry/O95396. Furthermore, the Moeb-like domain is made up of a central height strands β-sheet that is encircled by eight helices, as predicted by the structure of MoeB homologs (Lake *et al.,* 2001). We looked for conserved residues or sequence motifs in the two domains across distant sequences from the 316 sequences that blast-P was able to retrieve from the Uniprot database using human MOCS3, Arabidopsis MOCS3 (CNX5/STR13), or yeast MOCS3 as templates. With respect to the MOCS3 Rhd domain, the catalytic loop exhibits a CxxGxD/R consensus sequence. Site-directed mutagenesis was used on the separately expressed C-terminal MOCS3 Rhd to examine the function of the remaining five amino acids of the active site loop of MOCS3 for thiosulfate sulfurtransferase activity (Matthies *et al*., 2004). In the MoeB domain, a cysteine residue (Cys239) that is thought to be crucial for MOCS3 activity is conserved in addition to di-cysteines motifs involved in zinc cation coordination (Cys222XXCys225 and Cys297XXCys300), which have been suggested to be necessary for the folding of the protein. In addition, Cys412, the first residue of the human

MOCS3's six amino acid active site loop, was shown to forms a persulfide group during catalysis, which is necessary for thiosulfate sulfurtransferase activity (Matthies *et al*., 2004: Matthies *et al*., 2005).

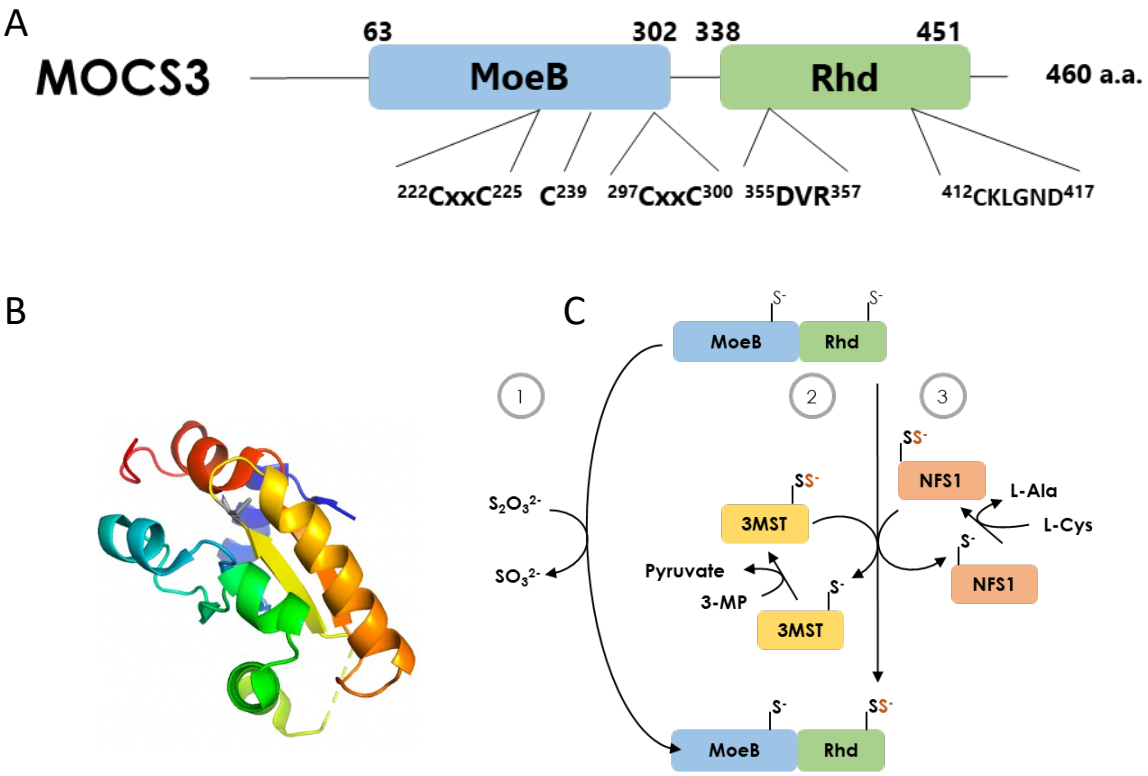

Figure 22*:* Structural features and proposed physiological partners of MOCS3.
(A) Modular organization of MOCS3 and conserved motives in distant protein sequences identified. (B) Cartoon representation of MOCS3-Rhd domain structure (PDB 3I2V). (C) Described sulfur donors for the human MOCS3 (1), the 3MST (2) or the cysteine desulfurase NFS1 (3). (adapted from Krepinsky & Leimkühler, 2007).

Low sulfurtransferase activity was demonstrated for isolated MOCS3-Rhd in the presence of thiosulfate and DTT *in vitro* (Leimkühler & Rajagopalan, 2001). Indeed, compared to bovine Rhodanese, the MOCS3-Rhd thiosulfate-dependent activity is 1000-fold lower, indicating that thiosulfate is probably not the physiological substrate of MOCS3. This may be related to the specific catalytic loop sequence, as evidenced by a 36- to 165-fold increase in sulfurtransferase activity when the CRKGVT sequence from bovine Rhodanese was replaced for the MOCS3 catalytic loop (Krepinsky & Leimkühler, 2007). Interestingly, the fact that NFS1 L-Cysteine desulfurase and 3MST were shown to interact both *in vitro* with MOCS3-Rhd and *in cellulo* with MOCS3 suggests that they could be its physiological donor substrates (Figure 22) (Fräsdorf *et al.,* 2014; Marelja *et al.,* 2008). Thus, MOCS3 is likely the first human

sulfurtransferase involved in protein to protein sulfur atom trafficking.

As isolated proteins, MoeB members catalyze ATP-dependent adenylation of C-terminal Glycine residue from sulfur carrier proteins. In the context of the MOCS3 protein, both MoeB and Rhd domains cooperate sequentially to catalyze the C-terminal thiocarboxylation of partner proteins, e.g. MOCS2 (Molybdenum cofactor synthesis 2) or URM1 (Ubiquitin-related modifier 1) that are involved in molybdenum cofactor maturation, tRNA thiolation, or proteins post-translational modifications, such as peroxiredoxin urmylation (Figure 23) (Chowdhury *et al.,* 2012; Furukawa *et al.,* 2000). From studies of human MOCS3 and homologs, it was proposed that MOCS3 activates MOCS2 in the presence of ATP by formation of a thioester bond between conserved C239 of the MoeB domain and MOCS2 C-terminal glycinyl residue. This covalent linkage is proposed to be essential for MOCS2 correct orientation relative to the Rhd domain during the catalysis, which consists of the nucleophilic attack of the persulfidated MOCS3-Rhd on the thiocarboxylated MOCS2 to form an acyl persulfide intermediate. Finally, release of the MOCS2 thiocarboxylate requires an unknown electron provider (Matthies *et al.,* 2004; Termathe & Leidel, 2018; Pabis *et al.,* 2020).

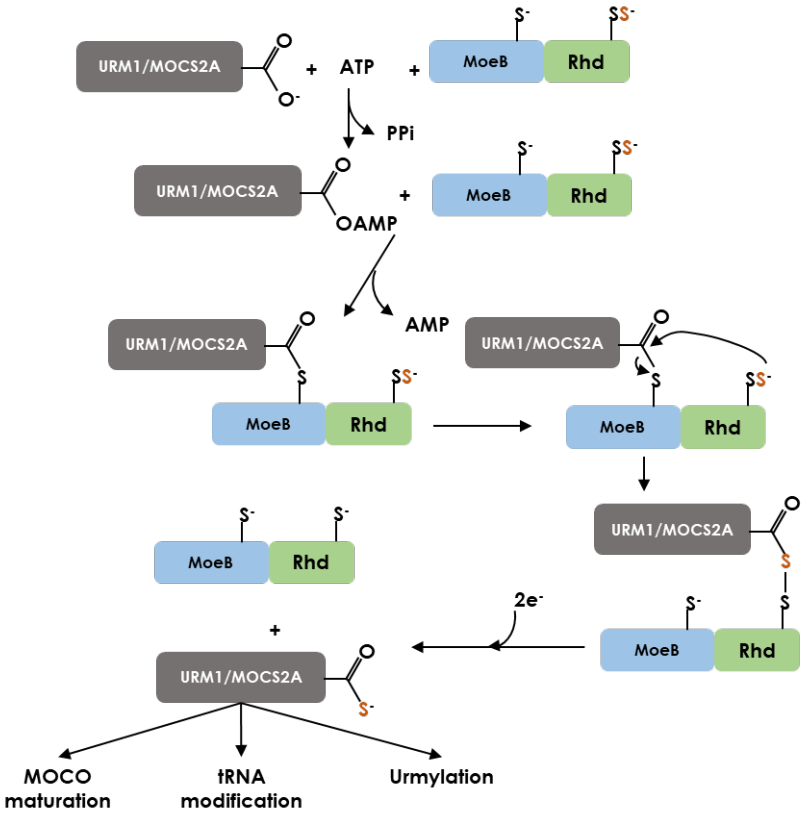

Figure 23: Proposed mechanism for the MOCS3 catalyzed-reaction.
Sequential cooperation of MoeB and Rhd domains into URM1/MOCS2A thiocarboxylation.

IV. TrhO

Recently, a new Rhd-containing enzyme was identified. Indeed, using reverse genetics and comparative genomics, Sakai *et al*. identify a new enzyme from *E. coli* named TrhO responsible for 5-hydroxyuridine (ho5U) formation, which is the first step of the cmo5U synthesis in tRNAs (Sakai *et al.,* 2019). In bacterial tRNAs, 5-carboxymethoxyuridine (cmo5U) at the first position of the anticodon facilitate non-Watson–Crick base pairing with guanosine and pyrimidines at the third positions of codons, thereby expanding decoding capabilities. In *E. coli*, two pathways exist for 5-hydroxyuridine (ho5U): a prephenate-dependent ho5U formation catalysed by TrhP (a peptidase U32 family protein), and an oxygen-dependent ho5U formation catalysed by TrhO (Figure 24). Moreover, phylogenetic tree of organisms possessing or lacking TrhO show that TrhO orthologs predominated in bacteria and eukaryotes but are absent in Archaea and obligate anaerobic bacteria.

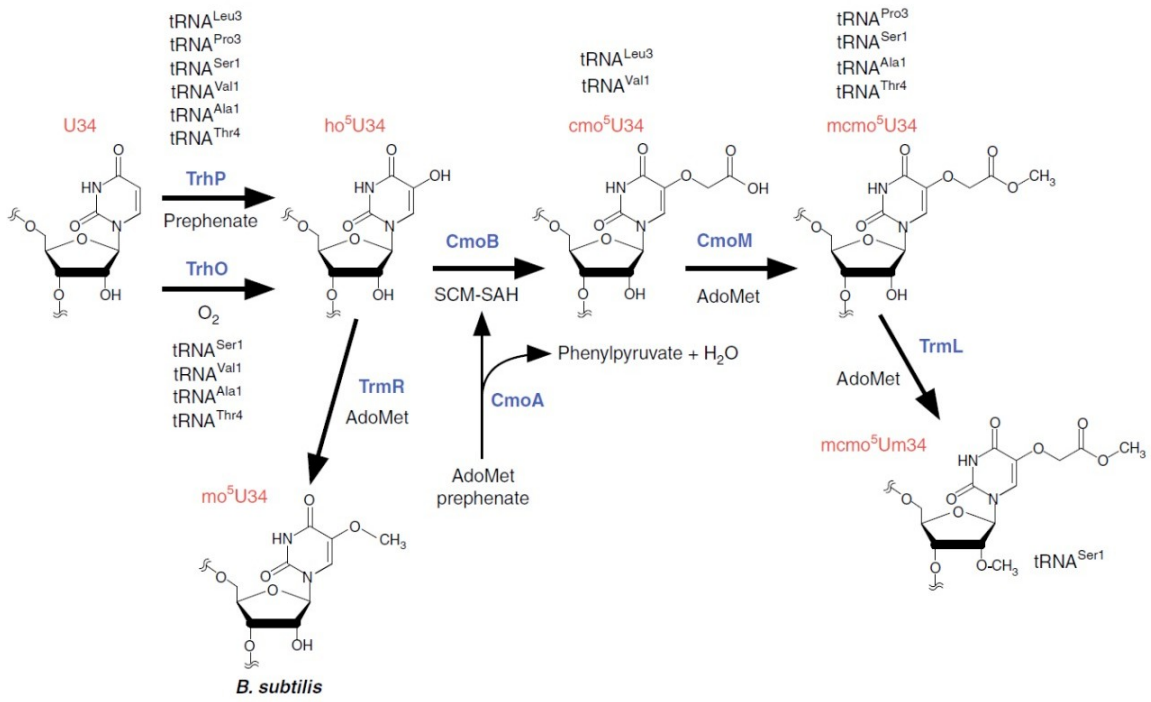

Figure 24: Biogenesis of mcmo5U34 and derivatives (from Sakai *et al*., 2019).
At the first step, U34 is redundantly hydroxylated by independent pathways mediated by TrhP and TrhO to form ho5U34 in tRNAs responsible for decoding NYN codons. TrhP requires prephenate as a metabolite for ho5U34 formation, whereas TrhO uses O_2 to hydroxylate U34 to form ho5U34 under aerobic conditions. CmoA synthesizes SCM-SAH from prephenate and AdoMet. CmoB uses SCM-SAH for carboxymethylation of ho5U34 to yield cmo5U34. Four tRNAs (Ala1, Ser1, Pro3, and Thr4) are further methylated by CmoM to yield mcmo5U34. In Gram-positive bacteria, including *B. subtilis*, ho5U34 is methylated by TrmR to yield mo5U34.

TrhO consists of two known domains, including a N-terminal acylphosphatase domain (UPF0176/IPR001792) and a C-terminal Rhd domain (Figure 25). On a structural point of view, only the 3D-structure of the *Legionella pneumophila* orthologous protein is available (PDB 4F67) (Figure 25). The Rhd domain loop contains the canonical Rhd CX_4R catalytic motif.

In human, TrhO homolog is named Thiosulfate SulfurTransferase-like Domain containing 2 isoform 1 (TSTD2) and encoded by the *TSTD2* gene composed of 33,289 nucleotides, including 10 exons. The gene is localized on chromosome 9 (9q22.33). TSTD2 protein contains 516 residues, but the presence of an alternative translation initiation start generates a shorter isoform of the TSTD2 protein that contains 167 residues and only the Rhd domain.

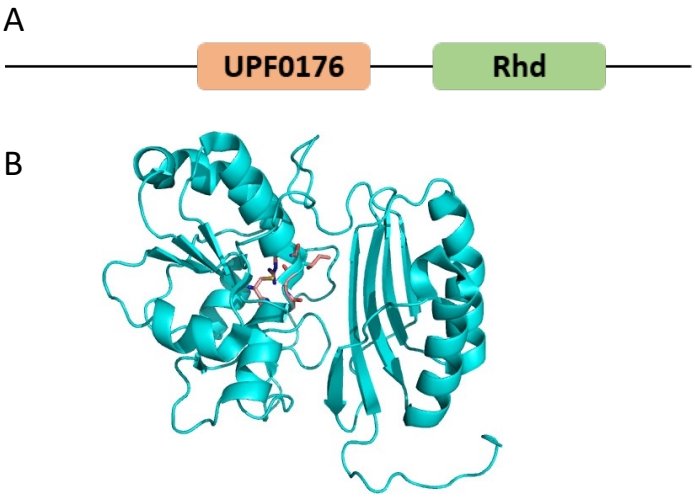

Figure 25: The *Legionella pneumophila* TrhO modular organization (A) and 3D-structure (B). The enzyme is represented in "ribbons and arrows" mode on the Pymol software version 2.4.1. It is composed of Acylphosphatase (UPF0176/IPR001792) and Rhd domains. Putative catalytic loop residues of the Rhd domain are represented as stick (PDB 4F67).

Regarding biochemical properties of TrhO, functional complementation of an *E. coli* mutant by variants of the TrhO protein underlined the role of several residues belonging to the Acylphosphatase domain (K112) or to the Rhd catalytic loop (C200, T201, G203, R205), in the production of oxygen-dependent ho5U34 hydroxylated tRNAs (Sakai *et al.,* 2019). However, the mechanism whereby catalysis occurs remains to be elucidated. TrhO is specific for a sub-set of tRNAs (Ser1, Val1, Ala1 or Thr4), and tRNAs recognition could be achieved by the positively charged β-sheet present in the acylphosphatase domain near the Rhd active-site loop. The acylphosphatase domain is also described in the InterPro databank as catalysing the hydrolysis of acyl-phosphate groups to release a carboxylic group and a phosphate molecule, but no biochemical data support this assumption.

V. CDC25 phosphatases

CDC25 phosphatases were first discovered in 1979 in the yeast *Schizosaccharomyces pombe* (Fantes, 1979). Subsequently, these proteins were characterized in all eukaryotes except plants (Boudolf *et al.,* 2006). CDC25 (Cell Division Cycle 25) phosphatases being able to dephosphorylate both the phosphothreonine and phosphotyrosine residues of their substrates places them in the dual-specificity phosphatase family. In this situation, cyclin-dependent kinases, or CDKs, are the only CDC25 substrates that are currently identified. Enabling the dephosphorylation of their residues pThr14 and pTyr15 (for CDK1), CDC25s are essential for regulating the cell cycle both in normal conditions and in response to DNA damage (Nilsson & Hoffman, 2000). All eukaryotes have different isoforms of the CDC25 phosphatase enzyme. There are three isoforms in human, and each can have various splicing variations (Baldin *et al.,* 1997; Wegener *et al.,* 2000; Forrest *et al.,* 1999). The three human CDC25 isoforms are called CDC25A, CDC25B, and CDC25C (Bordo & Bork, 2002; Kristjansdottir & Rudolph, 2004) and these isoforms have a special ability to dephosphorylate phosphotyrosine and phosphothreonine residues on particular CDKs.

CDC25s display an HCX_5R active-site motif and lack of overall sequence homology to other phosphatases. The structure of CDC25s can be divided into two main domains, the extremely divergent regulatory N-terminal domain and the catalytic C-terminal Rhd domain (Figure 26). The N-termini of CDC25s have nuclear import and export signals, multiple phosphorylation sites, and are 20-25% similar in sequence to one another (Rudolph *et al.,* 2001). The catalytic core is in the C-termini of CDC25s, which share a sequence that is more than 60% identical. The length of the active-site loop, which in CDC25s is formed by seven residues (CX_5R), is the most significant structural difference between rhodanese and CDC25s. This leads to a larger catalytic pocket that can fit a phosphorous atom, which exhibits a van der Waals radius slightly bigger than a sulfur atom (Bordo & Bork, 2002).

Currently, available 3D structures for CDC25s only concern their respective Rhd domain (CDC25B-Rhd and CDC25C-Rhd, Figure 26). The catalytic Cys residue into the HCX_5R loop sequence of the Rhd domain, is in a binding pocket for the substrate's phosphate group. The five X residues contribute not their side chains but rather their backbone amides toward the functionality of the active site. In structures with bound sulfate, these amides, along with the arginine of the motif, form multiple hydrogen bonds with the oxygen atoms of the sulfate, a mimic of a bound phosphorylated substrate (Figure 26). In contrast to other phosphatases,

the CDC25s do not have a loop containing an aspartic acid (i.e. the catalytic acid) overhanging the active site.

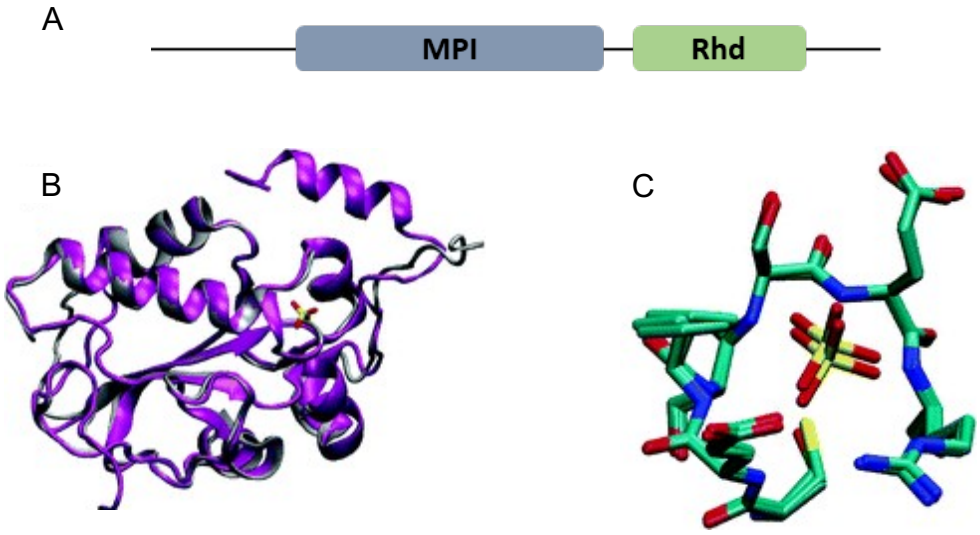

Figure 26: The CDC25s modular organization (A), structure of the catalytic domain (B) and of the active site (B) (Rudolph, 2007).
(A) Modular organization of CDC25s. (B) Overlay of CDC25A (1C25, gray) and CDC25B (1QB0, purple) structures shown as ribbon diagrams. The active site region can be identified by the bound sulfate in CDC25B, a phosphate mimic, shown in licorice. (C) Overlay of the active site loop of CDC25B (Cys473-Arg489) bound to sulfate (1QB0), as the apoenzyme (1YMK), and as the C473S mutant bound to sulfate (2A2K).

CDC25s use the classical two-steps catalytic mechanism described for other phosphatases using as catalytic residues, a thiolate and a protonated acid (Figure 27). In the first chemical step of the reaction, the thiolate attacks the P-O bond directly as the catalytic cysteine's thiolate is located directly below the phosphoryl group. The catalytic acid protonates the oxyanion, facilitating the leaving group's departure and the creation of the phospho-cysteine intermediate (Zhang *et al.,* 1994a; Zhang *et al.,* 1994b; Denu & Dixon, 1995; Zhang *et al.,*1995; Denu *et al.,* 1996). In the second chemical step, the acid residue functions as a base to activate the water molecule while water acts as a nucleophile in the hydrolysis of the phospho-enzyme intermediate. The identity of the catalytic acid is not known, even though many parts of this general mechanism have been experimentally verified for the CDC25s (Rudolph, 2007).

CDC25B and CDC25C both also have arsenate reductase activity. However, for CDC25B and CDC25C, the rates of arsenate reduction in the presence of 2 mM GSH were 25 and 7 times lower, respectively, than the rates of dephosphorylation. When the GSH concentration was raised to 5 mM, the CDC25s displayed 4-fold greater arsenate reductase activity (Bhattacharjee *et al*., 2010).

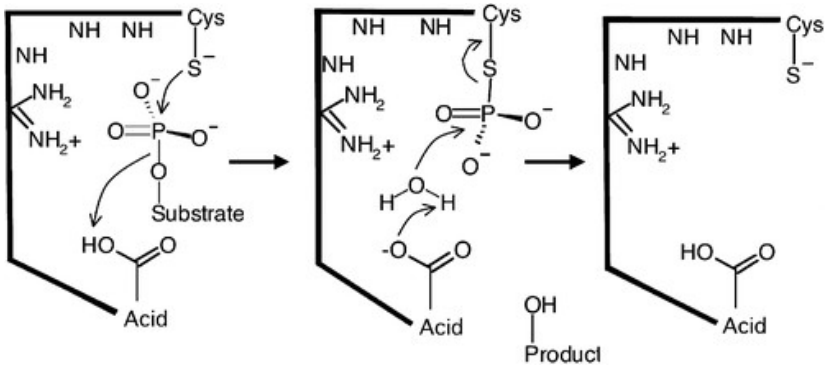

Figure 27: General catalytic mechanism of dual specificity phosphatases. (Rudolph, 2007)

CDC25s are essential for controlling cell division during mitosis, the G1-to-S and G2-to-M transitions, and the various CDC25 isoforms function in concert at different steps of the cell cycle. As important CDK/cyclin activators, CDC25s have also emerged as possible targets for the creation of anticancer treatments (Kristjánsdóttir & Rudolph, 2004). During the normal course of the cell cycle, the dephosphorylation by CDC25s mark the final activation of CDK/cyclin activity (Nilson & Hoffmann, 2000; Boutros *et al.,* 2006). While CDC25B and CDC25C are regulators of the G2-to-M transition, CDC25A oversees both the G1-to-S and G2-to-M transitions. In the checkpoint response that avoids CDK/cyclin activation after DNA damage, the CDC25s are also crucial (Figure 28) (Iliakis *et al.,* 2003; Karlsson-Rosenthal &Millar, 2006).

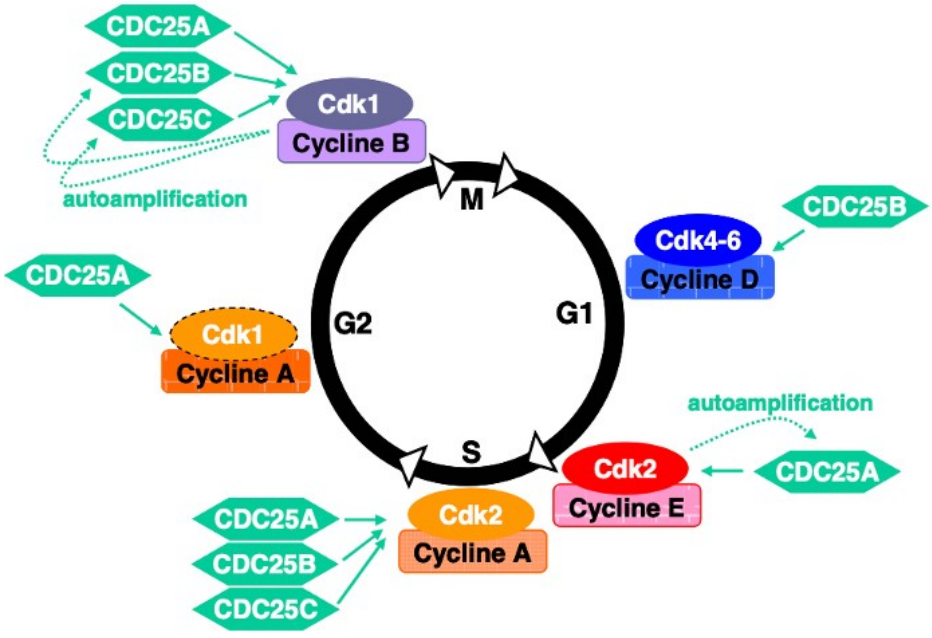

Figure 28: Different CDC25 isoforms in cell cycle regulation. (Boutros *et al.,* 2006).
CDC25 phosphatase activities toward CDK/Cyclin complexes play key roles in cell cycle in regulating both G2-to-M and G1-to-S transitions. CDC25 activities are enhanced or inhibited by various kinases activities at different cell cycle phases.

Different cases of prostate, lung, colon, oesophageal, pancreatic, head, and neck cancers have been linked to an overexpression of CDC25A and B isoforms (Figure 29) (Boutros *et al.* 2007). The information displayed in Figure 29 includes studies where a reported overexpression of the CDC25 protein level was found. On the opposite, only few numbers of overexpression cases involving isoform C have been documented in the literature (Wang *et al.*, 2010).

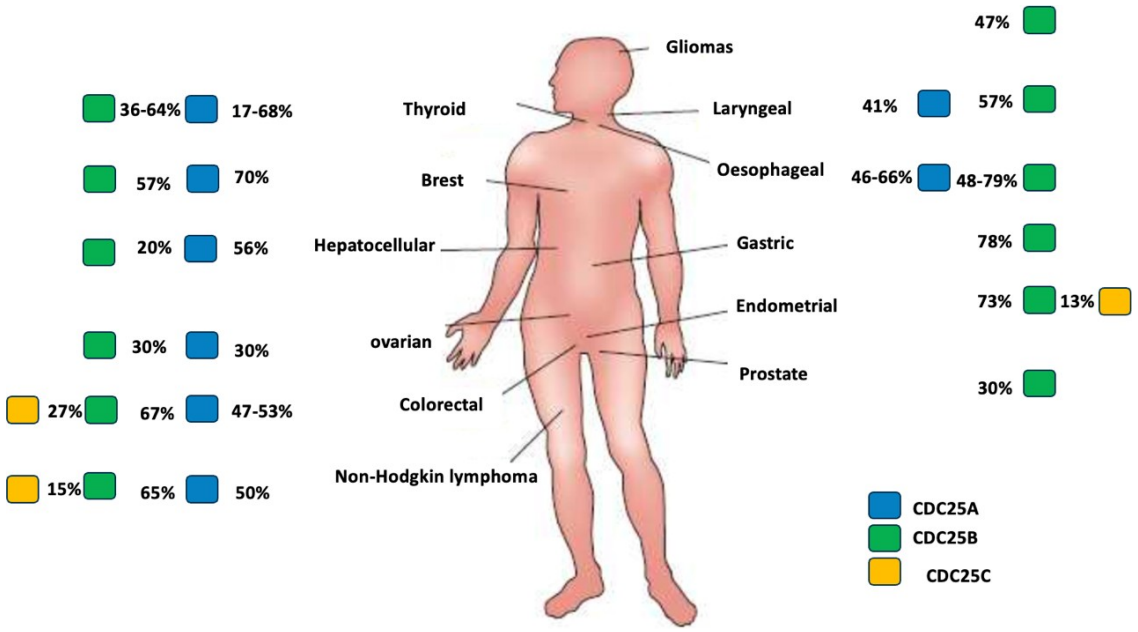

Figure 29: The overexpression of CDC25 phosphatases in several human cancer types (Boutros *et al.*, 2007). Primary tumor samples from patients with breast, prostate, ovarian, endometrial, colorectal, oesophageal, thyroid, laryngeal, gastric, and hepatocellular cancers, glioma, neuroblastoma, or non-Hodgkin lymphoma, have been shown to overexpress CDC25s. The percentage of tumors that have overexpressed CDC25A, CDC25B, or CDC25C are shown; if overexpression has been documented in multiple studies, a range of percentages is provided.

VI. Arsenate reductases

One family of arsenate reductases is also related to class 3 Rhd-containing enzymes. These enzymes are found in eukaryotes except in mammals, even though mammalian liver efficiently reduces As(V) to As(III) (Radabaugh & Aposhian, 2000). Several members of this family have been characterized to date: *Sc*Acr2p from the yeast *Saccharomyces cerevisiae* (Bobrowicz *et al.,* 1997; Mukhopadhyay & Rosen1998), *Lm*ACR2 from the parasitic protozoan *Leishmania major* (Zhou *et al*., 2004), *Pv*ACR2 from the fern *Pteris vilata* (Ellis *et al.,* 2006), *Os*ACR2 from rice *Oryza sativa* (Duan *et al*., 2007), and *At*ACR2 from *Arabidopsis thaliana* (Bleeker *et al*., 2006; Dhankher *et al.,* 2006).

These eukaryotic arsenate reductases have a six-residues long catalytic loop with a CX_5R signature identical to that of CDC25s. Only the crystal structure of *Lm*ACR2 has been reported (Mukhopadhyay *et al*., 2009). Structural comparison between *Lm*ACR2 and the catalytic domains of human CDC25 (each contains a CX_5R signature motif) shows an overall structural similarity and a similar active site loop conformation.

These eukaryotic arsenate reductases catalyze the two-electron reduction of inorganic As(V) to As(III) using glutaredoxin (Grx) and glutathione (GSH) as reductants, by a mechanism proposed to be identical to that of the bacterial arsenate reductase ArsC (Figure 30) (Zhou *et al*., 2004; Duan *et al*., 2007; Ellis *et al*., 2006; Mukhopadhyay *et al*., 2000; Martin *et al*., 2001).

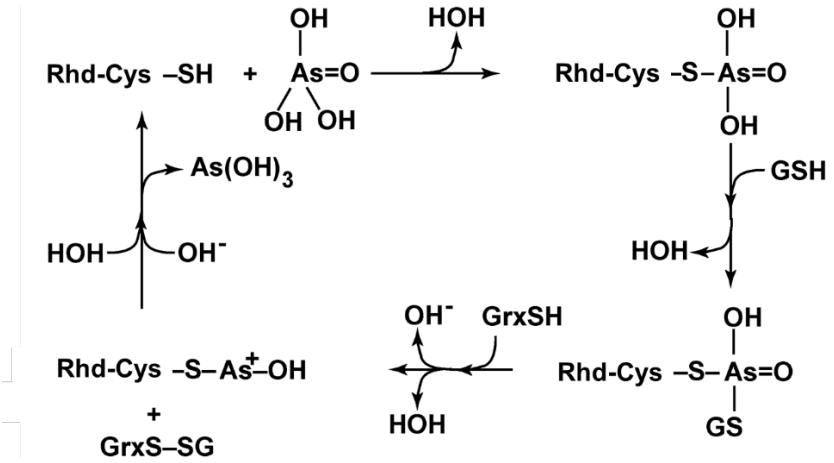

Figure 30: Proposed catalytic mechanism of Rhd-arsenate reductases (Martin *et al.,* 2001)

These reductases also exhibit significant variability in their biochemical activities, some of them displaying *in vitro* phosphatase activity. Indeed, both *Sc*Acr2p and *Pv*ACR2 lack phosphatase activity (Ellis *et al.,* 2006), although *Sc*Acr2p can be converted from a reductase to a phosphatase by a small number of mutations (Mukhopadhyay *et al.,* 2003). On the other hand, *Lm*ACR2, *At*ACR2, and *Os*ACR2 exhibit both arsenate reductase and phosphatase activities (Duan *et al.,* 2007; Bleeker *et al.,* 2006; Mukhopadhyay *et al.,* 2003; Zhou *et al.,* 2006).

OBJECTIVES

The redox group of the molecular enzymology team has a long-standing interest in enzymes which depend on the complex chemistry of sulfur and a project developed by S. Boschi-Muller and F. Talfournier focuses on the catalytic mechanisms and substrate specificities of sulfurtansferases belonging to the rhodanese family. As presented in the introduction section,the 3MST mechanism has already been investigated and published (Lec *et al.,* 2018). Moreover,the persulfide formation mechanism of TSTs has also been investigated recently (data not published). By using single turn-over kinetic approaches coupled with site-directed mutagenesis experiments, the results show that, unexpectedly, TSTD1 is a better 3MST than TST. Moreover, sulfur-sulfur bond breaking is critically dependent of charges neutralization provided by the Glu31/Arg84 pattern, whereas persulfide formation mechanism from 3MP is performed through a different catalytic strategy (Figure 31).

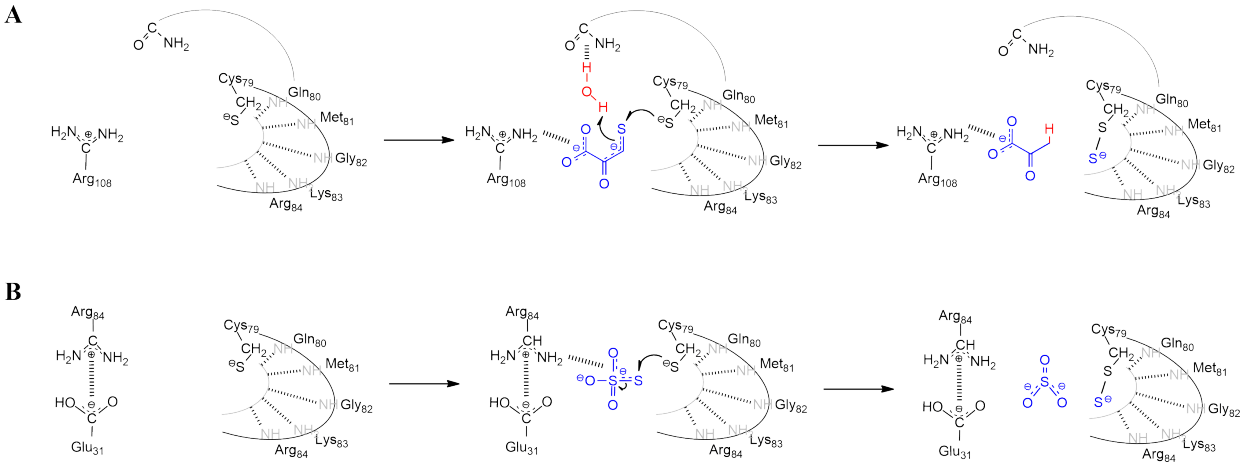

Figure 31: Proposed catalytic mechanisms for the persulfide formation catalyzed by TSTD1 from 3MP (A) and thiosulfate (B).
Substrates are represented in blue, catalytic residues in dark and water molecule in red.

Indeed, this study reveals the presence of two paired residues located on opposite faces within the active site and specifically dedicated to sulfur-sulfur bond cleavage for the Glu31/Arg84 pair (Figure 31A) or carbon-sulfur bond cleavage for the Gln80/Arg108 pair (Figure 31B), respectively. A search for the presence of these signatures in other TST members whose sequences are highly divergent was achieved. A sequence alignment of Rhd-containing enzymes was generated from the superimposition of fourteen 3D-structures using the Multiseq module in the VMD program (Figure 32). After addition of the human Rhodanese sequence, two families can be identified: a major TSTD1-like family with the Glu/Asp31 and

Arg84 signature, and another one containing human and bovine Rhodaneses, and *E. coli* GlpE and PspE (Figure 32). While these latter four enzymes have been shown to be TSTs, among the 11 TSTD1-like, TST activity has only been characterized for TSTD1, the enzyme from *Azotobacter vinelandii* (1e0c) (Forlani *et al.,* 2003) and the bifunctional persulfide dioxygenase-rhodanese enzyme from *Burkholderia phytofirmans* (5ve3,Motl *et al.,* 2017). It is interesting to find in this family the catalytic domain of human CDC25B and *L. major* arsenate reductase, which have the Glu31/Arg84 signature but a catalytic loop one residue longer (CX_5R vs. CX_4R). As previously described in the introduction part, these two enzymes display promiscuous phosphatase and arsenate reductase activity (Bhattacharjee *et al.,* 2010; Zhang *et al.,* 2003) and the presence of the TSTD1-like signature suggests the existence of sulfurtransferase activity. Moreover, the active site of all these enzymes is suitable for stabilizing oxyanions or thiolates, but the discriminating factor seems to be the length of the catalytic loop, as proposed for *A. vinelandii* RhdA, whose phosphatase activity was revealed after lengthening the loop by one residue (Forlani *et al.,* 2003). The fact that the loop is longer in CDC25s and arsenate reductases should not be an obstacle to the existence of TST-type activity, as the side chains of residues Cys79, Glu31 and Arg84 are perfectly superimposable (Figure 32).

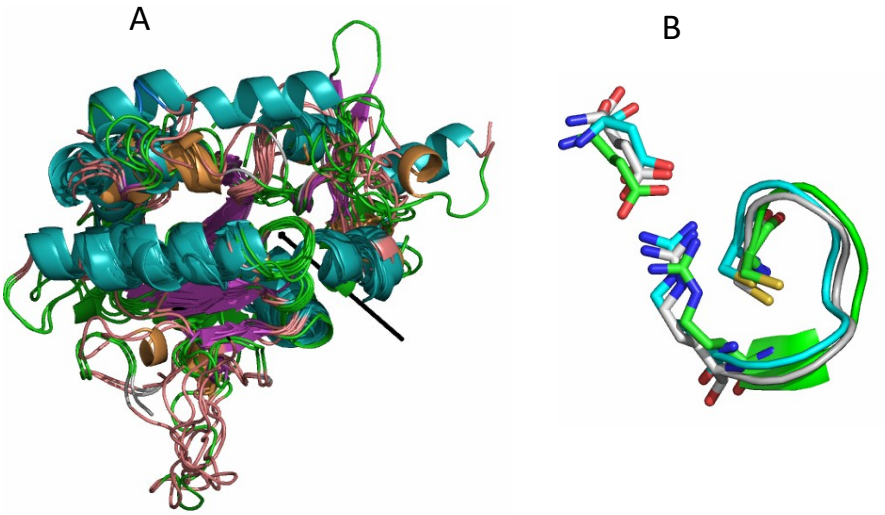

Figure 32: Superimposition of the 14 3D-structures (A) and of the conserved Glu/Asp, Cys and Arg residues of human TSTD1 (green), human CDC25B (grey) and arsenate reductase from *L. major* (cyan) (B).
The arrow indicates the position of the catalytic loop. The figure was produced using PyMol software (Delano Scientific LLC).

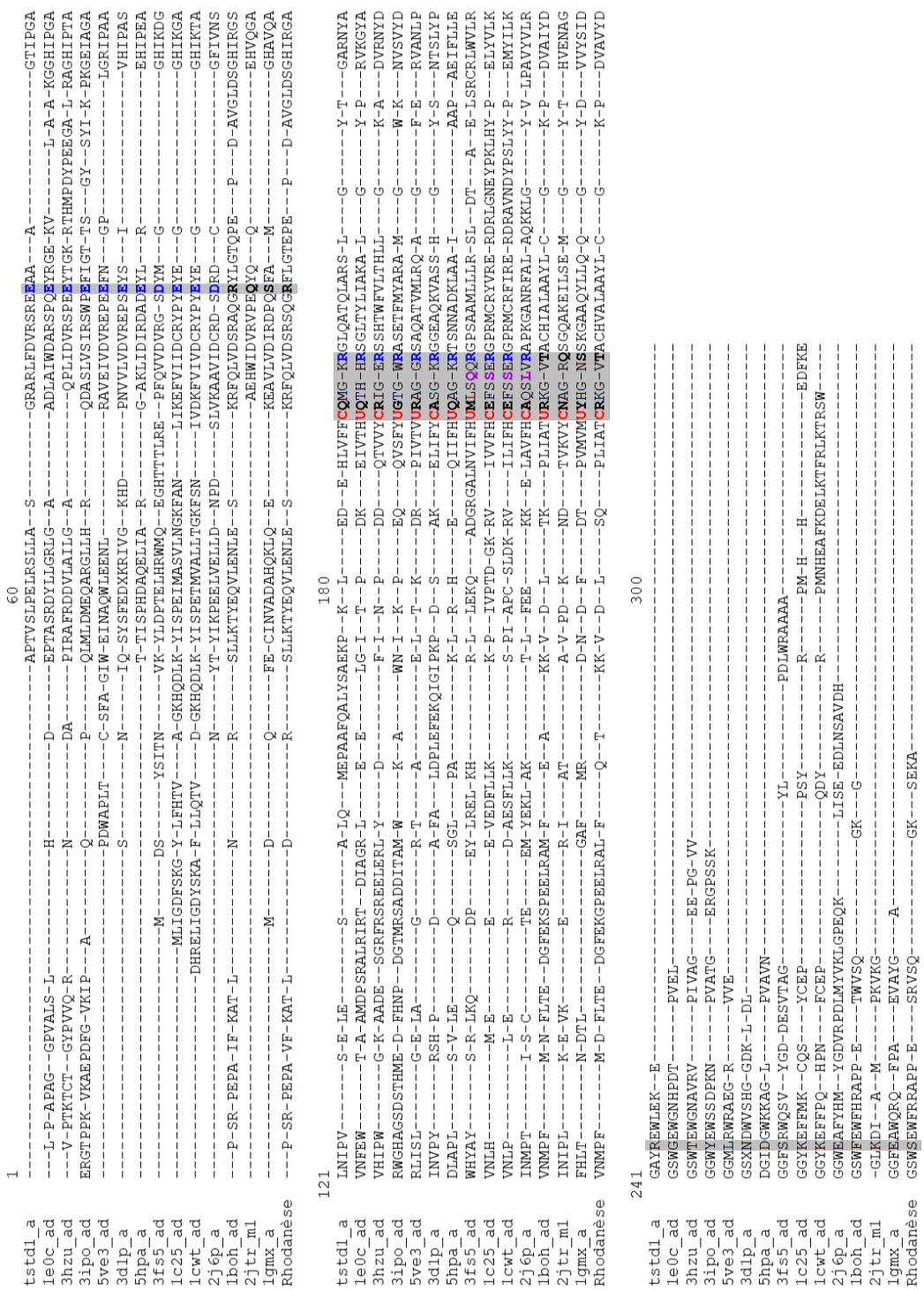

Figure 33: Multi-sequence alignment of TSTD1 and selected TSTs.
The sequences correspond to human TSTD1 (tstd1_a), RhdA from *Azobacter vinelandii* (1e0c_ad), TST from *Mycobacterium* (3hzu_ad), YnjE from *E. coli* (3ipo_ad), the bifunctional persulfide dioxygenase-rhodanese from *Burkholderia phytofirmans* (5ve3_ad), RDL1 from *Saccharomyces cerevisiae* (3d1p_a), Ygap from *E. coli* (5hpa_a), Ygr203w from *Saccharomyces cerevisiae* (3fs5_ad), human Cdc25A (1c25_ad) and B (1cwt_ad), arsenate reductase from *L. major* (2j6p_a), bovine Rosbov (1boh_ad), PspE from *E. coli* (2jtr), GlpE from *E. coli* (1gmx), and human Rhodanese (Rhd). Sulfur-sulfur bond cleavage signature (31/84 pair) is highlighted in blue. Catalytic cysteine residue (under reduced C or persulfide U form) is in red.

In this context, the main axes of my PhD project focused on:

1) Identification of the molecular basis responsible for the promiscuous activities of Rhd-fold enzymes with particular emphasis on the relation between the length and the sequence of the catalytic loop and the catalytic properties (sulfurtransferase, phosphatase and arsenate reductase). TSTD1 and CDC25B are used as initial models because the Glu31/Arg84 signature known to be essential for the thiosulfate sulfurtransferase activity of TSTD1 is also present in CDC25B.

By structure-function relationship studies the aim was to answer the following questions: Is CDC25B able to catalyze sulfur transfer? Does TSTD1 display phosphatase and arsenate reductase activities? Is there any relation between loop length and sequence and these activities? and what about other members of Rhd sulfurtransferase family?

2) Characterization of the substrate specificity of human sulfurtransferase MOCS3. Indeed, isolated MOCS3-Rhd was shown to present a low sulfurtransferase activity in the presence of thiosulfate, suggesting that thiosulfate is not its physiological substrate. On the other hand, NFS1 L-Cysteine desulfurase and 3MST have been proposed as interacting protein of MOCS3, suggesting that MOCS3 could act as a sulfurtransferase involved in sulfur atom trafficking. These raise the following questions: What about other small molecules as donor substrate for MOCS3? Are really NFS1 and 3MST sulfur donors for MOCS3? What about the sulfur acceptor? Is the Rhd-domain responsible for substrate specificities of MOCS3?

Materials and Methods

1. Biological materials

Detailed information regarding the biological materials employed in this study, culture media is compiled in Table 1. A comprehensive list of all cell strains is presented in Table2 , while Table3 & 4 details the plasmid and buffers utilized in this research.

Table1: media used to produce proteins of interest.

Name	Description	Uses
Luria Broth (LB) rich medium	Tryptone 10 g/L, yeast extract 5 g/L, NaCl 5 g/L. The pH is adjusted to 7.5 by adding NaOH.	Medium used for cultures and precultures.
ZYM5052	LB medium, glucose (10%), lactose (12%), glycerol (5%).	Medium used for cultures.
LBNB Medium	LB/antibiotic medium was inoculated at a 1:10 dilution and incubated at 37°C with shaking until the OD600nm reached 0.6. At this point, 0.5 M NaCl and 2 mM betaine were added to the medium. The culture was incubated for 1 hour at 47°C with shaking, followed by an incubation at 20°C with shaking for another hour. Finally, the expression system was induced by adding 1 mM IPTG. The culture was then incubated at 20°C with stirring for 3 hours.	Medium used for cultures
SOC medium	Tryptone 20 g/L, yeast extract 5 g/L, NaCl 10 mM, KCl 2.5 mM, MgCl2 10 mM, MnSO4 10 mM, Glucose 20 mM. The pH is adjusted to 7.5.	Medium used for the regeneration of cell membranes after transformation by heat shock.

Table 2. Cells used to produce proteins of interest.

Name	Description	Uses
E.coli BL21(DE3)	Derived from strain B834: F- dcm ompT hsdS rB- mB-) gal λ (DE3)	Protein production from pET vectors
E. coli C41(DE3)	Derived from strain BL21 (DE3): F- dcm ompT hsdSB (rB-mB-) gal (DE3) and two uncharacterized mutations	Protein production from pET vector
E. coli tuner 10 (DE3)	Strain derived from strain BL21 (DE3): F- ompT hsdSB (rB- mB-) dcm lacY1 gal (DE3) The lac permease (lacY) mutation allows uniform entry of IPTG into all cells in the population, which produces a concentration-dependent, homogeneous level of induction	Protein production from pET vector.
E. coli DH5α	supE44, ΔlacU169 (Φ80 lacZΔM15), hsdR17, recA1, endA1, gyrA96, thi-1, relA1	Preparation of plasmid DNA

Table 3. Plasmids used.

Name	Description	Uses
pET28b TSTD1	Plasmid pET28b comprising the coding sequence of the human *KAT* gene under the dependence of the promoter recognized by the phage T7 polymerase in phase with a polyHis tag at the 5' end.	Production of TSTD1
pCARGHO-CDC25B$_{cd}$	pET plasmid containing the coding sequence of the catalytic domain of human CDC25B fused to the coding sequence of the CRD tag, placed under the control of a promoter recognized by the T7 phage polymerase.	Production of CRD-CDC25B$_{cd}$
pET28a-CDC25B$_{cd}$	pET28b plasmid containing the coding sequence of the catalytic domain of human CDC25B under the dependence of the promoter recognized by the phage T7 polymerase in phase with a polyHis tag at the 5' end	Production of His-CDC25B$_{cd}$
pet28a-ArsC	Plasmid pET28b comprising the coding sequence of the *E. coli arsC* gene under the dependence of the promoter recognized by the phage T7 polymerase in phase with a polyHis tag at the 5' end.	Production of ArsC
pET28a	Plasmid pET28a(+) containing a Kan resistance and a multiple cloning site	Subcloning of MOCS3-Rhds
pCDNA3.1-MOCS3	Homo sapiens MOCS3 (Accession OHu00422C)	Subcloning of MOCS3-Rhds

Table 4: Buffers used.

Buffers	Compositions
Buffer A	Tris-HCl 50 mM, EDTA 2 mM, pH 8.0
Buffer B	Tris-HCl 50 mM, KCl 100 mM, pH 8
Buffer C	Tris-HCl 50 mM, EDTA 2 mM, pH 8.5
Buffer D	Tris-HCl 50 mM, KCl 100 mM, pH 8.5
Buffer E	KPi 500 mM, pH 7
Buffer F	KPi 500 mM + 40mM imidazole pH 7
Buffer G	Kpi 500 mM + 1 M imidazole pH 7
Buffer H	6M urea + 10 mM DTT + Tris-HCl 50 mM, EDTA 2 mM, pH 8.0
Buffer I	Tris-HCl 50 mM, EDTA 2 mM, pH 8.0 + 400 mM NaCl + 10 % glycerol + 10 unit of benzonase per mL + 2 mM $MgSO_4$ and 5 mM of DTT
Buffer J	Tris-HCl 50 mM, EDTA 2 mM, pH 8.0 + 400 mM NaCl and 10 % glycerol.
Buffer K	Tris-HCl 50 mM, EDTA 2 mM, pH 8.0 + 400 mM NaCl and 10 % glycerol. + 200 mM lactose
Buffer L	Tris-HCl 50 mM, EDTA 2 mM, pH 8.0 + 50 mM NaCl and 10 % glycerol
Buffer M	Tris-HCl 50 mM, EDTA 2 mM, pH 8.0 + 1 M NaCl and 10 % glycerol
Buffer N	Borate 50 mM, $MgSO_4$ 1 M pH 9.3
Buffer P	Tris-HCl 50 mM, 40mM imidazole , pH 8.0

2. Genetic engineering techniques

2.1. Site-directed mutagenesis

Site-directed mutagenesis was carried out by PCR in the presence of DNA polymerase from *Pyrococcus furiosus* (Fermentas), of two oligodeoxyribonucleotides complementary to

one of the two strands of the plasmid and carrying the mutation to be introduced, of the plasmid to be mutated and dNTP (Fermentas). *Pfu®* DNA polymerase was used because of its high fidelity, due to its 3'-exonuclease activity which allows the correction of replication errors. The PCR mixtures were then treated with the enzyme Dpn I (Thermofisher), which is an endonuclease, for 30 minutes at 37°C, followed by inactivation of the enzyme for 5 minutes at 80°C. A portion of the mixture is then used to transform competent DH5α bacteria. To do this, a fraction of the mixture is brought into contact with the DH5α cells for 30 minutes in ice, then a thermal shock is carried out at 42°C for 40 seconds. After adding 150 µL of SOC, the cells are placed for 1 hour at 37°C with stirring before spreading on selective solid medium (LB with kanamycin 50 mg/L) and incubating overnight at 37°C. The bacterial clones that were obtained are subsequently used to inoculate cultures in selective liquid medium (10 mL of LB and 50 mg/L of kanamycin) thereafter placed overnight at 37°C with stirring. The plasmid DNA from these cultures is then extracted using a Nucleo-Spin®Plasmid kit (Macherey-Nagel) and analyzed by sequencing (GATC Biotech. Company).

2.2. DNA sub-cloning

The coding sequence of the human MOCS3 303 and MOCS3 335 were PCR-amplified with specific primer pairs (Sigma®) from the synthetized commercial plasmid purchased at Genescript® (pCDNA3.1-MOCS, accession OHu00422C, https://www.genscript.com/). The amplification was performed according to manufacturer recommendations (0.2 mM dNTPs, 100 ng of the matrix DNA, 10 µM of each oligonucleotide, 1 U of Phusion High-Fidelity DNA Polymerase and 5x Phusion HF buffer, *Thermo Scientific™*) with a *T100™* Thermal Cycler**.** PCR products were separated on 1 % agarose gel and purified using the *NucleoSpin® Gel* and *PCR Clean-up* kit (*Macherey Nagel*) and eluted in 25 µL of water. The DNA concentration was measured using NanoDrop® ND-100 spectrophotometer.

Plasmid DNA (200 ng) and PCR amplified insert DNA were one tube (quantity ratio 1/3 or 1/5 depending on the insert size) double digested with specific restriction enzymes (*Thermo Scientific™*) to create compatible ends, the reaction was performed during 3 h at 37 °C according to manufacturer recommendations. Digested plasmid and insert DNA were then one column purified (*NucleoSpin® Gel* and *PCR Clean-up* kit, *Macherey Nagel*) and eluted in 25 µL water. 20 µL of digested vector and thereafter insert DNA mixtures were joined using

T4 DNA ligase according to manufacturer recommendations (*Thermo Scientific™*). The ligation reaction was gently mixed and incubated at room temperature overnight.

A fraction of the ligation mixture (5 µL) was used to transform chemically competent *E. coli* DH5α bacteria. The competent cells were stored in - 80°C and were thawed on ice before use. Tubes were incubated on ice for 30 minutes, thereafter transferred at 42°C for 40 seconds and further incubated on ice for one minute. After bacteria regeneration (37°C, 30 min) cells were plated on solid LB medium containing kanamycin and grown overnight at 37°C. Bacteria having integrated the plasmid were analysed by colony PCR using the *DreamTaq* DNA Polymerase (*Thermo Scientific™*) in 25 µL reaction mixture according manufacturer recommendations. The PCR amplification was carried out with a *T100™* Thermal Cycler**.** PCR positive colonies were amplified by 5-mL LB liquid culture with antibiotics. Plasmid DNA from selected bacterial clones was extracted by the *NucleoSpin®* kit (*Macherey-Nagel*) according to manufacturer recommendations. Samples concentrations were measured using the *NanoDrop ND-100* spectrophotometer.

Restriction of DNA *via* endonucleases was used for control digestion, for this reason the following reaction was set up: 200 - 400 ng of DNA, 1.5µL 10x green buffer, and 2µL of restriction endonucleases, and set up by sterile H_20 15 µL. The reaction was incubated at 37°C for 1 hour and checked by migration on a 1% agarose gel. The plasmid DNAs were also analyzed by sequencing (GATC Biotech. Compagny).

2.3. Agarose gel electrophoresis

Agarose gel electrophoresis was applied to separate DNA fragments. Gels were casted with 1% agarose to resolve the expected fragments of sizes between 731 and 7881 bp. Agarose gels were prepared by weighing 0,5 g agarose (ThermoFisher Scientific) and adding 50 ml of 1x Tris/Acetic Acid/EDTA (TAE) buffer (1,0g/100 ml) (BioRad). The mixture was brought to the boiling point, gently mixed and re-heated until a clear solution was attained. 5 µl of DNA dye SYBRSafe (ThermoFisher Scientific) was added to the clear solution, gently mixed and poured to a gel mold with a well-comb. The gel was hardened for approximately 35-45 minutes. The well-comb was carefully removed, and the gel was placed in a gel electrophoresis chamber. 1xTAE buffer was poured in the gel

electrophoresis chamber, enough to cover the gel. The samples were prepared by adding 10 µl Gel loading dye purple (6x) (Biolabs) to the samples before loading the gel.

The gel was run at 100V for approximately 25 min. The DNA fragments were visualized by using a Chemidoc system with a CCD-camera and a UV light table for excitation of the DNA dye.

3. Production and purification of recombinant enzymes

3.1. Transformation of competent bacteria

The conventional heat shock method is used to transform the competent bacteria *E. coli* tuner10 (DE3), BL21 (DE3), or C41 (DE3) with the expression plasmid. The bacterial cells have undergone a treatment causing an increase in the permeability of their membrane: micropores are formed by the action of salts such as $CaCl_2$. A mixture consisting of 1 to 100 ng of plasmid and 50 µL of competent bacteria is cooled for 30 minutes in ice and then subjected to a thermal shock at 42°C for 30 seconds, followed by cooling for 2 minutes in ice. A regeneration step is carried out by adding SOC medium and incubating for 1 hour at 37°C with stirring. After transformation, the selection of bacteria having integrated the plasmid is done on solid LB medium supplemented with an antibiotic of appropriate resistance to the plasmid used.

3.2. Production and purification of TSTD1

TSTD1 was produced in a *E. coli* C41(DE3) transformed with the plasmid pET28b-TSTD1. The cultures are inoculated in LB medium supplemented with 50 mg/L of kanamycin, then placed at 37°C with stirring until the OD600nm reaches 0.8. At this stage, the expression of the gene encoding TSTD1 is induced by adding 1 mM IPTG and the cells are then placed overnight at 37°C with shaking. The cells are harvested by centrifugation at 4000 g for 30 min.

The cell pellets are taken up in 20 mL of buffer A for TSTD1. Cell lysis is obtained by sonication at 4°C, under a power of 40 W per period of two times two minutes for 50% of the time. Cellular debris is removed by centrifugation at 20,000 g for 35 min. The supernatant

(SSO) is filtered at 0.45 µm before being injected onto a Nickel-Sepharose affinity chromatography column coupled to the ÄKTA™ Avent FPLC system (GE Healthcare®) previously equilibrated with buffer P for TSTD1. The elution is carried out by an imidazole gradient ranging from 0 to 1 M. The collected fractions are deposited on a 15% SDS-PAGE electrophoresis gel. Those containing TSTD1 is combined and dialyzed overnight in buffer A to remove imidazole. Finally, enzyme solution is frozen in liquid nitrogen before being stored at -80°C.

3.3. Production and purification of TSTD1+Ser

TSTD1+Ser is produced in *E. coli* C41 (DE3) transformed with the plasmid pET28b-TSTD1+Ser. The cultures are inoculated in LB medium supplemented with 50 mg/L of kanamycin, then placed at 37°C with stirring until the OD600nm reaches 0.8. At this stage, the expression of the gene encoding TSTD1+Ser is induced by adding 1 mM IPTG and the cells are then placed overnight at 37°C with shaking. The cells are harvested by centrifugation at 4000 g for 30 min.

The cell pellets are taken up in 20 mL of buffer A. Cell lysis is obtained by sonication at 4°C, under a power of 40 W per period of two times two minutes for 50% of the time. Cellular debris is removed by centrifugation at 20,000 g for 35 min. The supernatant (SSO) is filtered at 0.45 µm before being injected onto a Nickel-Sepharose affinity chromatography column coupled to the ÄKTA™ Avent FPLC system (GE Healthcare®) previously equilibrated with buffer P for TSTD1+Ser . The elution is carried out by an imidazole gradient ranging from 0 to 1 M. The collected fractions are deposited on a 15% SDS-PAGE electrophoresis gel. Those containing TSTD1+Ser is combined and dialyzed overnight in buffer A to remove imidazole. Finally, enzyme solution is frozen in liquid nitrogen before being stored at -80°C.

3.4. Production and purification of EX-MUT-TSTD1

EX-MUT-TSTD1 is produced in *E. coli* BL21 (DE3) transformed with the plasmid pET28b-EX-MUT-TSTD1. The cultures are inoculated in LB medium supplemented with 50 mg/L of kanamycin, then placed at 37°C with stirring until the OD600nm reaches 0.8. At this stage, the expression of the gene encoding EX-MUT-TSTD1 is induced by adding 0.2 mM IPTG and the

cells are then placed overnight at 37°C with shaking. The cells are harvested by centrifugation at 4000 g for 30 min.

The cell pellets are taken up in 20 mL of buffer A. Cell lysis is obtained by sonication at 4°C, under a power of 40 W per period of two times two minutes for 50% of the time. Pellet is retrieved by centrifugation at 20,000 g for 35 min, and suspended in 6 M urea, in buffer A followed by two successive dialysis at 4°C in the presence of decreasing urea concentration (3 and 0 M) in the same buffer. The supernatant is then filtered at 0.45µm before being injected onto a Nickel-Sepharose affinity chromatography column coupled to the ÄKTA™ Avent FPLC system (GE Healthcare®) previously equilibrated with buffer P. The elution is carried out by an imidazole gradient ranging from 0 to 1 M. The collected fractions are deposited on a 15% SDS-PAGE electrophoresis gel. Those containing EX-MUT-TSTD1 is combined and dialyzed overnight in buffer A to remove imidazole. Finally, enzyme solution is frozen in liquid nitrogen before being stored at -80°C.

3.5. Production and purification of CRD-CDC25B$_{cd}$

CRD-CDC25B$_{cd}$ was produced in *E. coli* BL21(DE3) transformed with the plasmid pCARGHO-CDC25B$_{cd}$. The cultures are inoculated in liquid medium (LB with ampicillin 200 mg/L), then placed at 37°C with stirring until the OD600nm reaches 0.8. At this stage, the expression of the gene encoding CDC25B$_{Cd}$ is induced by adding 1 mM IPTG and the cells are then placed overnight at 20°C with shaking. The cells are harvested by centrifugation at 4000 g for 30 min.

The cell pellets are taken up in 20 mL of buffer A in the presence of 400 mM NaCl, 10% glycerol to which 10 units of benzonase per mL have been added as well as 2 mM MgSO4 and 5 mM DTT. Cell lysis is obtained by sonication at 4°C, under a power of 40 W per period of two times two minutes for 50% of the time. Cellular debris is removed by centrifugation at 20,000 g for 35 min. The supernatant (SSO) is filtered at 0.45 µm before being injected onto a Lactose-Sepharose HP affinity chromatography column coupled to an Aktä Avant system (GE Healthcare) and equilibrated with buffer A in the presence of 400 mM of NaCl and 10% glycerol. The protein sample is then injected, and the elution is carried out in one step by adding 200 mM lactose, the latter will compete with the lectin domain (CRD) thus allowing

the elution of the protein of interest. The collected fractions are analyzed by 12.5 % SDS-PAGE electrophoresis and those containing the protein of interest are combined. Those containing CRD-CDC25B$_{cd}$ are pooled and injected onto a SP-Sepharose cation exchange chromatography column previously equilibrated with buffer A. Elution is carried out using a gradient from 0 to 1 M KCl. The collected fractions are deposited on a 12.5 % SDS-PAGE electrophoresis gel. Those containing CRD-CDC25B$_{cd}$ are pooled, concentrated on an Amicon® Ultra-15 10 kDa ultrafiltration unit (Millipore) and frozen in liquid nitrogen before being stored at -80°C.

3.6. Production and purification of His-CDC25B$_{cd}$

His-CDC25B$_{cd}$ is produced in a strain of *E. coli* Tuner 10 (DE3) transformed with the plasmid pET28a-CDC25B$_{cd}$. The cultures are inoculated in LB medium supplemented with 50 mg/L of kanamycin, then placed at 37°C with stirring until the OD600nm reaches 0.8. At this stage, the expression of the gene encoding His-CDC25B$_{cd}$ is induced by adding 0.2 mM IPTG and the cells are then placed overnight at 20°C with shaking. The cells are harvested by centrifugation at 4000 g for 30 min.

The cell pellets are taken up in 20 mL of buffer E. Cell lysis is obtained by sonication at 4°C, under a power of 40 W per period of two times two minutes for 50% of the time. Cellular debris is removed by centrifugation at 20,000 g for 35 min. The supernatant (SSO) is filtered at 0.45 µm before being injected onto a Nickel-Sepharose affinity chromatography column coupled to the ÄKTATM Avent FPLC system (GE Healthcare®) previously equilibrated with buffer F. The elution is carried out by an imidazole gradient ranging from 0 to 1 M. The collected fractions are deposited on a 15% SDS-PAGE electrophoresis gel. Those containing His-CDC25B$_{cd}$ is combined and dialyzed overnight in buffer A. The mixture is injected onto a Q-Sepharose anion exchange chromatography column previously equilibrated with buffer A. Elution is carried out using a gradient from 0 to 1 M KCl. The collected fractions are deposited on a 15% SDS-PAGE electrophoresis gel. Those containing His-CDC25B$_{cd}$ are pooled, concentrated on an Amicon® Ultra-15 10 kDa ultrafiltration unit (Millipore) and frozen in liquid nitrogen before being stored at -80°C.

3.7. Production and purification of His-CDC25B$_{cd}$ΔSer

His-CDC25B$_{cd}$ΔSer is produced in *E. coli* Tuner 10 (DE3) transformed with the plasmid pET28a-His-CDC25B$_{cd}$ΔSer. The cultures are inoculated in LB medium supplemented with 50 mg/L of kanamycin, then placed at 37°C with stirring until the OD600nm reaches 0.8. At this stage, the expression of the gene encoding His-CDC25B$_{cd}$ΔSer is induced by adding 0.2 mM IPTG and the cells are then placed overnight at 20°C with shaking. The cells are harvested by centrifugation at 4000 g for 30 min.

The cell pellets are taken up in 20 mL of buffer A. Cell lysis is obtained by sonication at 4°C, under a power of 40 W per period of two times two minutes for 50% of the time. Cellular debris is removed by centrifugation at 20,000 g for 35 min.

For purification from the soluble fraction, the supernatant (SSO) is filtered at 0.45 µm before being injected onto a Nickel-Sepharose affinity chromatography column coupled to the ÄKTATM Avent FPLC system (GE Healthcare®) previously equilibrated with buffer P. The elution is carried out by an imidazole gradient ranging from 0 to 1 M. The collected fractions are deposited on a 15% SDS-PAGE electrophoresis gel. Those containing His-CDC25B$_{cd}$ΔSer are combined and dialyzed overnight in buffer A. The mixture is injected onto a Q-Sepharose anion exchange chromatography column previously equilibrated with buffer A. Elution is carried out using a gradient from 0 to 1 M KCl. The collected fractions are deposited on a 15% SDS-PAGE electrophoresis gel. Those containing His-CDC25B$_{cd}$ΔSer are pooled, concentrated on an Amicon® Ultra-15 10 kDa ultrafiltration unit (Millipore) and frozen in liquid nitrogen before being stored at -80°C.

For purification from the insoluble fraction, the pellet suspended in 6 M urea, in buffer A followed by two successive dialysis at 4°C in the presence of decreasing urea concentration (3 and 0 M) in the same buffer. The supernatant is then filtered at 0.45 µm. finally, before being injected onto a Nickel-Sepharose affinity chromatography column coupled to the ÄKTATM Avent FPLC system (GE Healthcare®) previously equilibrated with buffer P. The elution is carried out by an imidazole gradient ranging from 0 to 1 M. The collected fractions are deposited on a 15% SDS-PAGE electrophoresis gel. Those containing His-CDC25B$_{cd}$ΔSer ares combined and dialyzed overnight in buffer A. The mixture is injected onto a Q-Sepharose anion exchange chromatography column previously equilibrated with

buffer A. Elution is carried out using a gradient from 0 to 1 M KCl. The collected fractions are deposited on a 15% SDS-PAGE electrophoresis gel. Those containing His-CDC25B$_{cd}$ΔSer are pooled, concentrated on an Amicon® Ultra-15 10 kDa ultrafiltration unit (Millipore) and frozen in liquid nitrogen before being stored at -80°C.

3.8. Production and purification of EX-MUT-CDC25B$_{cd}$

EX-MUT-CDC25B$_{cd}$ is produced in *E. coli* Tuner 10 (DE3) transformed with the plasmid pET28a-EX-MUT-CDC25B$_{cd}$. The cultures are inoculated in LB medium supplemented with 50 mg/L of kanamycin, then placed at 37°C with stirring until the OD600nm reaches 0.8. At this stage, the expression of the gene encoding His-EX-MUT-CDC25B$_{cd}$ is induced by adding 0.2 mM IPTG and the cells are then placed 3H at 37°C with shaking. The cells are harvested by centrifugation at 4000 g for 30 min.

The cell pellets are taken up in 20 mL of buffer A. Cell lysis is obtained by sonication at 4°C, under a power of 40 W per period of two times two minutes for 50% of the time. Soluble part is removed by centrifugation at 20,000 g for 35 min. The pellet is suspended in 6 M urea, in buffer A followed by two successive dialysis at 4°C in the presence of decreasing urea concentration (3 and 0 M) in the same buffer. The supernatant is then filtered at 0.45 µm. finally, before being injected onto a Nickel-Sepharose affinity chromatography column coupled to the ÄKTATM Avent FPLC system (GE Healthcare®) previously equilibrated with buffer P. The elution is carried out by an imidazole gradient ranging from 0 to 1 M. The collected fractions are deposited on a 15% SDS-PAGE electrophoresis gel. Those containing EX-MUT-CDC25B$_{cd}$ ares combined and dialyzed overnight in buffer A. The mixture is injected onto a Q-Sepharose anion exchange chromatography column previously equilibrated with buffer A. Elution is carried out using a gradient from 0 to 1 M KCl. The collected fractions are deposited on a 15% SDS-PAGE electrophoresis gel. Those containing EX-MUT-CDC25B$_{cd}$ are pooled, concentrated on an Amicon® Ultra-15 10 kDa ultrafiltration unit (Millipore) and frozen in liquid nitrogen before being stored at -80°C.

3.9. Production and purification of ArsC

ArsC was produced in *E. coli* BL21 (DE3) cells using the pet28a-ArsC vector transformed with the plasmid pET28b/Arsenate. The cultures are inoculated in LB medium supplemented with 50 mg/L of kanamycin, then placed at 37°C with stirring until the OD600nm reaches 0.8. At this stage, the expression of the gene encoding ArC is induced by adding 0.2 mM IPTG and the cells are then placed overnight at 20°C with shaking. The cells are harvested by centrifugation at 4000 g for 30 min.

The cell pellets are taken up in 20 mL of buffer A. Cell lysis is obtained by sonication at 4°C, under a power of 40 W per period of two times two minutes for 50% of the time. Cellular debris is removed by centrifugation at 20,000 g for 35 min. The supernatant (SSO) is filtered at 0.45 µm before being injected onto a Nickel-Sepharose affinity chromatography column coupled to the ÄKTATM Avent FPLC system (GE Healthcare®) previously equilibrated with buffer P for ArC. The elution is carried out by an imidazole gradient ranging from 0 to 1 M. The collected fractions are deposited on a 15% SDS-PAGE electrophoresis gel. Those containing ArsC are combined and dialyzed overnight in buffer A. The mixture is injected onto a Q-Sepharose anion exchange chromatography column previously equilibrated with buffer A. Elution is carried out using a gradient from 0 to 1 M KCl. The collected fractions are deposited on a 15% SDS-PAGE electrophoresis gel. Those containing ArsC are pooled, concentrated on an Amicon® Ultra-15 10 kDa ultrafiltration unit (Millipore) and frozen in liquid nitrogen before being stored at -80°C.

3.10. Production and purification of **MOCS3 303**

MOCS3 303 is produced in*. coli* BL21 (DE3) transformed with the plasmid pET28a-MOCS3 303. The cultures are inoculated in LB medium supplemented with 50 mg/L of kanamycin, then placed at 37°C with stirring until the OD600nm reaches 0.8. At this stage, the expression of the gene encoding MOCS3 303 is induced by adding 0.1 mM IPTG and the cells are then placed overnight at 37°C with shaking. The cells are harvested by centrifugation at 4000 g for 30 min.

The cell pellets are taken up in 20 mL of buffer A. Cell lysis is obtained by sonication at 4°C, under a power of 40 W per period of two times two minutes for 50% of the time. Cellular

debris is removed by centrifugation at 20,000 g for 35 min. The supernatant (SSO) is filtered at 0.45 µm before being injected onto a Nickel-Sepharose affinity chromatography column coupled to the ÄKTATM Avent FPLC system (GE Healthcare®) previously equilibrated with buffer P. The elution is carried out by an imidazole gradient ranging from 0 to 1 M. The collected fractions are deposited on a 15% SDS-PAGE electrophoresis gel. Those containing MOCS3 303 are combined and dialyzed overnight in buffer A. The mixture is injected onto a Q-Sepharose anion exchange chromatography column previously equilibrated with buffer I. Elution is carried out using a gradient from 0 to 1 M KCl. The collected fractions are deposited on a 15% SDS-PAGE electrophoresis gel. Those containing MOCS3 303 are pooled, concentrated on an Amicon® Ultra-15 10 kDa ultrafiltration unit (Millipore) and frozen in liquid nitrogen before being stored at -80°C.

3.11. Production and purification of **MOCS3 335**

MOCS3 335 is produced in a strain of *E. coli* BL21 (DE3) transformed with the plasmid pET28a-MOCS3 335. The cultures are inoculated in LB medium supplemented with 50 µg/L of kanamycin, then placed at 37°C with stirring until the OD600nm reaches 0.8. At this stage, the expression of the gene encoding MOCS3 335 is induced by adding 0.1 mM IPTG and the cells are then placed overnight at 37°C with shaking. The cells are harvested by centrifugation at 4000 g for 30 min.

The cell pellets are taken up in 20 mL of buffer C. Cell lysis is obtained by sonication at 4°C, under a power of 40 W per period of two times two minutes for 50% of the time. Soluble part is removed by centrifugation at 20,000 g for 35 min. The pellet is suspended in 6 M urea, in buffer C followed by two successive dialysis at 4°C in the presence of decreasing urea concentration (3 and 0 M) in the same buffer, and then filtered at 0.45 µm before being injected onto a Nickel-Sepharose affinity chromatography column coupled to the ÄKTATM Avent FPLC system (GE Healthcare®) previously equilibrated with buffer C. The elution is carried out by an imidazole gradient ranging from 0 to 1 M. The collected fractions are deposited on a 15% SDS-PAGE electrophoresis gel. Those containing MOCS3 335 are combined and dialyzed overnight in buffer C. The mixture is injected onto a Q-Sepharose anion exchange chromatography column previously equilibrated with buffer C. Elution is carried out using a gradient from 0 to 1 M KCl. The collected fractions are deposited on a 15%

SDS-PAGE electrophoresis gel. Those containing MOCS3 335 are pooled, concentrated on an Amicon® Ultra-15 10 kDa ultrafiltration unit (Millipore) and frozen in liquid nitrogen before being stored at -80°C.

4. Biochemical characterization of recombinant enzymes

4.1. Polyacrylamide Gel Electrophoresis under denaturing Conditions (SDS-PAGE)

This technique allows for monitoring the progression of the enzyme's purification process. Initially, proteins are concentrated by migration in a 5% polyacrylamide gel and then separated based on their size in a 12.5 % or 15 % polyacrylamide gel. The proteins are specifically stained with Coomassie blue R-250 (152) for visualization.

4.2. Determination of protein concentrations

Theoretical molar extinction coefficients at 280 nm were determined from the protein sequences using the ProtParam tool on Swiss-Prot site. Molar protein concentrations were determined spectrophotometrically using the molar extinction coefficients at 280 nm of 11,460 $M^{-1}.cm^{-1}$, 12,950 $M^{-1}.cm^{-1}$, 36,330 $M^{-1}.cm^{-1}$, 17,085 $M^{-1}.cm^{-1}$, 15,595 $M^{-1}.cm^{-1}$, and 4,470 $M^{-1}.cm^{-1}$, for TSTD1, CRD-CDC25B_{cd}, His-CDC25B_{cd}, MOCS3 303, MOCS3 335, and ArsC, respectively.

4.3. Determination of the molecular mass of recombinant proteins by mass spectrometry

Mass spectrometry is a technique requiring the use of a sample showing no trace of non-volatile salts. The recombinant proteins were desalted by a succession of dilution/concentration by ultrafiltration in an Amicon cell equipped with a YM 10 membrane with a capacity of 0.5 mL. The protein thus desalted is recovered in buffer W. The protein fraction is then analyzed using an electrospray mass spectrometer (MicrOTOF-Q Bruker Daltonics) under denaturing conditions in order to determine the molecular masses of wild-

type and mutated. The analyzes were carried out by Dr. Hortense Mazon within the joint mass spectrometry service of UMR 7565 CNRS-UL, Institut Jean Barriol.

5. Enzymatic properties of recombinant enzymes

Prior to any study, the protein sample is centrifuged at 12,000 g at 4°C to remove any protein aggregates. The enzyme concentration is calculated from the optical density at 280 nm, using the specific molar extinction coefficient of the studied protein.

5.1. Sulfurtransferase activity

Stock solutions of 3-mercaptopyruvate (3MP) were prepared at 100 mM. The kinetic studies occurred out in the presence of variable concentrations of substrate under single catalytic cycle conditions were performed using “stopped-flow” (SX19MV-R, Applied Photophysics) allowing the variation in fluorescence emission of the enzyme over short periods of time to be monitored. One syringe contains the enzyme and the other substrate in buffer A (Figure 34). The excitation is set at 284-285 nm and the use of a 320 nm “cut-off” filter makes it possible to specifically observe the fluorescence emission at wavelengths greater than 320 nm. The experimental data were fitted to the equation of a single or double exponential using Pro-Data SX software (Applied Photophysics).

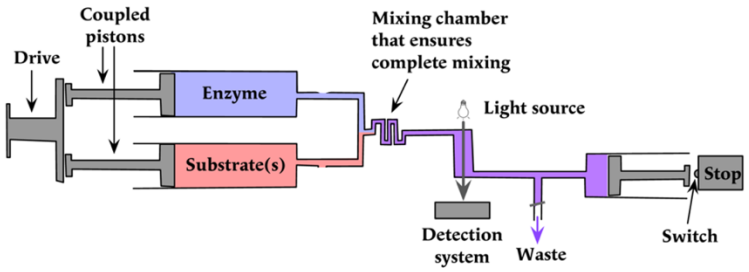

Figure 34: Operating principle of a "stopped-flow" apparatus. The stopped-flow apparatus enables rapid mixing of the enzyme (E) and substrate (S) solutions, allowing for real-time monitoring of reaction progress from the initial stages.

5.2. Phosphatase activity

a) With pNPP substrate

The para nitrophenol phosphate (pNPP) substrate was purchased in solution at a concentration of 500 mM in water (Sigma). The appearance of the product, para-nitrophenolate (pNP), which absorbs at 405 nm with a molar extinction coefficient of 18,000 $M^{-1}.cm^{-1}$, is followed over time using a SAFAS UVmc2 spectrophotometer. A preliminary blank is established by following the increase in the OD_{405nm} over time, in the absence of enzyme, due to the hydrolysis of the pNPP in the buffer. This rate is subtracted from the reaction rate in the presence of enzyme. The reaction mixture contains 1 µM of enzyme and variable concentrations of pNPP (from 2.5 to 75 mM) in a total volume of 500 µL.

b) With 4-MUP substrate

4-methylunbelliferyl phosphate (4-MUP) was purchased from Sigma. 4-MUP assays were realized under steady-state conditions. Hydrolysis of 4-MUP to 4-methyl-unbelliferon (4-MU, fluorescent) and inorganic phosphate was followed by fluorescence emission at 445 nm wavelength (excitation: 372 nm, PM 300) in 50 mM borate, 1 M $MgSO_4$ buffer, pH 9.3 on a SAFAS Xenius fluorimeter.

5.3. Arsenate reductase activity

Arsenate activity was assayed under steady-state conditions in the presence of 5 mM sodium arsenate, 30 mM NADPH, 4 mM glutathion (GSH), 85 nM glutathione reductase (GR), 1.5 µM glutaredoxine (GRX), in buffer A (Figure 35). Arsenate reduction coupled to NADPH oxidation was monitored by following at 30°C the decrease in absorbance at 340 nm (ε = 6220 $M^{-1}.cm^{-1}$) using a SAFAS UVmc2 spectrophotometer. The kinetic experiments were performed in the presence of 10 µM enzyme and variable concentrations of arsenate (5 to 35 mM).

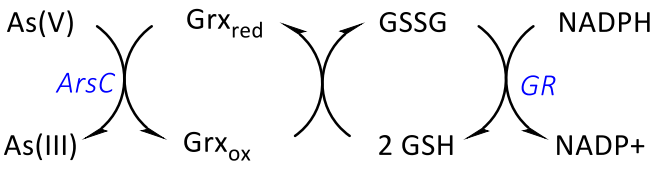

Figure 35: Principle of the arsenate reductase assay.
As(V), arsenate; As(III); arsenite, Grx_{red} and Grx_{ox}, reduced and oxidized glutaredoxin; GSH, reduced glutathione; GSSG, oxidized glutathione; GR, glutathione reductase.

5.4. Kinetic data fitting

Kinetic data were fitted using the SciDAVis software (version 2.3.0) to the following equations:

- Michaelis-Menten equation for steady state experiments: $$k_{obs} = \frac{k_{cat} \times [S]}{K_M + [S]}$$

- Hill equation for sigmoidal behaviour: $$k_{obs} = \frac{k_{cat} \times [S^n]}{K^n_{0.5} + [S^n]}$$

- Hyperbola equation for single turn-over experiments: $$k_{obs} = \frac{k_{max} \times [S]}{K + [S]}$$

Results

Axis 1:

This axis focused on the identification of the molecular basis responsible for the promiscuous activities of rhodanese-fold enzymes with particular emphasis on the relation between the length and the sequence of the catalytic loop and the catalytic properties (sulfurtransferase, phosphatase and arsenate reductase).

For this, two human enzymes have been used as models: a sulfurtransferase named TSTD1 previously studied in the group for its sulfurtransferase activity, and the catalytic domain of tyrosine phosphatase CDC25B, hereafter referred as $CDC25B_{cd}$, already known to display phosphatase and arsenate reductase activities and thus promiscuity. To evaluate the relationship between the loop length and the activities, the strategy was to perform structure-function relationship study on various enzymes variants: 1) a TSTD1 variant with an extended CX_5R catalytic loop obtained by addition of a Ser residue between Gly85 and Lys86 residues (TSTD1+Ser), 2) a TSTD1 variant in which the catalytic loop of $CDC25B_{cd}$ (CEFSSER) was introduced (named EX-MUT-TSTD1), 3) a $CDC25B_{cd}$ variant with a shorter CX_4R catalytic loop, i.e. without the Ser86 residue ($CDC25B_{cd}\Delta Ser$), and 4) a $CDC25B_{cd}$ variant exhibiting the catalytic loop of TSTD1 (CQMGKR), named EX-MUT-$CDC25B_{cd}$. The choice to introduce a Ser residue in the catalytic loop of TSTD1 between the Gly85 and Lys86 residues is justified by the presence of this same residue in the rhodanese domain proteins with CX_5R signature and which exhibit phosphatase activity (like $CDC25B_{cd}$, Bhattacharjee *et al.,* 2010).

In the following section, I will successively present results concerning the production and purification of the various enzymes, and the characterization of their kinetic properties.

A) Production and purification of TSTD1 and its variants

1- TSTD1

Employing the established laboratory protocol, TSTD1 was produced as a fused protein with an N-terminal poly-His-tag in *E. coli* C41 (DE3) cells transformed with a pET28b-TSTD1 vector. The purification protocol consists of two steps: (1) cell lysis by sonication to recover the enzyme in the soluble fraction, and (2) Ni-Sepharose affinity chromatography (elution at 200 mM of imidazole). This protocol allowed to obtain the wild-type form of TSTD1 purified to homogeneity and in large quantity (yield approx. 43 mg/L of culture). A table summarizing the different steps of purification and the SDS-PAGE used to evaluate the purity state of the enzyme are presented in figure 36.

A

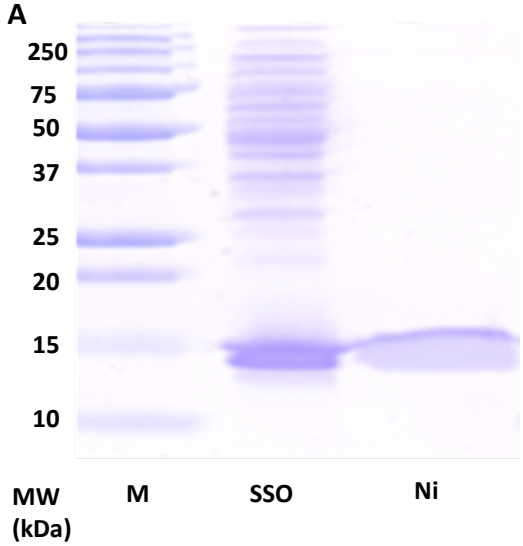

B

Step	Volume	OD_{280}	OD_{260}	Ratio
SSO	94 mL	79	143	0.55
Nickel-Sepharose	22 mL	6.1	3.2	1.9

Figure 36: Purification of recombinant TSTD1.
A) 15% SDS-PAGE analysis of the different steps of purification. B) Summary table of the steps used to purify TSTD1. The enzyme was produced in *E. coli* C41 (DE3) transformed with pET28b-TSTD1 and grown in 4 L LB/K overnight at 37°C after 1 mM IPTG induction. MW: marker, SSO: sonication supernatant, Ni-Sepharose: eluate of the Ni-Sepharose column. Ratio: OD_{280}/OD_{260}. Purified enzymatic solution with concentration 530 µM was stored at -80°C.
*Molar Mass of TSTD1= 12 kDa.

2- TSTD1+Ser

Site-directed mutagenesis was employed to generate a pET28b-TSTD1+Ser vector. The same protocol as for wild-type TSTD1 production and purification was used for TSTD1+Ser. TSTD1+Ser was produced in *E. coli* C41 (DE3) cells harboring the pET28b-TSTD1+Ser vector.

The purification protocol comprises two steps: (1) cell lysis by sonication to recover the enzyme in the soluble fraction, and (2) Ni-Sepharose affinity chromatography (elution at 200 mM imidazole). This protocol yielded significant amount of highly purified TSTD1 variant (approximately 28 mg/L of culture). A table summarizing the purification steps and the SDS-PAGE analysis used to monitor the enzyme's purity is presented in figure 37.

A

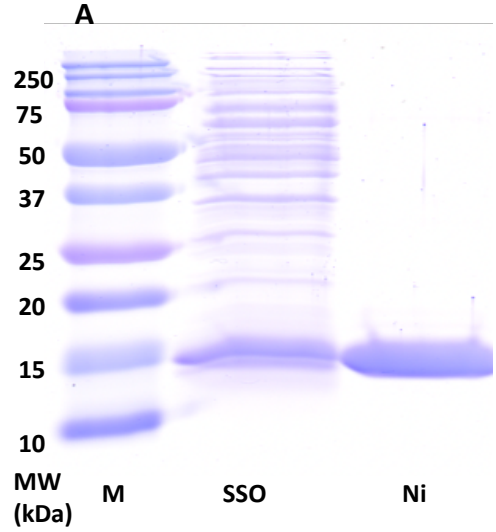

B

Step	Volume	OD_{280}	OD_{260}	Ratio
SSO	92 mL	66.4	127.7	0.51
Nickel-Sepharose	20 mL	4.4	2.5	1.7

Figure 37: Purification of TSTD1+Ser
A) 15% SDS-PAGE analysis of the different steps of purification. B) Summary table of the steps used to purify TSTD1+Ser. The enzyme was produced in *E. coli* C41(DE3) transformed with pET28b-TSTD1+Ser and grown in 4 L LB/K overnight at 37°C after 1mM IPTG induction. MW: marker, SSO: sonication supernatant, Ni-Sepharose: eluate of the Ni-Sepharose column. Ratio: OD_{280}/OD_{260}. Purified enzymatic solution with concentration 380 µM was stored at -80°C.
*Molar Mass of TSTD1+Ser = 12 kDa.

3- EX-MUT-TSTD1

Site-directed mutagenesis was performed to generate a pET28b-EX-MUT-TSTD1 vector. Unfortunately, initial production tests conducted in *E. coli* BL21 (DE3) cells using this vector and classical conditions (LB medium at 37°C) showed that the enzyme was mainly detected in the insoluble fraction after cell disruption (data not shown). We then assayed various protocols to identify the most favorable conditions to produce a soluble form of this variant.

To increase the amount of soluble EX-MUT-TSTD1, different bacterial strains and culture protocols were tested. Two *E. coli* strains were used: BL21(DE3) and C41(DE3) (specifically adapted to produce proteins that might be toxic).

Two culture protocols were also tested: the classic LB protocol (LB medium with 0.2 to 1mM IPTG induction and incubation from 3 h to overnight at 37°C or 20°C), and a LBNB protocol (LB medium with addition of 0.5 M NaCl and 2 mM betaine to induce an osmotic shock, followed by a thermal shock for 1 h at 47°C inducing the production of *E. coli* chaperones, and finally 0.2 to 1 mM IPTG induction followed by overnight at 20°C).

To check whether the variant was overproduced, bacterial crude extracts were analyzed by 15% SDS-PAGE for all these assays, Representative examples of these gels are shown in figure 38. As expected, protein production was much higher after overnight incubation, compared to 3 hours, but no difference in production level was detected irrespective of the conditions used (except for condition 5, figure 38B).

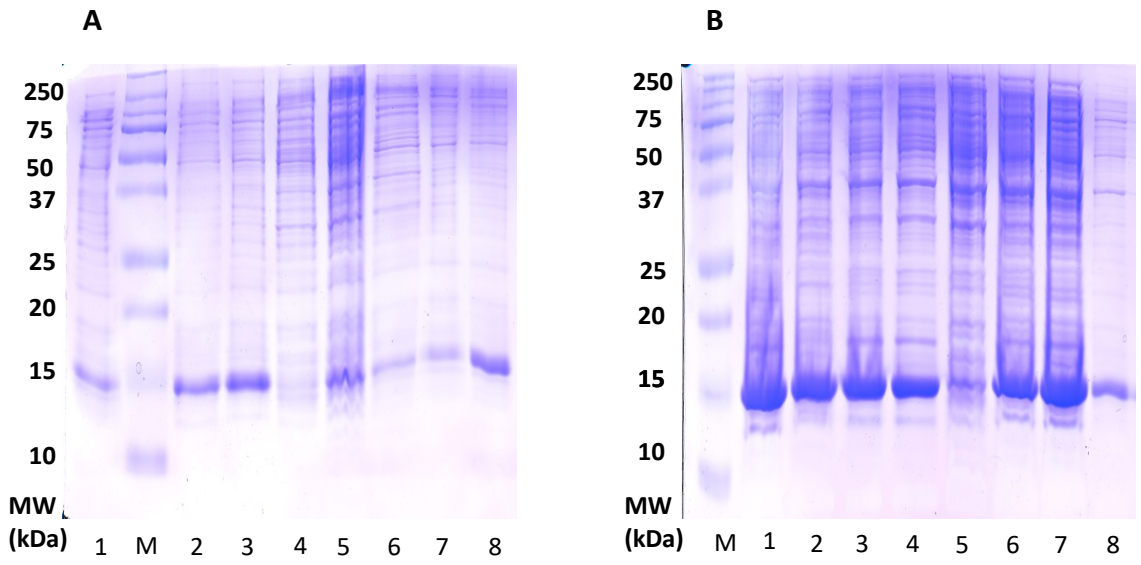

Figure 38: Overexpression for EX-MUT-TSTD1.
A) After 3h: 1: Classic LB 0.2 mM IPTG BL21(DE3) 20°C , 2: Classic LB 0.2 mM IPTG BL21(DE3) 37°C, 3: Classic LB 1 mM IPTG BL21(DE3) 37°C, 4 : Classic LB 0.2 mM IPTG C41(DE3) 20°C, 5 : Classic LB 0.2 mM IPTG C41(DE3) 37°C, 6 : Classic LB 1 mM IPTG C41(DE3) 37°C, 7: Classic LB 0.2 mM IPTG Tuner(DE3) 20°C, 8: Classic LB 0.2 mM IPTG Tuner(DE3) 37°C.
B) Overnight: 1: Classic LB 0.2 mM IPTG BL21(DE3) 20°C , 2: Classic LB 0.2 mM IPTG BL21(DE3) 37°C, 3: Classic LB 1 mM IPTG BL21(DE3) 37°C, 4 : Classic LB 0.2 mM IPTG C41(DE3) 20°C, 5 : Classic LB 0.2 mM IPTG C41(DE3) 37°C, 6 : Classic LB 1 mM IPTG C41(DE3) 37°C, 7: Classic LB 0.2 mM IPTG Tuner(DE3) 20°C, 8: Classic LB 0.2 mM IPTG Tuner(DE3) 37°C.
*Molar Mass of EX-MUT-TSTD1 = 12 kDa.

Insoluble and soluble fractions were analyzed by 15% SDS-PAGE after sonication and centrifugation to evaluate the amount of soluble variant in various buffers (50 mM Tris-HCl, 2 mM EDTA, pH 8; 50 mM, 100 mM or 500 mM KPi, pH 7). Unfortunately, the overproduced EX-MUT-TSTD1 was almost entirely recovered as an insoluble form within the sonication pellet irrespective of the buffers used, as evidenced by the electrophoretic profiles presented in figure 39.

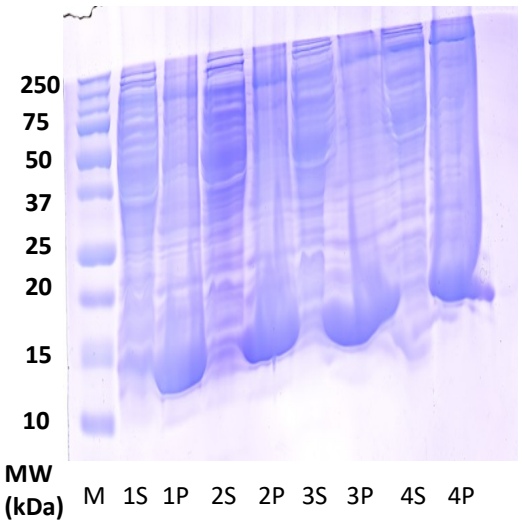

Figure 39: EX-MUT-TSTD1 solubility tests using different buffers.
1: 50 mM Tris-HCl, 2 mM EDTA, pH 8; 2: 50 mM KPi, pH 7; 3: 100 mM KPi, pH 7; 4: 500 mM KPi, pH 7. S: supernatant and P: pellet.
*Molar Mass of EX-MUT- TSTD1= 12 kDa.

The strategy was then to purify the variant from the pellet, i.e. to use the chaotropic agent urea (6 M) to recover the variant from the solubilized pellet content. Protein refolding was then realized by two successive dialyses against 3 M and 0 M urea in various buffers (50 mM Tris-HCl, pH 8 or 500 mM KPi, pH 7). The last step consists of a centrifugation to separate insoluble and soluble forms. As shown by SDS-PAGE analysis, this protocol permitted to obtain high amount of soluble EX-MUT-TSTD1 with the two buffers tested (Figure 40).

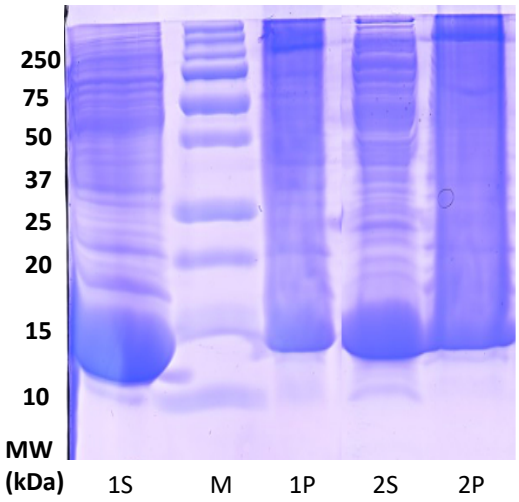

Figure 40: EX-MUT-TSTD1 resolubilization tests from the insoluble form.
1: 50 mM Tris-HCl, pH 8, buffer; 2: 50 mM KPi, pH 7 buffer. S: supernatant and P: pellet.
*Molar Mass of EX-MUT-TSTD1= 12 kDa.

EX-MUT-TSTD1 was produced in *E. coli* BL21 (DE3) transformed with pET28b-EX-MUT-TSTD1 with a classical LB protocol (0.2 mM IPTG, incubation overnight at 37°C after induction). The protocol of purification consists of four steps: (1) cell lysis by sonication to recover the enzyme in the insoluble fraction, (2) suspension of the pellet in 6 M urea, 10 mM DTT, 50 mM Tris-HCl, pH 8, buffer followed by (3) two successive dialysis at 4°C in the presence of decreasing urea concentration (3 and 0 M) in 50 mM Tris-HCl, pH 8, buffer, and (4) Ni-Sepharose affinity chromatography. This protocol allowed to obtain the EX-MUT-TSTD1 purified to homogeneity (yield approx. 13 mg/L of culture). A table summarizing the different steps of purification and the SDS-PAGE used to follow the purity state of the enzyme are presented in figure 41.

A

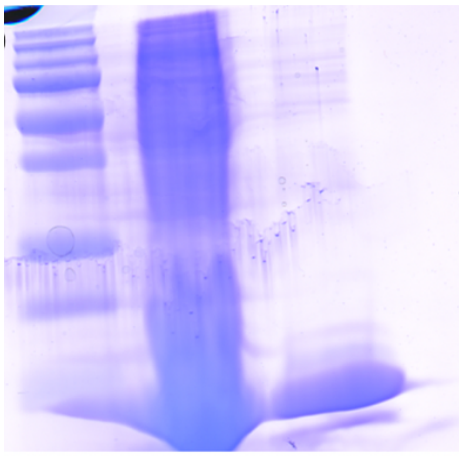

B

Step	Volume	OD_{280}	OD_{260}	Ratio
SU	72 mL	22.5	23.1	0.97
Nickel-Sepharose	21 mL	1.9	1.5	1.2

Figure 41: Purification of EX-MUT-TSTD1
A) 15% SDS-PAGE analysis of the different steps of purification. B) Summary table of the steps used to purify EX-MUT-TSTD1. The enzyme was produced in *E. coli* BL21 (DE3) transformed with pET28b-EX-MUT-TSTD1 and grown in 4 L LB/K overnight at 37°C after 0.2 mM IPTG induction. MW: marker, SU: supernatant after urea denaturation and refolding by dialysis, Ni-Sepharose: eluate of the Ni-Sepharose column. Ratio: OD_{280}/OD_{260}. Prior storage at -80°C, Purified enzymatic solution with concentration 380 µM 160 µM was stored at -80°C.
*Molar Mass of EX-MUT-TSTD1 = 12 kDa.

4- Preliminary quality controls

LC-ESI-MS experiments were performed to assess the integrity of all TSTD1 forms. As shown in Figure 42, all measured molecular masses agreed perfectly with the theoretical ones: 14562.40 ± 0.05 Da vs 14562.4 Da, 14649.50 ± 0.05 Da vs 14649.5 Da and 14640.33 ± 0.07 Da vs 14640.3 Da, for wild type, TSTD1+Ser and EX-MUT-TSTD1, respectively.

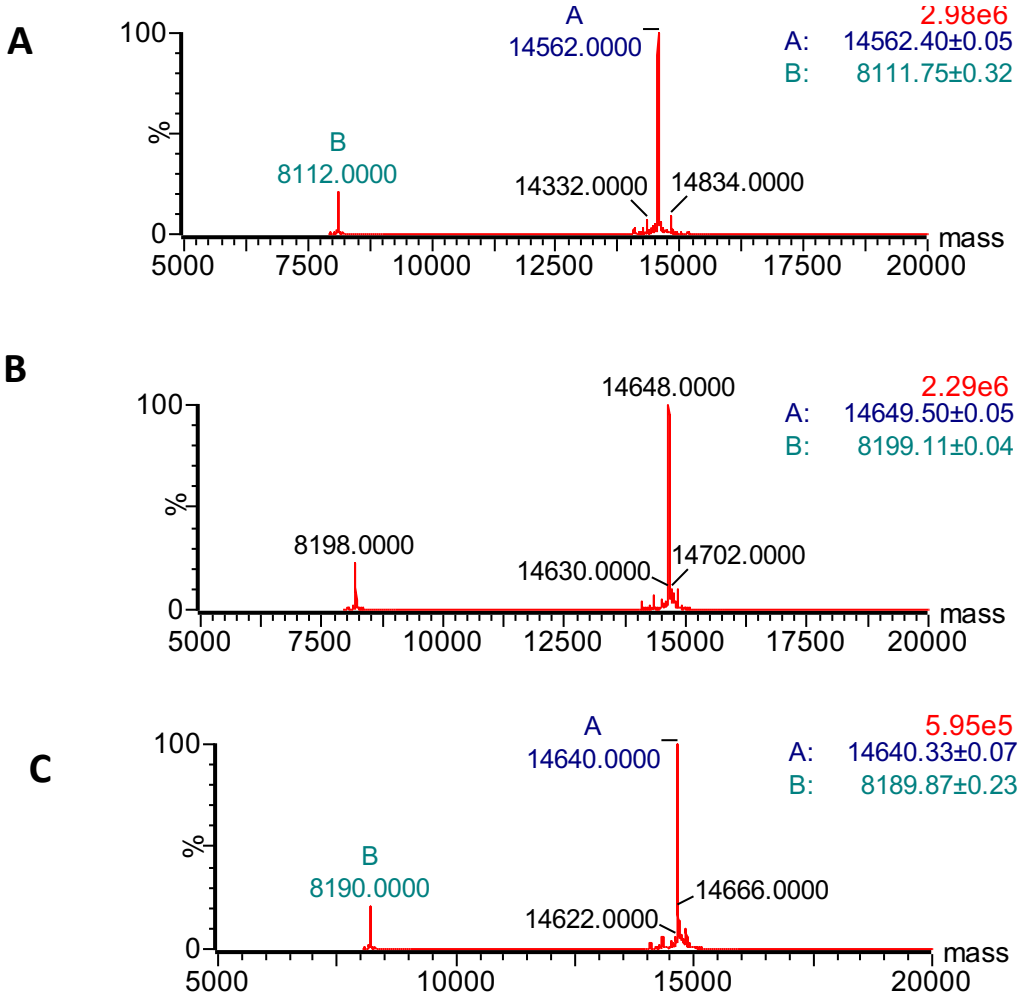

Figure 42: Mass spectrometry spectra of wild-type and mutated TSTD1s (A-C) by LC-ESI-MS
Distribution of charge states of the proteins by ESI-Q-TOF MS. For analysis, proteins were diluted to 10 µM in H_2O/Acetonitrile/ammonium buffer (50:50:1). The theoretical molecular masses of the proteins without the N-terminal Met are: 14562,4 Da for TSTD1 (A), 14649,5 Da for TSTD1+Ser (B), and 14640,3 Da for EX-MUT-TSTD1 (C).

B) Production and purification of CDC25B$_{cd}$ and its variants

1- CRD-CDC25B$_{cd}$

Employing the previously established laboratory protocol, CDC25Bcd was produced in *E. coli* BL21(DE3) cells using the pCARGHO-CDC25B$_{cd}$ vector. This vector allows the production of the enzyme fused to a N-terminus CRD tag (CRD stands for "Carbohydrate Recognition Domain" of a truncated form of galectin 3). The purification protocol comprises three steps: (1) cell lysis by sonication to recover the enzyme in the soluble fraction, (2) lactose-Sepharose affinity chromatography, enabled by the CRD tag, and (3) SP-Sepharose cation exchange

chromatography. This protocol yielded approximately 12 mg/L of culture of purified CRD-CDC25B$_{cd}$. A table summarizing the purification steps and the SDS-PAGE analysis employed to monitor the enzyme's purity is presented in figure 43.

A

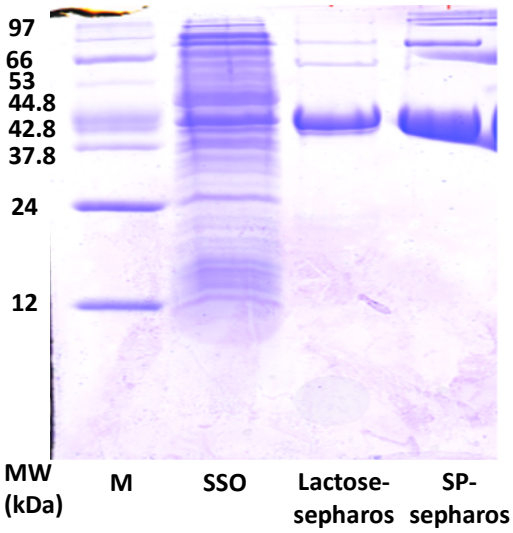

B

Steps	Volume	OD_{280}	OD_{260}	Ratio
SSO	95 mL	102	190	0.54
Lactose-Sepharose	119 mL	0.50	0.31	1.62
SP-Sepharose	33 mL	0.47	0.27	1.74

Figure 43: Purification of recombinant CRD-CDC25B$_{cd}$.
A) 12.5% SDS-PAGE analysis of the different steps of purification. B) Summary table of the steps used to purify CRD-CDC25B$_{cd}$. The enzyme was produced in *E. coli* BL21(DE3) transformed with pCARGHO-CDC25B$_{cd}$ and grown in 4 L LB/A overnight at 20°C after 1 mM IPTG induction. MW: marker, SSO: sonication supernatant, Lactose-Sepharose: eluate of the Lactose-Sepharose column, SP-Sepharose: eluate of the SP-Sepharose column. Ratio: OD_{280}/OD_{260}.
*Molar Mass of CRD-CDC25B$_{cd}$= 21 kDa.

2- His-CDC25B$_{cd}$

The production of CRD-CDC25B$_{cd}$ being low and unreproducible, we decided to change our strategy to produce the CDC25B$_{cd}$ fused to an His-tag. For this, a pET28a-CDC25B$_{cd}$ vector, allowing the production of a N-terminal poly-His tagged version of the enzyme, was purchased.

His-CDC25B$_{cd}$ production was first evaluated using various protocols presented previously (page 67), including different strains (BL21(DE3), C41(DE3), and Tuner10 (DE3)), media (LB, LBNB), to identify the optimal conditions (Figure 43). An auto inducible medium permitting a smooth induction was also assayed (ZYM protocol) and it was expected to minimize the production of insoluble forms. Analysis of bacterial crude extracts on SDS-PAGE

showed that the best production level was obtained with the Tuner (DE3) strain and a classical LB protocol with 0.2 mM IPTG and overnight incubation at 20°C (Figure 44).

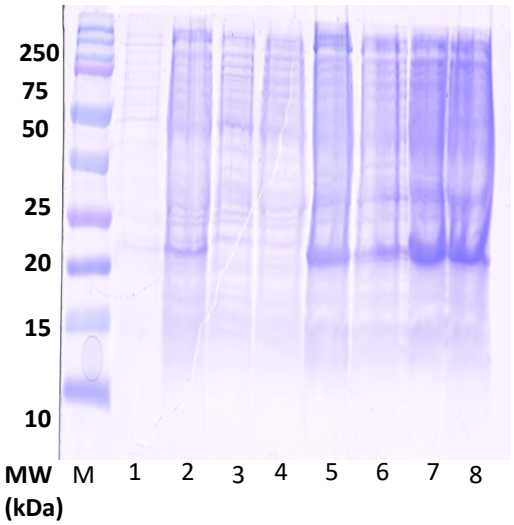

Figure 44: Production of His-CDC25B$_{cd}$.
1: Classical LB protocol before addition of IPTG Tuner (DE3); 2: LBNB protocol before addition of IPTG Tuner(DE3); 3: Classical LB protocol 3 hours at 20°C after addition of 0.2 mM IPTG Tuner (DE3); 4: LBNB protocol 3 hours at 20°C after addition of 0.2 mM IPTG Tuner(DE3); 5: Classical LB protocol overnight at 20°C after addition of 0.2 mM IPTG Tuner(DE3); 6: LBNB protocol overnight at 20°C after addition of 0.2 mM IPTG Tuner(DE3); 7: ZYM protocol BL21(DE3), 8: ZYM protocol Tuner(DE3). *Molar Mass of His-CDC25B$_{cd}$ = 21 kDa.

Before commencing with the purification, the solubility state of the produced protein was evaluated. Analysis of insoluble and soluble fractions was realized by 15 % SDS-PAGE after sonication and centrifugation to evaluate the solubility of the protein in various buffers (50 mM Tris-HCl, 100 mM KCl, 40 mM Imidazole, pH 8 buffer; 100 mM or 500 mM KPi buffer, pH 7; with or without 10% glycerol). As evidenced by the electrophoretic profile presented in figure 45, His-CDC25B$_{cd}$ was present both in insoluble and soluble form with all buffers, with no obvious difference between the two except when 100 mM KPi pH 7 was used.

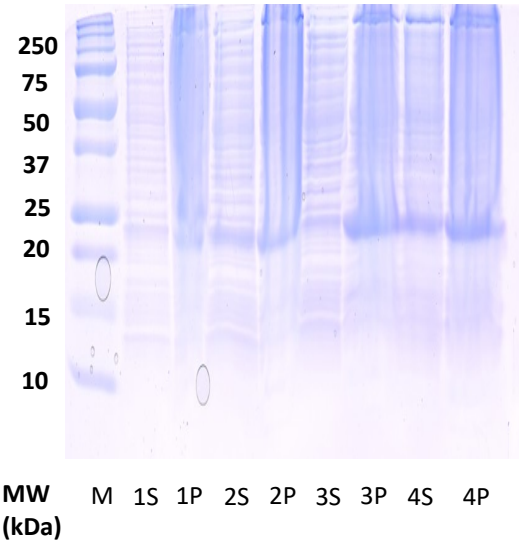

Figure 45: His-CDC25B$_{cd}$ solubility tests with different buffers.
1: 50 mM Tris-HCl, 100 mM KCl, 40 M imidazole, pH 8; 2: same buffer as 1 with 10 % glycerol; 3: 100 mM KPi, pH 7; 4: 500 mM KPi, pH 7. S: supernatant and P: pellet. *Molar Mass of His-CDC25B$_{cd}$ = 21 kDa.

Based on these data, His-CDC25B$_{cd}$ production were achieved using *E. coli* Tuner (DE3) cells with a pET28a-CDC25B$_{cd}$ vector, and the following three steps protocol was used for purification: (1) cell lysis by sonication using 500 mM KPi as buffer to isolate the enzyme in the soluble fraction, (2) Ni-Sepharose affinity chromatography, and (3) Q-Sepharose anion exchange chromatography. A table summarizing the purification steps and the SDS-PAGE analysis used to monitor the enzyme's purity is presented in figure 46. This protocol yielded approximately 3 mg/L of culture of purified wild-type His-CDC25B$_{cd}$. This yield is comparable to that obtained with the CRD-CDC25B$_{cd}$, but this protocol has been shown to be much more reproductible (data not shown).

A

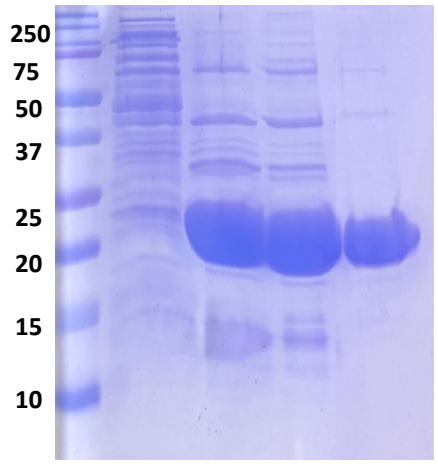

B

Step	Volume	OD_{280}	OD_{260}	Ratio
SSO	102 mL	87.9	162.7	0.54
Ni-Sepharose	15 mL	3.5	2.5	1.3
Q-Sepharose	19 mL	1.1	0.5	1.9

Figure 46: Purification of His-CDC25B$_{cd}$.
A) 15% SDS-PAGE analysis of the different steps of purification. B) Summary table of the steps used to purify His-CDC25B$_{cd}$. The enzyme was produced in *E. coli* Tuner (DE3) transformed with pET28a-CDC25B$_{cd}$ and grown in 4 L LB/K overnight at 20°C after 0.2 mM IPTG induction. MW M: marker; SSO: sonication supernatant, Ni-Sepharose: eluate of the Ni-Sepharose column, Dialysis: dialysis of the Ni fraction to eliminate imidazole, Q-Seph: eluate of the Q-Sepharose column. Ratio: OD_{280}/OD_{260}. Prior storage at -80°C, purified enzymatic solution was concentrated by ultrafiltration to 150 µM without significant loss of proteins (yield of 84 %). *Molar Mass of His-CDC25B$_{cd}$= 21 kDa.

3- His-CDC25B$_{cd}$ΔSer

Site-directed mutagenesis was used to produce a pET28a-CDC25B$_{cd}$ΔSer plasmid. Using a strategy similar to that depicted for His-CDC25B$_{cd}$, the production of the variant was first tested with various protocols, encompassing different strains, culture media, IPTG concentrations, and incubation temperatures. Analysis of bacterial crude extracts on SDS-PAGE showed that a reasonable amount of protein was obtained with the Tuner (DE3) strain

using a classical LB protocol with 0.2 mM IPTG and incubation overnight at 20°C (Figure 47 lane 5).

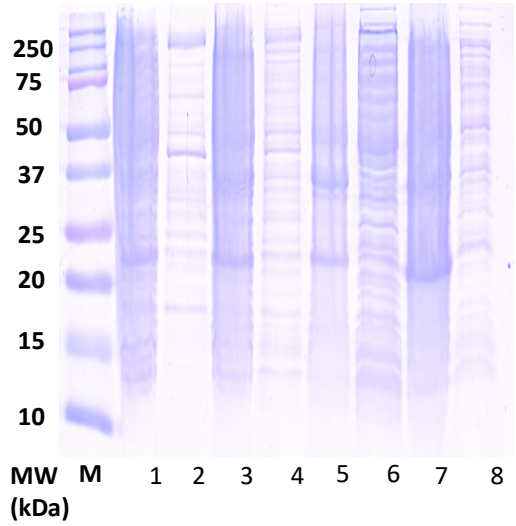

Figure 47: His-CDC25B$_{cd}$ΔSer overexpression tests
1: Classical LB protocol before addition of IPTG Tuner (DE3); 2: LBNB protocol before addition of IPTG Tuner (DE3); 3: Classical LB protocol 3 hours at 20°C after addition of 0.2 mM IPTG Tuner (DE3); 4: LBNB protocol 3 hours at 20°C after addition of 0.2 mM IPTG Tuner (DE3); 5: Classical LB protocol overnight at 20°C after addition of 0.2 mM IPTG Tuner (DE3); 6: LBNB protocol overnight at 20°C after addition of 0.2 mM IPTG Tuner (DE3); 7: ZYM protocol BL21(DE3), 8: ZYM protocol Tuner (DE3). *Molar Mass of His-CDC25B$_{cd}$ΔSer = 21 kDa.

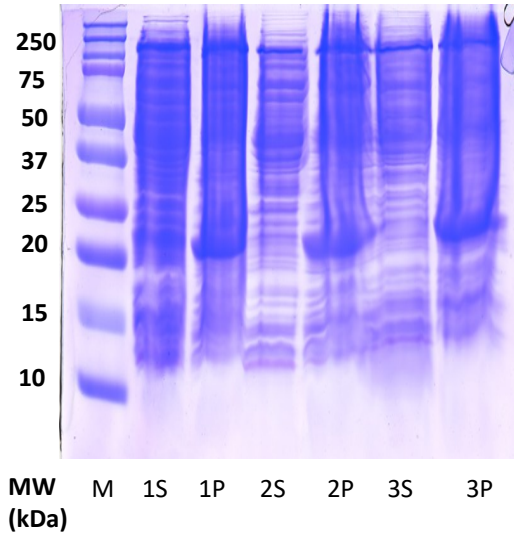

Figure 48: His-CDC25B$_{cd}$ΔSer.solubility tests with different buffers
1) Tris-HCl 50mM, EDTA mM, pH 8; 2) 100 mM KPi pH 7; 3) 500mM KPi pH 7; S: supernatant and P: pellet. *Molar Mass of His-CDC25B$_{cd}$ΔSer = 21 kDa.

Then, we checked whether this variant was produced, at least partially, as a soluble form. Although, the protein is almost entirely retrieved in the insoluble fraction irrespective of the buffer used, as illustrated in Figure 48, we first tried to perform the purification from the soluble fraction. His-CDC25B$_{cd}$ΔSer produced in *E. coli* Tuner (DE3) cells using a pET28a-CDC25B$_{cd}$ΔSer vector was purified after a three-step procedure: (1) cell lysis by sonication to recover the enzyme in the soluble fraction, (2) Ni-Sepharose affinity chromatography, and (3) Q-Sepharose anion exchange chromatography. This protocol yielded approximately 1 mg/L of culture of purified His-CDC25B$_{cd}$ΔSer. A table summarizing the purification steps and the SDS-PAGE analysis used to monitor the enzyme's purity is presented in Figure 49.

A

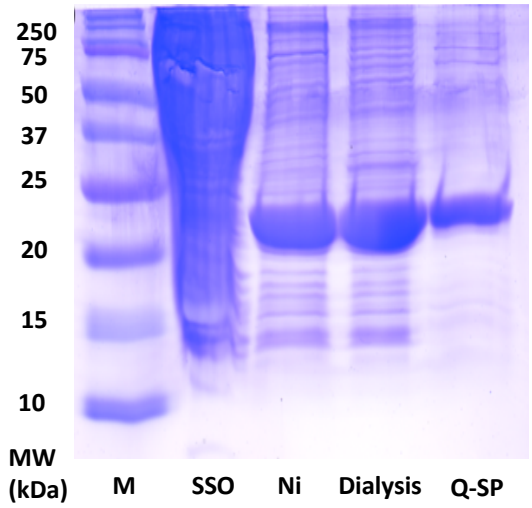

B

Steps	Volume	OD_{280}	OD_{260}	Ratio
SSO	92 mL	20.6	30.7	0.67
Ni-Sepharose	15mL	3.6	3.4	1.14
Q-Sepharose	26 mL	0.3	0.15	2

Figure 49: Purification of His-CDC25B$_{cd}$ΔS from the soluble fraction.
A) 15% SDS-PAGE analysis of the different steps of purification. MW, M: marker, SSO: sonication supernatant, Ni: eluate of the Ni-Sepharose column, Dialysis: dialysis of the Ni fraction to eliminate imidazole, Q-SP: eluate of the Q-Sepharose column. B) Summary table of the steps used to purify His-CDC25B$_{cd}$ΔSer. The enzyme was produced in *E. coli* Tuner (DE3) transformed with pET28a- CDC25B$_{cd}$ΔSer and grown in 4 L LB/K overnight at 20°C after 0.2 mM IPTG induction. Prior storage at -80°C, purified enzymatic solution was concentrated by ultrafiltration to 150 µM with a significant loss of proteins (yield of 60 %). *Molar Mass of His-CDC25B$_{cd}$ΔSer = 21 kDa.

We managed to purify this variant but its purity grade revealed by the electrophoretic profile (Figure 49 lane Q-SP) cannot be considered as sufficient to perform kinetic experiments. Thus, we decided to perform the purification from the sonication pellet using the procedure already depicted for EX-MUT-TSTD1 (page 69). First, we tried to define which buffer provides the best results (Figure 50).

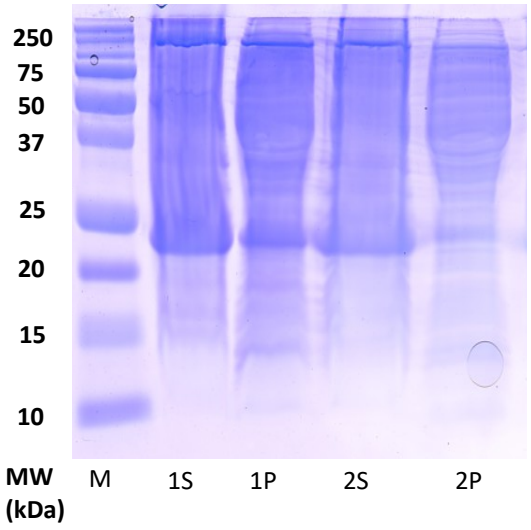

Figure 50: His-CDC25B$_{cd}$ΔSer resolubilization tests from the insoluble form.
1: 50 mM Tris-HCl, 2 mM EDTA, pH 8; 2: 500 mM KPi, pH 7. S: supernatant and P: pellet. *Molar Mass of His-CDC25B$_{cd}$ΔSer = 21 kDa.

The purification protocol from the insoluble fraction is identical to that used for the soluble part, except for the post-sonication steps. Following sonication, the pellet was solubilized using 6 M urea, 10 mM DTT, and TE buffer. This was followed by serial dialysis steps against buffer containing 3 M urea for 2 hours and 0 M urea overnight (Figure 51).

A

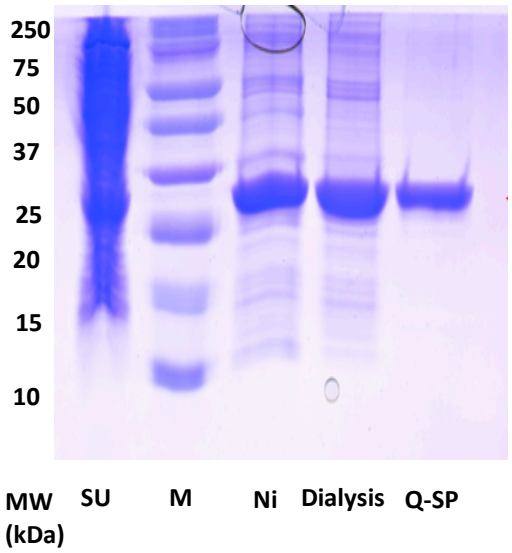

B

Steps	Volume	OD_{280}	OD_{260}	Ratio
SU	62 mL	28.6	48.6	0.54
Ni-Sepharose	15 mL	2.23	2.1	1.06
Q-Sepharose	16 mL	0.18	0.76	2.43

Figure 51: Purification of His-CDC25B$_{cd}$ΔSer from the insoluble fraction.
A) 15 % SDS-PAGE analysis of the different steps of purification. MW, M: marker, SU: supernatant after urea denaturation and refolding by dialysis, Ni: eluate from Ni-Sepharose column, Dialysis: dialysis of the Ni fraction to eliminate imidazole, Q-SP: eluate from the Q-Sepharose column. B) Summary table of the steps used to purify His- CDC25B$_{cd}$ ΔSer. The enzyme was produced in *E. coli* Tuner (DE3) transformed with pET28a- CDC25B$_{cd}$ ΔSer and grown in 4 L LB/K overnight at 20°C after 0.2 mM IPTG induction. Prior storage at -80°C, purified enzymatic solutions was concentrated by ultrafiltration to 300 µM with a significant loss of proteins leading to a yield of 1 mg / L of culture. *Molar Mass of His-CDC25B$_{cd}$ΔSer = 21 kDa.

4- EX-MUT-CDC25B$_{cd}$

Site-directed mutagenesis was performed to exchange the CDC25B$_{cd}$ catalytic loop by the shorter one issued from TSTD1 thus producing the pET28a-EX- MUT- CDC25B$_{cd}$ plasmid. Again, the production of the variant was first assayed using various protocols i.e. different strains, IPTG concentrations and incubation temperatures. Analysis of bacterial crude extracts on 15 % SDS-PAGE showed that growing the BL21 (DE3) or Tuner (DE3) cells at 37°C for 3h after IPTG induction are the best conditions to obtain significant amount of protein (Figure 52 lanes 2,3, 5 & 6).

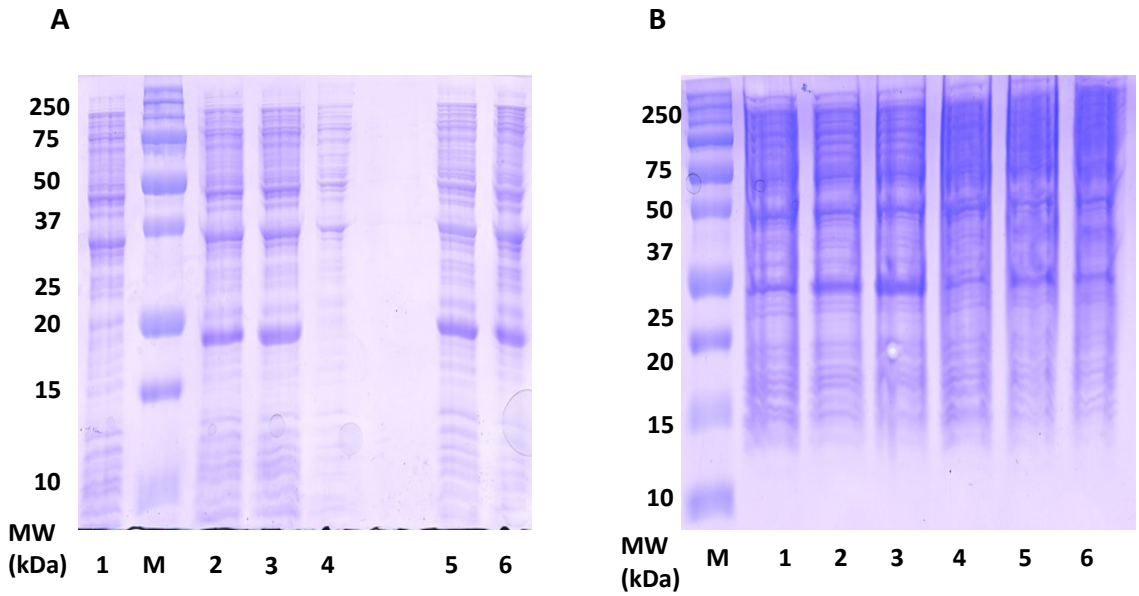

Figure 52: EX-MUT-CDC25B$_{cd}$ overexpression tests using classic LB protocol.
A) 3 h culture : 1 : 0.2 mM IPTG BL21(DE3) 20°C; 2: 0.2 mM IPTG BL21(DE3) 37°C; 3: 1 mM IPTG BL21(DE3) 37°C; 4: 0.2 mM IPTG Tuner (DE3) 20°C; 5: 0.2 mM IPTG Tuner (DE3) 37°C ; 6: 1mM IPTG Tuner (DE3) 37°C.
B) Overnight culture : 1 : 0.2 mM IPTG BL21(DE3) 20°C; 2: 0.2 mM IPTG BL21(DE3) 37°C; 3: 1 mM IPTG BL21(DE3) 37°C; 4: 0.2 mM IPTG Tuner (DE3) 20°C; 5: 0.2 mM IPTG Tuner (DE3) 37°C; 6: 1 mM IPTG Tuner (DE3) 37°C .
*Molar Mass of EX-MUT-CDC25B$_{cd}$= 21 kDa.

Then, the solubility of this variant was evaluated by SDS-PAGE analysis using different sonication buffers. As shown on Figure 53, the protein is detected but almost entirely in the insoluble fraction as already observed for His-CDC25B$_{cd}$ΔSer, and in high amount except when 500 mM KPi is used (lanes 4S & 4P).

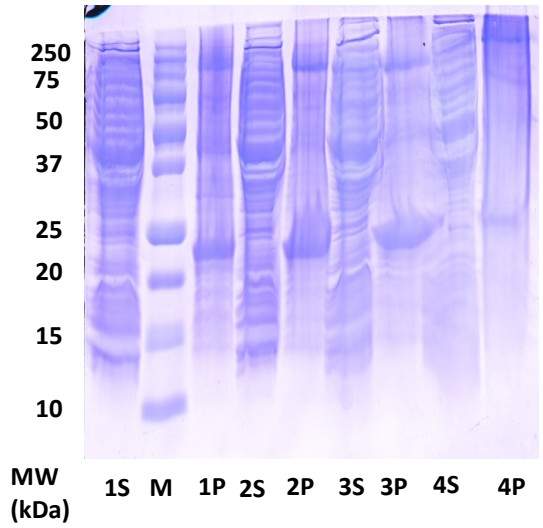

Figure 53: EX-MUT-CDC25B$_{cd}$ solubility tests using different buffers.
1: 50mM Tris-HCl, 2 mM EDTA, pH 8; 2: 50 mM KPi, pH 7.0, 3: 100 mM KPi, pH 7.0; 4: 500 mM KPi, pH 7.0; S: Supernatant and P: pellet.
*Molar Mass of EX-MUT--CDC25B$_{cd}$ = 21 kDa.

Additionally, we decided to perform the purification from the sonication pellet using the procedure already depicted for His-CDC25B$_{cd}$ΔSer (page 76-77). First, we tried to define which buffer provides the best results and as seen on the electrophoretic profile efficient refolding of this variant is only observed with 50 mM Tris-HCl, 2 mM EDTA, pH 8 buffer (Figure 54 Lane 1S).

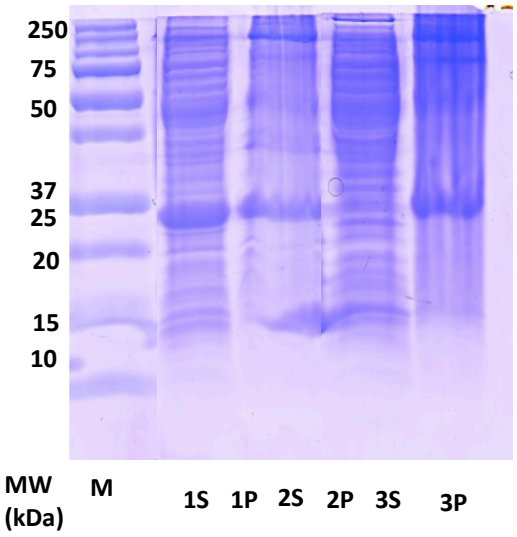

Figure 54: EX-MUT-CDC25B$_{cd}$ resolubilization tests from the insoluble form.
1: 50 mM Tris-HCl, 2 mM EDTA, pH 8; 2: 50 mM KPi, pH 7. S: supernatant and P: pellet.
*Molar Mass of EX-MUT-CDC25B$_{cd}$= 21 kDa.

EX- MUT- CDC25B$_{cd}$ was thus produced in *E. coli* Tuner (DE3) cells transformed by pET28a-EX-MUT- CDC25B$_{cd}$ vector using the classic LB protocol, 0.2 mM IPTG and growth at 37°C for 3 h. The purification protocol consists of four steps: (1) cell lysis by sonication using 50 mM Tris-HCl, 2 mM EDTA, pH 8 to recover the enzyme in the insoluble fraction, (2) suspension of the pellet in 6 M urea, 10 mM DTT, 50 mM Tris-HCl, 2 mM EDTA pH 8 buffer followed by two successive dialysis at 4°C in the presence of decreasing urea concentration (3 and 0 M) in 50 mM Tris-HCl, 2 mM EDTA pH 8 buffer, (3) Ni-Sepharose affinity chromatography and (4) Q-Sepharose anion exchange chromatography. . This protocol allowed to obtain the EX-MUT-CDC25B$_{cd}$ purified to homogeneity (yield approx. 0.2 mg/L of culture). A table summarizing the different steps of purification and the SDS-PAGE used to follow the purity state of the enzyme are presented in Figure 55.

A

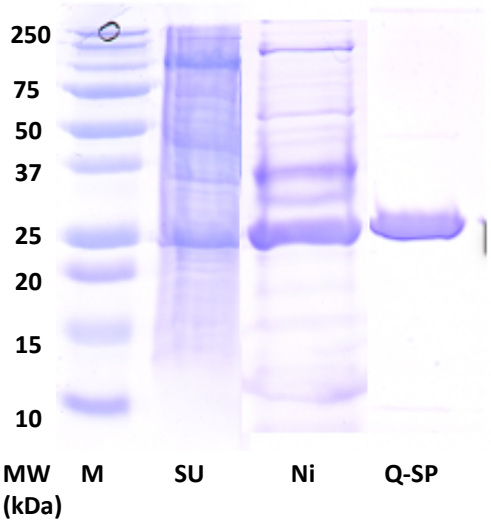

B

Steps	Volume	OD_{280}	OD_{260}	Ratio
SU	82 mL	78.2	105.4	0.74
Ni-Sepharose	28 mL	0.5	0.8	0.62
Q-Sepharose	20 mL	1.9	1.7	1.1

Figure 55: Purification of EX-MUT-CDC25B_{cd} from the insoluble fraction.
A) 15 % SDS-PAGE analysis of the different steps of purification. MW, M: marker, SU: supernatant after urea denaturation and refolding by dialysis, Ni: eluate from the Ni-Sepharose column, Q-SP: eluate from the Q-Sepharose column. B) Summary table of the steps used to purify EX-MUT-CDC25B_{cd}. The enzyme was produced in *E. coli* Tuner (DE3) transformed with pET28a- EX-MUT-CDC25B_{cd} and grown in 4 L LB/K 3 h at 37°C after 0.2 mM IPTG induction. Prior storage at -80°C, purified enzymatic solution was concentrated by ultrafiltration with a 99 % loss of proteins leading to a yield of around 0.01 mg / L of culture. To avoid this protein leakage, purified enzymatic solutions were stored without concentration. *Molar Mass of EX-MUT-CDC25B_{cd}= 21 kDa.

5- Storage concerns for wild-type and mutated CDC25B_{cd}s

Prior storage at -80°C, purified enzymatic solutions were concentrated by ultrafiltration and for all CDC25B_{cd} variants a significant/drastic loss of proteins is observed ranging from 40 to 99 % compared to the yields mentioned in the previous sections. We thus hypothesized that the proteins remain partially stuck on the ultrafiltration unit membrane because no aggregate was observed in concentrated solution. However, it likely reflects the moderate stability of these enzymes that is even more pronounced for thawed samples (i.e. aggregates are observed in solution). LC-ESI-MS experiments were performed to assess their integrity and as shown in Figure 56, a molecular mass of 23405.7 ± 0.1 Da was determined for wild-type His-CDC25B_{cd} in agreement with the theoretical one (23405.6 Da). Unfortunately, no exploitable data was obtained for both variants (data not shown).

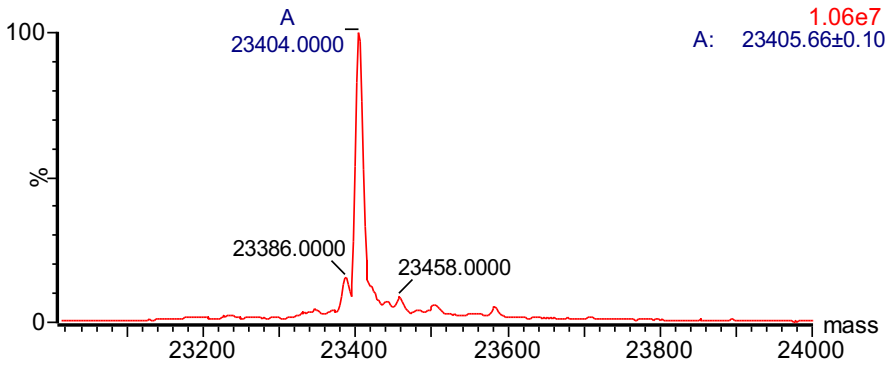

Figure 56: Mass spectrometry spectra of wild-type CDC25B$_{cd}$ by LC-ESI-MS
Distribution of charge states of the proteins by ESI-Q-TOF MS. For analysis, proteins were diluted to 10 µM in H_2O/Acetonitrile/ammonium buffer (50:50:1). The theoretical molecular mass of the protein without the N-terminal Met is 23405,6 Da for CDC25B$_{cd}$.

C) Characterization of the catalytic properties

Characterization focused on the sulfurtransferase, phosphatase and arsenate reductase activities of wild-type and mutated forms of TSTD1 and His-CDC25B$_{cd}$ (hereinafter referred to as CDC25B$_{cd}$).

1- Sulfurtransferase activity

The sulfurtransferase activity was assayed under single turn-over conditions (*i.e*. in the absence of acceptor substrate) to specifically evaluate the capacity of the enzyme to catalyze the sulfur transfer from a donor substrate, *i.e*. 3MP, to its catalytic Cys to form a persulfide intermediate (Figure 57), as already established for wild-type TSTD1 (A-L Claudel thesis, 2022).

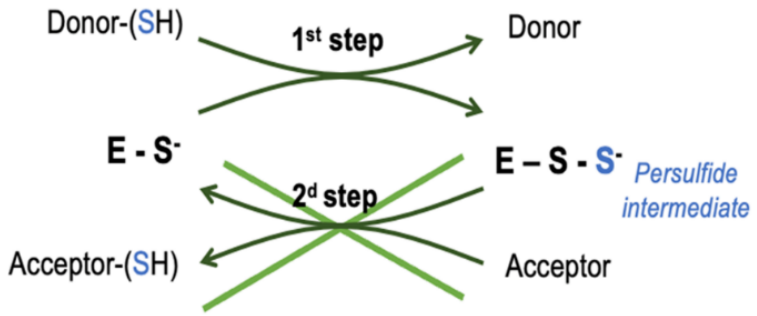

Figure 57: Sulfurtransferase reaction under single turn-over conditions.
The sulfur atom is first transferred from the donor substrate to the thiolate group of the catalytic Cys (E-S$^-$) (1st step) leading to formation of a persulfide intermediate (E-S-S$^-$). In the absence of acceptor substrate, the persulfide intermediate accumulates.

To monitor the sulfur transfer reaction, we took advantage of the change in fluorescence emission intensity of the enzyme Trp residue(s) upon persulfide formation. Because this reaction was expected to be rapid, the kinetic experiments were performed using a SX19-MV stopped-flow under fluorescence mode (Applied Photophysics). One syringe contained the enzyme, the other one the 3MP substrate. After selective excitation of the enzyme Trp residues, the reaction of persulfide formation was monitored using a 320 nm cut-off filter.

1.1 Wild-type and mutated TSTD1s

To check whether a change in the fluorescence properties of the TSTD1 variants occurs in presence of 3MP, emission spectra were recorded before and after substrate addition using Flx-SAFAS® fluorimeter. As already observed for the wild type, an approx. 10 % decrease in fluorescence intensity is measured for both variants (data not shown), suggesting that sulfur transfer still occurs upon 3MP addition.

Kinetic experiments were thus performed at 30°C in 50 mM Tris-HCl, 2 mM EDTA buffer pH 8.0 in the presence of 10 µM enzyme and variable 3MP concentrations (1.5 to 55 mM). A decrease in the fluorescence emission of the enzyme is observed, while no significant change occurs in the absence of 3MP (data not shown). For each 3MP concentration, the biphasic kinetic trace was fitted to an expression combining mono-exponential decay and linear functions (EX-MUT-TSTD1) or a biexponential expression (TSTD1 & TSTD1+Ser) to determine the k_{obs} value of the fast-decreasing phase (Figure 58). Fitting the k_{obs} = f ([3MP]) profile by nonlinear regression analysis to a hyperbola yielded values for the apparent affinity constant for 3MP (K_{3MP}) and for the maximum rate constant associated with the first sulfur transfer step (k_{max}) (Figure 57). Modifying the TSTD1 catalytic loop only led to a 3- to 4.4-fold increase in the K_{3MP} values with no significant change in k_{max}. This moderate impact on the sulfur transfer efficiency is further confirmed when comparing the k_{max} /K_{3MP} ratio that range from 11875 $M^{-1}.s^{-1}$ to 2441 $M^{-1}.s^{-1}$ for TSTD1 and EX-MUT-TSTD1, respectively.

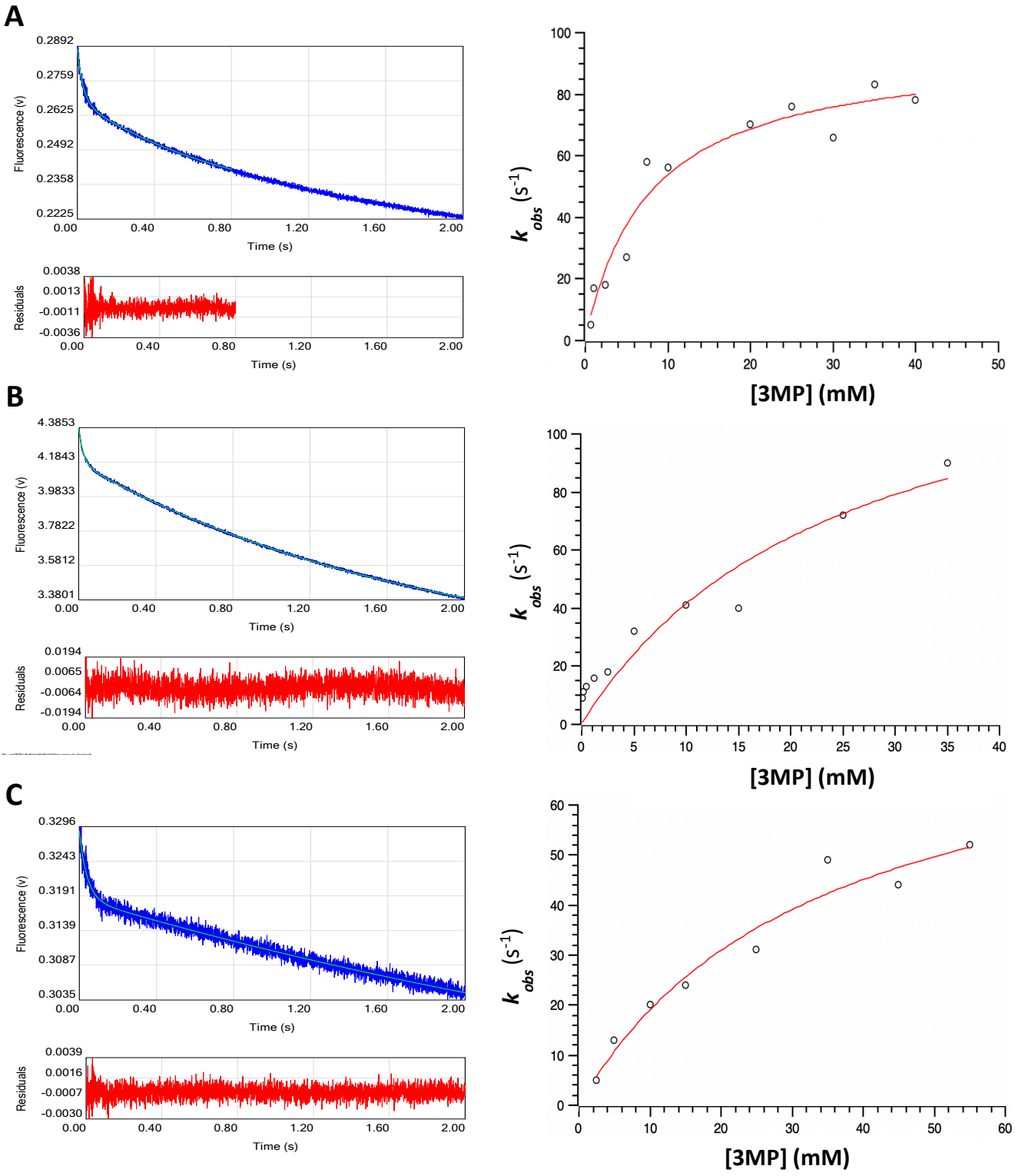

Figure 58: Kinetics of the first step of sulfur transfer under single turn-over conditions catalyzed by TSTD1 (A), TSTD1+Ser (B) and EX-MUT-TSTD1 (C)

Left: Representative data obtained in the presence of 10 mM, 10 mM and 2.5 mM 3MP for TSTD1 (A), TSTD1+Ser (B) and EX-MUT-TSTD1 (C), respectively. Right: **A:** Resulting k_{obs} data (●) were fitted to the equation $k_{obs} = k_{max} * [3MP]/(K_{3MP} + [3MP])$, yielding k_{max} and K_{3MP} values of 95 +/- 8 s^{-1} and 8 +/- 2 mM, respectively; **B:** k_{max} and K_{3MP} , values of 145 +/- 44 s^{-1} and 25 +/- 14 mM, respectively & **C:** k_{max} and K_{3MP}, values of 83 +/- 14 s^{-1} and 34 +/- 12 mM, respectively.

1.2 Wild-type and mutated CDC25B$_{cd}$s

To determine the kinetic parameters of the first step of sulfur transfer from the donor substrate to the enzyme in a similar way to that used for TSTD1s, it was necessary to verify the fluorescence emission properties of the Trp residues of the enzymes. The spectra obtained show that in the presence of 3MP, a 60 % and 80 % decrease in the fluorescence emission signal is observed for His-CDC25B$_{cd}$ and His-CDC25B$_{cd}$ΔSer, respectively, suggesting that 3MP is indeed a donor substrate for these enzymes (Figure 59).

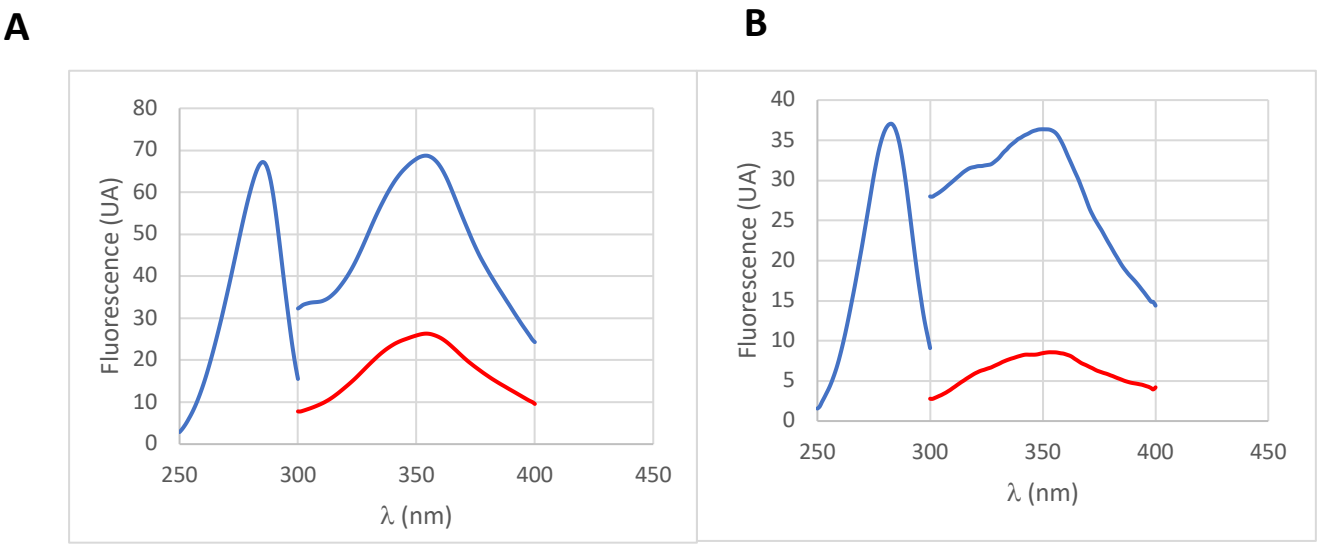

Figure 59: Variation of the fluorescence emission spectra of the Trp residues of His-CDC25B$_{cd}$ (A) His-CDC25B$_{cd}$Δser (B) in the presence (red) or absence (blue) of the sulfur donor substrate 3MP.
Spectra were recorded in the presence of 5 µM enzyme and 1 mM 3MP in 50 mM Tris-HCl, 2 mM EDTA pH 8 at 25 °C. Excitation spectra were obtained using an emission wavelength of 352 nm, while emission intensities were monitored after excitation at 285 nm.

To determine the kinetic parameters of this step, experiments were performed using a SX19-MV stopped-flow (Applied Photophysics) as already depicted for TSTD1 and its variants. One syringe contained the enzyme, the other one the 3MP substrate and after selective excitation of the Trp residues at 285 nm, the reaction of sulfur transfer was monitored using a 320 nm cut-off filter. In the presence of 2.5 to 10 µM of enzyme and variable concentrations of 3MP (1.5 to 45 mM), a decrease in the fluorescence emission of the enzyme is observed, while no significant decrease in the fluorescence emission is observed in the absence of 3MP. For each 3MP concentration, the traces were clearly biphasic and were thus fitted to an expression combining mono-exponential decay and linear functions (EX-MUT-CDC25B$_{cd}$) or a

biexponential expression ($CDC25B_{cd}$ & $CDC25B_{cd}\Delta Ser$) to determine the k_{obs} value of the fast-decreasing phase (Figure 60). For $CDC25B_{cd}$, fitting the k_{obs} = f ([3MP]) profile by nonlinear regression analysis to a hyperbola made possible the determination of the values of the apparent affinity constant for 3MP (K_{3MP} = 7.4 ± 1.2 mM) and of the maximum rate constant for the first sulfur transfer step (k_{max} = 101 ± 6 s^{-1}) (Figure 59). In contrast, because no saturation was observed until 45 mM 3MP for both variants, only second order rate constants (k_2) were determined from the linear regressions. These k_2 values were compared to the k_{max} / K_{3MP} obtained for the wild-type, and for $CDC25B_{cd}\Delta Ser$, reducing the loop length led to a 22-fold decrease in catalytic efficiency, while for EX-MUT-$CDC25B_{cd}$, exchanging the loop led to a 8.4-fold decrease. The fact that the k_{obs} value measured at 40 mM 3MP for EX-MUT-$CDC25B_{cd}$ is close to the $CDC25B_{cd}$ k_{max} value (68 s^{-1} vs 101 s^{-1}), it shows that the decreased catalytic efficiency of this variant is not associated to a *k* effect, but probably to a *K* one. The corresponding k_{obs} value for $CDC25B_{cd}\Delta Ser$ is lower (approx. 25 s^{-1}), suggesting that its reduced catalytic efficiency originates from both *k* and *K* effects.

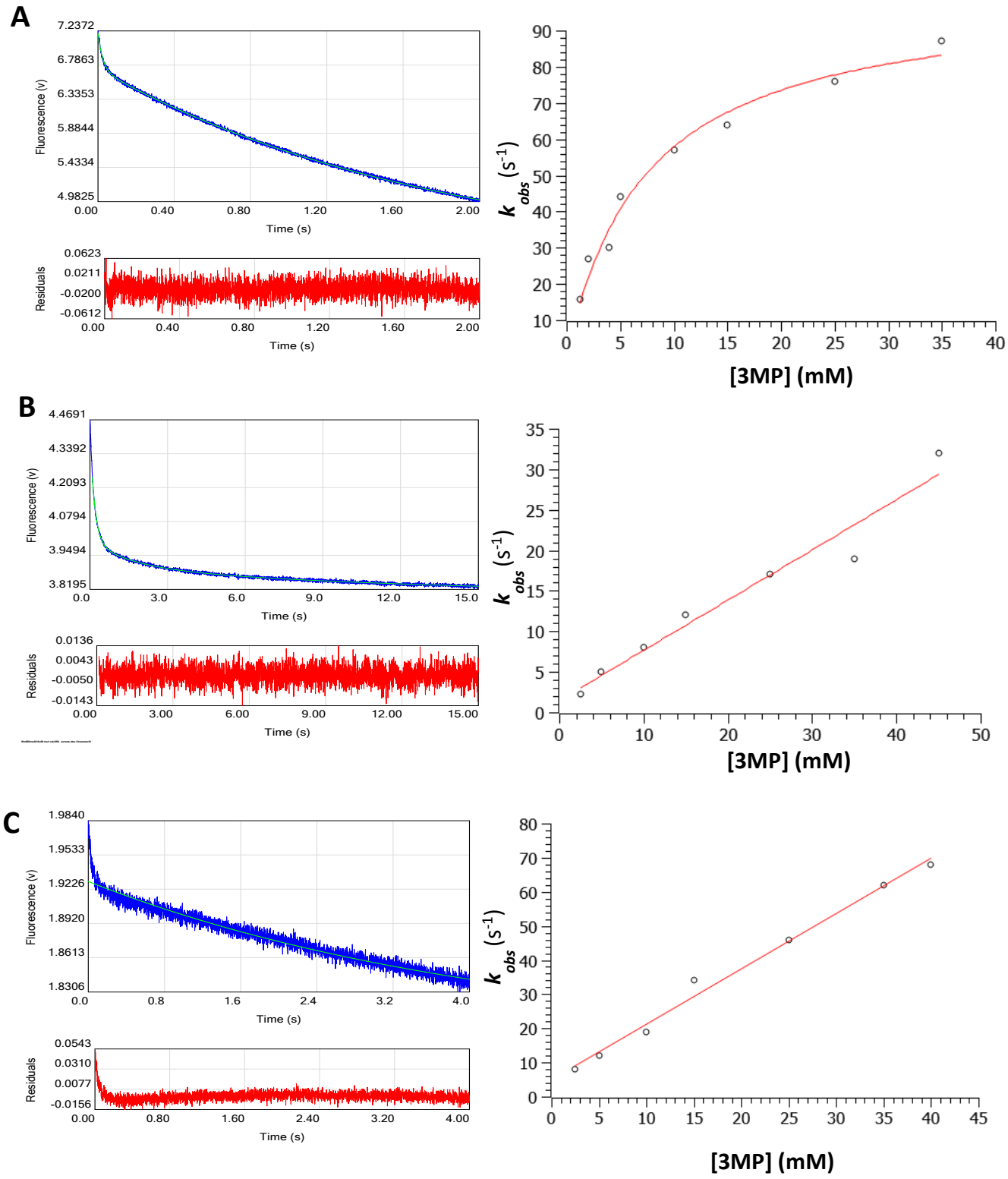

Figure 60: Kinetics of the first step of sulfur transfer under single turn-over conditions catalyzed by $CDC25B_{cd}$ (A) $CDC25B_{cd}$ ΔSer (B) and EX-MUT-$CDC25B_{cd}$ (C).

Left: Representative data obtained in the presence of 10 mM, 25 mM and 2.5 mM 3MP for CDC25Bcd (A) CDC25Bcd ΔSer (B) and EX-MUT-$CDC25B_{cd}$ (C), respectively. Right: A: Resulting k_{obs} data (●) were fitted to the equation $k_{obs} = k_{max} * [3MP]/(K_{3MP} + [3MP])$, yielding k_{max} and K_{3MP} values of 101 ± 6 s^{-1} and 7.4 ± 1.2 mM, respectively, B, C: Resulting k_{obs} data (●) were fitted to a linear equation, yielding a slope value of 620 ± 59 and 1622 ± 71 $M^{-1}.s^{-1}$ for B and C, respectively.

2- Phosphatase activity

2.1 Wild-type and mutated CDC25B$_{cd}$s

Phosphatase activity was assayed under steady-state conditions in the presence of para- nitrophenyl phosphate (pNPP), a classical substrate analog. The hydrolysis of pNPP was followed at 30 °C in 50 mM Tris-HCl, 2 mM EDTA, pH 8 by measuring on a SAFAS UVmc2 spectrophotometer the absorbance at 405 nm of p-nitrophenolate released during the reaction (Figure 61 A). A commercial alkaline phosphatase (1 µM) was used as positive control and in the presence of 25 mM pNPP an increase in absorbance at 405 nm is indeed observed (Figure 61 B).

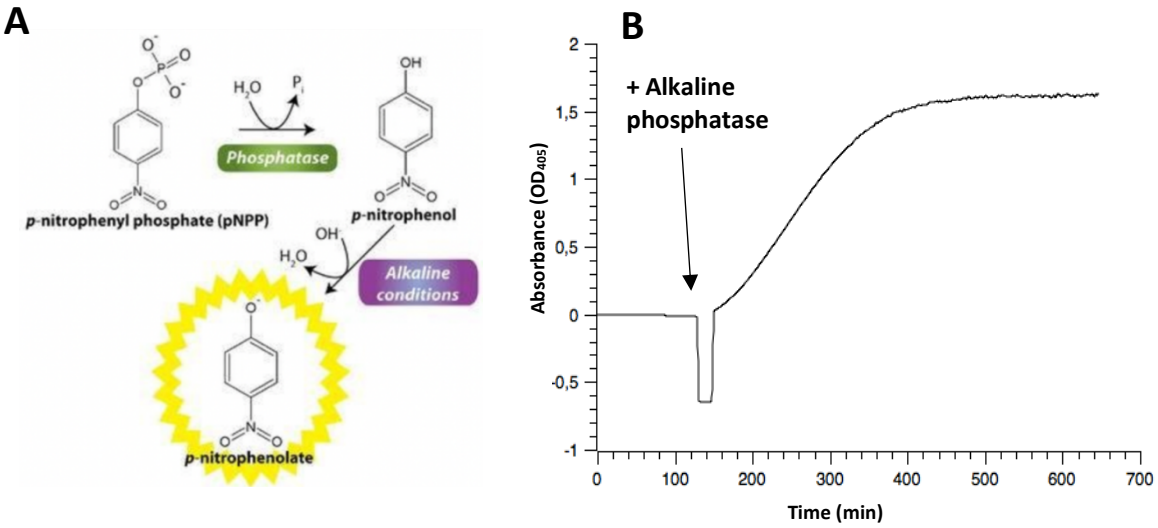

Figure 61: pNPP hydrolysis catalyzed by phosphatases.
A: The reaction leads to formation of para-nitrophenolate which absorbs at 405 nm and monitoring this signal over time allows the determination of initial rates. B: Time course of pNPP hydrolysis catalysed by alkaline phosphatase.

The phosphatase activity of CDC25B$_{cd}$ was evaluated in the presence of 1 µM enzyme and 0.75 to 20 mM pNPP. Corrections were made for spontaneous hydrolysis of the pNPP under the same experimental conditions. For all substrate concentrations tested, an increase in the absorption over time was observed (Figure 62A), proportional to enzyme concentration (i.e. initial rate conditions, data not shown). Experimental data were fitted to the Michaelis–Menten equation using non-linear least-squares regression analysis (Figure 61A) yielding k_{cat} and K_M values of 0.20 ± 0.01 s^{-1} and 1.6 ± 0.2 mM, respectively (Figure 63).

As expected, these parameters are consistent with those already published ($k_{cat} \approx 0.3\ s^{-1}$ and $K_M \approx 9$ mM, Bhattacharjee *et al*., 2010).

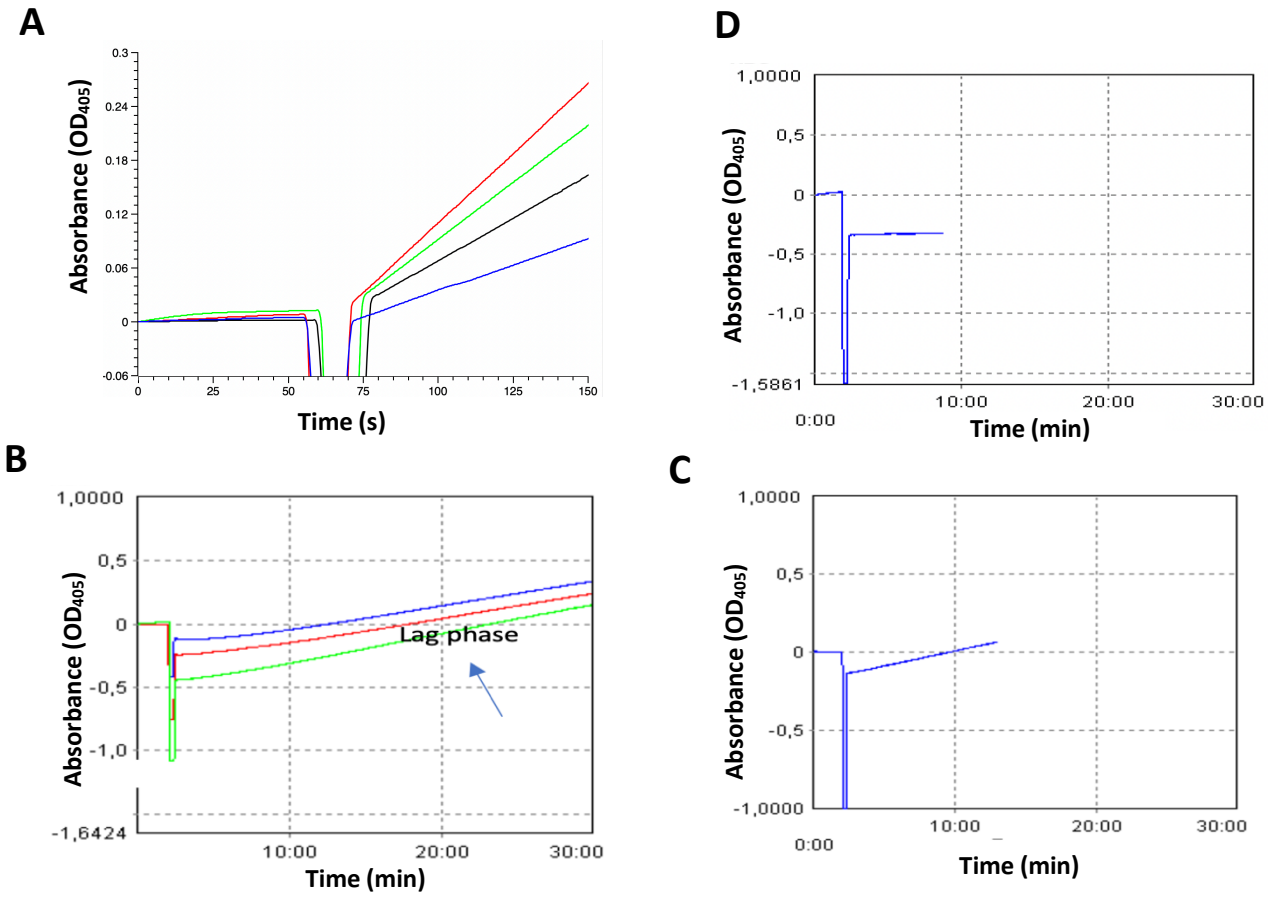

Figure 62: Kinetic assays for the phosphatase activity of CDC25B$_{cd}$ (A), CDC25B$_{cd}$ΔSer (B, C) and EX-MUT- CDC25B$_{cd}$ (D)

Representative data obtained for various pNPP concentrations. Spontaneous pNPP hydrolysis was monitored and then enzyme was added to measure initial velocity. (A) Representative data obtained for 1 µM CDC25B$_{cd}$ in presence of 2.5 to 10mM of pNPP. (B) Representative data obtained with 30 µM CDC25B$_{cd}$ΔSer in presence of 5, 10 and 30 mM of pNPP with a 10 min lag phase. (C) Data observed in the presence of 5 mM pNPP after preincubation of 30 µM CDC25B$_{cd}$ΔSer with 500 mM KPi buffer pH 7 during 20 min at room temperature. (D) Data obtained for 60 µM EX-MUT-CDC25B$_{cd}$ in the presence of 200 mM pNPP.

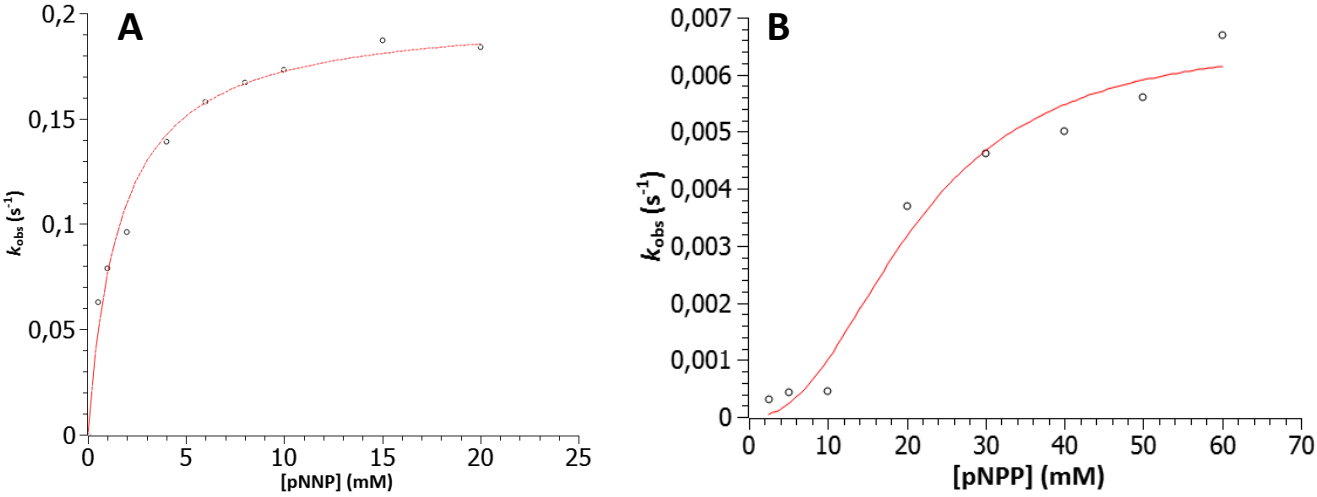

Figure 63: Kinetic assays for the phosphatase activity of CDC25B$_{cd}$ (A) and CDC25B$_{cd}$ΔSer (B)
A: Experimental k_{obs} data (●) were fitted to the equation $k_{obs} = k_{cat}.[pNPP]/(K_M + [pNPP])$, yielding k_{cat} and K_M values of 0.20 ± 0.01 s^{-1} and 1.6 ± 0.2 mM, respectively. B: Experimental k_{obs} data (●) were fitted to the $k_{obs} = k_{cat}.[pNPP]^n/(K_{0.5}^n + [pNPP]^n)$ equation, yielding k_{cat}, $K_{0.5}$ and n values of 0.007 ± 0.001 s^{-1}, 21 ± 4 mM and 2.3 ± 0.7, respectively.

For CDC25B$_{cd}$ΔSer, I used the same conditions but I observed a lag phase whose duration is approx. 10 min in the presence of 5 mM pNPP (Figure 62B). Experimental data were fitted to the Hill equation using non-linear least-squares regression analysis (Figure 63B). Because this sigmoidal profile may rely on conformational changes involving at least the catalytic loop, as already observed for sulfurtransferases (^{h}3-MST, GlpE, Rhodanese), I preincubated the mutant with phosphate buffer to check whether this lag could be eliminated. As shown on Figure 62C, incubation with 500 mM KPi buffer pH 7.0 for 20 min at room temperature is required to fully remove the lag.

In terms of kinetic parameters, reducing the loop length for CDC25B$_{cd}$ΔSer led to a 30-fold decrease in k_{cat}. For EX-MUT-CDC25B$_{cd,}$ no increase in the absorption over time was observed up to 60 µM of enzyme and 200 mM of pNPP (Figure 62D), showing that exchanging the loop abolishes the phosphatase activity.

2.2 Wild-type and mutated TSTD1

The phosphatase activity of wild-type and mutated TSTD1s was also evaluated in the presence of 1 to 60 µM of enzyme and 25 to 200 mM of pNPP. No increase in the absorption over time was observed which means that wild-type and mutated TSTD1s have no detectable phosphatase activity (data not shown). These results could show that 1) TSTD1 displays no promiscuous phosphatase activity even in the presence of a longer catalytic loop, or 2) pNPP is a poor substrate. To discriminate between these hypotheses, phosphatase activity was tested in the presence of another artificial substrate, the 4-methylunbelliferyl phosphate (4-MUP) (Figure 63).

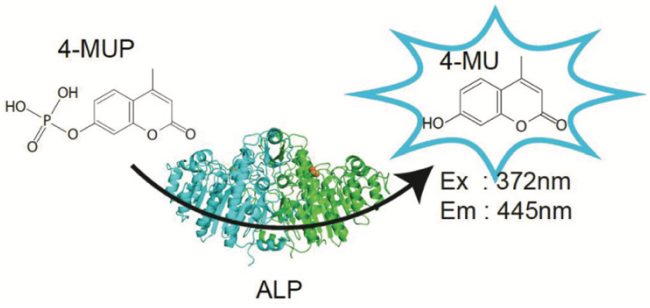

Figure 64: 4-MUP hydrolysis catalyzed by alkaline phosphatase (ALP). While 4-MUP is non-fluorescent, the 4-MU product is fluorescent.

4-MUP assays were realized under steady-state conditions. Hydrolysis of 4-MUP to 4-methylunbelliferon (4-MU, fluorescent) and inorganic phosphate was followed by fluorescence emission at 445 nm wavelength (excitation: 372 nm) in 50 mM borate, 1 M $MgSO_4$ buffer, pH 9.3 on a SAFAS Xenius fluorimeter. $CDC25B_{cd}$ was used as positive control and in the presence of 0.1 mM 4-MUP and 1 µM of enzyme, an increase in fluorescence emission is indeed observed (Figure 65A). The phosphatase activity of wild-type and mutated TSTD1s was evaluated in the presence of 50 µM of enzyme and 0.1 mM of 4-MUP. In all cases, no increase in the fluorescence emission over time was observed, showing that wild-type and mutated TSTD1s have no detectable phosphatase activity with 4-MUP (A representative data obtained for TSTD1 is presented in figure 65B). Moreover, comparable result was observed for EX-MUT-$CDC25B_{cd}$ up to 50 µM of enzyme.

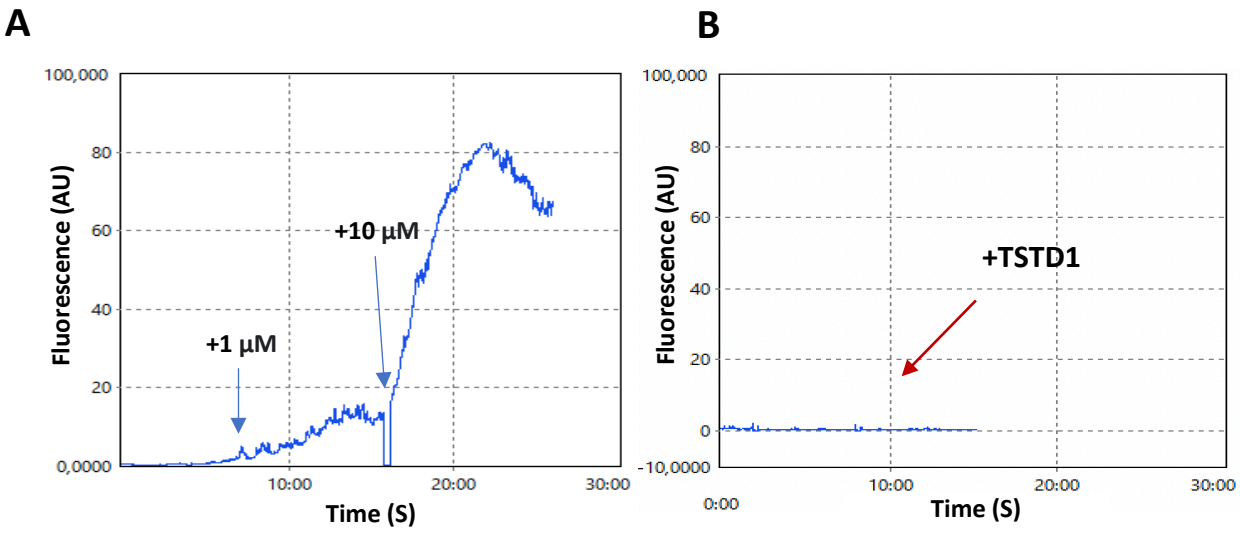

Figure 65: Kinetic assays for the phosphatase activity with 4-MUP substrate of CDC25B$_{cd}$ (A) and TSTD1 (B). Data obtained in the presence of 0.1 mM 4-MUP. A: Spontaneous 4-MUP hydrolysis was measured and then CDC25B$_{cd}$ (1 µM, and after 10 µM) was added to measure initial velocity. B: Spontaneous 4-MUP hydrolysis was measured and then 50 µM TSTD1 was added.

3- Arsenate reductase

The first goal was to set up an activity test based on the protocol described by Gladysheva *et al*. (1994). The strategy consisted in using: 1) sodium arsenate and glutaredoxin (GRX) / glutathione (GSH) as substrates, 2) a coupled assay with NADPH and glutathione reductase (GR) for detection, and 3) the *E. coli* arsenate reductase (ArsC) as positive control.

3.1 Production and purification of ArsC

To produce ArsC in *E. coli* cells, a pET28a-ArsC vector allowing the production of the enzyme fused with an His tag at the N-terminus has been designed and purchased from Genscript®. The production was first assayed using various classical protocols i.e. different strains (BL21(DE3) and C41(DE3)) and incubation temperature (20°C and 37 °C) after induction in the presence of 0.2 mM IPTG. Cells pellets, obtained after overnight incubation, were resuspended in 50 mM Tris-HCl, 2 mM EDTA, pH 8 buffer before sonication and centrifugation to separate soluble and insoluble fractions. As shown on Figure 66, the protein is detected almost entirely in the soluble fraction and in high amount whatever the strain and temperature used.

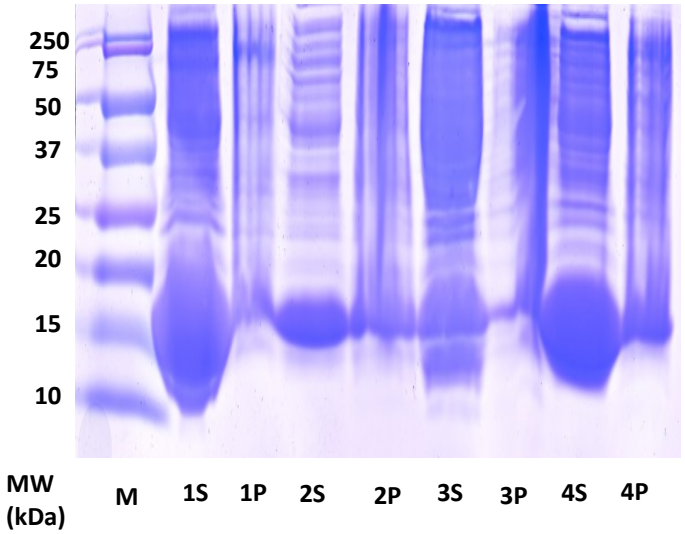

Figure 66: ArsC overexpression tests
1: BL21(DE3) 20°C; 2: BL21(DE3) 37°C; 3: C41(DE3) 20°C; 4: C41(DE3) 37°C. S: Supernatant and P: pellet. *Molar Mass of ArsC= 17.9 kDa.

Based on these data, arsenate reductase was produced in *E. coli* BL21 (DE3) cells using the pet28a-ArsC vector. The protocol for purification consists of three steps: (1) cell lysis by sonication to recover the enzyme in the soluble fraction, (2) Ni-Sepharose affinity chromatography, and (3) Q-Sepharose anion exchange chromatography. This protocol allowed to obtain the enzyme purified to homogeneity (yield approx. 7 mg/L of culture). A table summarizing the different steps of purification and the SDS-PAGE used to follow the purity state of the enzyme are presented in (Figure 67).

A

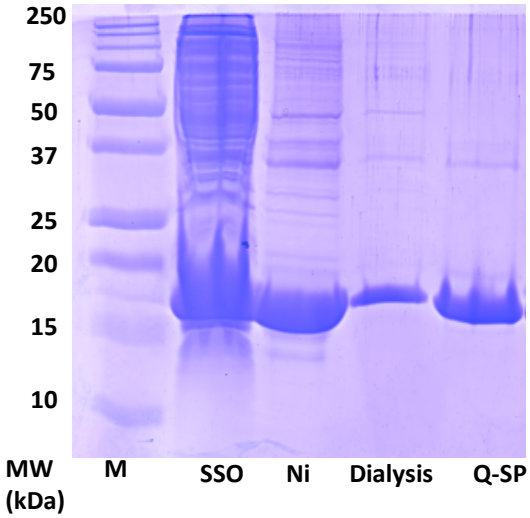

B

Steps	Volume	OD_{280}	OD_{260}	Ratio
SSO	99 mL	120	206	0.57
Ni-Sepharose	19 mL	1.00	0.86	1.1
Q-Sepharose	30 mL	0.19	0.12	1.5

Figure 67: Purification of Ars C
A) 15% SDS-PAGE analysis of the different steps of purification. MW, M: marker, SSO: sonication supernatant, Ni: eluate of the Ni-Sepharose column, Dialysis: Dialysis: dialysis of the Ni fraction to eliminate imidazole, Q-SP: eluate of the Q-Sepharose column. B) Summary table of the steps used to ARsC. The enzyme was produced in *E. coli* BL21(DE3) transformed with pET28a-ArsC and grown in 4

L LB/K overnight at 20°C after 0.2 mM IPTG induction. Prior storage at -80°C, purified enzymatic solution was concentrated by ultrafiltration to 400 µM with no significant loss of proteins. *Molar Mass of ArsC= 17.9 kDa.

3.2 Kinetics with ArsC

Arsenate activity was assayed under steady-state conditions in the presence of 5 mM sodium arsenate as substrate, 30 mM NADPH, 4 mM glutathion (GSH), 85 nM glutathione reductase (GR), 1.5 µM glutaredoxine (GRX), in 50 mM Tris-HCl, 2 mM EDTA buffer, pH 8. Arsenate reduction coupled to NADPH oxidation was monitored by following at 30°C the decrease in absorbance at 340 nm (ε = 6220 $M^{-1}.cm^{-1}$) using a SAFAS UVmc2 spectrophotometer. The kinetic experiments were performed in the presence of 10 µM enzyme and variable concentrations of arsenate (5 to 35 mM). Fitting the profile k_{obs} = f ([substrate]) to linear equation yielded k_2 value of 3.8 $M^{-1}.s^{-1}$ (Figure 68).

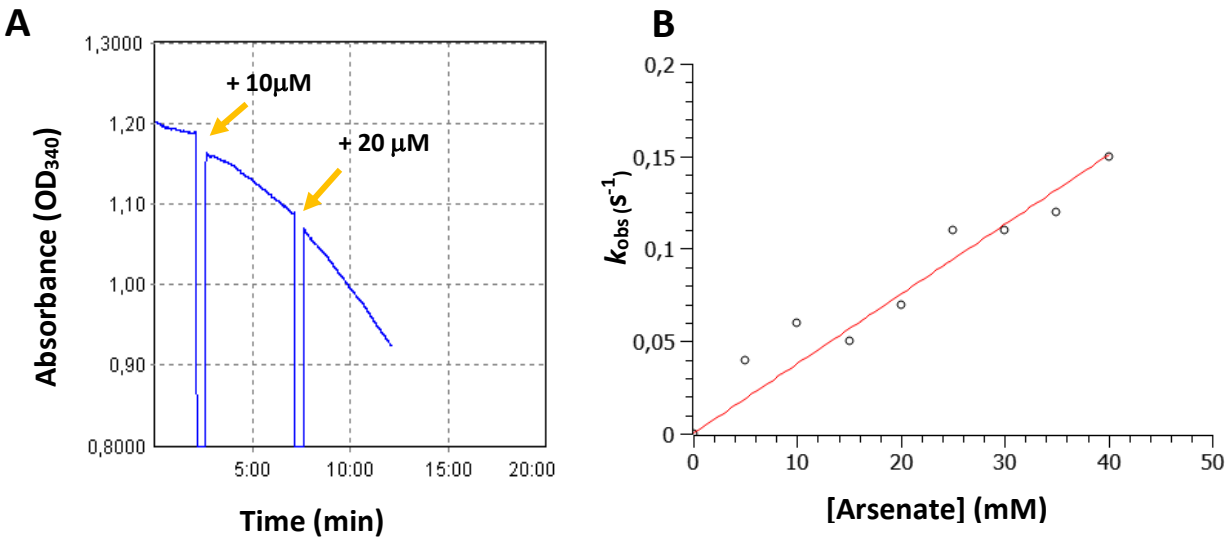

Figure 68: Kinetic assays for the arsenate reductase activity of ArsC.
A: Representative data obtained for various ArsC concentrations. Background signal due to the coupled assay was measured (P0) and then ArsC (10 µM(P1) then 20 µM(P2)) was added. Observed slope values: P0 = 0.006, P1 = 0.016, P2 = 0.032 ΔDO/min. B: Resulting k_{obs} data (●) obtained with 10 µM ArsC were fitted to a linear equation, yielding a slope value of 3.8 ± 0.2 $M^{-1}.s^{-1}$.

3.3 Kinetics with wild-type and mutated $CDC25B_{cd}S$

The arsenate activity was evaluated in the presence of 10 µM enzyme and variable concentrations of arsenate (5 to 50 mM). For $CDC25B_{cd}$ and $CDC25B_{cd}$ΔSer, a decrease in the absorption over time was observed (Data not shown) allowing determination of the observed

rate constant (k_{obs}). For $CDC25B_{cd}$, experimental data were fitted to the Michaelis–Menten equation using non-linear least-squares regression analysis yielding k_{cat} and K_M values of 0.09 ± 0.02 s^{-1} and 15 ± 12 mM, respectively (Figure 69A). For $CDC25B_{cd}\Delta Ser$, experimental data were fitted to the Hill equation using non-linear least-squares regression analysis yielding k_{max}, K_M and n values of 0.12 ± 0.03 s^{-1}, 38 ± 6 mM and 3.7 ± 0.9, respectively (Figure 69 B). For EX-MUT-$CDC25B_{cd}$, no decrease in the absorption over time was observed up to 40 mM of arsenate (Figure 69 C).

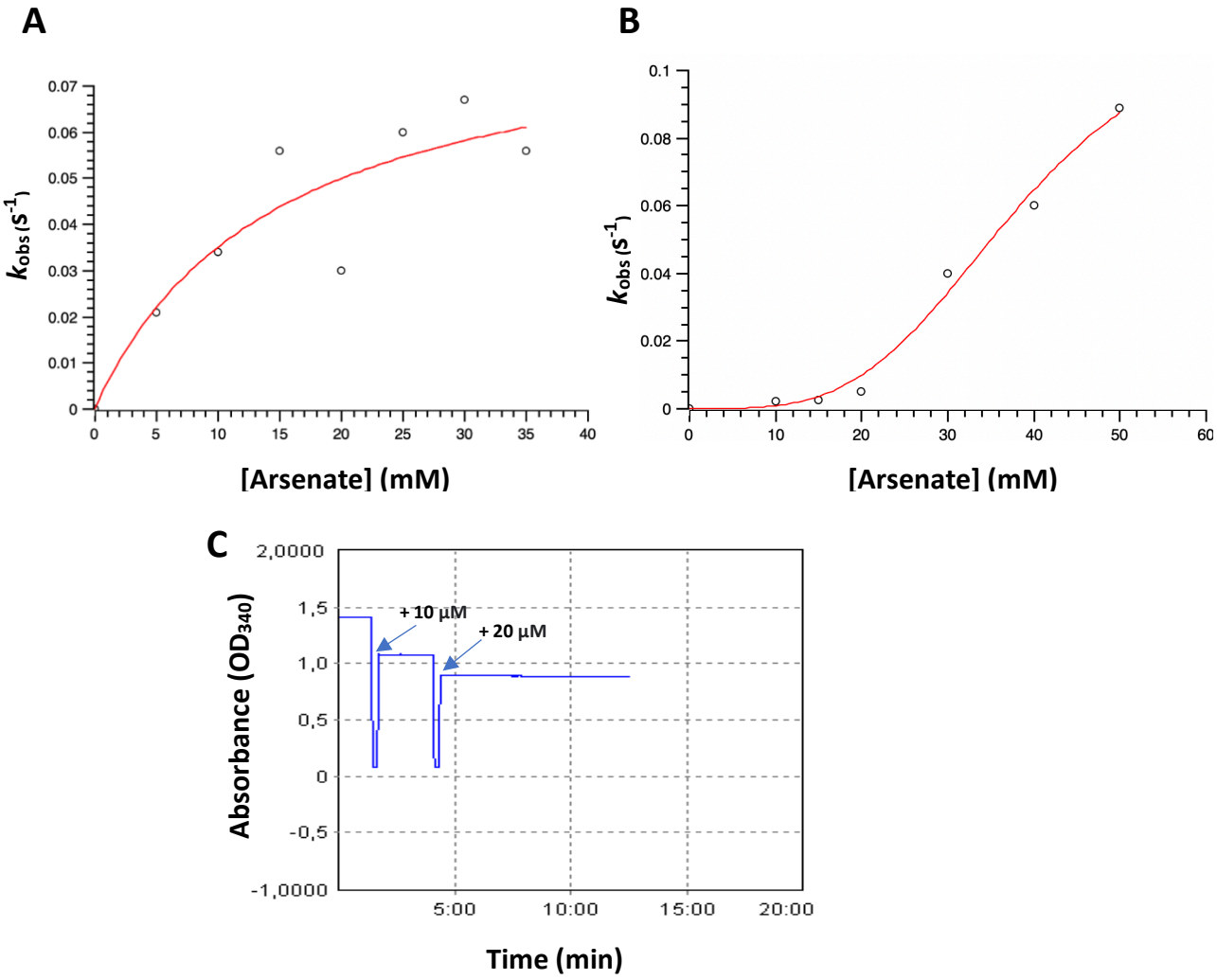

Figure 69: Kinetics assays for the arsenate reductase activity of $CDC25B_{cd}$ (A), $CDC25B_{cd}\Delta Ser$ (B), and EX-MUT-$CDC25B_{cd}$ (C).
A: Resulting k_{obs} data (○) were fitted to the equation $k_{obs} = k_{max}.[arsenate]/(K_M + [arsenate])$, yielding k_{max} and K_M values of 0.09 ± 0.02 s^{-1} and 15 ± 12 mM, respectively. B: k_{obs} data (○) were fitted to the Hill equation yielding k_{max}, $K_{0.5}$ and n values of 0.12 ± 0.03 s^{-1}, 38 ± 6 mM and 3.7 ± 0.9 , respectively. C: Representative data obtained for various EX-MUT-$CDC25B_{cd}$ concentrations. Background signal due to the coupled assay was measured (P_0) and then EX-MUT-$CDC25B_{cd}$ (10µM (P_1) then 20µM (P_2)) was added. Observed slope values: P_0 = 0.004, P_1 = 0.001, P_2 = 0.0004 DOD/min.

The k_{max}/K_M value of $CDC25B_{cd}$ is comparable to the k_2 value determined under the same conditions for ArsC (5.8 vs 3.8 $M^{-1}.s^{-1}$), suggesting that $CDC25B_{cd}$ is a good arsenate reductase. In terms of kinetic parameters, reducing the loop length for $CDC25B_{cd}\Delta$Ser had no significant impact on k_{cat} (0.09 vs 0.12 s^{-1}). Finally, exchanging the loop abolishes the arsenate activity.

3.4 Kinetics with wild-type and mutated TSTD1s

The arsenate activity was evaluated in the presence of 10 µM enzyme and variable concentrations of arsenate (5 to 50 mM). For all TSTD1s, no decrease in the absorption over time was observed up to 40 mM of arsenate (data not shown).

Axis 2:

This axis focused on the characterization of substrate specificity of MOCS3-Rhd, which implied first to obtain this domain under soluble form and in great amount. For this, the strategy was to produce two forms: 1) a 193 amino acid long form corresponding to the domain produced in Matthies *et al.*, 2004 named MOCS3 303, and 2) a shorter 161 amino acid long form corresponding to the MOCS-Rhd domain describe in the pdb 3i2v file named MOCS3 335 (Figure 69).

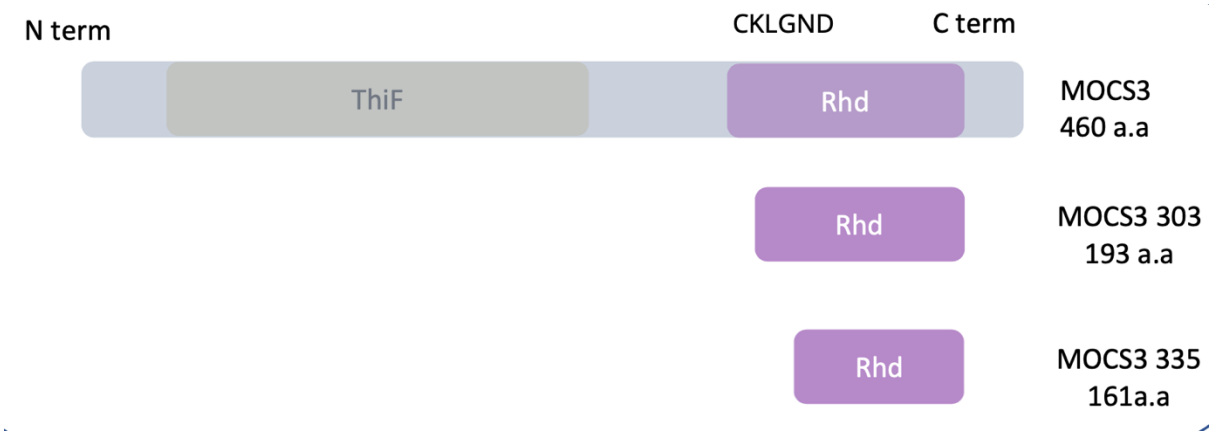

Figure 70: Schemes of MOCS3 and the two desired constructs.

In the following section, I will successively present results concerning the construction of the vectors and the production and purification of the MOCS3 303 and MOCS3 335.

1- Construction of the expression vectors

To produce the two forms of MOCS3-Rhd, we developed a subcloning strategy consisting in introducing the sequences encoding the MOCS3 303 and MOCS3 335 forms into the pET28a plasmid, enabling the addition of a His6 tag. For that, the coding sequence of the human MOCS3 303 and MOCS3 335 were PCR-amplified from the synthetized commercial plasmid purchased at Genescript® (https://www.genscript.com/). PCR products were separated on 1 % agarose gel and purified (Figure 71A). PCR amplified DNAs were inserted in a pET28a plasmid between unique *BamH*1 and *Xho*1 restricted site to generate pET28a-MOCS3 303 and pET28a-MOCS3 335 vectors. Presence of the inserts was confirmed by *Nde*1/*Xho*1 digestion (Figure 71B). Finally, the absence of unwanted mutations in the coding sequences was validated by sequencing.

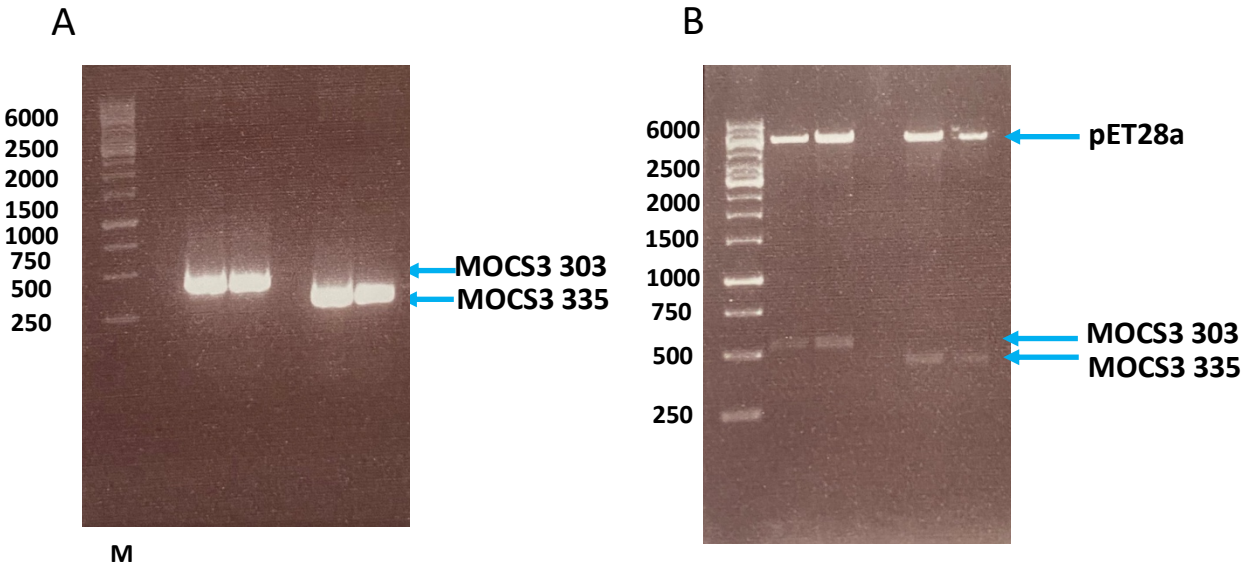

Figure 71: Electrophoretic profiles on 1% agarose gels of PCR products (A) and digested plasmids (B)
A: Expected product sizes were 480 bp for MOCS3 303 and 384 bp for MOCS3 335. B: Expected product sizes were 525 bp for MOCS3 303 and 429 bp for MOCS3 335, corresponding to the coding sequence with the polyHis tag. M: size marker.

2- Tests production of MOCS3 303 and MOCS3 335

MOCS3-Rhds production was first evaluated using the classical protocol with BL21(DE3), 0.1 mM IPTG and 3 hours or overnight incubation at 37°C or 20°C. Analysis of bacterial crude extracts on SDS-PAGE showed that production was obtained in all conditions (Figure 72).

Before commencing with the purification, the solubility state of the produced proteins was evaluated. Analysis of insoluble and soluble fractions was realized by SDS-PAGE after sonication and centrifugation to evaluate the solubility of the protein in 50 mM Tris-HCl, 2 mM EDTA, pH 8 buffer. As evidenced by the electrophoretic profile presented in figure 73, MOCS3 303 was only partially soluble and MOCS3 335 was almost entirely in the insoluble fraction.

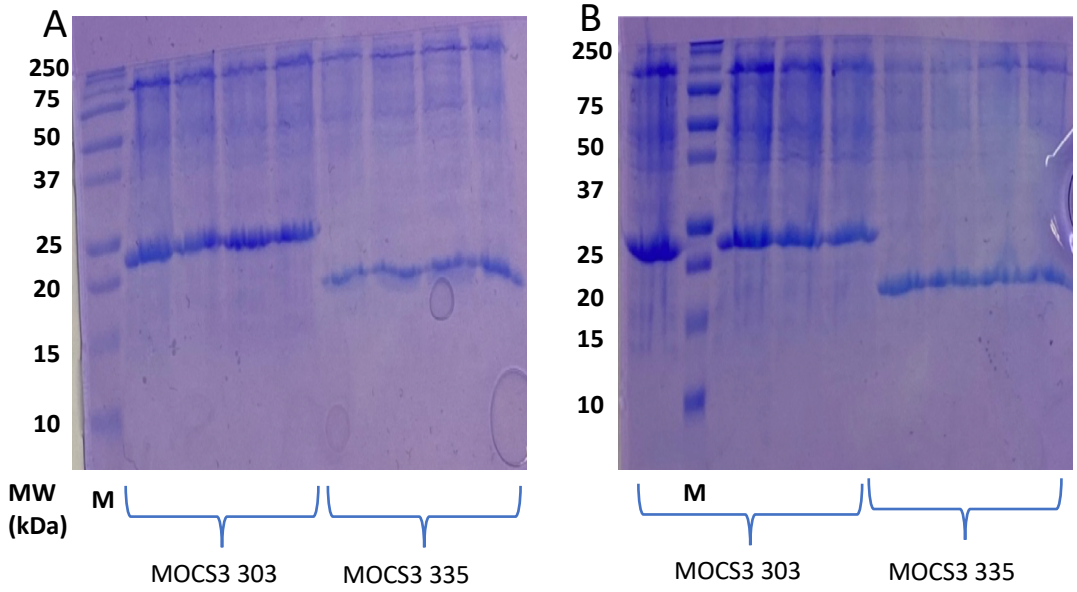

Figure 72: Overexpression for MOCS3 303 and MOCS3 335.
Expression tests were realized in BL21(DE3) with the classical LB protocol and 0.1 mM IPTG for 3 hours (A) or overnight (B). 1,2,3&4: 37°C; 5,6,7&8:20°C. *Molar Mass of MOCS3 303= 21 kDa. & Molar Mass of MOCS3 335= 17 kDa.

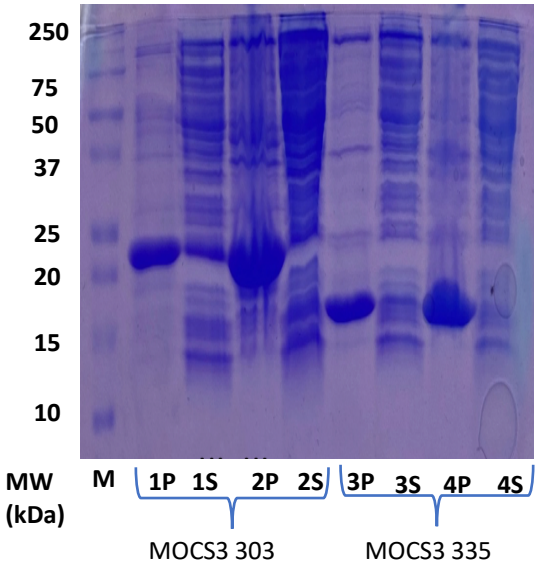

Figure 73: Solubility tests for MOCS3 303 and MOCS3 335.
Cells pellets from cultures at 37°C were resuspended in 50 mM Tris-HCl, 2 mM EDTA, pH 8 buffer, and sonicated before centrifugation. 1: MOCS3 303 after 3 H, 2: MOCS3 303 overnight, 3:

MOCS3 335 after 3 H, 2: MOCS3 335 overnight. S: supernatant and P: pellet. Molar Mass of MOCS3 303= 21 kDa. & Molar Mass of MOCS3 335= 17 kDa.

3- Production and purification of MOCS3 303

MOCS3 303 was produced in *E. coli* BL21 (DE3) cells using the pET28a-MOCS3 303 vector which permits the production of the enzyme fused with a polyHis tag at the N-terminus. The recombinant enzyme being partly soluble, we designed a purification protocol consisting in three steps: (1) cell lysis by sonication to recover the enzyme in the soluble fraction, (2) Ni-Sepharose affinity chromatography, and (3) Q-Sepharose anion exchange chromatography. This protocol allowed to obtain the MOCS3 303 purified to homogeneity (yield approx. 6 mg/L of culture). A table summarizing the different steps of purification and the SDS-PAGE used to follow the purity state of the enzyme are presented in figure 74.

A

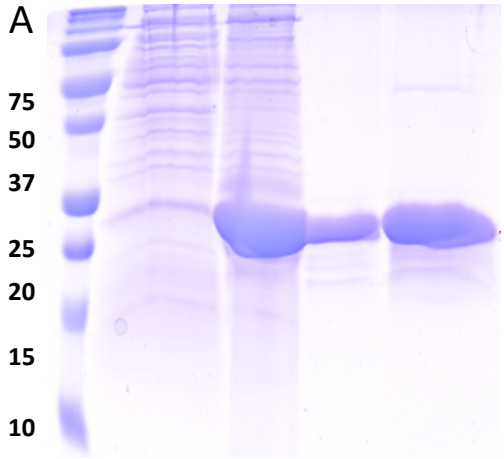

B

Steps	Volume	OD_{280}	OD_{260}	Ratio
SSO	90 mL	68.3	133.1	0.74
Ni-Sepharose	14 mL	3.3	2.71	0.62
Q-Sepharose	40 mL	0.46	0.37	1.11

Figure 74: Purification of MOCS3 303 from the soluble fraction
A) 15% SDS-PAGE analysis of the different steps of purification. MW, M: marker, FT: Flow through from Ni-Sepharose column, Ni: eluate of the Ni-Sepharose column, Dialysis: dialysis of the Ni fraction to eliminate imidazole, Q-SP: eluate of the Q-Sepharose column. B) Summary table of the purification steps. The enzyme was produced in *E. coli* BL21 (DE3) cells transformed with the pET28a-MOCS3 303 and grown in 4 L LB/K overnight at 37°C after 0.1 mM IPTG induction. Prior storage at -80°C, purified enzymatic solution was concentrated by ultrafiltration to 110 µM with moderate loss of proteins (yield of 70 %). Molar Mass of MOCS3 303= 21 kDa.

4- Production and purification of MOCS3 335

MOCS3 335 was produced in *E. coli* BL21 (DE3) cells using the pET28a-MOCS3 335 vector which permits the production of the enzyme fused with a polyHis tag at the N-terminus. The recombinant enzyme is totally unsoluble. For this reason, I decided to use the "urea protocol" developed in axis 1, and I designed a purification protocol consisting in four steps: (1) cell lysis by sonication to recover the enzyme in the pellet, (2) suspension of the pellet in 6 M urea, 10 mM DTT, 50 mM Tris-HCl, 2 mM EDTA pH 8 buffer followed by two successive dialysis at 4°C in the presence of decreasing urea concentration (3 and 0 M) in 50 mM Tris-HCl, 2 mM EDTA pH 8 buffer, (3) Ni-Sepharose affinity chromatography, and (4) Q-Sepharose anion exchange chromatography. This protocol allowed to obtain the MOCS3 335 purified to homogeneity (yield approx. 10 mg/L of culture). A table summarizing the different steps of purification and the SDS-PAGE used to follow the purity state of the enzyme are presented in figure 75.

A

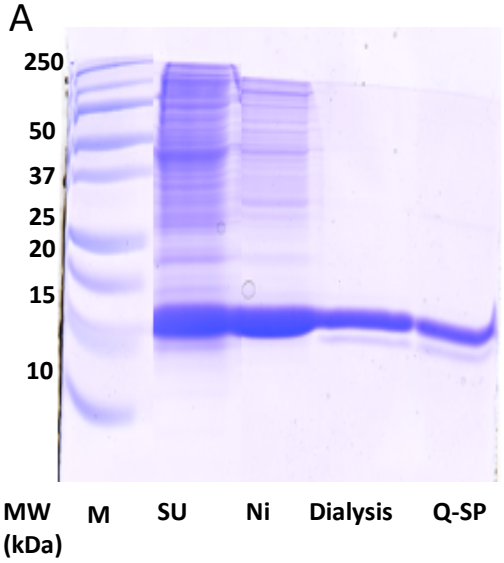

B

Steps	Volume	OD_{280}	OD_{260}	Ratio
SU	80mL	116	131	0.88
Ni-Sepharose	30 mL	2.1	1.37	1.5
Q-Sepharose	45 mL	0.79	0.52	1.53

Figure 75: Purification of MOCS3 335 from the insoluble fraction.
A) 15% SDS-PAGE analysis of the different steps of purification. MW, M: marker, SU: supernatant after urea denaturation and refolding by dialysis, Ni: eluate from the Ni-Sepharose column, Dialysis: dialysis of the Ni fraction to eliminate imidazole, Q-SP: eluate from the Q-Sepharose column. B) Summary table of the purification steps. The enzyme was produced in *E. coli* BL21 (DE3) cells transformed with the pET28a-MOCS3 335 and grown in 4 L LB/K overnight at 37°C after 0.1 mM IPTG induction. Prior storage at -80°C, purified enzymatic solution was concentrated by ultrafiltration to 120 µM with moderate loss of proteins (yield of 60 %). *Molar Mass of MOCS3 335= 17 kDa.

DISCUSSION & PERSPECTIVES

The first axis of my thesis was to determine whether two human Rhodanese-fold containing enzymes i.e. $CDC25B_{cd}$ and TSTD1 were promiscuous or not with particular emphasis on the link existing, if any, between the length and the sequence of the active site loops and their catalytic capabilities.

1. Native $CDC25B_{cd}$ is intrinsically promiscuous

The strategy to reveal a putative additional promiscuous sulfurtransferase activity of the $CDC25B_{cd}$ was first to produce a CRD-tagged version of this Rhd domain. Addition of a lectinic domain was expected to improve the yield in soluble recombinant form and to permit a quite straight-forward purification protocol. Unfortunately, this was not really the case due to a low amount of soluble form irrespective of the conditions used for the production (*E. coli* strains, media, temperature, induction strategy …) and a lack of reproducibility. However, I managed to confirm that this bulky tag did not drastically impair the phosphatase activity compared to the wild-type form. More importantly, I showed that, under single turn-over conditions, CRD-$CDC25_{cd}$ was able to catalyse a sulfur transfer reaction from 3-MP to its catalytic Cys, thus revealing a promiscuous sulfurtransferase activity (data not shown). Because, we aimed to evaluate the consequences of mutating the CX_5R loop either by removing the Ser residue or by introducing the shorter TSTD1 loop, it was necessary to obtain higher amounts of recombinant $CDC25B_{cd}$ to perform all the kinetic experiments. Expecting a more efficient and reliable production & purification protocol, we decided to generate His-tagged versions as done by Bhattacharjee et al (2010).

His-$CDC25B_{cd}$ (hereafter referred to as $CDC25B_{cd}$) displays phosphatase and sulfurtransferase activities, as previously shown for CRD-$CDC25B_{cd}$. In terms of catalytic efficiencies, the His-tagged version is approx. 5.7-fold or 341-fold more efficient than the CRD-$CDC25B_{cd}$ for the phosphatase (125 vs 22 $M^{-1}. s^{-1}$, Table 5) or the sulfurtransferase activity (13650 vs 40 $M^{-1}. s^{-1}$), respectively. The slight difference observed for the phosphatase activity is likely not resulting from steric hindrance provided by the CRD tag, because more drastic effects would have been observed, but rather it may reveal changes even minor in the structure and/or the dynamics of the Rhd domain especially within the active site. The picture clearly differs for the sulfurtransferase activity, but in that case the very low catalytic efficiency of CRD-$CDC25B_{cd}$ reflects a probable lack of stability of this form under stopped-flow

conditions (pressure & shear stress). Interestingly, $CDC25B_{cd}$ is even a slightly more efficient sulfurtransferase than TSTD1 when 3MP is used as donor substrate (k_{max}/K_{3MP} 13650 vs 11870 $M^{-1}. s^{-1}$, respectively, Table 5). Because the TSTD1 Gln80/Arg108 pair shown to be specifically dedicated to sulfur transfer from 3MP (Figure 31A) can be considered as conserved in $CDC25B_{cd}$ (i.e. Glu80/Lys108, Figure 76), $CDC25B_{cd}$'s high catalytic efficiency is not so surprising. Moreover, this explains, at least partially, why this enzyme exhibits promiscuous sulfurtransferase activity. This question will be addressed by substituting Glu80 and/or Lys108. Although, it is tempting to discuss the fact that this promiscuous activity is 100-fold more efficient than the native one (13650 vs 125 $M^{-1}. s^{-1}$), it would be however too speculative because phosphatase activity was assayed with a substrate analog (pNPP).

	$CDC25B_{cd}$	**$CDC25B_{cd}$△Ser**	**EX-MUT-$CDC25B_{cd}$**
Phosphatase activity			
k_{cat} (s^{-1})	0.20 ± 0.01	0.007 ± 0.001	No activity
K_M (pNPP) (mM)	1.6 ± 0.2	21 ± 4 [a]	
k_{cat} / K_M ($M^{-1}.s^{-1}$)	125	22	
Sulfurtransferase activity			
k_{max} (s^{-1})	101 ± 6	N.D.	N.D.
K_{3MP} (mM)	7.4 ± 1.2	N.D.	N.D.
k_{max} / K_{3MP} ($M^{-1}.s^{-1}$)	$13.6.10^3$	620 ± 59 [b]	1622 ± 71 [c]
Arsenate reductase activity			
k_{cat} (s^{-1})	0.09 ± 0.02	0.12 ± 0.03	No activity
K_M (arsenate) (mM)	15 ± 12	38 ± 6 [d]	
k_{cat} / K_M ($M^{-1}.s^{-1}$)	5.8	3.1	

Table 5: Kinetic parameters determined for wild-type and mutated $CDC25B_{cd}$s
[a] $K_{0.5}$ value (n = 2.3 ± 0.7); [b, c] k_2 values; [d] $K_{0.5}$ value (n = 3.7 ± 0.9).

By contrast, no activity could be detected in the presence of thiosulfate (up to 80 mM) highlighting a strict specificity for 3MP in contrast to what has been determined for TSTD1 ($k_{max}/K_{Thiosulfate}$ of 2. 10^3 $M^{-1}. s^{-1}$, A-L Claudel, 2022). This result is rather surprising because the Glu31/Arg84 pair responsible for the sulfur-sulfur bond cleavage in TSTD1 is conserved in $CDC25B_{cd}$ (Figure 76). Thus, one could hypothesize that the thiosulfate cannot access to the

active site due to steric hindrance (Thiosulfate is more bulky than 3MP) but this can be ruled out for two reasons: 1) the CDC25B$_{cd}$'s active is really surface exposed; 2) a sulfate molecule occupies the active site in the CDC25B$_{cd}$ X-ray structure (Figure 76). Therefore, this lack of activity likely results from the formation of a CDC25B$_{cd}$/thiosulfate Michaelian complex that is not competent for catalysis due to an incorrect positioning of the distal sulfur atom of the thiosulfate relative to the thiolate group of the catalytic Cys79.

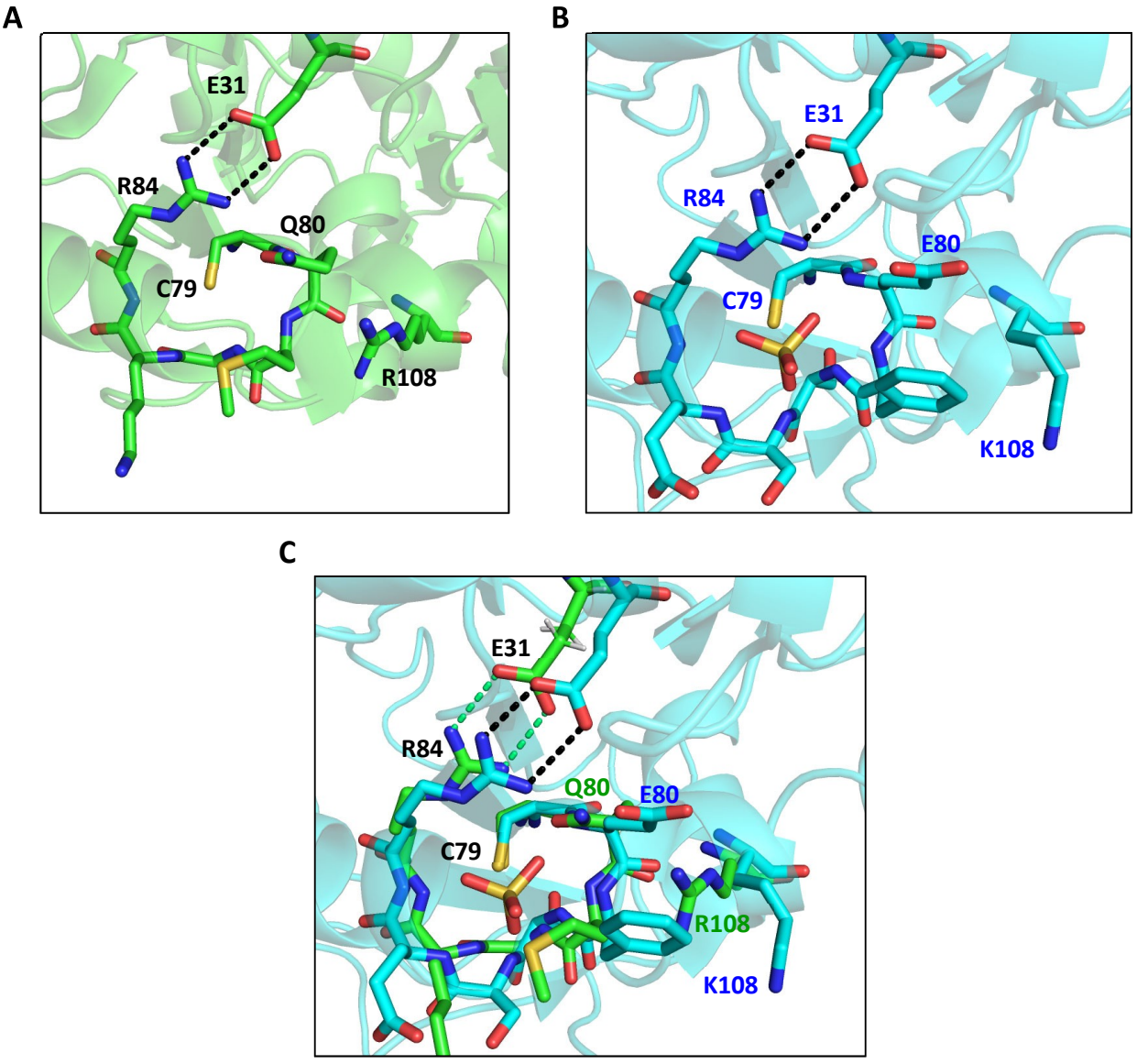

Figure 76: Active sites of TSTD1 (**A**, PDB code 4JGT) and CDC25B$_{cd}$ (**B**, PDB code 1CWT). **(C)** Superimposition of the active site of TSTD1 (green) and CDC25B$_{cd}$ (cyan). Residues at positions 31, 79, 80, 84 and 108 are represented as sticks colored according to the corresponding active site and the sulfate molecule present within the CDC25B$_{cd}$'s active site, as well. The sulfur atom of the catalytic Cys79 is shown in yellow, and the figures were generated using PyMOL version 2.0.1.

As already mentioned, the formation of the Cys persulfide intermediate is very efficient in the presence of 3MP but what about the second step i.e. the sulfur transfer from this intermediate towards an acceptor substrate? Several classical acceptors either physiological (Trx, DHLA) or artificial (DTT) could be tested under steady-state conditions: for Trx using the NADPH/Trx reductase coupled assay, and for DHLA and DTT using a H_2S-specific microelectrode, as previously optimized in the team for 3MSTs and TSTs. If such an activity is revealed, this will raise the question of its physiological relevance regarding the dual nucleo-cytoplasmic localization of CDC25B (Sur & Agrawal, 2016).

2. Modifying the catalytic loop of CDC25B$_{cd}$ does not improve but rather abolish its promiscuity

For the CDC25B$_{cd}$ ΔSer variant, reducing the loop length led to a 5.7-fold decrease in phosphatase catalytic efficiency and to a 22-fold decrease in the sulfurtransferase one. For EX-MUT- CDC25B$_{cd,}$ exchanging the loop abolished the phosphatase activity and led to an 8.4-fold decrease in sulfurtransferase catalytic efficiency (Table 5). In contrast, the promiscuous arsenate reductase activity is preserved for CDC25B$_{cd}$ ΔSer variant but not for EX-MUT-CDC25B$_{cd}$.

Interestingly, when the phosphatase activity is assayed under steady-state conditions for CDC25B$_{cd}$ ΔSer variant a lag phase of approx. 10 min is observed in the presence of 5 mM pNPP (Figure 62 p. 88). This means that the Michaelian complex initially formed is not fully catalytically competent and requires conformational changes, even minor, to reach the steady-state regime. This assumption is first supported by the fact that phosphate binding drives a conformational change whose nature remains to be defined. The pNPP phosphate group is known to be anchored by contributions of backbone amides and Arg84 side-chain of the catalytic loop for the phosphatase reaction to occur. Therefore, one can hypothesize that this binding mode is altered when the loop length is reduced, a conformational adaptation that could be restricted to this active site part is thus required to restore a productive binding. Secondly, the sigmoidal k_{obs} = f([pNPP]) profile (Figure 63B p. 89) reveals kinetic cooperativity. This may result from hysteresis and one can propose a kinetic scheme derived from the one proposed for human and *E. coli* 3-MSTs (Lec *et al.*, 2018). Briefly, it relies on local

conformational transitions that have to occur within the active site between the two steps of the reaction, with two conformations catalytically competent for the first and the second step, respectively. For $CDC25B_{cd}$ ΔSer, transitions between these two conformations are not rapid enough to be at equilibrium during catalysis and lead to kinetic cooperativity (Figure 77). Based on this model, the absence of cooperative behavior for $CDC25B_{cd}$ can be explained by much faster transitions likely associated with loop dynamics.

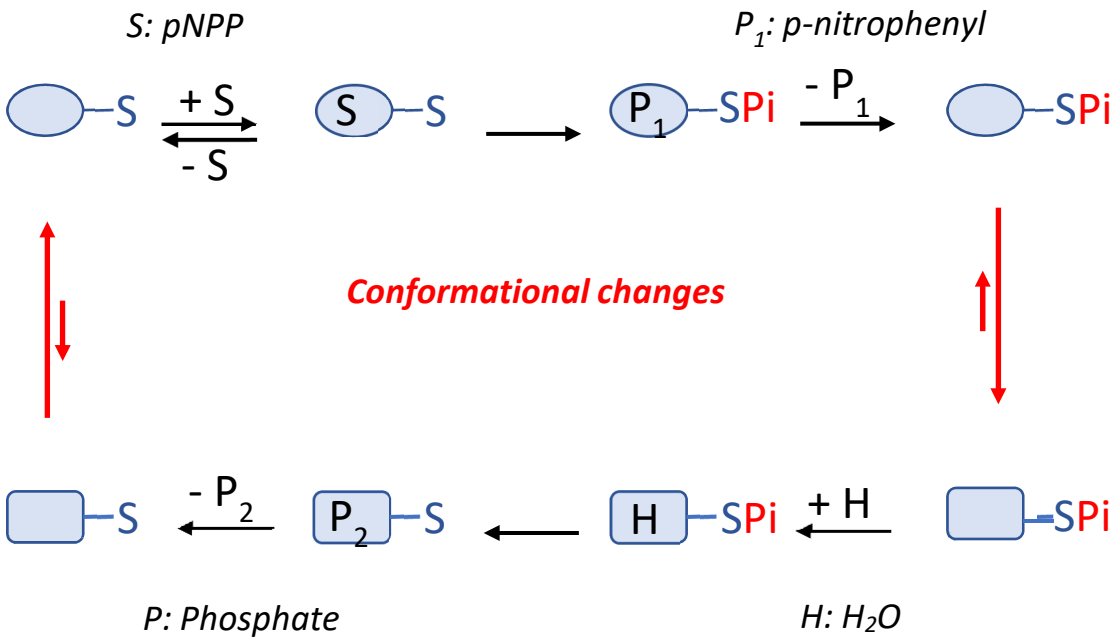

Figure 77: Proposed kinetic model for the $CDC25B_{cd}$-catalyzed phosphatase reaction.
The conformation adapted for the first step is an ellipsis, whilst the rectangle represents the one adapted for hydrolysis of the phospho-enzyme intermediate (SPi). The blue S symbolizes the sulfur atom of the catalytic Cys79.

The picture clearly differs for EX-MUT-$CDC25B_{cd}$ because introducing the TSTD1 catalytic loop totally impairs the phosphatase activity. This drastic effect cannot be explained by the loop length which is similar to the $CDC25B_{cd}$ ΔSer one, but rather by its sequence. Considering the key contribution of the loop conformation/dynamics in the phosphatase activity, this data suggests that the TSTD1 loop is intrinsically not adapted to bind phosphate in a productive way. Because Arg84 is not only conserved, but also anchored by the salt-bridge with Glu31 (Figure 76C) in both enzymes, differences originate from backbone amides positioning relative to the phosphate oxygens.

Regarding the consequences induced by the catalytic loop changes on the promiscuous arsenate reductase activity, reducing the loop length by one residue has no significant impact on the kinetic parameters (Table 5). However, and similarly to what was observed for the phosphatase activity, kinetic cooperativity is revealed. In addition, exchanging the catalytic loop also fully abolishes the activity. Therefore, the conclusions drawn for the phosphatase activity can reasonably be extended to the arsenate reductase activity and it would be expected given that phosphate and arsenate are considered as chemical analogues.

The situation is rather different when looking at the sulfurtransferase properties of the $CDC25B_{cd}$ variants because EX-MUT-$CDC25B_{cd}$ remains active. The moderate decrease in catalytic efficiency observed for both variants is mainly due to a K_{3MP} effect thus higher substrate concentrations are required to form enzyme/3MP competent complexes. However, once formed, these complexes are fully adapted for an efficient sulfur transfer as shown by the rate constant values close to that determined for $CDC25B_{cd}$ (see results page 85). These data suggest that irrespective the loop length/sequence the presence of a Glu80/Lys108 or Gln80/Lys108 pair in $CDC25B_{cd}$ ΔSer or EX-MUT-$CDC25B_{cd}$, respectively, is sufficient to permit an efficient catalysis. To further define the specific impact of the length/sequence of the loop on the sulfur transfer, it would be interesting to check whether a Thiosulfate-dependent activity exits for both $CDC25B_{cd}$ variants. Indeed, the presence of the Glu31/Arg84 pair combined to a CX_4R catalytic loop is favorable for a sulfur-sulfur bond cleavage activity.

3. TSTD1 and related catalytic loop variants do not exhibit promiscuity

Regarding the sulfurtransferase activity, modifying the catalytic loop does not significantly impact the carbon-sulfur bond cleavage efficiency of the TSTD1 variants (Table 6). As already discussed for $CDC25B_{cd}$, the 3MP-dependent sulfurtransferase activity depends on the presence of the 80/108 pair, which is "conserved" for both variants explaining the minor changes in catalytic efficiency (2- to 5-fold decrease in k_{max}/K_{3MP}). However, compared to the $CDC25B_{cd}$ context, the key difference lies in the fact that 3MP recognition is preserved (i.e. saturation is observed) irrespective of the catalytic loop version. This suggest that TSTD1 active site is intrinsically more adapted to catalyze this sulfur transfer reaction. This property

may rely on local dynamics but it remains to be checked/validated by in silico studies. In this view, it would be very interesting to verify whether the same is true when thiosulfate is used as sulfur donor. Although one could predict no significant change in the sulfur-sulfur bond cleavage efficiency because the thiosulfate Glu31/Arg84 specific pair is conserved in the two TSTD1 variants, we cannot rule out the possibility that increasing the loop length will impair the productive binding of the substrate within the active site, as proposed for $CDC25B_{cd}$. Finally, to provide a more complete picture of the role of this loop on the kinetic properties of the TSTD1 variants, the second step of sulfur transfer will be studied using approaches already described for $CDC25B_{cd}$ (page 104).

	TSTD1	TSTD1+Ser	EX-MUT-TSTD1
Sulfurtransferase activity			
k_{max} (s^{-1})	95 ± 8	145 ± 44	83 ± 14
K_{3MP} (mM)	8 ± 2	25 ± 14	34 ± 12
k_{max} / K_{3MP} ($M^{-1}.s^{-1}$)	$11.9.10^3$	$5.8.10^3$	$2.4.10^3$
Phosphatase activity			
		Not detectable	
Arsenate reductase activity			
		Not detectable	

Table 6: Kinetic parameters determined for wild-type and mutated TSTD1s

In contrast to what was observed for $CDC25B_{cd}$, no promiscuous activity is revealed with TSTD1s irrespective of the loop version. For TSTD1, previous data showed that this so-called TST rather belongs to the 3MST family (A-L Claudel, 2022) and this property could result from an active site cavity not fully designed to stabilize/accommodate oxyanions like thiosulfate. Similarly, this may apply for oxyanions that are even bulkier i.e. phosphate and arsenate. For both TSTD1 variants, the catalytic loop is one residue longer thus making room for phosphate or arsenate binding, but they remain inactive even with the $CDC25B_{cd}$-loop. One may argue for the TSTD1+Ser variant that the mutated TSTD1 loop is not better suited than the native version to bind oxyanions. However, this proposal is no more valid for EX-MUT-

TSTD1. In this case, the absence of any promiscuous activity likely highlights the critical role of the molecular environment (i.e. shift from a $CDC25B_{cd}$ native context to the TSTD1 heterologous context) in modulating the contribution of the $CDC25B_{cd}$ loop in catalysis, which is here totally abolished. Whether this relies on altered loop dynamics remains to be evaluated.

4. What about other sulfurtransferases?

The absence under our experimental conditions of any promiscuous activity for TSTD1 raised the question of the generality of this selectivity/specialization among the sulfurtransferase family. To address this point, phosphatase activity was assayed on two other sulfurtransferases: *E. coli* GlpE and human 3MST that contain one- and two-Rhd domain(s), respectively. Again, irrespective of the substrate analog used (pNPP or 4-MUP), no phosphatase activity was detected (data not shown). Interestingly, this property seems to be independent of the protein scaffold, the domain organization and the loop sequence for the native forms. To gain more insights, it would be informative to elongate the catalytic loop of these two enzymes and check whether phosphatase or arsenate reductase activity can be detected. In fact, this was done on RhdA, a two Rhd-domains enzyme from *A. vinelandii* (Forlani *et al.*, 2003), but very low phosphatase activity was obtained at the detriment of the native sulfurtransferase one. Altogether, these data further support the idea that sulfurtransferases are more specialized and so less adapted than $CDC25B_{cd}$s to catalyze unnatural reactions.

Concerning the second axis, I managed to produce and purify two versions of MOCS3-Rhd domain. However, due to time constraints I was not able to go further in their biochemical characterization. Prior to any kinetic experiments, it will be necessary to assess the quality of the purified proteins by first validating their molecular masses by ESI-MS, their homogeneity by DLS and their overall structural integrity by far- and near-UV CD analyses. To assay the sulfurtransferase activity, a prerequisite is to validate that a variation in Trp fluorescence emission occurs upon addition of 3MP or thiosulfate (two Trp residues in both MOCS3-Rhds), as shown for other Rhd-containing sulfurtransferases. If so, fast kinetic experiments will be performed to study the sulfur transfer step towards the catalytic Cys. Although, MOCS3- and TSTD1-Rhd domains superimpose quite well, in particular for the catalytic loop, the Glu31/Arg84 and Gln80/Arg108 pairs are not conserved in MOCS3-Rhd (Figure 78). Thus, no activity is expected with these two chemical sulfur donors. It would be however in agreement with the proposed physiological substrates i.e. persulfidated- 3MST or cysteine desulfurase NFS1 (Figure 22 page 32). In that case, the sulfur transfer is likely to be promoted by protein-protein interactions that will ensure the adequate positioning of the sulfur atom to be transferred relative to the catalytic Cys. It is therefore of interest first, to check whether such complexes are indeed formed in vitro, and then if direct sulfur transfer occurs from the persulfidated-proteins to MOCS3-Rhd. In a cellular context, the MOCS3-Rhd active site is proposed to be located at the Rhd/Adenylyltransferase interface (AF-095396-F1-model_v4), if this model is valid the additional domain has to be mobile enough to permit a protein- protein sulfur transfer.

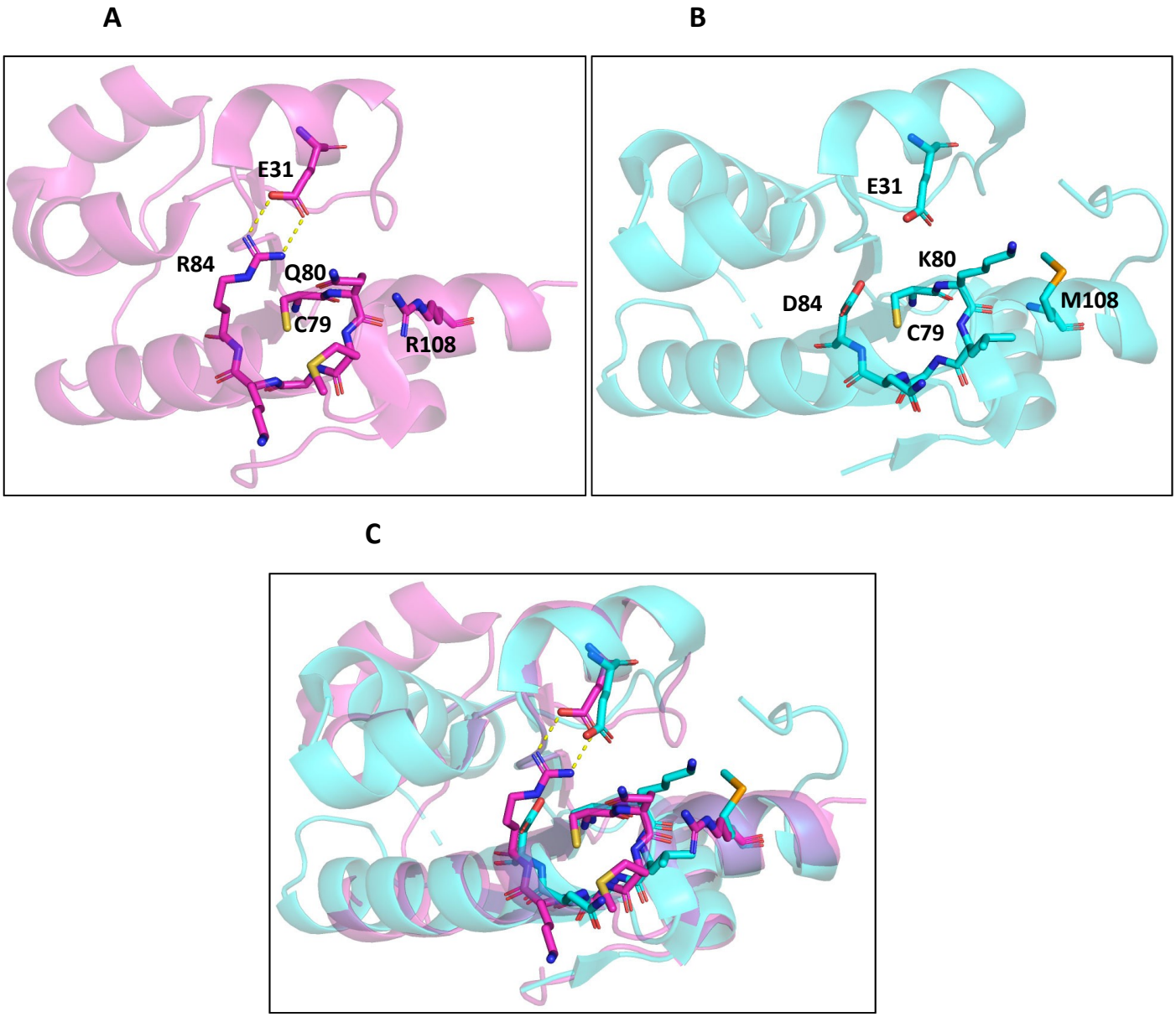

Figure 78: Active sites of TSTD1 (**A**, PDB code 4JGT) and MOCS3 (**B**, PDB code 3I2V). **(C)** Superimpositionof the active site of TSTD1 (pink) and MOCS3 (cyan) with RMSD of 1.047 Å on 69 C_α. Residues at positions 31, 79, 80, 84 and 108 are represented as sticks colored according to the corresponding active site. The sulfur atom of the catalytic Cys is shown in yellow, and the figures were generated using PyMOL version 2.0.1.

References

References

Abdolrasulnia, R., & Wood, J.L. (1980). Persulfide properties of thiocystine and related trisulfides. *Bioorganic Chemistry, 9*, 253-260.

Adams H, Teertstra W, Koster M, Tommassen J. PspE (phage-shock protein E) of Escherichia coli is a rhodanese. *FEBS Lett.* 2002 May 8;518(1-3):173-6. doi: 10.1016/s0014-5793(02)02695-9.

Afriat L, Roodveldt C, Manco G, Tawfik DS. The latent promiscuity of newly identified microbial lactonases is linked to a recently diverged phosphotriesterase. *Biochemistry*. 2006 Nov 21;45(46):13677-86. doi: 10.1021/bi061268r.

Aita N, Ishii K, Akamatsu Y, Ogasawara Y, Tanabe S. Cloning and expression of human liver rhodanese cDNA*. Biochem Biophys Res Commun*. 1997 Feb 3;231(1):56-60. doi: 10.1006/bbrc.1996.6046.

Alphey, M.S., Williams, R.A.M., Mottram, J.C., Coombs, G.H., Hunter, W.N., (2003). The crystal structure of Leishmania major 3-mercaptopyruvate sulfurtransferase. A three- domain architecture with a serine protease-like triad at the active site. *J. Biol. Chem.* **278**, 48219–48227.

Amitai G, Gupta RD, Tawfik DS. Latent evolutionary potentials under the neutral mutational drift of an enzyme. *HFSP J.* 2007 May;1(1):67-78. doi: 10.2976/1.2739115/10.2976/1.

Avvakumov, G.V., Walker, J.R., Xue, S., Finerty, P.J., Mackenzie, F., Newman, E.M., and Dhe-Paganon, S. (2006). Amino-terminal dimeriza,on, NRDP1-rhodanese interac,on, and inhibited cataly,c domain conforma,on of the ubiqui,n-specific protease 8 (USP8). *J. Biol. Chem. 281*, 38061–38070.

Azumi, Y., and Watanabe, A. (1991). Evidence for a senescence-associated gene induced by darkness*. Plant Physiol*. *95*, 577–583.

Baldin V, Cans C, Superti-Furga G, Ducommun B. Alternative splicing of the human CDC25B tyrosine phosphatase. Possible implications for growth control? *Oncogene.* 1997 May 22;14(20):2485-95. doi: 10.1038/sj.onc.1201063

Bebrone C. Metallo-beta-lactamases (classification, activity, genetic organization, structure, zinc coordination) and their superfamily. *Biochem Pharmacol*. 2007 Dec 15;74(12):1686-701. doi: 10.1016/j.bcp.2007.05.021.

Bergthorsson U, Andersson DI, Roth JR. Ohno's dilemma: evolution of new genes under continuous selection. *Proc Natl Acad Sci U S A.* 2007 Oct 23;104(43):17004-9. doi: 10.1073/pnas.0707158104.

Bhattacharjee H, Sheng J, Ajees AA, Mukhopadhyay R, Rosen BP. Adventitious arsenate reductase activity of the catalytic domain of the human Cdc25B and Cdc25C phosphatases. *Biochemistry*. 2010 Feb 2;49(4):802-9. doi: 10.1021/bi9019127.

Bimai O, Arragain S, Golinelli-Pimpaneau B. Structure-based mechanistic insights into catalysis by tRNA thiolation enzymes. *Curr Opin Struct Biol*. 2020 Dec;65:69-78. doi: 10.1016/j.sbi.2020.06.002.

Bleeker PM, Hakvoort HW, Bliek M, Souer E, Schat H. Enhanced arsenate reduction by a CDC25-like tyrosine phosphatase explains increased phytochelatin accumulation in arsenate-tolerant Holcus lanatus. *Plant J*. 2006 Mar;45(6):917-29. doi: 10.1111/j.1365-313X.2005.02651.x.

Bobrowicz P, Wysocki R, Owsianik G, Goffeau A, Ułaszewski S. Isolation of three contiguous genes, ACR1, ACR2 and ACR3, involved in resistance to arsenic compounds in the yeast Saccharomyces cerevisiae. *Yeast.* 1997 Jul;13(9):819-28. doi: 10.1002/(SICI)1097-0061(199707)13:9<819::AID-YEA142>3.0.CO;2-Y

Bordo D, Bork P. The rhodanese/Cdc25 phosphatase superfamily. Sequence-structure-function relations. EMBO Rep. 2002 Aug;3(8):741-6. doi: 10.1093/embo-reports/kvf150.

Bordo, D., Deriu, D., Colnaghi, R., Carpen, A., Pagani, S., Bolognesi, M., (2000). The crystal structure of a sulfurtransferase from Azotobacter vinelandii highlights the evolutionary relationship between the rhodanese and phosphatase enzyme families. *J. Mol. Biol.* **298**, 691–704.

Bornscheuer UT, Kazlauskas RJ. Catalytic promiscuity in biocatalysis: using old enzymes to form new bonds and follow new pathways. *Angew Chem Int Ed Engl*. 2004 Nov 19;43(45):6032-40. doi: 10.1002/anie.200460416.

Boudolf V, Inzé D, De Veylder L. What if higher plants lack a CDC25 phosphatase? *Trends Plant Sci*. 2006 Oct;11(10):474-9. doi: 10.1016/j.tplants.2006.08.009.

Boutros R, Dozier C, Ducommun B. The when and wheres of CDC25 phosphatases. *Curr Opin Cell Biol*. 2006 Apr;18(2):185-91. doi: 10.1016/j.ceb.2006.02.003

Boutros R, Lobjois V, Ducommun B. CDC25 phosphatases in cancer cells: key players? Good targets? *Nat Rev Cancer*. 2007 Jul;7(7):495-507. doi: 10.1038/nrc2169.

Buonvino S, Arciero I, Melino S. Thiosulfate-Cyanide Sulfurtransferase a Mitochondrial Essential Enzyme: From Cell Metabolism to the Biotechnological Applications. *Int J Mol* Sci. 2022 Jul 30;23(15):8452. doi: 10.3390/ijms23158452

Carbonell P, Lecointre G, Faulon JL. Origins of specificity and promiscuity in metabolic networks. *J Biol Chem*. 2011 Dec 23;286(51):43994-44004. doi:10.1074/jbc.M111.274050.

Chauncey TR, Westley J. The catalytic mechanism of yeast thiosulfate reductase. *J Biol Chem.* 1983 Dec 25;258(24):15037-45.

Chen Z, Zhang X, Li H, Liu H, Xia Y, Xun L. The Complete Pathway for Thiosulfate Utilization in Saccharomyces cerevisiae. *Appl Environ Microbiol*. 2018 Oct 30;84(22):e01241-18. doi: 10.1128/AEM.01241-18.

Schmidt DM, Mundorff EC, Dojka M, Bermudez E, Ness JE, Govindarajan S, Babbitt PC, Minshull J, Gerlt JA. Evolutionary potential of (beta/alpha)8-barrels: functional promiscuity produced by single substitutions in the enolase superfamily. *Biochemistry*. 2003 Jul 22;42(28):8387-93. doi: 10.1021/bi034769a.

Chng SS, Dutton RJ, Denoncin K, Vertommen D, Collet JF, Kadokura H, Beckwith J. Overexpression of the rhodanese PspE, a single cysteine-containing protein, restores disulphide bond formation to an Escherichia coli strain lacking DsbA. *Mol Microbiol.* 2012 Sep;85(5):996-1006. doi: 10.1111/j.1365-2958.2012.08157.x.

Chowdhury MM, Dosche C, Löhmannsröben HG, Leimkühler S. Dual role of the molybdenum cofactor biosynthesis protein MOCS3 in tRNA thiolation and molybdenum cofactor biosynthesis in humans. *J Biol Chem*. 2012 May 18;287(21):17297-17307. doi: 10.1074/jbc.M112.351429.

Cipollone R, Ascenzi P, Visca P. Common themes and variations in the rhodanese superfamily. *IUBMB Life*. 2007 Feb;59(2):51-9. doi: 10.1080/15216540701206859.

Colin PY, Kintses B, Gielen F, Miton CM, Fischer G, Mohamed MF, Hyvönen M, Morgavi DP, Janssen DB, Hollfelder F. Ultrahigh-throughput discovery of promiscuous enzymes by picodroplet functional metagenomics. *Nat Commun*. 2015 Dec 7;6:10008. doi: 10.1038/ncomms10008.

Colnaghi, R., Cassinelli, G., Drummond, M., Forlani, F., Pagani, S., (2001). Properties of the Escherichia coli rhodanese-like protein SseA: contribution of the active-site residue Ser240 to sulfur donor recognition. *FEBS Lett.* **500**, 153–156.

Copley SD, Newton MS, Widney KA. How to Recruit a Promiscuous Enzyme to Serve a New Function. *Biochemistry.* 2023 Jan 17;62(2):300-308. doi: 10.1021/acs.biochem.2c00249.

Copley SD. An evolutionary perspective on protein moonlighting. Biochem Soc Trans. 2014 Dec;42(6):1684-91. doi: 10.1042/BST20140245.

Copley SD. Enzymes with extra talents: moonlighting functions and catalytic promiscuity. *Curr Opin Chem Biol*. 2003 Apr;7(2):265-72. doi: 10.1016/s1367-5931(03)00032-2.

Copley SD. Evolution of efficient pathways for degradation of anthropogenic chemicals. *Nat Chem Biol*. 2009 Aug;5(8):559-66. doi: 10.1038/nchembio.197.

Copley SD. Shining a light on enzyme promiscuity. *Curr Opin Struct Biol*. 2017 Dec;47:167-175. doi: 10.1016/j.sbi.2017.11.001.

Cornilescu G, Vinarov DA, Tyler EM, Markley JL, Cornilescu CC. Solution structure of a single-domain thiosulfate sulfurtransferase from Arabidopsis thaliana. *Protein Sci*. 2006 Dec;15(12):2836-41. doi: 10.1110/ps.062395206.

Cortese MS, Caplan AB, Crawford RL. Structural, functional, and evolutionary analysis of moeZ, a gene encoding an enzyme required for the synthesis of the Pseudomonas metabolite, pyridine-2,6-bis(thiocarboxylic acid). *BMC Evol Biol*. 2002 Apr 23;2:8. doi: 10.1186/1471-2148-2-8.

Denu, J. M., and Dixon, J. E. (1995) A cataly,c mechanism for the dual-specific phosphatases, *Proc. Natl. Acad. Sci. U.S.A. 92*, 5910-5914.

Denu, J. M., Stuckey, J. A., Saper, M. A., and Dixon, J. E. (1996) Form and func,on in protein dephosphoryla,on, *Cell 87*, 361- 364.

Dhankher, O. P., Rosen, B. P., McKinney, E. C., and Meagher, R. B. (2006) Hyperaccumula<on of arsenic in the shoots of Arabidopsis silenced for arsenate reductase (ACR2). *Proc. Natl. Acad. Sci. U.S.A.* 103, 5413–5418

Duan,G. L., Zhou, Y., Tong, Y. P., Mukhopadhyay, R., Rosen, B. P., and Zhu, Y. G. (2007) A CDC25 homologue from rice functions as an arsenate reductase. *New Phytol.* 174, 311–321

Edwards DR, Lohman DC, Wolfenden R. Catalytic proficiency: the extreme case of S-O cleaving sulfatases*. J Am Chem Soc*. 2012 Jan 11;134(1):525-31. doi: 10.1021/ja208827q.

Ellis DR, Gumaelius L, Indriolo E, Pickering IJ, Banks JA, Salt DE. A novel arsenate reductase from the arsenic hyperaccumulating fern Pteris vittata. *Plant Physiol*. 2006 Aug;141(4):1544-54. doi: 10.1104/pp.106.084079.

Fantes P. (1979). Epistatic gene interactions in the control of division in fission yeast. *Nature* 279, 428-430.

Fauman EB, Cogswell JP, Lovejoy B, Rocque WJ, Holmes W, Montana VG, Piwnica-Worms H, Rink MJ, Saper MA. Crystal structure of the catalytic domain of the human cell cycle control phosphatase, Cdc25A. *Cell.* 1998 May 15;93(4):617-25. doi: 10.1016/s0092-8674(00)81190-3.

Fernández-Gacio A, Codina A, Fastrez J, Riant O, Soumillion P. Transforming carbonic anhydrase into epoxide synthase by metal exchange*. Chembiochem.* 2006 Jul;7(7):1013-6. doi: 10.1002/cbic.200600127.

Forlani F, Carpen A, Pagani S. Evidence that elongation of the catalytic loop of the Azotobacter vinelandii rhodanese changed selectivity from sulfur- to phosphate-containing substrates. *Protein Eng.* 2003 Jul;16(7):515-9. doi: 10.1093/protein/gzg061.

Forrest AR, McCormack AK, DeSouza CP, Sinnamon JM, Tonks ID, Hayward NK, Ellem KA, Gabrielli BG. Multiple splicing variants of cdc25B regulate G2/M progression. *Biochem Biophys Res Commun*. 1999 Jul 5;260(2):510-5. doi: 10.1006/bbrc.1999.0870.

Fräsdorf B, Radon C, Leimkühler S. Characterization and interaction studies of two isoforms of the dual localized 3-mercaptopyruvate sulfurtransferase TUM1 from humans. *J Biol Chem*. 2014 Dec 12;289(50):34543-56. doi: 10.1074/jbc.M114.605733.

Furne, J.; Springfield, J.; Koenig, T.; DeMaster, E.; Levi2, M.D. Oxida,on of Hydrogen Sulfide and Methanethiol to Thiosulfate by Rat Tissues: A Specialized Func,on of the Colonic Mucosa. *Biochem. Pharmacol.* **2001**, *62*, 255–259.

Furukawa K, Mizushima N, Noda T, Ohsumi Y. A protein conjugation system in yeast with homology to biosynthetic enzyme reaction of prokaryotes. *J Biol Chem*. 2000 Mar 17;275(11):7462-5. doi: 10.1074/jbc.275.11.7462.

Gatti-Lafranconi P, Hollfelder F. Flexibility and reac,vity in promiscuous enzymes. *Chembiochem*. 2013 Feb 11;14(3):285-92. doi: 10.1002/cbic.201200628.

Gladysheva TB, Oden KL, Rosen BP. Properties of the arsenate reductase of plasmid R773. *Biochemistry*. 1994 Jun 14;33(23):7288-93. doi: 10.1021/bi00189a033

GREEN JR, WESTLEY J. Mechanism of rhodanese action: polarographic studies. *J Biol Chem.* 1961 Nov;236:3047-50.

Gupta RD, Tawfik DS. Directed enzyme evolution via small and effective neutral drift libraries. *Nat Methods*. 2008 Nov;5(11):939-42. doi: 10.1038/nmeth.1262.

Gupta, R.D. Recent advances in enzyme promiscuity. *Sustain Chem Process* **4**, 2 (2016). doi:10.1186/s40508-016-0046-9.

Hannestad U, Mårtensson J, Sjödahl R, Sörbo B. 3-mercaptolactate cysteine disulfiduria: biochemical studies on affected and unaffected members of a family. *Biochem Med*. 1981 Aug;26(1):106-14. doi: 10.1016/0006-2944(81)90035-1.

Hatzfeld Y, Saito K. Evidence for the existence of rhodanese (thiosulfate:cyanide sulfurtransferase) in plants: preliminary characterization of two rhodanese cDNAs from Arabidopsis thaliana. *FEBS Lett*. 2000 Mar 24;470(2):147-50. doi: 10.1016/s0014-5793(00)01311-9.

Hill, A.C., 1898. LXVI.—Reversible zymohydrolysis. *Journal of the Chemical Society, Transactions*, *73*, pp.634-658.

HIMWICH WA, SAUNDERS JP. Enzymatic conversion of cyanide to thiocyanate. *Am J Physiol*. 1948 May 1;153(2):348-54. doi: 10.1152/ajplegacy.1948.153.2.348

Hofmann K, Bucher P, Kajava AV. A model of Cdc25 phosphatase catalytic domain and Cdk-interaction surface based on the presence of a rhodanese homology domain. *J Mol Biol*. 1998 Sep 11;282(1):195-208. doi: 10.1006/jmbi.1998.1998.

Hughes AL. The evolution of functionally novel proteins after gene duplication. *Proc Biol Sci.* 1994 May 23;256(1346):119-24. doi: 10.1098/rspb.1994.0058.

Hult K, Berglund P. Enzyme promiscuity: mechanism and applications. *Trends Biotechnol*. 2007 May;25(5):231-8. doi: 10.1016/j.tibtech.2007.03.002.

Jackson RC, Handschumacher RE. 1970. *Escherichia coli* L-asparaginase. Catalytic activity and subunit nature. *Biochemistry* 9:3585–90

Jensen RA. Enzyme recruitment in evolution of new function. *Annu Rev Microbiol*. 1976;30:409-25. doi: 10.1146/annurev.mi.30.100176.002205

Kabil O, Banerjee R. Characterization of patient mutations in human persulfide dioxygenase (ETHE1) involved in H2S catabolism. *J Biol Chem.* 2012 Dec 28;287(53):44561-7. doi: 10.1074/jbc.M112.407411.

Karlsson-Rosenthal C, Millar JB. Cdc25: mechanisms of checkpoint inhibition and recovery. *Trends Cell Biol.* 2006 Jun;16(6):285-92. doi: 10.1016/j.tcb.2006.04.002.

Kastle, J.H. and Loevenhart, A.S. (1900) Concerning lipase, the fat- slitting enzyme, and the reversibility of its action*. Am. Chem. J*. 24, 491–5253

Kawano Y, Onishi F, Shiroyama M, Miura M, Tanaka N, Oshiro S, Nonaka G, Nakanishi T, Ohtsu I. Improved fermentative L-cysteine overproduction by enhancing a newly identified thiosulfate assimilation pathway in Escherichia coli. *Appl Microbiol Biotechnol*. 2017 Sep;101(18):6879-6889. doi: 10.1007/s00253-017-8420-4.

Khanal A, Yu McLoughlin S, Kershner JP, Copley SD. Differential effects of a mutation on the normal and promiscuous activities of orthologs: implications for natural and directed evolution. *Mol Biol Evol*. 2015 Jan;32(1):100-8. doi: 10.1093/molbev/msu271.

Khersonsky O, Roodveldt C, Tawfik DS. Enzyme promiscuity: evolutionary and mechanistic aspects. *Curr Opin Chem Biol*. 2006 Oct;10(5):498-508. doi: 10.1016/j.cbpa.2006.08.011.

Khersonsky O, Tawfik DS. Enzyme promiscuity: a mechanistic and evolutionary perspective. *Annu Rev Biochem*. 2010;79:471-505. doi: 10.1146/annurev-biochem-030409-143718.

Khersonsky O, Tawfik DS. The histidine 115-histidine 134 dyad mediates the lactonase activity of mammalian serum paraoxonases. *J Biol Chem*. 2006 Mar 17;281(11):7649-56. doi: 10.1074/jbc.M512594200.

Kim J, Kershner JP, Novikov Y, Shoemaker RK, Copley SD. Three serendipitous pathways in E. coli can bypass a block in pyridoxal-5'-phosphate synthesis. *Mol Syst Biol*. 2010 Nov 30;6:436. doi: 10.1038/msb.2010.88.

Krepinsky K, Leimkühler S. Site-directed mutagenesis of the active site loop of the rhodanese-like domain of the human molybdopterin synthase sulfurase MOCS3. Major differences in substrate specificity between eukaryotic and bacterial homologs. *FEBS J*. 2007 Jun;274(11):2778-87. doi: 10.1111/j.1742-4658.2007.05811.x

Kristjánsdóttir K, Rudolph J. Cdc25 phosphatases and cancer. *Chem Biol*. 2004 Aug;11(8):1043-51. doi: 10.1016/j.chembiol.2004.07.007

Lake MW, Wuebbens MM, Rajagopalan KV, Schindelin H. Mechanism of ubiquitin activation revealed by the structure of a bacterial MoeB-MoaD complex. *Nature.* 2001 Nov 15;414(6861):325-9. doi: 10.1038/35104586.

Lang, K. (1933). Die rhodanbildung in tierkorper. *Biochem Z* 259, 243 – 256.

Lec, J.-C., Boutserin, S., Mazon, H., Mulliert, G., Boschi-Muller, S., and Talfournier, F. (2018). Unraveling the Mechanism of Cysteine Persulfide Formation Catalyzed by 3-Mercaptopyruvate Sulfurtransferases. ACS Catal. *8*, 2049–2059.

Leimkühler S, Rajagopalan KV. A sulfurtransferase is required in the transfer of cysteine sulfur in the in vitro synthesis of molybdopterin from precursor Z in Escherichia coli. *J Biol Chem*. 2001 Jun 22;276(25):22024-31. doi: 10.1074/jbc.M102072200.

Li, H., Yang, F., Kang, X., Xia, B., Jin, C., (2008). Solution Structures and Backbone Dynamics of Escherichia coli Rhodanese PspE in Its Sulfur-Free and Persulfide-Intermediate Forms: Implications for the Catalytic Mechanism of Rhodanese. *Biochemistry* **47**, 4377–4385.

liakis G, Wang Y, Guan J, Wang H. DNA damage checkpoint control in cells exposed to ionizing radiation. *Oncogene.* 2003 Sep 1;22(37):5834-47. doi: 10.1038/sj.onc.1206682.

Libiad M, Motl N, Akey DL, Sakamoto N, Fearon ER, Smith JL, Banerjee R. Thiosulfate sulfurtransferase-like domain-containing 1 protein interacts with thioredoxin. *J Biol Chem*. 2018 Feb 23;293(8):2675-2686. doi: 10.1074/jbc.RA117.000826.

Libiad M, Yadav PK, Vitvitsky V, Martinov M, Banerjee R. Organization of the human mitochondrial hydrogen sulfide oxidation pathway. *J Biol Chem*. 2014 Nov 7;289(45):30901-10. doi: 10.1074/jbc.M114.602664.

Lozovsky ER, Chookajorn T, Brown KM, Imwong M, Shaw PJ, Kamchonwongpaisan S, Neafsey DE, Weinreich DM, Hartl DL. Stepwise acquisition of pyrimethamine resistance in the malaria parasite. *Proc Natl Acad Sci U S A*. 2009 Jul 21;106(29):12025-30. doi: 10.1073/pnas.0905922106

Marelja Z, Stöcklein W, Nimtz M, Leimkühler S. A novel role for human Nfs1 in the cytoplasm: Nfs1 acts as a sulfur donor for MOCS3, a protein involved in molybdenum cofactor biosynthesis. *J Biol Chem*. 2008 Sep 12;283(37):25178-25185. doi: 10.1074/jbc.M804064200.

Martin P, DeMel S, Shi J, Gladysheva T, Gatti DL, Rosen BP, Edwards BF. Insights into the structure, solvation, and mechanism of ArsC arsenate reductase, a novel arsenic detoxification enzyme. *Structure*. 2001 Nov;9(11):1071-81. doi: 10.1016/s0969-2126(01)00672-4

Matthies A, Rajagopalan KV, Mendel RR, Leimkühler S. Evidence for the physiological role of a rhodanese-like protein for the biosynthesis of the molybdenum cofactor in humans. *Proc Natl Acad Sci U S A*. 2004 Apr 20;101(16):5946-51. doi: 10.1073/pnas.0308191101.

Matthies, A., Nimtz, M., and Leimkühler, S. (2005). Molybdenum cofactor biosynthesis in humans: identification of a persulfide group in the rhodanese-like domain of MOCS3 by mass spectrometry. Biochemistry *44*, 7912–7920.

Meister, A. (1954). Enzymatic transfer of alpha-amino groups. *Science*, *120*(3106), 43-50.

Melaku, L., & Mossie, A. (2017). Molecular Characterization of Hydrogen Sulfide Role in Vascular System and Method of Endogenous Production Detections with Common Ion Channels Used to Produce Its Biological Effect. *Biochem Physiol*, *6*(222), 2.

Melideo SL, Jackson MR, Jorns MS. Biosynthesis of a central intermediate in hydrogen sulfide metabolism by a novel human sulfurtransferase and its yeast ortholog. *Biochemistry*. 2014 Jul 22;53(28):4739-53. doi: 10.1021/bi500650h.

Mendel RR, Schwarz G. Biosynthesis and molecular biology of the molybdenum cofactor (Moco). *Met Ions Biol Syst*. 2002;39:317-68.

Mikami, Y., Shibuya, N., Kimura, Y., Nagahara, N., Ogasawara, Y., Kimura, H., (2011). Thioredoxin and dihydrolipoic acid are required for 3-mercaptopyruvate sulfurtransferase to produce hydrogen sulfide. *Biochem. J.* **439**, 479–485.

Miles ZD, Roberts SA, McCarty RM, Bandarian V. Biochemical and structural studies of 6-carboxy-5,6,7,8-tetrahydropterin synthase reveal the molecular basis of catalytic promiscuity within the tunnel-fold superfamily. *J Biol Chem*. 2014 Aug 22;289(34):23641-52. doi: 10.1074/jbc.M114.555680.

Mintel R, Westley J. The rhodanese reaction. Mechanism of thiosulfate binding. *J Biol Chem*. 1966 Jul 25;241(14):3386-9.

Miyamoto, R., Otsuguro, K.-I., Yamaguchi, S., and Ito, S. (2014). Contribution of cysteine aminotransferase and mercaptopyruvate sulfurtransferase to hydrogen sulfide production in peripheral neurons. J. Neurochem. *130*, 29–40.

Motl, N., Skiba, M.A., Kabil, O., Smith, J.L., Banerjee, R., (2017). Structural and biochemical analyses indicate that a bacterial persulfide dioxygenase-rhodanese fusion protein functions in sulfur assimilation. *J. Biol. Chem.* **292**, 14026–14038.

Mukhopadhyay R, Rosen BP. Saccharomyces cerevisiae ACR2 gene encodes an arsenate reductase. *FEMS Microbiol Lett.* 1998 Nov 1;168(1):127-36. doi: 10.1111/j.1574-6968.1998.tb13265.x.

Mukhopadhyay R, Zhou Y, Rosen BP. Directed evolution of a yeast arsenate reductase into a protein-tyrosine phosphatase. *J Biol Chem*. 2003 Jul 4;278(27):24476-80. doi: 10.1074/jbc.M302610200.

Mukhopadhyay, R., Bisacchi, D., Zhou, Y., Armiroh, A., and Bordo, D. (2009) Structural characteriza<on of the As/Sb reductase LmACR2 from Leishmania major. *J. Mol. Biol*. 386, 1229–1239

Mukhopadhyay, R., Shi, J., and Rosen, B. P. (2000) Purification and characterization of Acr2p, the Saccharomyces cerevisiae arsenate reductase. *J. Biol. Chem*. 275, 21149–21157

Nagahara N, Koike S, Nirasawa T, Kimura H, Ogasawara Y. Alternative pathway of H_2S and polysulfides production from sulfurated catalytic-cysteine of reaction intermediates of 3-mercaptopyruvate sulfurtransferase. *Biochem Biophys Res Commun.* 2018 Feb 5;496(2):648-653. doi: 10.1016/j.bbrc.2018.01.056.

Nagahara, N.; Nishino, T. *J. Biol. Chem*. **1996**, *271*, 27395-401.

Nagahara,N.,Okazaki,T.,andNishino,T.(1995).Cytosolicmer- captopyruvate sulfurtransferase is evolu,onarily related to mito- chondrial rhodanese. *J. Biol. Chem*. *270*, 16230–16235.

NakagawaY,BenderML.1969.Modificationofalpha-chymotrypsinbymethylp nitrobenzenesulfonate. *J. Am. Chem. Soc.* 91:1566–67

Nandi, D.L., Westley, J., (1998). Reduced thioredoxin as a sulfur-acceptor substrate for rhodanese. *Int. J. Biochem. Cell Biol.* **30**, 973–977.

Neuberg C, Hirsch J (1921) An enzyme which brings about union into carbon chain (carboligase). *Biochem. Z.* **115**: 282–310.

Nilsson I, Hoffmann I. Cell cycle regulation by the Cdc25 phosphatase family. *Prog Cell Cycle Res*. 2000;4:107-14. doi: 10.1007/978-1-4615-4253-7_10. PMID: 10740819.

Nobeli I, Favia AD, Thornton JM. Protein promiscuity and its implications for biotechnology. *Nat Biotechnol*. 2009 Feb;27(2):157-67. doi: 10.1038/nbt1519.

O'Brien PJ, Herschlag D. Catalytic promiscuity and the evolution of new enzymatic activities. *Chem Biol*. 1999 Apr;6(4):R91-R105. doi: 10.1016/S1074-5521(99)80033-7.

O'Brien PJ, Herschlag D. Functional interrelationships in the alkaline phosphatase superfamily: phosphodiesterase activity of Escherichia coli alkaline phosphatase. *Biochemistry.* 2001 May 15;40(19):5691-9. doi: 10.1021/bi0028892.

Obach & Isoherranen, Atkinson's Principles of Clinical Pharmacology (Fourth Edition), 2022

Pabis M, Termathe M, Ravichandran KE, Kienast SD, Krutyhołowa R, Sokołowski M, Jankowska U, Grudnik P, Leidel SA, Glatt S. Molecular basis for the bifunctional Uba4-Urm1 sulfur-relay system in tRNA thiolation and ubiquitin-like conjugation. *EMBO J.* 2020 Oct 1;39(19):e105087. doi: 10.15252/embj.2020105087

Park HS, Nam SH, Lee JK, Yoon CN, Mannervik B, Benkovic SJ, Kim HS. Design and evolution of new catalytic activity with an existing protein scaffold. *Science*. 2006 Jan 27;311(5760):535-8. doi: 10.1126/science.1118953.

Pecci L, Pensa B, Costa M, Cignini PL, Cannella C. Reaction of rhodanese with dithiothreitol. *Biochim Biophys Acta.* 1976 Aug 12;445(1):104-11. doi: 10.1016/0005-2744(76)90163-7.

phosphatases, *Proc. Natl. Acad. Sci. U.S.A. 91*, 1624-1627.

Piedrafita G, Keller MA, Ralser M. The Impact of Non-Enzymatic Reactions and Enzyme Promiscuity on Cellular Metabolism during (Oxidative) Stress Conditions. *Biomolecules*. 2015 Sep 10;5(3):2101-22. doi:10.3390/biom5032101.

Ploegman JH, Drent G, Kalk KH, Hol WG, Heinrikson RL, Keim P, Weng L, Russell J. The covalent and tertiary structure of bovine liver rhodanese. *Nature*. 1978 May 11;273(5658):124-9. doi: 10.1038/273124a0.

Pocker Y, Stone JT. The catalytic versatility of erythrocyte carbonic anhydrase. The enzyme-catalyzed hydrolysis of rho-nitrophenyl acetate. *J Am Chem Soc*. 1965 Dec 5;87(23):5497-8. doi: 10.1021/ja00951a049.

Radabaugh TR, Aposhian HV. Enzymatic reduction of arsenic compounds in mammalian systems: reduction of arsenate to arsenite by human liver arsenate reductase*. Chem Res Toxicol*. 2000 Jan;13(1):26-30. doi: 10.1021/tx990115k.

Rahimi M, van der Meer JY, Geertsema EM, Poddar H, Baas BJ, Poelarends GJ. Mutations Closer to the Active Site Improve the Promiscuous Aldolase Activity of 4-Oxalocrotonate Tautomerase More Effectively than Distant Mutations. *Chembiochem.* 2016 Jul 1;17(13):1225-8. doi: 10.1002/cbic.201600149.

Ramos JL, Gonzalez-Perez MM, Caballero A, van Dillewijn P. 2005. Bioremediation of polynitrated aromatic compounds: plants and microbes put up a fight. *Curr Opin Biotechnol* 16:275–281.

Rao SP, Dobariya P, Bellamkonda H, More SS. Role of 3-Mercaptopyruvate Sulfurtransferase (3-MST) in Physiology and Disease. *Antioxidants (Basel).* 2023 Mar 1;12(3):603. doi: 10.3390/antiox12030603.

Ray WK, Zeng G, Potters MB, Mansuri AM, Larson TJ. Characterization of a 12-kilodalton rhodanese encoded by glpE of Escherichia coli and its interaction with thioredoxin. *J Bacteriol*. 2000 Apr;182(8):2277-84. doi: 10.1128/JB.182.8.2277-2284.2000.

ReidTW,FahrneyD.1967.Thepepsincatalyzedhydrolysisofsulfiteesters.*J.Am.Chem.Soc.*89:3941– 43.

Renata H, Wang ZJ, Arnold FH. Expanding the enzyme universe: accessing non-natural reactions by mechanism-guided directed evolution. *Angew Chem Int Ed Engl*. 2015 Mar 9;54(11):3351-67. doi: 10.1002/anie.201409470.

Rona, P., Ammon, R. and TRURNIT, H., 1931. Studies on the enzymatic ester formation and ester hydrolysis. *Biochem. Z*, *247*, pp.113-145

Rudolph J. Cdc25 phosphatases: structure, specificity, and mechanism. *Biochemistry.* 2007 Mar 27;46(12):3595-604. doi: 10.1021/bi700026j.

Sakai Y, Kimura S, Suzuki T. Dual pathways of tRNA hydroxylation ensure efficient translation by expanding decoding capability. *Nat Commun*. 2019 Jun 28;10(1):2858. doi: 10.1038/s41467-019-10750-8.

Selles B, Moseler A, Caubrière D, Sun SK, Ziesel M, Dhalleine T, Hériché M, Wirtz M, Rouhier N, Couturier J. The cytosolic Arabidopsis thaliana cysteine desulfurase ABA3 delivers sulfur to the sulfurtransferase STR18. *J Biol Chem*. 2022 Apr;298(4):101749. doi: 10.1016/j.jbc.2022.101749.

Selles, B., Moseler, A., Rouhier, N., and Couturier, J. (2019a). Rhodanese domain-containing sulfurtransferases: mul,faceted proteins involved in sulfur trafficking in plants. *J. Exp. Bot*. *70*, 4139– 4154.

Shen J, Keithly ME, Armstrong RN, Higgins KA, Edmonds KA, Giedroc DP. Staphylococcus aureus CstB Is a Novel Multidomain Persulfide Dioxygenase-Sulfurtransferase Involved in Hydrogen Sulfide Detoxification. *Biochemistry*. 2015 Jul 28;54(29):4542-54. doi: 10.1021/acs.biochem.5b00584.

Shibuya N, Tanaka M, Yoshida M, Ogasawara Y, Togawa T, Ishii K, Kimura H. 3-Mercaptopyruvate sulfurtransferase produces hydrogen sulfide and bound sulfane sulfur in the brain. *Antioxid Redox Signal*. 2009 Apr;11(4):703-14. doi: 10.1089/ars.2008.2253.

Shih VE, Abroms IF, Johnson JL, Carney M, Mandell R, Robb RM, Cloherty JP, Rajagopalan KV. Sulfite oxidase deficiency. Biochemical and clinical investigations of a hereditary metabolic disorder in sulfur metabolism. *N Engl J Med*. 1977 Nov 10;297(19):1022-8. doi: 10.1056/NEJM197711102971902.

Smirnov A, Comte C, Mager-Heckel AM, Addis V, Krasheninnikov IA, Martin RP, Entelis N, Tarassov I. Mitochondrial enzyme rhodanese is essential for 5 S ribosomal RNA import into human mitochondria*. J Biol Chem*. 2010 Oct 1;285(40):30792-803. doi: 10.1074/jbc.M110.151183.

Smirnov A, Entelis N, Martin RP, Tarassov I. Biological significance of 5S rRNA import into human mitochondria: role of ribosomal protein MRP-L18. *Genes Dev.* 2011 Jun 15;25(12):1289-305. doi: 10.1101/gad.624711

Sorbo, B. On the Proper,es of Rhodanese. *Acta Chem. Scand.* **1951**, *5*, 724–726.

Spallarossa A, Forlani F, Carpen A, Armirotti A, Pagani S, Bolognesi M, Bordo D. The "rhodanese" fold and catalytic mechanism of 3-mercaptopyruvate sulfurtransferases: crystal structure of SseA from Escherichia coli. *J Mol Biol.* 2004 Jan 9;335(2):583-93. doi: 10.1016/j.jmb.2003.10.072.

Spallarossa, M., et al. (2001). Crystal structure of the Escherichia coli GlpE thiosulfate sulfurtransferase: insights into the cataly,c mechanism of rhodanese-type enzymes. *Journal of molecular biology*, 307(1), 23-36.

Sur S, Agrawal DK. Phosphatases and kinases regulating CDC25 activity in the cell cycle: clinical implications of CDC25 overexpression and potential treatment strategies. *Mol Cell Biochem.* 2016 May;416(1-2):33-46. doi: 10.1007/s11010-016-2693-2

Sylvester M, Sander C. Immunohistochemical localization of rhodanese. *Histochem J*. 1990 Apr;22(4):197-200. doi: 10.1007/BF02386005.

Tabita R, Silver M, Lundgren DG. The rhodanese enzyme of Ferrobacillus ferrooxidans (Thiobacillus ferrooxidans). *Can J Biochem*. 1969 Dec;47(12):1141-5. doi: 10.1139/o69-184.

Termathe M, Leidel SA. The Uba4 domain interplay is mediated via a thioester that is critical for tRNA thiolation through Urm1 thiocarboxylation. *Nucleic Acids Res*. 2018 Jun 1;46(10):5171-5181. doi: 10.1093/nar/gky312

Tseng HC, Martin CH, Nielsen DR, Prather KL. Metabolic engineering of Escherichia coli for enhanced production of (R)- and (S)-3-hydroxybutyrate. *Appl Environ Microbiol*. 2009 May;75(10):3137-45. doi: 10.1128/AEM.02667-08.

Wackett LP. Questioning our perceptions about evolution of biodegradative enzymes. *Curr Opin Microbiol*. 2009 Jun;12(3):244-51. doi: 10.1016/j.mib.2009.05.001

Wang Q, Li H, Xia Y, Xun L, Liu H. *Saccharomyces cerevisiae* Rhodanese RDL2 Uses the Arg Residue of the Active-Site Loop for Thiosulfate Decomposition. *Antioxidants (Basel)*. 2021 Sep 26;10(10):1525. doi: 10.3390/antiox10101525.

Wang R. Physiological implications of hydrogen sulfide: a whiff exploration that blossomed. *Physiol Rev*. 2012 Apr;92(2):791-896. doi: 10.1152/physrev.00017.2011.

Wang Z, Trope CG, Florenes VA, Suo Z, Nesland JM, Holm R. Overexpression of CDC25B, CDC25C and phospho-CDC25C (Ser216) in vulvar squamous cell carcinomas are associated with malignant features and aggressive cancer phenotypes. *BMC Cancer*. 2010 May 25;10:233. doi: 10.1186/1471-2407-10-233.

Wegener S, Hampe W, Herrmann D, Schaller HC. Alternative splicing in the regulatory region of the human phosphatases CDC25A and CDC25C. *Eur J Cell Biol*. 2000 Nov;79(11):810-5. doi: 10.1078/0171-9335-00115.

Weng L, Heinrikson RL, Westley J. Active site cysteinyl and arginyl residues of rhodanese. A novel formation of disulfide bonds in the active site promoted by phenylglyoxal. *J Biol Chem*. 1978 Nov 25;253(22):8109-19.

Wenzel, K., Felix, S.B., Flachmeier, C., Heere, P., Schulze, W., Grunewald, I., Pankow, H., Hewelt, A., Scherneck, S., Bauer, D., et al. (2003). Identification and Characterization of

KAT, a Novel Gene Preferentially Expressed in Several Human Cancer Cell Lines. *384*, 763–775. doi.org/10.1515/BC.2003.085.

Westley J. Rhodanese. *Adv Enzymol Relat Areas Mol Biol*. 1973;39:327-68. doi: 10.1002/9780470122846.ch5.

Westley J. Thiosulfate: cyanide sulfurtransferase (rhodanese). *Methods Enzymol.* 1981;77:285-91. doi: 10.1016/s0076-6879(81)77039-3.

Westrop, G.D., Georg, I., Coombs, G.H., (2009). The mercaptopyruvate sulfurtransferase of Trichomonas vaginalis links cysteine catabolism to the production of thioredoxin persulfide. *J. Biol. Chem.* **284**, 33485–33494.

Williams, R.A.M., Kelly, S.M., Mottram, J.C., Coombs, G.H., (2003). 3-Mercaptopyruvate sulfurtransferase of Leishmania contains an unusual C-terminal extension and is involved in thioredoxin and antioxidant metabolism. *J. Biol. Chem.* **278**, 1480–1486.

Yadav, P.K., Yamada, K., Chiku, T., Koutmos, M., Banerjee, R., (2013). Structure and Kinetic Analysis of H2S Production by Human Mercaptopyruvate Sulfurtransferase. *J. Biol. Chem.* **288**, 20002–20013.

Yang K, Metcalf WW. A new activity for an old enzyme: Escherichia coli bacterial alkaline phosphatase is a phosphite-dependent hydrogenase. *Proc Natl Acad Sci U S A*. 2004 May 25;101(21):7919-24. doi: 10.1073/pnas.0400664101.

Yokoyama S, Watanabe T, Murao K, Ishikura H, Yamaizumi Z, Nishimura S, Miyazawa T. Molecular mechanism of codon recognition by tRNA species with modified uridine in the first position of the anticodon. *Proc Natl Acad Sci U S A*. 1985 Aug;82(15):4905-9. doi: 10.1073/pnas.82.15.4905.

Zhang, Z. Y. (2003). Chemical and mechanistic approaches to the study of protein tyrosine phosphatases. *Accounts of chemical research*, *36*(6), 385-392.

Zhang, Z. Y., Zhou, G. C., Denu, J. M., Wu, L., Tang, X. J., Mondesert, O., Russell, P., Butch, E., and Guan, K. L. (1995) Purifica,on and Characteriza,on of the Low Molecular Weight. *Plant Physiology,* 163(3), 273-286.

Zhang, Z.-Y., Wang, Y., and Dixon, J. E. (1994a) Dissec,ng the mechanism of protein-tyrosine

Zhang, Z., Harms, E., and Van E2en, R. L. (1994b) Asp129 of low molecular weight protein tyrosine phosphatase is involved in leaving group protona,on, *J. Biol. Chem. 269*, 25947-25950. 58.

Zhou Y, Bhattacharjee H, Mukhopadhyay R. Bifunctional role of the leishmanial antimonate reductase LmACR2 as a protein tyrosine phosphatase. *Mol Biochem Parasitol*. 2006 Aug;148(2):161-8. doi: 10.1016/j.molbiopara.2006.03.009.

Zhou Y, Messier N, Ouellette M, Rosen BP, Mukhopadhyay R. Leishmania major LmACR2 is a pentavalent antimony reductase that confers sensitivity to the drug pentostam. *J Biol Chem*. 2004 Sep 3;279(36):37445-51. doi: 10.1074/jbc.M404383200.

Annexe

antioxidants

MDPI

Review

Rhodanese-Fold Containing Proteins in Humans: Not Just Key Players in Sulfur Trafficking

Razan Alsohaibani †, Anne-Lise Claudel †, Romain Perchat-Varlet †, Séverine Boutserin, François Talfournier, Sandrine Boschi-Muller * and Benjamin Selles *

IMoPA, CNRS, Université de Lorraine, F-54000 Nancy, France

* Correspondence: sandrine.boschi@univ-lorraine.fr (S.B.-M.); benjamin.selles@univ-lorraine.fr (B.S.)

† These authors contributed equally to this work.

Abstract: The Rhodanese-fold is a ubiquitous structural domain present in various protein subfamilies associated with different physiological functions or pathophysiological conditions in humans. Proteins harboring a Rhodanese domain are diverse in terms of domain architecture, with some representatives exhibiting one or several Rhodanese domains, fused or not to other structural domains. The most famous Rhodanese domains are catalytically active, thanks to an active-site loop containing an essential cysteine residue which allows for catalyzing sulfur transfer reactions involved in sulfur trafficking, hydrogen sulfide metabolism, biosynthesis of molybdenum cofactor, thio-modification of tRNAs or protein urmylation. In addition, they also catalyse phosphatase reactions linked to cell cycle regulation, and recent advances proposed a new role into tRNA hydroxylation, illustrating the catalytic versatility of Rhodanese domain. To date, no exhaustive analysis of Rhodanese containing protein equipment from humans is available. In this review, we focus on structural and biochemical properties of human-active Rhodanese-containing proteins, in order to provide a picture of their established or putative key roles in many essential biological functions.

Keywords: Rhodanese-fold; sulfur trafficking; cysteine persulfide; promiscuous activities; MoCo maturation; tRNA thiolation

check for updates

Citation: Alsohaibani, R.; Claudel, A.-L.; Perchat-Varlet, R.; Boutserin, S.; Talfournier, F.; Boschi-Muller, S.; Selles, B. Rhodanese-Fold Containing Proteins in Humans: Not Just Key Players in Sulfur Trafficking. *Antioxidants* **2023**, *12*, 843. https://doi.org/10.3390/antiox12040843

Academic Editor: Stanley Omaye

Received: 2 March 2023
Revised: 21 March 2023
Accepted: 28 March 2023
Published: 31 March 2023

Copyright: © 2023 by the authors. Licensee MDPI, Basel, Switzerland. This article is an open access article distributed under the terms and conditions of the Creative Commons Attribution (CC BY) license (https://creativecommons.org/licenses/by/4.0/).

1. Introduction

Proteins harboring a Rhodanese (Rhd) domain are ubiquitous and are involved in a variety of physiological processes, from metabolic pathways and signaling to protein posttranslational modifications [1–4]. The role of Rhd-containing proteins in most of these pathways resides in the capability of such functional protein domains to catalyze sulfur atom transfers from a donor molecule to an acceptor one, thus, participating in sulfur atom trafficking. In particular, they are now recognized as key players in the emerging gasotransmitter hydrogen sulfide (H_2S) homeostasis in humans. H_2S is described as an ubiquitous and pleiotropic molecule with a broad spectrum of targets, including nuclear factor-kappa (NF-κB), p38 mitogen-activated kinase (p38 MAPK), nuclear factor erythroid 2-related factor 2 (Nrf2), p53 and mTOR, the target of rapamycin [5–8]. Based on its chemical properties, the reactions involving H_2S are categorized into the following three groups: 1—reactions with metal centers, 2—cross-talks with ROS and RNS, 3—protein persulfide formation [9]. More recently, Rhd-containing proteins were reported to be involved in tRNA thiolation (i.e., post-transcriptional modifications), stabilizing tRNA tertiary structure and/or permitting fine-tune decoding processes [10], or in maturation of the molybdenum cofactor (MoCo), a prosthetic group present in essential proteins, such as sulfite oxidase (SO), xanthine oxidoreductase (XOR), and aldehyde oxidase (AO) [11].

Hence, understanding the Rhd structural domain landscape is an essential step to understanding the importance of such proteins in human physiology. Here we summarize the current understanding on active human Rhd proteins, in both mechanistic and physiological terms.

2. The Rhodanese-Fold and Domains Organization

The so called "rhodanese" fold is an α/β structural arrangement, containing around 100 residues, found in a broad range of protein structures, encoded by prokaryotes and eukaryotes genomes (Figure 1a) [1,2].

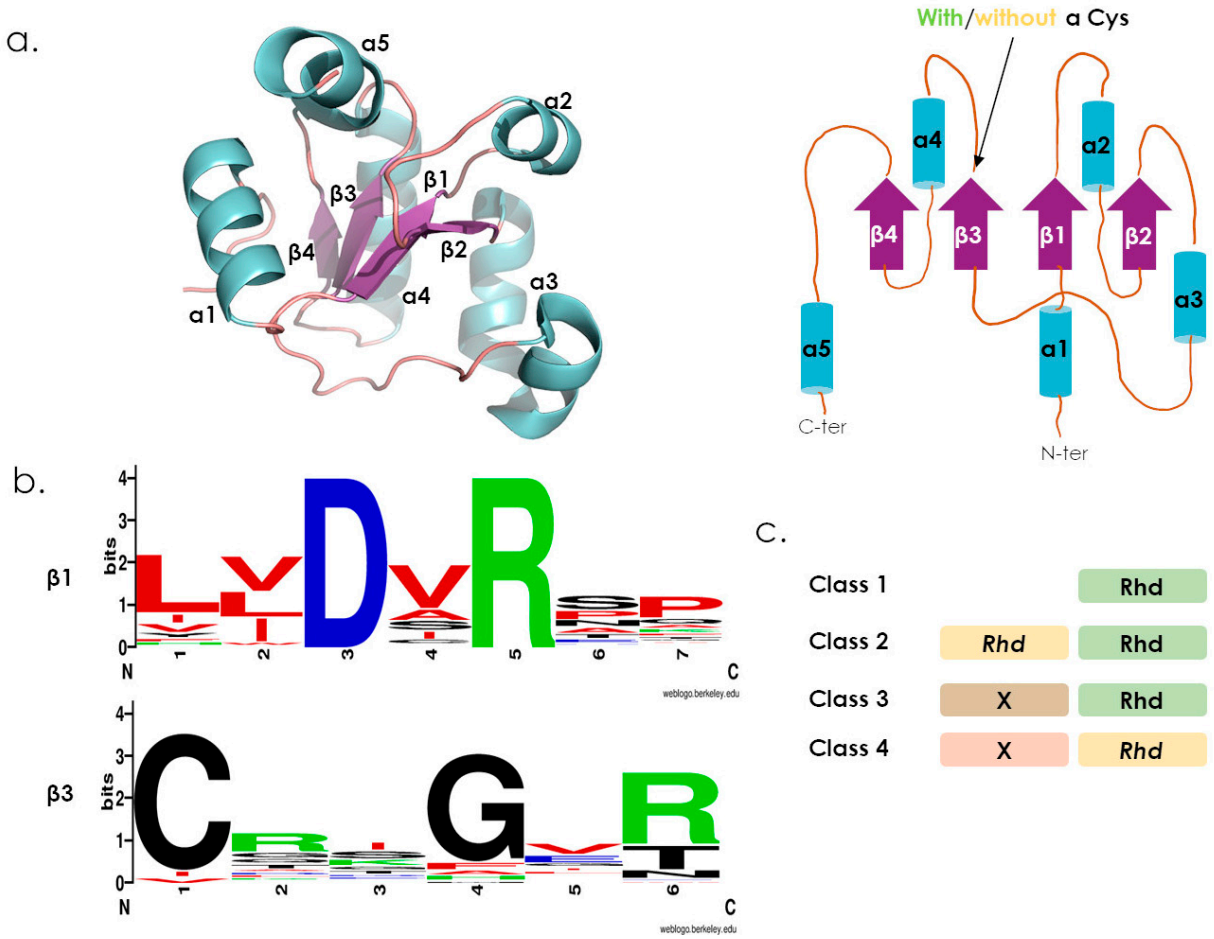

Figure 1. Rhodanese-fold features of Rhd-containing proteins. (**a**) 3D structure of TSTD1 (PDB 6BEV), with its topological representation. (**b**) WebLogo-generated representation (https://weblogo.berkeley.edu/logo.cgi, accessed on 07 October 2022) of the patterns issued from a multiple alignment of 50 sequences (identified by Blast with TSTD1 as template, UniProt, https://www.uniprot.org/, accessed on 20 September 2022) that cover the two structural regions located at the end of β-1 and β-3 strands in Rossmann-like fold. (**c**) The different subclasses of Rhd domain-containing proteins. Active Rhd domains are represented in green, inactive Rhd domains are in yellow, other structural domains (X) are represented in brown and pink.

Despite a conserved overall structural arrangement, primary structures adopting the Rhd fold are highly variable, making global sequence comparison between functionally or evolutionary distant Rhd-containing proteins difficult. Meanwhile, the growing number of available Rhd 3D structures from a variety of proteins (215 entries at RCSB database, https://www.rcsb.org accessed on 5 September 2022) allows a direct inspection of Rhd-domain conserved structural signatures. As an example, an in silico large scale identification and analysis of Rossmann-like structural domains revealed that the Rhd fold belongs to this vast family. Its structure is composed of a three-layered α/β sandwich (a characteristic of Rossmann-like protein) in which, the central parallel β sheet is surrounded by 4 to 5 α-helices (Figure 1a) [12]. Authors also identified two highly conserved structural motifs within the Rhd domain, at the end of the β1 strand, corresponding to a DxR motif of unknown function, and the end of the β3 strand corresponding to a

(C/D)$x_{4/5}$(R/T) loop motif (Figure 1b, Supplemental File S1, Supplemental Materials) [1,3]. Quite interestingly, despite some sequence variability, these two structural motifs are conserved within Rossmann-like subfamilies, revealing a promiscuous fold adapted to perform various functions. Thereby, Rhd domains can be defined as catalytically active or inactive, depending on the presence or absence, respectively, of a cysteine residue within the loop located at the end of the β3 strand (Figure 1a) [1]. For the active ones, the so-called catalytic loop is made of a Cx_4R/T or Cx_5R motif that supports various chemical reactions. By contrast, catalytically inactive Rhd domains are rather considered as protein–protein interaction mediators [13].

Rhd domain-containing proteins also exhibit variable domain organizations, with one or several Rhd domains fused or not to other functional domains [1–3,14,15]. Considering the catalytically active/inactive criteria previously defined, the following four classes can be defined (Figure 1c): (1) mono-domain proteins, with a unique active Rhd domain; (2) two-domain proteins, with an inactive and an active Rhd domains; (3) an active Rhd domain fused to unrelated domains; (4) an inactive Rhd domain fused to unrelated domains.

3. Reactions Catalyzed by Active Rhodanese Domains

The active Rhd domains, bearing a cysteine residue in the catalytic loop, are able to catalyze several classical reactions as follows: a sulfur transfer for sulfurtransferases, a phosphate group transfer for phosphatases, or an arsenate reduction for arsenate reductases. The latter two were reported for the CDC25 proteins [16,17].

Sulfurtransferases catalyze the transfer of a sulfur atom from a donor substrate to an acceptor one. Depending on their preferred donor substrate in vitro, these enzymes can be classified into the following two groups: thiosulfate sulfurtransferases (TSTs) for thiosulfate, and 3-mercaptopyruvate sulfurtransferases (3MSTs or MPSTs) for 3-mercaptopyruvate [2]. The two-step reaction is initiated by the nucleophilic attack of the catalytic cysteine on the sulfur atom of the substrate, leading to the formation of a persulfide intermediate. Then, the sulfur atom is transferred to an acceptor to form the product and regenerate the cysteine under thiolate form (Figure 2a) [18]. The two-step mechanism for the phosphatase-catalyzed reaction [19] starts with the nucleophilic attack of the catalytic cysteine on the substrate phosphate group to form a phosphoenzyme intermediate that is further hydrolyzed (Figure 2b). Finally, arsenate reductases catalyze the two-electron reduction in arsenate (As(+V)) to arsenite (As(+III)), and the proposed mechanism involves the nucleophilic attack of the catalytic cysteine on the arsenic atom of the substrate to form a thioarsenate intermediate, which is then reduced to arsenite by glutathione and glutaredoxin (Figure 2c) [20,21].

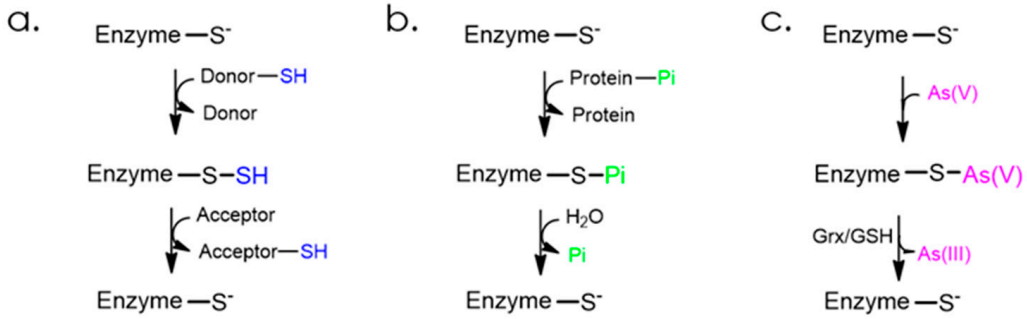

Figure 2. Two-step mechanisms for the reactions catalyzed by (**a**) sulfurtransferases, (**b**) phosphatases, and (**c**) arsenate reductases.

4. The Human Rhodanese Repertoire

Because of their highly divergent nature, sequence identity search programs cannot be used to exhaustively identify Rhd domains from sequence databases. A keyword-based search of the human Rhd domains present in the UniProt library [22] identified 30 proteins (Supplementary File S2), 23 of which possess a Rhd domain (the 7 remaining are

described as interacting with Rhd-containing proteins). Structural information is available for these 23 proteins, either PDB structures for 10 of them, or 3D models in the Alphafold database for all [23]. A thorough analysis of these structures or models shows that 8 of them possess a cysteine-containing catalytic loop and thus should be active (MPST, TST, TSTD1, CDC25A-B-C, MOCS3 and TSTD2) (Figure 3a). Interestingly, superimposing all the catalytic loops reveals noticeable structural homology, even for CDC25-type proteins containing a loop that is one residue longer (Figure 3b). Despite this structural homology, it was proposed by several studies that catalysis features and substrate specificities of the Rhd domain-containing protein are mostly driven by the residue composition of the catalytic loop [1,24,25].

a.

	Entry	Entry name	Length (a.a.)	Domain [FT]	pdb	Alphafold
MPST	P25325	THTM_HUMAN	297	DOMAIN 25..144	4JGT	
TST*	Q16762	THTR_HUMAN	297	DOMAIN 25..143		AF-Q16762-F1
TSTD1	Q8NFU3	TSTD1_HUMAN	115	DOMAIN 17..115	6BEV	
CDC25A	P30304	MPIP1_HUMAN	524	DOMAIN 376..482	1C25	
CDC25C	P30305	MPIP2_HUMAN	580	DOMAIN 431..538	1CWR	
CDC25B	P30307	MPIP3_HUMAN	473	DOMAIN 321..428	3OP3	
MOCS3	O95396	MOCS3_HUMAN	460	DOMAIN 347..458	3I2V	
TSTD2	Q5T7W7	TSTD2_HUMAN	516	DOMAIN 301..396		AF-Q5T7W7-F1

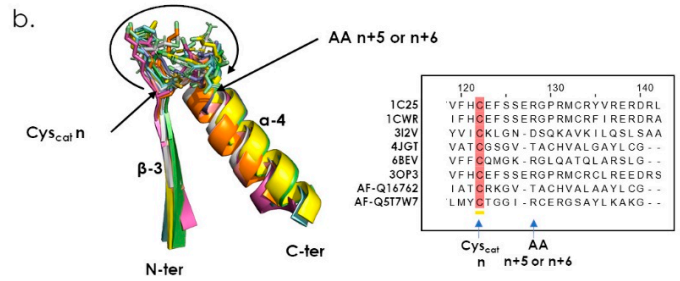

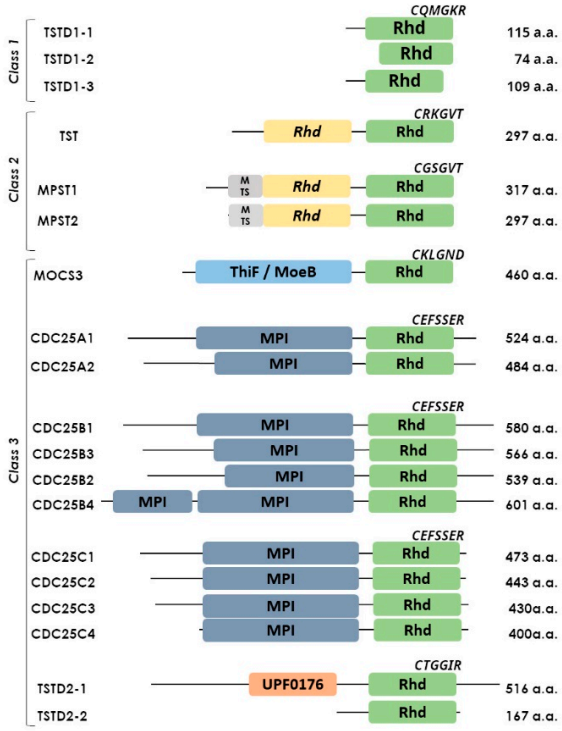

Figure 3. Human-active Rhd domain-containing proteins. (**a**) Eight human Rhd domain-containing proteins retrieved from the Uniprot database (https://www.uniprot.org/, accessed on 15 September 2022), indicating the length of the proteins and the position of the Rhd domain within the sequences. 3D-structures available in PDB, experimentally resolved or predicted structures by alphafold (https://alphafold.ebi.ac.uk/ accessed on 18 October 2022) are indicated. TST* is also known as Rhodanese. (**b**) Superimposition of active site loops (in sticks) flanked by the β-3 strand and the α-4 helix was made using CCP4MG software (https://www.ccp4.ac.uk/MG/ accessed on 5 July 2022) and is represented using Pymol (https://pymol.org/2/, version 2.4.1, accessed on 5 July 2002). Sequence alignment extracted from structure superimposition is represented in the right panel. (**c**) Modular organization of human-active Rhd domain-containing proteins and of their described isoforms. Active site loop sequences are indicated, and protein domains were defined using InterPro (https://www.ebi.ac.uk/interpro/, accessed on 25 September 2022).

Among the eight active Rhd-containing proteins, four catalyze a sulfur transfer reaction (MPST, TST, TSTD1, MOCS3) and three catalyze phosphatase reactions (CDC25A/B/C), whereas no typical Rhd-dependent activity is proposed for the last one (TSTD2). In terms of domain organization, TSTD1 belongs to class one, MPST and TST to class two, and CDCD25A/B/C, MOCS3 and TSTD2 to class three (Figure 3c). These 8 proteins were characterized in vitro and/or *in cellulo*, except for TSTD2 (Figure 4).

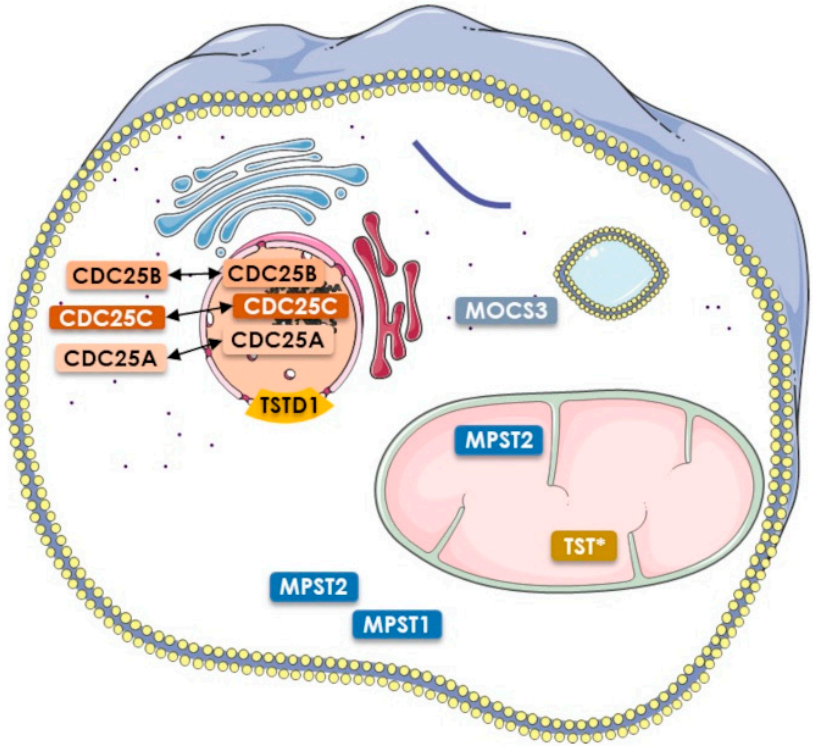

Figure 4. Reported sub-cellular localizations of human Rhd-containing proteins representatives [24,26–34].

5. TSTD1: The Unique Class One Rhd Enzyme, So Far

TSTD1 is encoded by the *KAT* gene located on chromosome 1 (1q23.3), which is 1.6 kilobases long and consists of 4 exons and 3 introns [30]. In vivo, three transcripts are generated from *KAT* by alternative splicing, thus leading to the production of 3 TSTD1 isoforms (1-1, 1-2, 1-3) (Figure 3c). The TSTD1-1 isoform (115 residues and 12,530 Da) is issued from the longest transcript, containing the four exons. The TSTD1-2 isoform (74 residues and 8274 Da) that is truncated at its N-terminus compared to TSTD1-1 corresponds to the shortest transcript, lacking exon 2. The TSTD1-3 isoform (109 residues and 11,750 Da) with a truncated C-terminal end and a decapeptide not present in TSTD1-1 and 1-2 (decapeptide encoded by intron 3) is produced from the medium transcript, lacking exon 4 and containing intron 3.

The sulfurtransferase activity of TSTD1 isoforms has been studied in vitro [35,36]. First, Melideo and colleagues have investigated potential sulfurtransferase activities of all three TSTD1 isoforms, with thiosulfate as donor and glutathione as acceptor, and they have demonstrated that TSTD1-1 is the only isoform displaying sulfurtransferase activity under such conditions [35]. In addition, Libiad and co-workers have investigated the thiosulfate sulfurtransferase activity of TSTD1-1, with various sulfur acceptor substrates (Figure 5b) [36]. In these conditions, the TSTD1-1 protein exhibits affinity for KCN, GSH, Cys or homocysteine (HCys) in the mM range, but a K_M for thioredoxin around 17 µM, a value close to those reported for other physiological thioredoxin partners [36–39]. This suggests that, in vitro, human thioredoxin is the final sulfur acceptor for TSTD1.

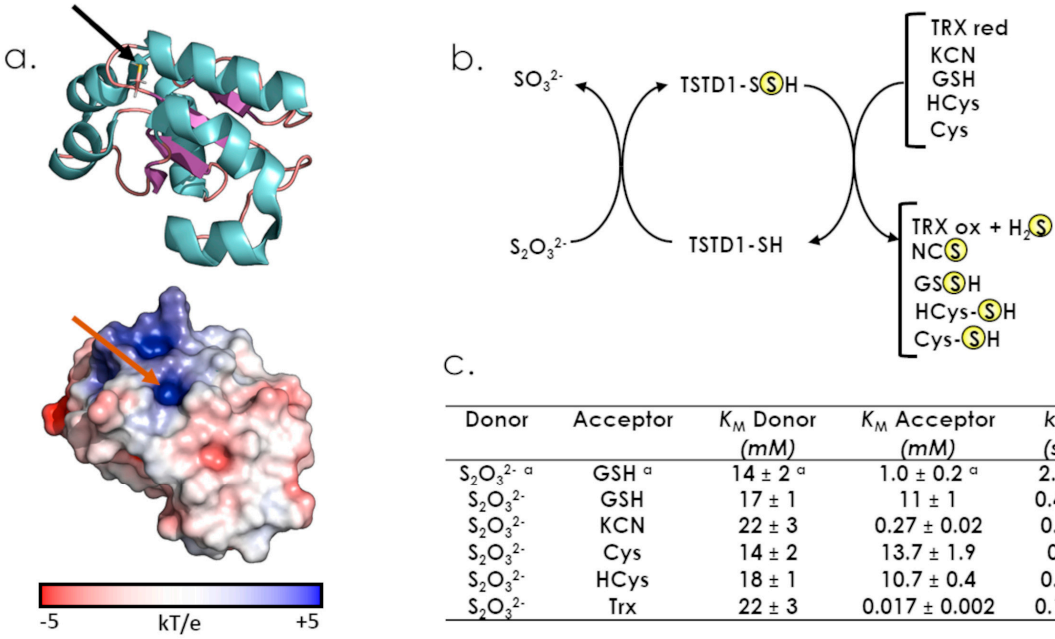

c.

Donor	Acceptor	K_M Donor (*mM*)	K_M Acceptor (*mM*)	k_{cat} (s^{-1})	k_{cat} / K_M (M^{-1}. s^{-1})
$S_2O_3^{2-}$ [a]	GSH [a]	14 ± 2 [a]	1.0 ± 0.2 [a]	2.7 [a]	-
$S_2O_3^{2-}$	GSH	17 ± 1	11 ± 1	0.432	25
$S_2O_3^{2-}$	KCN	22 ± 3	0.27 ± 0.02	0.52	24
$S_2O_3^{2-}$	Cys	14 ± 2	13.7 ± 1.9	0.7	50
$S_2O_3^{2-}$	HCys	18 ± 1	10.7 ± 0.4	0.61	34
$S_2O_3^{2-}$	Trx	22 ± 3	0.017 ± 0.002	0.116	23,000

Figure 5. Structural and catalytic properties of TSTD1. (**a**) Cartoon and surface representations of the TSTD1 structure (PDB 6BEV). The active site cysteine is represented in stick and indicated by a black (cartoon) or a red (surface) arrow. (**b**) describes sulfur donors and acceptors for TSTD1. (**c**) Steady-state kinetic parameters for the thiosulfate sulfurtransferase activity of TSTD1 ([36], except for [a] [35]).

In addition, Melideo and colleagues revealed a potential mechanistic crosstalk between TSTD1 and a protein with Persulfide Dioxygenase (PDO) activity. Indeed, they demonstrated that the presence of PDO accelerated the TSTD1 catalysis toward thiosulfate by consuming the TSTD1 reaction product (GSSH). Moreover, the fact that fusions between PDO and Rhd-fold protein domains exist proposes that TSTD1 protein is part of the mitochondrial sulfide oxidation unit complex (SOU complex), the main actor of H_2S detoxication in mammalian cells. Meanwhile, no in cellulo data supports this hypothesis so far.

A high resolution crystal structure of the TSTD1-1 isoform was recently reported (Figure 5a) [36]. TSTD1-1 possesses a canonical Rhd fold composed of five stranded β-sheet surrounded by six α-helices. Authors also identified a potential specific feature of TSTD1 protein compared to multidomain sulfurtransferases, because the catalytic cysteine lies in a shallow pocket, whereas it is more deeply buried for MPST or TST proteins.

In humans, *TSTD1* transcripts accumulate in different tissues, such as the kidney, liver, skeletal muscle, heart, colon, thymus, spleen, placenta, or lung [30]. In addition, TSTD1 proteins accumulate in various cancer derived cell lines [30]. Because the human colon is physiologically exposed to high levels of thiosulfate due to gut microbiome activities, Libiad and colleagues recently, investigated the TSTD1 protein localization within this tissue [36,40]. They demonstrated that TSTD1 accumulates within the luminal face of the colon, the potential major site of interaction between the microbiome and human cells.

6. The Two Rhd Classes, TST and MPST (Two Evolutionarily Related Sulfurtransferases with Different Functions)

6.1. TST

The human TST is also called Rhodanese in the literature, due to the name of the first characterized TST protein denominated as RhoBov (Bovin Rhodanese) [41–43]. The *TST* gene is located on chromosome 22 (22q12.3), and the protein (297 residues and 33 kDa) is produced from a unique 1.3 kb long mRNA [44]. Regarding 3D-structure, no information is available for the human enzyme, except for a model predicted by Alphafold

(https://alphafold.ebi.ac.uk/entry/Q16762, accessed on 18 October 2022). Nevertheless, the 3D-structure of the RhoBov homolog protein, with 89% sequence identity, is available in the PDB (PDB 1BOH). As previously mentioned, the TST protein is composed of two Rhd domains with a unique catalytic cysteine residue located in the C-terminal one (Figures 3c and 6a). The active site is walled in by residues from both domains and resides in the interdomain cleft. The catalytically active cysteine residue is embedded in the CRKGVT loop, whose sequence clearly differs from those of other sulfurtransferase family members [1]. In vitro, TST efficiently catalyzes the sulfur transfer from thiosulfate to cyanide to generate thiocyanate and sulfite (Figure 6b). This reaction explains the rationale for using thiosulfate as an antidote against cyanide poisoning. It has also been shown that TST has a 40-fold higher catalytic efficiency in the presence of glutathione-persulfide (GSSH) compared to thiosulfate (Figure 6c) [45]. In addition, sulfite is a rather good sulfur-acceptor substrate, which leads to the formation of thiosulfate. Altogether, formation of thiosulfate from sulfite and GSSH is much more efficient than the reverse reaction, with at least 400-fold higher k_{cat}/K_M value (Figure 6b,c), suggesting that TST preferentially produces, rather than utilizes, thiosulfate. Two other thiol acceptors, cysteine and homocysteine, showed higher efficiency than GSH, primarily due to higher k_{cat} values. However, one needs to keep in mind that steady-state kinetics are not totally appropriate to define the substrate specificities of this enzyme, since TST exhibited kinetic cooperativity with respect to many substrates. This may result from unexplained hysteresis behaviour and thus prevents relevant comparison of catalytic efficiencies [46].

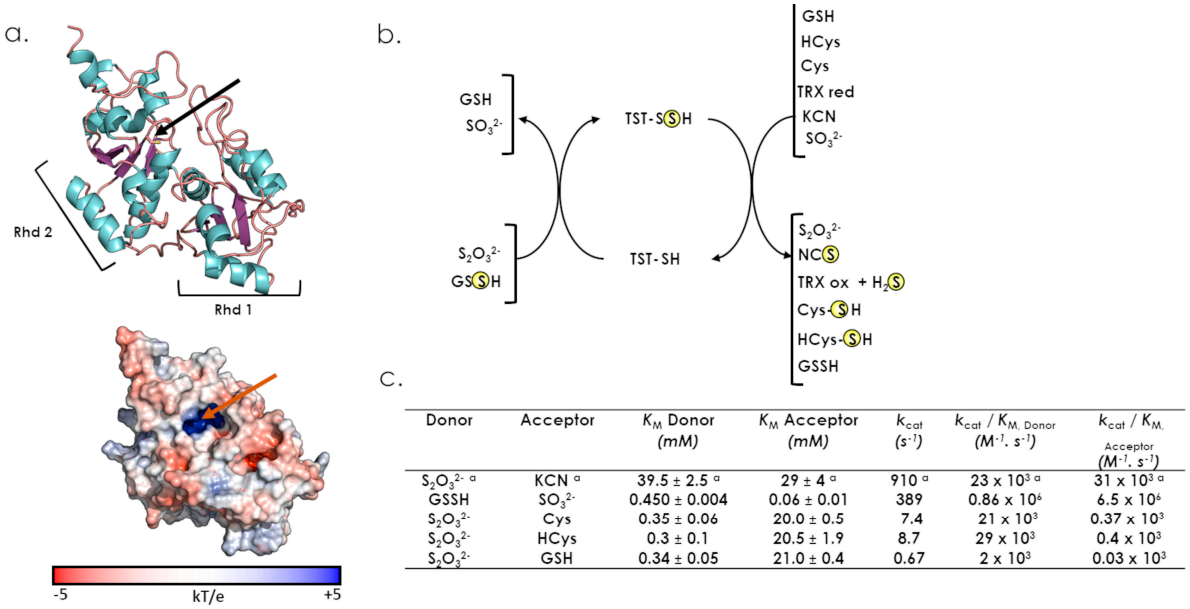

c.

Donor	Acceptor	K_M Donor (*mM*)	K_M Acceptor (*mM*)	k_{cat} (s^{-1})	k_{cat} / $K_{M,\ Donor}$ ($M^{-1}.\ s^{-1}$)	k_{cat} / $K_{M,\ Acceptor}$ ($M^{-1}.\ s^{-1}$)
$S_2O_3^{2-}$ [a]	KCN [a]	39.5 ± 2.5 [a]	29 ± 4 [a]	910 [a]	23 x 10^3 [a]	31 x 10^3 [a]
GSSH	SO_3^{2-}	0.450 ± 0.004	0.06 ± 0.01	389	0.86 x 10^6	6.5 x 10^6
$S_2O_3^{2-}$	Cys	0.35 ± 0.06	20.0 ± 0.5	7.4	21 x 10^3	0.37 x 10^3
$S_2O_3^{2-}$	HCys	0.3 ± 0.1	20.5 ± 1.9	8.7	29 x 10^3	0.4 x 10^3
$S_2O_3^{2-}$	GSH	0.34 ± 0.05	21.0 ± 0.4	0.67	2 x 10^3	0.03 x 10^3

Figure 6. Structural and catalytic properties of TST. (**a**) Cartoon and surface representations of the TST structure (Alphafold AF-Q16762). The two Rhd domains are indicated. The active site cysteine is represented in stick and is indicated by a black (cartoon) or a red (surface) arrow. (**b**) describes sulfur donors or acceptors for TST. (**c**) Steady-state kinetic parameters for the sulfurtransferase activity of TST ([45], except for [a] [46]).

Although the TST protein is targeted to mitochondria, it does not contain a N-terminal mitochondrial targeting sequence (Figures 3c and 4) [28,42,47]. Interestingly, investigation of 5S RNA mitochondrial targeting revealed that two protein components were essential to this process, the TST and the MRP-L18 proteins [28,29]. Mixed cellular and molecular experiments showed that a TST/5 S RNA complex is indeed formed, mediated by the 5S RNA γ-domain, and that the MRP-L18 protein is essential for the γ-domain conformational changes that are required to form this complex [28,29]. Meanwhile, the TST protein is successfully imported into mitochondria in the absence of 5S RNA, at least in vitro, indicating

that the molecular mechanism driving this process is still elusive [28]. This protein is also proposed to be involved in the mitochondrial sulfide oxidation pathway. This pathway begins with sulfide quinone oxidoreductase (SQOR) and includes a sulfur dioxygenase (also known as ETHE1 or persulfide dioxygenase, PDO) and TST. Indeed, combined kinetic data and simulations at physiologically-relevant substrate concentrations shows that SQOR predominantly catalyses the synthesis of GSSH, a substrate for TST [45,48,49].

The TST protein is abundant in the liver, kidney and colon, where it is important in the detoxification of H_2S produced by sulfate-reducing microbiota [46]. A role of TST in the regulation of fat mass has also been proposed. This assumption is supported by the fact that expression of the *TST* mRNA in adipose tissue is positively correlated with insulin sensitivity and negatively with fat mass. Thus, the *TST* gene as a beneficial regulator of mitochondrial adipocyte function could have therapeutic significance for people with type 2 diabetes [50].

Finally, a deficiency in TST activity is associated with Leber's disease, a rare hereditary pathology causing atrophy of the eye [51]. The study of liver biopsies of patients showed that TST activity decreases during the disease progression. Indeed, infusion of these patients with thiosulfate does not cause an increase in the urinary concentration of thiocyanate, in contrast to what is observed for healthy individuals [52]. This suggests that cyanide detoxification is suboptimal in patients with Leber's disease, probably due to decreased TST activity.

6.2. MPST

MPST, now well recognized as one of the enzymes involved in the generation of hydrogen sulfide (H_2S), has already been subject to a recent review focused on mechanistic and physiological aspects [53].

As expected, the reported crystal structure of MPST contains two Rhd domains as follows: an inactive N-terminal domain (residues 1–138) and an active C-terminal domain (residues 165–285), connected by a long linker (residues 139–164) that wraps around and interacts tightly with both domains (Figures 3c and 7a) [54]. A cleft located between the two domains houses the active site occupied by the complex formed after the first step of sulfur transfer. The catalytic cysteine persulfide (Cys_{248}-SSH) located in a CGSGVT loop and the pyruvate (Figure 7a) and both domains contribute residues that line the active site.

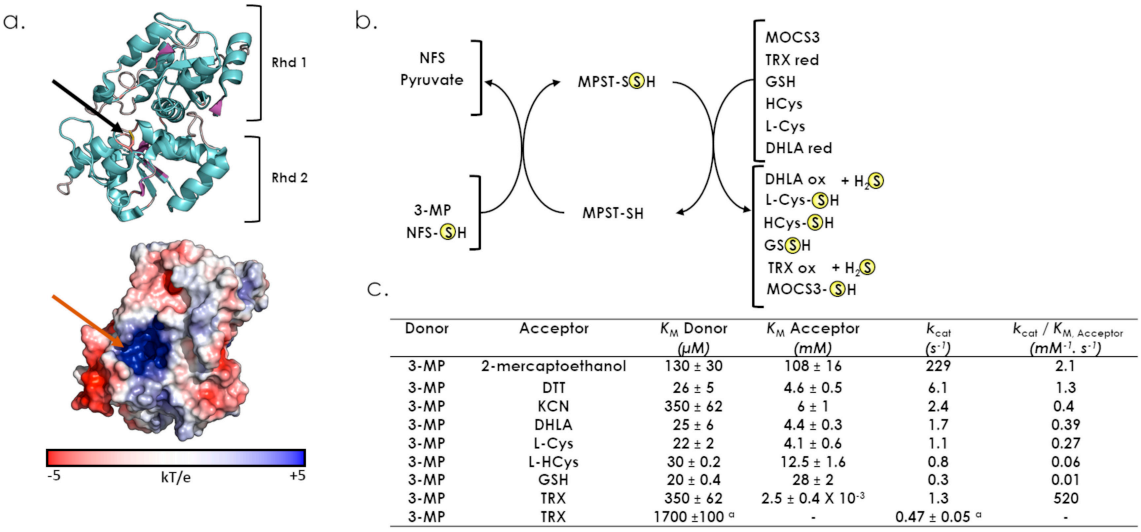

c.

Donor	Acceptor	K_M Donor (μM)	K_M Acceptor (mM)	k_{cat} (s^{-1})	k_{cat} / $K_{M,\ Acceptor}$ ($mM^{-1}.\ s^{-1}$)
3-MP	2-mercaptoethanol	130 ± 30	108 ± 16	229	2.1
3-MP	DTT	26 ± 5	4.6 ± 0.5	6.1	1.3
3-MP	KCN	350 ± 62	6 ± 1	2.4	0.4
3-MP	DHLA	25 ± 6	4.4 ± 0.3	1.7	0.39
3-MP	L-Cys	22 ± 2	4.1 ± 0.6	1.1	0.27
3-MP	L-HCys	30 ± 0.2	12.5 ± 1.6	0.8	0.06
3-MP	GSH	20 ± 0.4	28 ± 2	0.3	0.01
3-MP	TRX	350 ± 62	2.5 ± 0.4 X 10^{-3}	1.3	520
3-MP	TRX	1700 ±100 [a]	-	0.47 ± 0.05 [a]	-

Figure 7. Structural and catalytic properties of MPST. (**a**) Cartoon and surface representations of the MPST structure (PDB 4JGT). The active site cysteine is represented in stick and indicated by a black (cartoon) or a red (surface) arrow. (**b**) describes sulfur donors or acceptors for the MPST. (**c**) Steady-state kinetic parameters for the 3-mercaptopyruvate sulfurtransferase activity of MPST ([54], except for [a] [25]).

MPST transfers a sulfur atom from 3-MP to various physiological or artificial acceptors and, if the latter is a thiol compound, the decomposition of the product formed leads to H_2S production (Figure 7b) [2,55,56]. Non-physiological reductants that can liberate H_2S include DTT and 2-mercaptoethanol, whereas physiologically relevant ones are GSH, homocysteine, cysteine, dihydrolipoic acid (DHLA) and thioredoxin [25,54]. Based on steady-state kinetic parameters, thioredoxin is likely to be the better acceptor for MPST, as supported by a catalytic efficiency that is much higher than those obtained for the non-physiologically reductant DTT (k_{cat}/K_M 400-fold lower) or the small biologically-relevant reductant GSH (k_{cat}/K_M 52,000-fold lower) (Figure 7b). It is important to note that MPST displays non Michaelis-Menten kinetics, such as TST. This behaviour, that may result from hysteresis, could be explained by the requirement for conformational transitions to occur between the two steps of sulfur transfer (Lec et al., 2018). Moreover, MPST is the only Rhd-containing sulfurtransferase for which the persulfide formation mechanism has been deciphered [25,53]. This step is very efficient and critically depends on the electrostatic contribution provided by the CGSGVT catalytic loop. Furthermore, the water-mediated protonation of the pyruvate enolate and the S^0 transfer from the deprotonated 3-MP to the thiolate form of the catalytic cysteine occur concomitantly.

In the human genome, only one gene located on chromosome 22 (22q12.3) encodes a MPST (also known as TUM1 or 3-MST). The cytoplasmic and mitochondrial localization of human MPST is supported by immunofluorescence studies performed in human HEK293 cells (Figure 4) [27]. This dual subcellular localization is due to the existence of two MPST isoforms, resulting from an alternative translation initiation start. The shorter isoform possesses an accessible mitochondrion targeting sequence, whereas this sequence is masked by an additional N-terminal peptide of 20 residues for the longer one [27]. These features explain the strict cytosolic or the dual cytosolic–mitochondrial localization of the long or the short form, respectively (Figures 3c and 4). It should be noted that these two isoforms exhibit identical kinetic and physicochemical properties [27,57]. Moreover, the cytosolic isoform of MPST is able to interact with the cytosolic forms of the NFS1 cysteine desulfurase and MOCS3 sulfurtransferase, while the second one interacts with MOCS3 in the cytosol and NFS1 within mitochondria [27]. These results suggest additional roles for MPST depending on its subcellular location (thiolation of mitochondrial tRNAs for the MPST/NFS1complex and biosynthesis of molybdenum cofactors for the cytosolic MPST/MOCS3 complex).

MPST is involved in H_2S production in the brain, kidney, and liver at the mitochondrial level [58]. From a pathophysiological point of view, an MPST deficiency in humans is associated to a rare syndrome called mercaptolactate-cysteine disulfiduria, characterized by mental disorder and a specific form of disulfiduria [59–61].

7. The Class Three Rhd Enzymes in Humans, the Most Versatile Rhd Domains

This class is the most divergent in terms of domain nature and organization, catalytic activity and physiological function, with three enzymes, among which, one was recently discovered.

7.1. CDC25s

CDC25 (Cell Division Cycle 25) phosphatases belong to the family of dual-specificity phosphatases, i.e., they are able to dephosphorylate both the pThr and pTyr residues of their substrates, the cyclin-dependent kinases (CDK) [62].

The CDC25 family in humans is composed of three proteins (CDC25A, CDC25B and CDC25C) encoded by three different genes localized in chromosomes 3, 20 and 5, (3p21.31, 20p13 and 5q31.2), respectively. CDC25 genes produce transcripts that are subjected to alternative splicing, leading to the production of two variants for CDC25A and four variants for CDC25B or CDC25C (Figure 3c). Canonical representatives for CDC25s isoforms are 524, 580 and 473 residues, which are proteins for CDC25A, CDC25B and CDC25C, respectively (Figure 3c) [63–66].

The structure of CDC25s can be divided into two main domains, the extremely divergent regulatory N-terminal domain and the catalytic C-terminal Rhd domain (Figure 3c) [67]. To date, available 3D structures for CDC25s only concern their respective Rhd domain (Figure 8a). The catalytic Cys484 residue, included into the HCX_5R loop sequence of the Rhd domain, is located in a binding pocket for the substrate's phosphate group, whereas other key elements for substrate recognition are located about 20–30 Å from the active site [68,69]. The N-terminal regulatory domain contains phosphorylation and ubiquitination sites that regulate phosphatase activity, and there are large differences between the three isoforms (sequence similarity is less than 25% and they vary in length). Moreover, this domain contains other sequence motifs, which determine the subcellular localization of the CDC25s (Figure 4) [70].

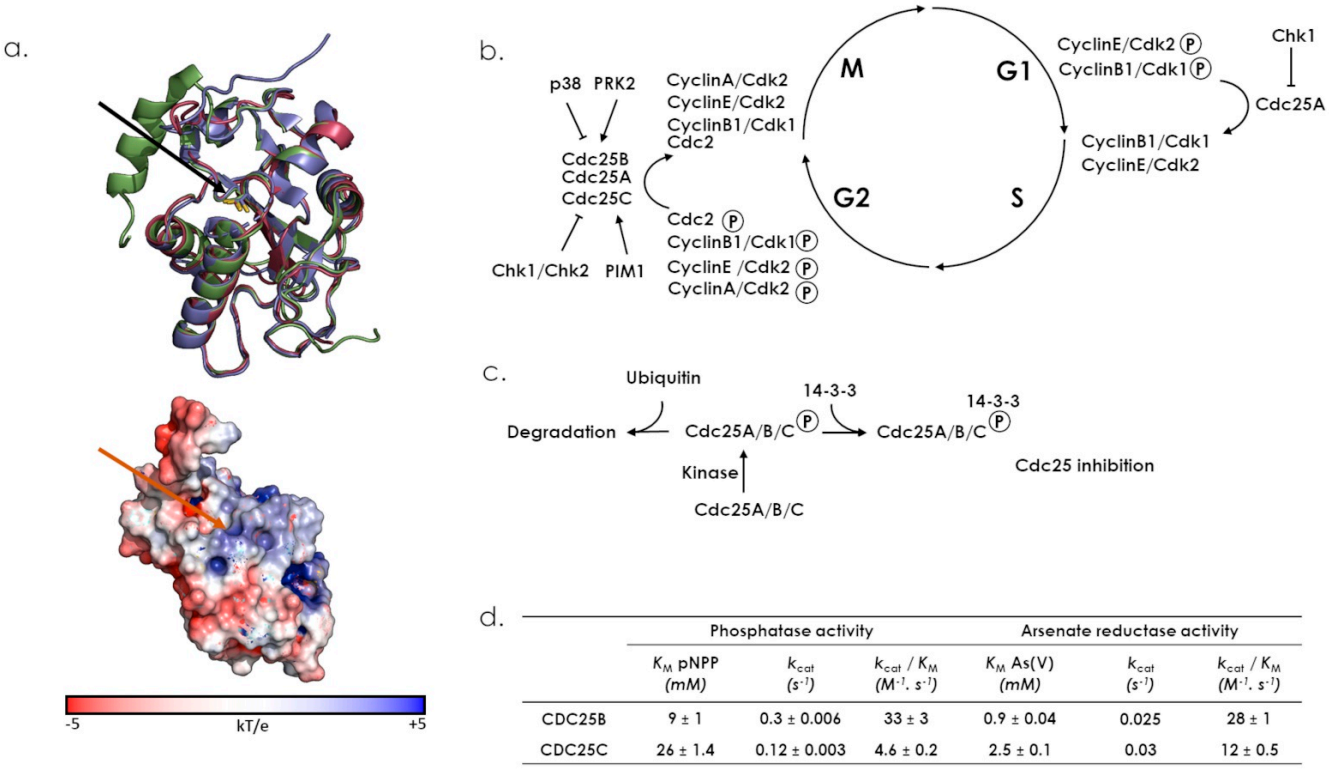

d.

	Phosphatase activity			Arsenate reductase activity		
	K_M pNPP (*mM*)	k_{cat} (s^{-1})	k_{cat} / K_M (M^{-1}. s^{-1})	K_M As(V) (*mM*)	k_{cat} (s^{-1})	k_{cat} / K_M (M^{-1}. s^{-1})
CDC25B	9 ± 1	0.3 ± 0.006	33 ± 3	0.9 ± 0.04	0.025	28 ± 1
CDC25C	26 ± 1.4	0.12 ± 0.003	4.6 ± 0.2	2.5 ± 0.1	0.03	12 ± 0.5

Figure 8. Structural features, catalytic properties and biological functions of CDC25s. (**a**) Upper panel: superimposition of Rhd domains 3D structures from CDC25A (1C25, red), CDC25B (3OP3, purple) and CDC25C (1CWR, green) using Pymol (version 2.4.1). RMSD values: 0.600 Å (1CRW versus 1C25) for 956 remaining atoms; 0.677 Å (1CRW versus 3OP3) for 951 remaining atoms; 0.913 Å (1C25 versus 3OP3) for 959 remaining atoms. Catalytic Cys are represented in sticks and indicated by a black arrow. Lower panel: surface charge representation of 1C25, position of the catalytic Cys is indicated by a red arrow. (**b**) CDC25 phosphatase activities toward Cyclin/Cdk complexes play key roles in cell cycle in regulating both G2/M and G1/S transitions. CDC25 activities are enhanced or inhibited by various kinases activities at different cell cycle phases. (**c**) CDC25 activities are also regulated by 14-3-3 reversible inhibition or proteasome activity. (**d**) Kinetic parameters of the phosphatase and arsenate reductase activities of purified Rhd domains of CDC25s [17]. Phosphatase activity was obtained from the rate of hydrolysis of p-nitrophenyl phosphate (pNPP), and arsenate reductase activity was determined using a coupled assay combining GSH, glutathione reductase, NADPH and glutaredoxine.

The catalytic mechanism of phosphatase activity is a classical two-step mechanism (Figure 2b) [71]. In the Michaelian complex, the phosphate group of the substrate is probably stabilized by hydrogen bonds, with the arginine and X residues of the HCx_5R motif. Although Glu474 was recently proposed for CDC25B, the residue involved in acid/base

catalysis for leaving group protonation and water molecule activation remains to be identified. Moreover, arsenate reductase activity was revealed for the catalytic domain of the human CDC25B and CDC25C, as these two enzymes were shown to catalyze in vitro inorganic arsenate reduction in the presence of glutathion and glutaredoxin (Figure 8b) [17]. Substituting alanine for the cysteine and arginine residues of the HCx_5R catalytic motif led to the loss of both reductase and phosphatase activities, suggesting that the Rhd catalytic domain shares the same active site for dephosphorylation and arsenate reduction. CDC25s serve as key activators of the Cdk/cyclins activity during normal cell cycle progression [62,72]. CDC25A controls both the G1-to-S and G2-to-M transitions, whereas CDC25B and CDC25C regulate the G2-to-M transition (Figure 8c). The CDC25s also play an important role in the checkpoint response that prevents Cdk/cyclin activation following DNA damage [73,74]. CDC25A is mainly localized in the nucleus (Figure 4) [75]. CDC25B, the "initiator" phosphatase, is located in the nucleus during interphase, but shuttles back and forth between the cytoplasm and nucleus during the entire cell cycle. It translocates to the cytoplasm during the G2 phase, activates the cyclin B1/CDK1 complex, and then re-enters the nucleus to initiate mitosis (Figures 4 and 8c) [70,76]. Moreover, CDC25s are cell cycle control proteins whose overexpression is frequently associated with a wide variety of cancers. The downregulation of CDC25C induces cell cycle arrest in G2/M phase in response to DNA damage via p53-mediated signal transduction, and its abnormal expression is associated with cancer initiation, development, metastasis and occurrence. Indeed, many studies revealed that CDC25C is highly expressed in lung, liver, gastric, bladder, prostate, esophageal and colorectal cancers and in acute myeloid leukemia, correlated to poor prognosis and low survival rates [77].

7.2. MOCS3

The human MOCS3 protein is encoded by the *MOCS3* gene composed of a unique 1383 bp long exon, located on chromosome 20 (20q13.13). MOCS3 is a protein of 461 residues (49 kDa), constituted of two structural domains (Figures 3c and 9a) [24], a Rhd C-terminal domain and a N-terminal domain, exhibiting similarity with bacterial ThiF/MoeB/HesA family or E1 ubiquitin-like activating enzymes [1,78]. Little information is available regarding MOCS3 3D arrangement, with only one structure for the Rhd domain of the protein (Figure 9b) (PDB 3I2V). An Alphafold prediction is also available (https://alphafold.ebi.ac.uk/entry/O95396, accessed on 17 October 2022) and, as expected from the structure of MoeB homologs, the human Moeb-like domain is constituted of a central height strands β-sheet, surrounded by height helices [78]. From the 316 sequences retrieved by blast-P from Uniprot database with human MOCS3, Arabidopsis MOCS3 (CNX5/STR13) or yeast MOCS3 (also known as Uba4p) as templates, we searched whether conserved residues or sequence motifs are conserved in the two domains throughout distant sequences (Figure 9a, Supplemental File S3). Regarding the MOCS3 Rhd domain, the DxR structural motif is strictly conserved, and the catalytic loop displays a CxxGxD/R consensus sequence. In MoeB/ThiF domain, dicysteines motifs involved in zinc cation coordination ($Cys_{222}XXCys_{225}$ and $Cys_{297}XXCys_{300}$), reported to be essential for the folding of the protein, are conserved in addition to a cysteine residue (Cys_{239}), proposed to be essential for MOCS3 function.

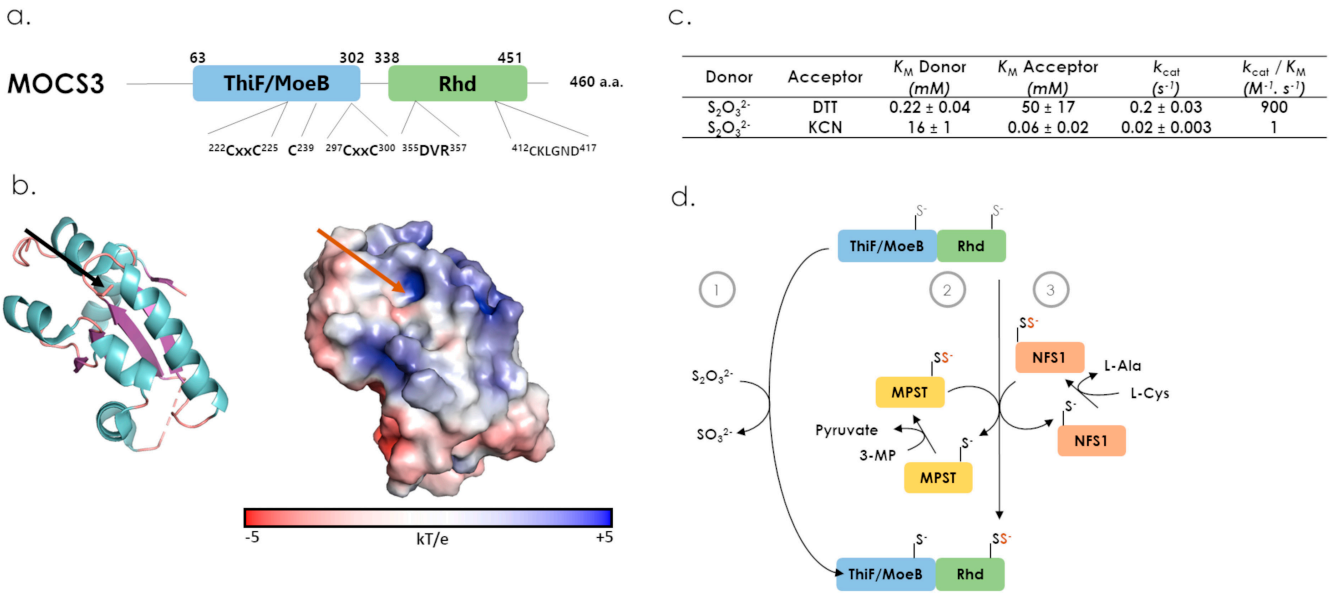

Donor	Acceptor	K_M Donor (mM)	K_M Acceptor (mM)	k_{cat} (s^{-1})	k_{cat} / K_M (M^{-1}. s^{-1})
$S_2O_3^{2-}$	DTT	0.22 ± 0.04	50 ± 17	0.2 ± 0.03	900
$S_2O_3^{2-}$	KCN	16 ± 1	0.06 ± 0.02	0.02 ± 0.003	1

Figure 9. Structural features, catalytic properties and proposed physiological partners of MOCS3. (**a**) Modular organization of MOCS3 and conserved motifs in distant protein sequences identified by BlastP ($Cys_{222}XXCys_{225}$, Cys_{239}, $Cys_{297}XXCys_{300}$, $_{355}DxR_{357}$ and $_{412}CxxGxD/R_{417}$). (**b**) Cartoon and surface representations of MOCS3-Rhd domain structure (PDB 3I2V). The active site cysteine is represented in stick and is indicated by a black (cartoon) or a red (surface) arrow. (**c**) Steady-state kinetic parameters for the thiosulfate sulfurtransferase activity of the Rhd domain from MOCS3 [79]. (**d**) describes sulfur donors for MOCS3 (1), MPST (2) or the cysteine desulfurase NFS1 (3).

In vitro, isolated MOCS3-Rhd was shown to present a low sulfurtransferase activity from thiosulfate to cyanide or DTT (Figure 9c) [24,79]. Indeed, the MOCS3-Rhd thiosulfate-dependent activity is 1000-fold lower, relative to bovine TST/Rhodanese, suggesting that thiosulfate is not the MOCS3 physiological substrate (Figure 9d). This could be linked with the particular catalytic loop sequence, as suggested by a 36- to 165-fold increase in sulfurtransferase activities when MOCS3 catalytic loop was substituted by the CRKGVT sequence issued from bovine Rhodanese [79]. Interestingly, the fact that NFS1 L-Cysteine desulfurase and MPST were shown to interact both in vitro with MOCS3-RhD and in cellulo with MOCS3 suggests that they could be its physiological donor substrates (Figure 9d) [27,80]. Thus, MOCS3 is likely the first human Rhd-containing enzyme involved in protein to protein sulfur atom trafficking.

As isolated proteins, MoeB/ThiF members catalyse ATP-dependent adenylation of C-terminal Glycine residue from sulfur carrier proteins [81]. In the context of the MOCS3 protein, both MoeB/ThiF and Rhd domains cooperate sequentially to catalyse the C-terminal thiocarboxylation of partner proteins, e.g., MOCS2 (Molybdenum cofactor synthesis 2) or URM1 (Ubiquitin-related modifier 1) that are involved in molybdenum cofactor maturation, tRNA thiolation, or proteins post-translational modification, such as peroxiredoxin urmylation (Figure 10) [26,82]. From studies of human MOCS3 and homologs, it was proposed that MOCS3 activates MOCS2 in the presence of ATP by formation of a thioester bond between conserved C239 of the MoeB/ThiF domain and MOCS2 C-terminal glycinyl residue. This covalent linkage is proposed to be essential for MOCS2 correct orientation relative to the Rhd domain during the catalysis, which consists of the nucleophilic attack of the persulfidated MOCS3-Rhd on the thiocarboxylated MOCS2 to form an acyl persulfide intermediate. Finally, release of the MOCS2 thiocarboxylate requires an unknown electron provider [24,83,84].

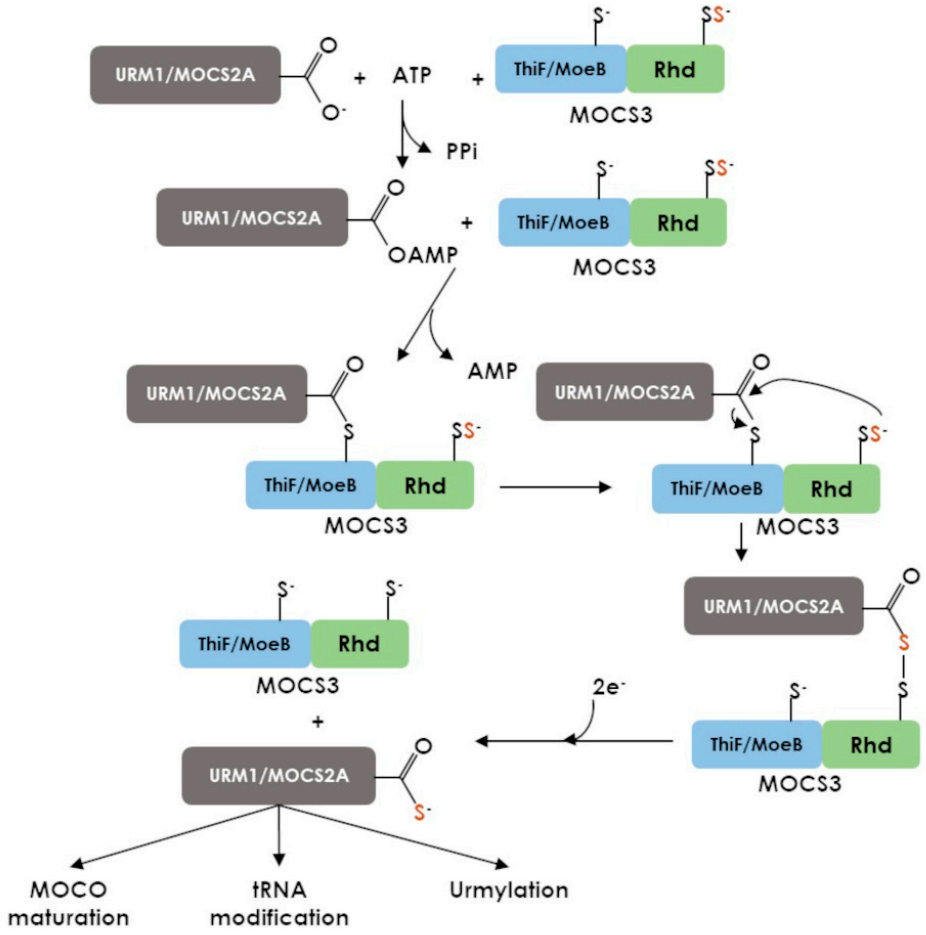

Figure 10. Proposed mechanism for the MOCS3-catalyzed reaction.

In human cells, the MOCS3 protein accumulates into the cytoplasm and participates in sulfur atom trafficking through two distinct pathways, tRNA thiolation and molybdenum cofactor maturation [24,26]. At the physiological level, molybdenum cofactor (MoCo) maturation pathway defect induces severe pathological conditions at the neonatal period, causing neurological abnormality, developmental delay, skeletal changes or feeding difficulties [11]. These symptoms are proposed to be due to inactivation of MoCo cofactor containing essential proteins, i.e., sulfite oxidase, xanthine oxidoreductase, or aldehyde oxidase, leading to the accumulation of toxic metabolites, such as sulfite, xanthine or hypoxanthine. MoCo deficiency symptoms were reported to be caused by mutation in *MOCS1* (Molybdenum cofactor synthesis 1), *MOCS2*, or *GPHN* (Gephyrin) genes [85]. In most cases, patients died at young age. Meanwhile, recent studies reported severe MoCo deficiency symptoms for two patients with mutation into *MOCS3* gene and highlighted the physiological importance of MOCS3 protein for MoCo maturation [86,87]. In the first case, the seventeen-year old patient presented intellectual disabilities, autism and dysmorphic features [86]. The second case was a newborn female who presented early microcephaly, hypotonia and hyper-reflexia [87]. In the two cases, biochemical/metabolites investigations related to MoCo deficiency revealed sulfocysteine, thiosulfate and xanthine, or uric acid and sulfite abnormal accumulation, respectively [86,87]. Moreover, HEK293T in cellulo investigation conducted on homozygote *MOCS3* mutant, generated by CRISPR-Cas9, offers the most complete picture of MOCS3 cellular functions [88]. First, this investigation reported a cell viability reduction as a consequence of *MOCS3* ($^{-}/^{-}$). Next, regarding MoCo maturation, it was demonstrated that sulfite oxidase (90% decrease) or aconitase (35% decrease) activity was impacted by *MOCS3* depletion [88]. Finally, authors also demon-

strated the essential role of MOCS3 in tRNA post-transcriptional modification, with an accumulation of mcm^{5}U-modified tRNA, the precursor of mcm^{5}s^{2}U tRNA molecules [88].

7.3. TSTD2

The human Thiosulfate SulfurTransferase-like Domain containing 2 isoform 1 (TSTD2) is encoded by the *TSTD2* gene composed of 33,289 nucleotides, including 10 exons. The gene is localized on chromosome 9 (9q22.33). *TSTD2* orthologs are widely distributed genes present in bacteria and eukaryotes, but are absent in Archaea and obligate anaerobic bacteria [89].

TSTD2 protein contains 516 residues and consists of two known domains, including a N-terminal acylphosphatase domain (UPF0176/IPR001792) and a C-terminal Rhd domain (Figure 11), but the alternative translation initiation start generates a shorter isoform of the TSTD2 protein that contains 167 residues and only the Rhd domain (Figure 3c). A model of the three-dimensional organization of the "full-length" TSTD2 protein generated from the 3D-structure of the *Legionella pneumophila* orthologous protein (PDB 4F67) is available in AlphaFold (AF-QT7W7) (Figure 11) [23]. The Rhd domain contains the canonical Rhd CX_4R catalytic motif (residues 355-400) localised on a loop (Figures 3 and 11).

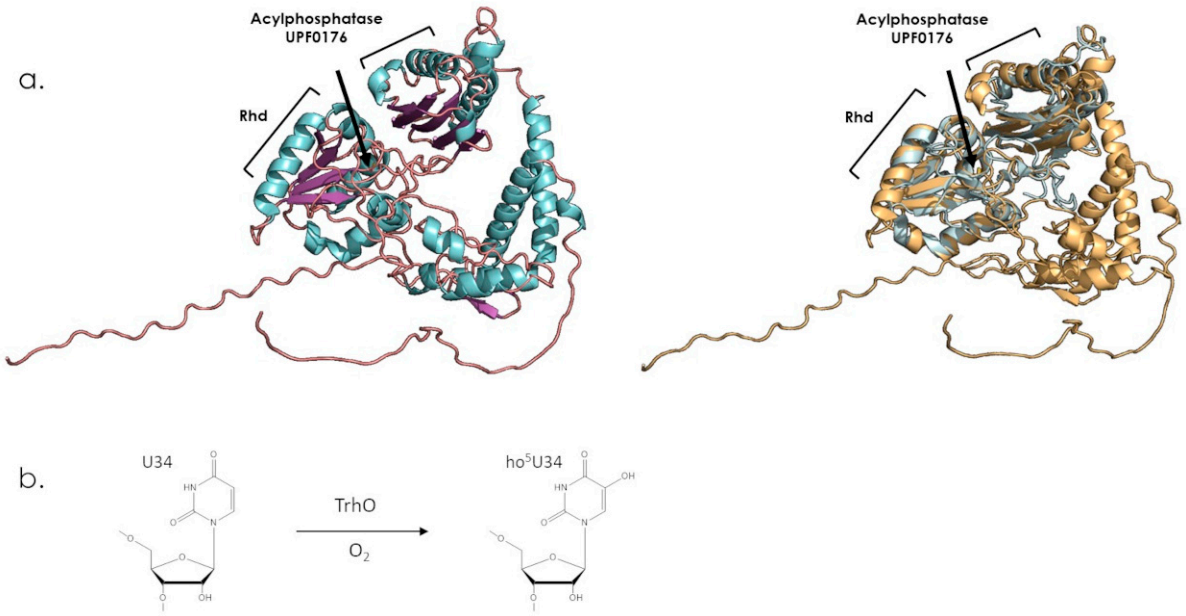

Figure 11. The TSTD2 structural model and reaction catalyzed by *E. coli* counterpart. (**a**) Left: the TSTD2 Alphafold predicted structure (AF-Q5T7W7). Acylphosphatase (UPF0176/IPR001792) and Rhd domains are indicated. Right: structure superimposition, using Pymol (version 2.4.1) (RMSD = 1.073 Å on remaining 1149 atoms), of the TSTD2 AlphaFold model (Gold) with the *Legionella pneumophila* protein structure (PDB 4F67, Pale green, Q5ZRP2, UniProt). Putative catalytic loop cysteine residue is represented as stick and is indicated by a black arrow. (**b**) The oxygen dependent tRNA U34 hydroxylation (^{ho5}U34) catalysed by TrhO, the TSTD2 orthologous protein from *E. coli* [89].

Regarding functions or biochemical properties of TSTD2, no information is available in the literature. Nevertheless, another orthologous protein from *E. coli*, named YceA or TrhO, was recently characterized [89]. The functional analysis of this protein in *E. coli* has highlighted its role in the hydroxylation of tRNAs, which initiates the cmo5U synthesis and improves decoding of codons ending in G (Figure 11) [89]. The functional complementation of an *E. coli* mutant by variants of the TrhO protein underlined the role of several residues belonging to the Acylphosphatase domain (K112) or to the Rhd catalytic loop (C200, T201, G203, R205), in the production of oxygen-dependent ^{ho5}U34 hydroxylated tRNAs. However, the mechanism whereby catalysis occurs remains to be elucidated. TrhO

is specific for a sub-set of tRNA (Ser1, Val1, Ala1 or Thr4), and tRNAs recognition could be achieved by the positively charged β-sheet present in the acylphosphatase domain near the Rhd active-site loop. The acylphosphatase domain is also described in the InterPro databank as catalysing the hydrolysis of acyl-phosphate groups to release a carboxylic group and a phosphate molecule, but no biochemical data support this assumption. Finally, no data indicate whether the TSTD2 Rhd domain is able to catalyse classical sulfur atom transfers, dephosphorylation reactions or arsenate reduction.

At the physiological level, the cellular functions of TSTD2 protein are still unknown. TSTD2's gene expression or protein accumulation variations were reported for human traits or diseases resistance/susceptibility, but, to date, this information is too preliminary to propose physiological implications [90–92].

8. Concluding Remarks

The increasing number of identified and characterized human Rhd domain-containing proteins supports the notion that the Rhd structural domain has evolved, as isolated protein or in combination with other domains, to fulfill different cellular functions. Although, the fine characterization of the active Rhd domains is still elusive, especially for the last one reported, the emerging picture in this catalytic promiscuity stressed the crucial role of the active-site loop, the structural domains organization and interaction networks, depending on subcellular localization. In the future, the exhaustive characterization of human Rhd-containing proteins at the biochemical and cellular level is a decisive step to better define the functions of Rhd-containing proteins, and to reveal their key contributions in human physio- and pathophysiology.

Supplementary Materials: The following are available online at https://www.mdpi.com/article/10.3390/antiox12040843/s1, Supplemental File S1: Sequence from mammals, plants, yeast or bacteria used for Rhd domain conserved motives DxR and CxxGxR, retrieve from BlastP using TSTD1 as template; Supplemental File S2: Human Rhd containing protein identified into the UniProt database; Supplemental File S3: Sequences retrieve by BlastP with *Arabidopsis thaliana* MOCS3 (STR13/Q9ZNWO), *Saccharomyces cerevisiae* MOCS3 (Uba4p/P38820) or Human MOCS3 (O95396) proteins sequences.

Funding: This work was supported by a grant from the "Université de Lorraine". The authors acknowledge support of the group by the "Impact Biomolecules" project of the "Lorraine Université d'Excellence" (Investissements d'avenir-ANR project number 15-004). R.A. was supported by the Kingdom of Saudi Arabia, A.-L.C. and R.P.V. were supported by the French Research Ministry.

Institutional Review Board Statement: Not applicable.

Informed Consent Statement: Not applicable.

Data Availability Statement: All data presented in this study are available in the article and Supplementary Materials.

Conflicts of Interest: The authors declare no conflict of interest.

References

1. Bordo, D.; Bork, P. The Rhodanese/Cdc25 Phosphatase Superfamily. Sequence-Structure-Function Relations. *EMBO Rep.* **2002**, *3*, 741–746. [CrossRef]
2. Cipollone, R.; Ascenzi, P.; Visca, P. Common Themes and Variations in the Rhodanese Superfamily. *IUBMB Life* **2007**, *59*, 51–59. [CrossRef] [PubMed]
3. Selles, B.; Moseler, A.; Rouhier, N.; Couturier, J. Rhodanese Domain-Containing Sulfurtransferases: Multifaceted Proteins Involved in Sulfur Trafficking in Plants. *J. Exp. Bot.* **2019**, *70*, 4139–4154. [CrossRef]
4. Termathe, M.; Leidel, S.A. Urm1: A Non-Canonical UBL. *Biomolecules* **2021**, *11*, 139. [CrossRef] [PubMed]
5. Yang, G.; Sun, X.; Wang, R. Hydrogen Sulfide-Induced Apoptosis of Human Aorta Smooth Muscle Cells via the Activation of Mitogen-Activated Protein Kinases and Caspase-3. *FASEB J.* **2004**, *18*, 1782–1784. [CrossRef] [PubMed]
6. Szabó, G.; Veres, G.; Radovits, T.; Gerő, D.; Módis, K.; Miesel-Gröschel, C.; Horkay, F.; Karck, M.; Szabó, C. Cardioprotective Effects of Hydrogen Sulfide. *Nitric Oxide* **2011**, *25*, 201–210. [CrossRef]

7. Calenic, B.; Yaegaki, K.; Ishkitiev, N.; Kumazawa, Y.; Imai, T.; Tanaka, T. P53-Pathway Activity and Apoptosis in Hydrogen Sulfide-Exposed Stem Cells Separated from Human Gingival Epithelium. *J. Periodontal Res.* **2013**, *48*, 322–330. [CrossRef]
8. Talaei, F.; van Praag, V.M.; Henning, R.H. Hydrogen Sulfide Restores a Normal Morphological Phenotype in Werner Syndrome Fibroblasts, Attenuates Oxidative Damage and Modulates MTOR Pathway. *Pharmacol. Res.* **2013**, *74*, 34–44. [CrossRef]
9. Filipovic, M.R.; Zivanovic, J.; Alvarez, B.; Banerjee, R. Chemical Biology of H_2S Signaling through Persulfidation. *Chem. Rev.* **2018**, *118*, 1253–1337. [CrossRef]
10. Bimai, O.; Arragain, S.; Golinelli-Pimpaneau, B. Structure-Based Mechanistic Insights into Catalysis by TRNA Thiolation Enzymes. *Curr. Opin. Struct. Biol.* **2020**, *65*, 69–78. [CrossRef]
11. Schwarz, G. Molybdenum Cofactor and Human Disease. *Curr. Opin. Chem. Biol.* **2016**, *31*, 179–187. [CrossRef] [PubMed]
12. Medvedev, K.E.; Kinch, L.N.; Schaeffer, R.D.; Grishin, N.V. Functional Analysis of Rossmann-like Domains Reveals Convergent Evolution of Topology and Reaction Pathways. *PLoS Comput. Biol.* **2019**, *15*, e1007569. [CrossRef]
13. Avvakumov, G.V.; Walker, J.R.; Xue, S.; Finerty, P.J.; Mackenzie, F.; Newman, E.M.; Dhe-Paganon, S. Amino-Terminal Dimerization, NRDP1-Rhodanese Interaction, and Inhibited Catalytic Domain Conformation of the Ubiquitin-Specific Protease 8 (USP8). *J. Biol. Chem.* **2006**, *281*, 38061–38070. [CrossRef] [PubMed]
14. Guretzki, S.; Papenbrock, J. Characterization of the Sulfurtransferase Family from Oryza Sativa L. *Plant Physiol. Biochem.* **2011**, *49*, 1064–1070. [CrossRef] [PubMed]
15. Moseler, A.; Selles, B.; Rouhier, N.; Couturier, J. Novel Insights into the Diversity of the Sulfurtransferase Family in Photosynthetic Organisms with Emphasis on Oak. *New Phytol.* **2019**, *226*, 967–977. [CrossRef] [PubMed]
16. Forlani, F.; Carpen, A.; Pagani, S. Evidence That Elongation of the Catalytic Loop of the Azotobacter Vinelandii Rhodanese Changed Selectivity from Sulfur- to Phosphate-containing Substrates. *Protein Eng. Des. Sel.* **2003**, *16*, 515–519. [CrossRef]
17. Bhattacharjee, H.; Sheng, J.; Ajees, A.A.; Mukhopadhyay, R.; Rosen, B.P. Adventitious Arsenate Reductase Activity of the Catalytic Domain of the Human Cdc25B and Cdc25C Phosphatases. *Biochemistry* **2010**, *49*, 802–809. [CrossRef]
18. Spallarossa, A.; Forlani, F.; Carpen, A.; Armirotti, A.; Pagani, S.; Bolognesi, M.; Bordo, D. The "Rhodanese" Fold and Catalytic Mechanism of 3-Mercaptopyruvate Sulfurtransferases: Crystal Structure of SseA from Escherichia Coli. *J. Mol. Biol.* **2004**, *335*, 583–593. [CrossRef]
19. Gottlin, E.B.; Xu, X.; Epstein, D.M.; Burke, S.P.; Eckstein, J.W.; Ballou, D.P.; Dixon, J.E. Kinetic Analysis of the Catalytic Domain of Human Cdc25B. *J. Biol. Chem.* **1996**, *271*, 27445–27449. [CrossRef]
20. Mukhopadhyay, R.; Shi, J.; Rosen, B.P. Purification and Characterization of Acr2p, TheSaccharomyces Cerevisiae Arsenate Reductase. *J. Biol. Chem.* **2000**, *275*, 21149–21157. [CrossRef]
21. Mukhopadhyay, R.; Bisacchi, D.; Zhou, Y.; Armirotti, A.; Bordo, D. Structural Characterization of the As/Sb Reductase LmACR2 from Leishmania Major. *J. Mol. Biol.* **2009**, *386*, 1229–1239. [CrossRef] [PubMed]
22. The UniProt Consortium. UniProt: The Universal Protein Knowledgebase in 2021. *Nucleic Acids Res.* **2021**, *49*, D480–D489. [CrossRef] [PubMed]
23. Jumper, J.; Evans, R.; Pritzel, A.; Green, T.; Figurnov, M.; Ronneberger, O.; Tunyasuvunakool, K.; Bates, R.; Žídek, A.; Potapenko, A.; et al. Highly Accurate Protein Structure Prediction with AlphaFold. *Nature* **2021**, *596*, 583–589. [CrossRef] [PubMed]
24. Matthies, A.; Rajagopalan, K.V.; Mendel, R.R.; Leimkühler, S. Evidence for the Physiological Role of a Rhodanese-like Protein for the Biosynthesis of the Molybdenum Cofactor in Humans. *Proc. Natl. Acad. Sci. USA* **2004**, *101*, 5946–5951. [CrossRef]
25. Lec, J.-C.; Boutserin, S.; Mazon, H.; Mulliert, G.; Boschi-Muller, S.; Talfournier, F. Unraveling the Mechanism of Cysteine Persulfide Formation Catalyzed by 3-Mercaptopyruvate Sulfurtransferases. *ACS Catal.* **2018**, *8*, 2049–2059. [CrossRef]
26. Chowdhury, M.M.; Dosche, C.; Löhmannsröben, H.-G.; Leimkühler, S. Dual Role of the Molybdenum Cofactor Biosynthesis Protein MOCS3 in TRNA Thiolation and Molybdenum Cofactor Biosynthesis in Humans. *J. Biol. Chem.* **2012**, *287*, 17297–17307. [CrossRef]
27. Fräsdorf, B.; Radon, C.; Leimkühler, S. Characterization and Interaction Studies of Two Isoforms of the Dual Localized 3-Mercaptopyruvate Sulfurtransferase TUM1 from Humans. *J. Biol. Chem.* **2014**, *289*, 34543–34556. [CrossRef]
28. Smirnov, A.; Comte, C.; Mager-Heckel, A.-M.; Addis, V.; Krasheninnikov, I.A.; Martin, R.P.; Entelis, N.; Tarassov, I. Mitochondrial Enzyme Rhodanese Is Essential for 5 S Ribosomal RNA Import into Human Mitochondria. *J. Biol. Chem.* **2010**, *285*, 30792–30803. [CrossRef]
29. Smirnov, A.; Entelis, N.; Martin, R.P.; Tarassov, I. Biological Significance of 5S RRNA Import into Human Mitochondria: Role of Ribosomal Protein MRP-L18. *Genes Dev.* **2011**, *25*, 1289–1305. [CrossRef]
30. Wenzel, K.; Felix, S.B.; Flachmeier, C.; Heere, P.; Schulze, W.; Grunewald, I.; Pankow, H.; Hewelt, A.; Scherneck, S.; Bauer, D.; et al. Identification and Characterization of KAT, a Novel Gene Preferentially Expressed in Several Human Cancer Cell Lines. *Biol. Chem.* **2003**, *384*, 763–775. [CrossRef]
31. Dalal, S.N.; Schweitzer, C.M.; Gan, J.; DeCaprio, J.A. Cytoplasmic Localization of Human Cdc25C during Interphase Requires an Intact 14-3-3 Binding Site. *Mol. Cell Biol.* **1999**, *19*, 4465–4479. [CrossRef] [PubMed]
32. Lindqvist, A.; Källström, H.; Lundgren, A.; Barsoum, E.; Rosenthal, C.K. Cdc25B Cooperates with Cdc25A to Induce Mitosis but Has a Unique Role in Activating Cyclin B1-Cdk1 at the Centrosome. *J. Cell Biol.* **2005**, *171*, 35–45. [CrossRef] [PubMed]
33. Leisser, C.; Rosenberger, G.; Maier, S.; Fuhrmann, G.; Grusch, M.; Strasser, S.; Huettenbrenner, S.; Fassl, S.; Polgar, D.; Krieger, S.; et al. Subcellular Localisation of Cdc25A Determines Cell Fate. *Cell Death Differ.* **2004**, *11*, 80–89. [CrossRef]

34. Zou, X.; Tsutsui, T.; Ray, D.; Blomquist, J.F.; Ichijo, H.; Ucker, D.S.; Kiyokawa, H. The Cell Cycle-Regulatory CDC25A Phosphatase Inhibits Apoptosis Signal-Regulating Kinase 1. *Mol. Cell Biol.* **2001**, *21*, 4818–4828. [CrossRef] [PubMed]
35. Melideo, S.L.; Jackson, M.R.; Jorns, M.S. Biosynthesis of a Central Intermediate in Hydrogen Sulfide Metabolism by a Novel Human Sulfurtransferase and Its Yeast Ortholog. *Biochemistry* **2014**, *53*, 4739–4753. [CrossRef] [PubMed]
36. Libiad, M.; Motl, N.; Akey, D.L.; Sakamoto, N.; Fearon, E.R.; Smith, J.L.; Banerjee, R. Thiosulfate Sulfurtransferase-like Domain-Containing 1 Protein Interacts with Thioredoxin. *J. Biol. Chem.* **2018**, *293*, 2675–2686. [CrossRef]
37. Boschi-Muller, S.; Olry, A.; Antoine, M.; Branlant, G. The Enzymology and Biochemistry of Methionine Sulfoxide Reductases. *Biochim. Biophys. Acta* **2005**, *1703*, 231–238. [CrossRef]
38. Schlecker, T.; Comini, M.A.; Melchers, J.; Ruppert, T.; Krauth-Siegel, R.L. Catalytic Mechanism of the Glutathione Peroxidase-Type Tryparedoxin Peroxidase of Trypanosoma Brucei. *Biochem. J.* **2007**, *405*, 445–454. [CrossRef]
39. Selles, B.; Hugo, M.; Trujillo, M.; Srivastava, V.; Wingsle, G.; Jacquot, J.-P.; Radi, R.; Rouhier, N. Hydroperoxide and Peroxynitrite Reductase Activity of Poplar Thioredoxin-Dependent Glutathione Peroxidase 5: Kinetics, Catalytic Mechanism and Oxidative Inactivation. *Biochem. J.* **2012**, *442*, 369–380. [CrossRef]
40. Furne, J.; Springfield, J.; Koenig, T.; DeMaster, E.; Levitt, M.D. Oxidation of Hydrogen Sulfide and Methanethiol to Thiosulfate by Rat Tissues: A Specialized Function of the Colonic Mucosa. *Biochem. Pharmacol.* **2001**, *62*, 255–259. [CrossRef]
41. Lang, K. Die Rhodanbildung Im Tierkörper. *Biochem. Z.* **1933**, *259*, 37.
42. Ploegman, J.H.; Drent, G.; Kalk, K.H.; Hol, W.G.J.; Heinrikson, R.L.; Keim, P.; Weng, L.; Russell, J. The Covalent and Tertiary Structure of Bovine Liver Rhodanese. *Nature* **1978**, *273*, 124–129. [CrossRef]
43. Pallini, R.; Guazzi, G.C.; Cannella, C.; Cacace, M.G. Cloning and Sequence Analysis of the Human Liver Rhodanese: Comparison with the Bovine and Chicken Enzymes. *Biochem. Biophys. Res. Commun.* **1991**, *180*, 887–893. [CrossRef] [PubMed]
44. Aita, N.; Ishii, K.; Akamatsu, Y.; Ogasawara, Y.; Tanabe, S. Cloning and Expression of Human Liver Rhodanese CDNA. *Biochem. Biophys. Res. Commun.* **1997**, *231*, 56–60. [CrossRef]
45. Libiad, M.; Yadav, P.K.; Vitvitsky, V.; Martinov, M.; Banerjee, R. Organization of the Human Mitochondrial Hydrogen Sulfide Oxidation Pathway. *J. Biol. Chem.* **2014**, *289*, 30901–30910. [CrossRef] [PubMed]
46. Libiad, M.; Sriraman, A.; Banerjee, R. Polymorphic Variants of Human Rhodanese Exhibit Differences in Thermal Stability and Sulfur Transfer Kinetics. *J. Biol. Chem.* **2015**, *290*, 23579–23588. [CrossRef]
47. Ploegman, J.H.; Drent, G.; Kalk, K.H.; Hol, W.G. Structure of Bovine Liver Rhodanese. I. Structure Determination at 2.5 A Resolution and a Comparison of the Conformation and Sequence of Its Two Domains. *J. Mol. Biol.* **1978**, *123*, 557–594. [CrossRef]
48. Jackson, M.R.; Melideo, S.L.; Jorns, M.S. Human Sulfide: Quinone Oxidoreductase Catalyzes the First Step in Hydrogen Sulfide Metabolism and Produces a Sulfane Sulfur Metabolite. *Biochemistry* **2012**, *51*, 6804–6815. [CrossRef]
49. Motl, N.; Skiba, M.A.; Kabil, O.; Smith, J.L.; Banerjee, R. Structural and Biochemical Analyses Indicate That a Bacterial Persulfide Dioxygenase-Rhodanese Fusion Protein Functions in Sulfur Assimilation. *J. Biol. Chem.* **2017**, *292*, 14026–14038. [CrossRef]
50. Morton, N.M.; Beltram, J.; Carter, R.N.; Michailidou, Z.; Gorjanc, G.; McFadden, C.; Barrios-Llerena, M.E.; Rodriguez-Cuenca, S.; Gibbins, M.T.G.; Aird, R.E.; et al. Genetic Identification of Thiosulfate Sulfurtransferase as an Adipocyte-Expressed Antidiabetic Target in Mice Selected for Leanness. *Nat. Med.* **2016**, *22*, 771–779. [CrossRef]
51. Whitehouse, D.B.; Poole, C.J.; Kind, P.R.; Hopkinson, D.A. Rhodanese Isozymes in Three Subjects with Leber's Optic Neuropathy. *J. Med. Genet.* **1989**, *26*, 113–115. [CrossRef]
52. Cagianut, B.; Schnebli, H.P.; Rhyner, K.; Furrer, J. Decreased Thiosulfate Sulfur Transferase (Rhodanese) in Leber's Hereditary Optic Atrophy. *Klin. Wochenschr.* **1984**, *62*, 850–854. [CrossRef]
53. Pedre, B.; Dick, T.P. 3-Mercaptopyruvate Sulfurtransferase: An Enzyme at the Crossroads of Sulfane Sulfur Trafficking. *Biol. Chem.* **2021**, *402*, 223–237. [CrossRef] [PubMed]
54. Yadav, P.K.; Yamada, K.; Chiku, T.; Koutmos, M.; Banerjee, R. Structure and Kinetic Analysis of H2S Production by Human Mercaptopyruvate Sulfurtransferase. *J. Biol. Chem.* **2013**, *288*, 20002–20013. [CrossRef] [PubMed]
55. Zheng, L.; White, R.H.; Cash, V.L.; Dean, D.R. Mechanism for the Desulfurization of L-Cysteine Catalyzed by the NifS Gene Product. *Biochemistry* **1994**, *33*, 4714–4720. [CrossRef] [PubMed]
56. Alphey, M.S.; Williams, R.A.M.; Mottram, J.C.; Coombs, G.H.; Hunter, W.N. The Crystal Structure of Leishmania Major 3-Mercaptopyruvate Sulfurtransferase a Three-Domain Architecture with a Serine Protease-like Triad at the Active Site. *J. Biol. Chem.* **2003**, *278*, 48219–48227. [CrossRef]
57. Yadav, P.K.; Vitvitsky, V.; Carballal, S.; Seravalli, J.; Banerjee, R. Thioredoxin Regulates Human Mercaptopyruvate Sulfurtransferase at Physiologically-Relevant Concentrations. *J. Biol. Chem.* **2020**, *295*, 6299–6311. [CrossRef]
58. Nagahara, N.; Koike, S.; Nirasawa, T.; Kimura, H.; Ogasawara, Y. Alternative Pathway of H2S and Polysulfides Production from Sulfurated Catalytic-Cysteine of Reaction Intermediates of 3-Mercaptopyruvate Sulfurtransferase. *Biochem. Biophys. Res. Commun.* **2018**, *496*, 648–653. [CrossRef]
59. Crawhall, J.C.; Parker, R.; Sneddon, W.; Young, E.P. Beta-Mercaptolactate-Cysteine Disulfide in the Urine of a Mentally Retarded Patient. *Am. J. Dis. Child.* **1969**, *117*, 71–82. [CrossRef]
60. Crawhall, J.C.; Bir, K.; Purkiss, P.; Stanbury, J.B. Sulfur Amino Acids as Precursors of Beta-Mercaptolactate-Cysteine Disulfide in Human Subjects. *Biochem. Med.* **1971**, *5*, 109–115. [CrossRef]
61. Hannestad, U.; Mårtensson, J.; Sjödahl, R.; Sörbo, B. 3-Mercaptolactate Cysteine Disulfiduria: Biochemical Studies on Affected and Unaffected Members of a Family. *Biochem. Med.* **1981**, *26*, 106–114. [CrossRef]

62. Nilsson, I.; Hoffmann, I. Cell Cycle Regulation by the Cdc25 Phosphatase Family. *Prog. Cell Cycle. Res.* **2000**, *4*, 107–114. [CrossRef] [PubMed]
63. Baldin, V.; Cans, C.; Superti-Furga, G.; Ducommun, B. Alternative Splicing of the Human CDC25B Tyrosine Phosphatase. Possible Implications for Growth Control? *Oncogene* **1997**, *14*, 2485–2495. [CrossRef] [PubMed]
64. Forrest, A.R.; McCormack, A.K.; DeSouza, C.P.; Sinnamon, J.M.; Tonks, I.D.; Hayward, N.K.; Ellem, K.A.; Gabrielli, B.G. Multiple Splicing Variants of Cdc25B Regulate G2/M Progression. *Biochem. Biophys. Res. Commun.* **1999**, *260*, 510–515. [CrossRef] [PubMed]
65. Wegener, S.; Hampe, W.; Herrmann, D.; Schaller, H.C. Alternative Splicing in the Regulatory Region of the Human Phosphatases CDC25A and CDC25C. *Eur. J. Cell Biol.* **2000**, *79*, 810–815. [CrossRef]
66. Bureik, M.; Rief, N.; Drescher, R.; Jungbluth, A.; Montenarh, M.; Wagner, P. An Additional Transcript of the Cdc25C Gene from A431 Cells Encodes a Functional Protein. *Int. J. Oncol.* **2000**, *17*, 1251–1258. [CrossRef] [PubMed]
67. Rudolph, J. Cdc25 Phosphatases: Structure, Specificity, and Mechanism. *Biochemistry* **2007**, *46*, 3595–3604. [CrossRef]
68. Reynolds, R.A.; Yem, A.W.; Wolfe, C.L.; Deibel, M.R.; Chidester, C.G.; Watenpaugh, K.D. Crystal Structure of the Catalytic Subunit of Cdc25B Required for G2/M Phase Transition of the Cell Cycle. *J. Mol. Biol.* **1999**, *293*, 559–568. [CrossRef] [PubMed]
69. Sohn, J.; Kristjánsdóttir, K.; Safi, A.; Parker, B.; Kiburz, B.; Rudolph, J. Remote Hot Spots Mediate Protein Substrate Recognition for the Cdc25 Phosphatase. *Proc. Natl. Acad. Sci. USA* **2004**, *101*, 16437–16441. [CrossRef]
70. Sur, S.; Agrawal, D.K. Phosphatases and Kinases Regulating CDC25 Activity in the Cell Cycle: Clinical Implications of CDC25 Overexpression and Potential Treatment Strategies. *Mol. Cell. Biochem.* **2016**, *416*, 33–46. [CrossRef]
71. Arantes, G.M. The Catalytic Acid in the Dephosphorylation of the Cdk2-PTpY/CycA Protein Complex by Cdc25B Phosphatase. *J. Phys. Chem. B* **2008**, *112*, 15244–15247. [CrossRef] [PubMed]
72. Boutros, R.; Dozier, C.; Ducommun, B. The When and Wheres of CDC25 Phosphatases. *Curr. Opin. Cell Biol.* **2006**, *18*, 185–191. [CrossRef] [PubMed]
73. Iliakis, G.; Wang, Y.; Guan, J.; Wang, H. DNA Damage Checkpoint Control in Cells Exposed to Ionizing Radiation. *Oncogene* **2003**, *22*, 5834–5847. [CrossRef]
74. Karlsson-Rosenthal, C.; Millar, J.B.A. Cdc25: Mechanisms of Checkpoint Inhibition and Recovery. *Trends Cell Biol.* **2006**, *16*, 285–292. [CrossRef] [PubMed]
75. Shen, T.; Huang, S. The Role of Cdc25A in the Regulation of Cell Proliferation and Apoptosis. *Anticancer Agents Med. Chem.* **2012**, *12*, 631–639. [CrossRef]
76. Fei, F.; Qu, J.; Liu, K.; Li, C.; Wang, X.; Li, Y.; Zhang, S. The Subcellular Location of Cyclin B1 and CDC25 Associated with the Formation of Polyploid Giant Cancer Cells and Their Clinicopathological Significance. *Lab. Investig.* **2019**, *99*, 483–498. [CrossRef]
77. Liu, K.; Zheng, M.; Lu, R.; Du, J.; Zhao, Q.; Li, Z.; Li, Y.; Zhang, S. The Role of CDC25C in Cell Cycle Regulation and Clinical Cancer Therapy: A Systematic Review. *Cancer Cell Int.* **2020**, *20*, 213. [CrossRef]
78. Lake, M.W.; Wuebbens, M.M.; Rajagopalan, K.V.; Schindelin, H. Mechanism of Ubiquitin Activation Revealed by the Structure of a Bacterial MoeB–MoaD Complex. *Nature* **2001**, *414*, 325–329. [CrossRef]
79. Krepinsky, K.; Leimkühler, S. Site-Directed Mutagenesis of the Active Site Loop of the Rhodanese-like Domain of the Human Molybdopterin Synthase Sulfurase MOCS3. Major Differences in Substrate Specificity between Eukaryotic and Bacterial Homologs. *FEBS J.* **2007**, *274*, 2778–2787. [CrossRef]
80. Marelja, Z.; Stöcklein, W.; Nimtz, M.; Leimkühler, S. A Novel Role for Human Nfs1 in the Cytoplasm: Nfs1 Acts as a Sulfur Donor for MOCS3, a Protein Involved in Molybdenum Cofactor Biosynthesis. *J. Biol. Chem.* **2008**, *283*, 25178–25185. [CrossRef]
81. Leimkühler, S.; Rajagopalan, K.V. A Sulfurtransferase Is Required in the Transfer of Cysteine Sulfur in the in Vitro Synthesis of Molybdopterin from Precursor Z in Escherichia Coli. *J. Biol. Chem.* **2001**, *276*, 22024–22031. [CrossRef] [PubMed]
82. Furukawa, K.; Mizushima, N.; Noda, T.; Ohsumi, Y. A Protein Conjugation System in Yeast with Homology to Biosynthetic Enzyme Reaction of Prokaryotes. *J. Biol. Chem.* **2000**, *275*, 7462–7465. [CrossRef] [PubMed]
83. Termathe, M.; Leidel, S.A. The Uba4 Domain Interplay Is Mediated via a Thioester That Is Critical for TRNA Thiolation through Urm1 Thiocarboxylation. *Nucleic Acids Res.* **2018**, *46*, 5171–5181. [CrossRef]
84. Pabis, M.; Termathe, M.; Ravichandran, K.E.; Kienast, S.D.; Krutyhołowa, R.; Sokołowski, M.; Jankowska, U.; Grudnik, P.; Leidel, S.A.; Glatt, S. Molecular Basis for the Bifunctional Uba4-Urm1 Sulfur-Relay System in TRNA Thiolation and Ubiquitin-like Conjugation. *EMBO J.* **2020**, *39*, e105087. [CrossRef] [PubMed]
85. Mendel, R.R.; Kruse, T. Cell Biology of Molybdenum in Plants and Humans. *Biochim. Biophys. Acta* **2012**, *1823*, 1568–1579. [CrossRef] [PubMed]
86. Huijmans, J.G.M.; Schot, R.; de Klerk, J.B.C.; Williams, M.; de Coo, R.F.M.; Duran, M.; Verheijen, F.W.; van Slegtenhorst, M.; Mancini, G.M.S. Molybdenum Cofactor Deficiency: Identification of a Patient with Homozygote Mutation in the MOCS3 Gene. *Am. J. Med. Genet.* **2017**, *173*, 1601–1606. [CrossRef]
87. Tian, Q.; Cao, Y.; Shu, L.; Chen, Y.; Peng, Y.; Wang, Y.; Chen, Y.; Wang, H.; Mao, X. Case Report: Compound Heterozygous Variants in MOCS3 Identified in a Chinese Infant With Molybdenum Cofactor Deficiency. *Front. Genet.* **2021**, *12*, 651878. [CrossRef]
88. Neukranz, Y.; Kotter, A.; Beilschmidt, L.; Marelja, Z.; Helm, M.; Gräf, R.; Leimkühler, S. Analysis of the Cellular Roles of MOCS3 Identifies a MOCS3-Independent Localization of NFS1 at the Tips of the Centrosome. *Biochemistry* **2019**, *58*, 1786–1798. [CrossRef]
89. Sakai, Y.; Kimura, S.; Suzuki, T. Dual Pathways of TRNA Hydroxylation Ensure Efficient Translation by Expanding Decoding Capability. *Nat. Commun.* **2019**, *10*, 2858. [CrossRef]

90. Weiss, B.; Eberle, B.; Roeth, R.; de Bruin, C.; Lui, J.C.; Paramasivam, N.; Hinderhofer, K.; van Duyvenvoorde, H.A.; Baron, J.; Wit, J.M.; et al. Evidence That Non-Syndromic Familial Tall Stature Has an Oligogenic Origin Including Ciliary Genes. *Front. Endocrinol.* **2021**, *12*, 660731. [CrossRef]
91. Si, T.; Ning, X.; Chen, H.; Hu, Z.; Dun, L.; Zheng, N.; Huang, P.; Yang, L.; Yi, P. ANTXR1 as a Potential Prognostic Biomarker for Hepatitis B Virus-Related Hepatocellular Carcinoma Identified by a Weighted Gene Correlation Network Analysis. *J. Gastrointest. Oncol.* **2021**, *12*, 3079–3092. [CrossRef] [PubMed]
92. Kubota, M.; Zhang, B.-S.; Li, S.-Y.; Yoshida, Y.; Wang, H.; Adachi, A.; Matsutani, T.; Mine, S.; Machida, T.; Kamitsukasa, I.; et al. Serum Anti-TSTD2 Antibody as a Biomarker for Atherosclerosis-induced Ischemic Stroke and Chronic Kidney Disease. *Med. Int.* **2022**, *3*, 4. [CrossRef] [PubMed]

Disclaimer/Publisher's Note: The statements, opinions and data contained in all publications are solely those of the individual author(s) and contributor(s) and not of MDPI and/or the editor(s). MDPI and/or the editor(s) disclaim responsibility for any injury to people or property resulting from any ideas, methods, instructions or products referred to in the content.

Abstract

The rhodanese domain (Rhd), composed of a central β sheet flanked by α helices, is found in all major evolutionary phyla and often in several proteins encoded by the same genome. Rhd-containing enzymes are classified into four families according to the number of Rhd domains and the presence, or not, of additional domains. Some of the Rhd-containing enzymes exhibit sulfurtransferase activities and are implicated in hydrogen sulfide metabolism and/or signaling processes as sulfur carriers. These enzymes catalyze a sulfur transfer reaction from a donor substrate like 3-mercaptopyruvate or thiosulfate for 3-mercaptopyruvate sulfurtransferases or thiosulfate sulfurtransferases, respectively. Human CDC25 phosphatases which catalyze the dephosphorylation of cyclin dependent kinases, belong also to this family. The fact that these enzymes exhibit a side arsenate reductase activity suggest that the Rhd-domain represents a new example of promiscuous catalyst exhibiting sulfurtransferase, phosphatase and arsenate reductase activities in the same active site. Interestingly, all these activities rely on the presence of a Cys-containing catalytic loop, but sulfurtransferases and phosphatases mainly differ by the size and sequence of the catalytic loop which is one residue longer in the later one (CX_5R vs CX_4R). Moreover, MOCS3, another human sulfurtransferase, was shown to display substrate specificity for protein persulfide.

In this context, my project aims to 1) characterize the promiscuous activities of rhodanese family enzymes, using the human TSTD1 sulfurtransferase and the catalytic domain of the CDC25B as model enzymes, and 2) characterize the substrate specificity of MOCS3. Using a structure-function relationship approach, I showed in particular that i) unlike TSTD1, CDC25B displays promiscuous sulfurtransferase, phosphatase and arsenate reductase activities, and ii) this promiscuity does not exclusively rely on the size and the sequence of the catalytic loop.

Keywords: Rhodanese family, sulfurtransferase, phosphatase, promiscuity, structure-function, specificity

Résumé

Le domaine rhodanèse (Rhd), composé d'un feuillet β central flanqué d'hélices α, est ubiquitaire et il est souvent retrouvé dans plusieurs protéines codées par le même génome. Les enzymes à domaine Rhd sont classées en quatre familles selon le nombre de domaines Rhd et la présence ou non de domaines supplémentaires. Certaines de ces enzymes sont des thioltransférases impliquées dans le métabolisme du sulfure d'hydrogène ou la signalisation par transpersulfuration. Ces enzymes catalysent une réaction de transfert de soufre d'un substrat donneur comme le 3-mercaptopyruvate ou le thiosulfate respectivement pour les 3-mercaptopyruvate thioltransférases ou les thiosulfate thioltransférases. Les phosphatases CDC25 humaines, qui catalysent la déphosphorylation des kinases dépendantes des cyclines, appartiennent également à cette famille. Le fait que ces enzymes présentent une activité secondaire de réduction de l'arsenate suggère que le domaine Rhd pourrait présenter une promiscuité d'activités thioltransférase, phosphatase et arsenate réductas. Il est intéressant de noter que toutes ces activités reposent sur la présence d'une boucle catalytique contenant une Cys, les thioltransférases et les phosphatases différant principalement par la taille et la séquence de cette boucle qui est plus longue d'un résidu dans ces dernières (CX_5R vs CX_4R). De plus, une autre thioltranférase humaine appelée MOCS3 semble être spécifique de substrats protéiques persulfurés.

Dans ce contexte, mon projet visait à 1) caractériser les activités de promiscuité des enzymes de la famille Rhd, en utilisant la thioltransférase humaine TSTD1 et le domaine catalytique de la CDC25B comme enzymes modèles, et 2) caractériser la spécificité de substrat de MOCS3. Par des approches de relations structure-fonction, j'ai notamment montré que i) contrairement à TSTD1, la CDC25B présente bien une activité promiscuitaire thioltransférase, phosphatase et arsenate réductase, et ii) cette promiscuité ne dépend pas uniquement de la taille et de la séquence de la boucle catalytique.

Mots clés : Famille Rhodanèse, thioltransférases, phosphatases, promiscuité, structure-fonction, spécificité

Résumé étendu en français

Caractérisation biochimique des activités promiscuitaires d'enzymes à domaine rhodanèse

Introduction et Objectifs

L'objectif principal de mon projet de thèse portait sur l'identification des bases moléculaires responsables de l'activité des enzymes à domaine rhodanèse (Rhd), en particulier le lien pouvant exister entre la longueur et la séquence de la boucle catalytique et les propriétés catalytiques (thioltransférase, phosphatase et arséniate réductase). Pour cette raison, les deux parties de l'introduction seront consacrées successivement à la promiscuité enzymatique et aux enzymes contenant un domaine Rhd.

I. Promiscuité enzymatique

La promiscuité enzymatique correspond à la capacité des enzymes à catalyser de multiples réactions, mettant en évidence la polyvalence de ces catalyseurs biologiques et soulignant leur capacité à répondre aux demandes métaboliques des organismes vivants (O'Brien & Herschlag, 1999 ; Bornscheuer & Kazlauskas, 2004). Bien que les enzymes présentent des spécificités, beaucoup d'entre elles sont aussi connues depuis longtemps pour leur promiscuité (Gupta, 2016). Comme Hult et Burglund (Hult & Berglund, 2007) le soulignent, la découverte de la catalyse de la synthèse des liaisons C-C par la pyruvate décarboxylase remonte à 1921. Des exemples encore plus anciens répondent à la définition de la littérature car une promiscuité a été observée dans l'inversion de l'activité enzymatique hydrolytique de la maltase dès 1898 (Hill, 1898) et en 1900 pour la lipase pancréatique (Kastle et Loevenhart, 1900).

Les mécanismes sous-jacents à la promiscuité enzymatique reposent sur la diversité conformationnelle du site actif des enzymes, la diversité de substrats et de cofacteurs, et l'existence de différents états de protonation et de sous-sites distincts au sein des sites actifs (Khersonsky et Tawfik, 2010 ; Copley, 2014). Selon les facteurs responsables de la promiscuité enzymatique, elle peut être classée en trois groupes principaux : (1) la promiscuité de substrat, (2) la promiscuité catalytique et (3) la promiscuité conditionnelle (Figure A).

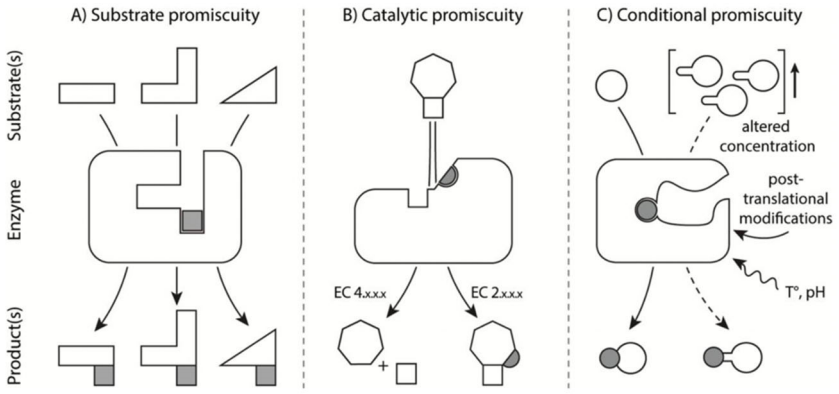

Figure A : Classification mécanistique de la promiscuité enzymatique (adaptée de Piedrafita et al., 2015). *(A) promiscuité ou multi-spécificité de substrat. Une enzyme peut effectuer la même réaction catalytique avec une gamme de substrats structuralement apparentés mais non identiques, présentant ainsi une spécificité de substrat plus large que celle initialement décrite. (B) promiscuité catalytique : Une enzyme peut catalyser plusieurs réactions chimiquement distinctes, élargissant ainsi son répertoire fonctionnel et lui permettant de participer à un plus large éventail de processus métaboliques. (C) promiscuité conditionnelle : les activités secondaires latentes d'une enzyme peuvent être induites ou activées dans des conditions environnementales spécifiques, telles que des concentrations accrues de substrats alternatifs (pour lesquels l'enzyme a une affinité moindre), ou des modifications post-traductionnelles qui déclenchent des changements de conformation.*

II. Les enzymes à domaine rhodanèse

Le domaine rhodanèse (Rhd) est un module structural commun aux trois principaux phyla de l'évolution. Il est constitué d'environ 100 résidus d'acides aminés qui forment un feuillet β central de cinq brins parallèles, flanqué de 4 à 5 hélices alpha (Selles et al., 2019). L'analyse des génomes de plus de 80 espèces suggère que plus de 500 séquences pourraient coder des protéines comportant au moins un domaine Rhd (Hofmann et al., 1998). Plusieurs protéines à domaine Rhd sont souvent codées par le même génome. Par exemple, le génome humain contient 47 protéines distinctes et *Escherichia coli* compte 7 protéines connues.

Le domaine Rhd présente une grande diversité de fonctions et participe à un large éventail de processus physiologiques. Certains domaines Rhd présentent une activité catalytique liée à la présence d'un résidu cystéine dans une boucle CX_n, n ayant une valeur de 5 ou 6 (Forlani *et al.*, 2003) et ils sont dénommés enzymes à domaine Rhd. Celles-ci ont été classées en quatre groupes en fonction du nombre de domaines Rhd et de la présence ou non de domaines additionnels (Figure B) *(*Bordo & Bork*,* 2002 *;* Cipollone *et al.,* 2007).

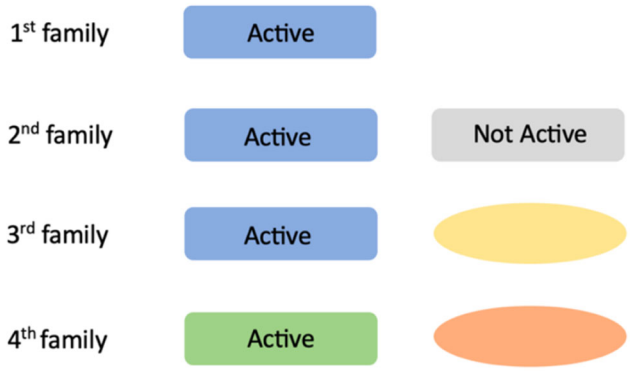

Figure B : Classification des enzymes à domaine Rhd en quatre familles en fonction du nombre de domaines Rhd et de la présence ou de l'absence de domaines supplémentaires (Bordo et Bork, 2002 ; Cipollone et al., 2007) *La première famille est composée d'enzymes possédant un seul domaine Rhd, comme la thioltransférase TSTD1. La deuxième famille est composée d'enzymes possédant deux domaines Rhd mais un seul est actif, comme la thioltransférase 3MST. Les troisième et quatrième familles contiennent un domaine supplémentaire associé à un domaine Rhd possédant une boucle catalytique conservée respectivement de six et sept résidus (cas de la phosphatase CDC25B humaine).*

Actuellement, les enzymes à domaine Rhd ont été décrites comme catalysant trois principaux types de processus chimiques, à savoir le transfert d'atomes de soufre (activité thioltransférase) ou de groupement phosphate (activité phosphatase) et la réduction de l'arséniate (activité arséniate réductase) (Forlani et al., 2003 ; Bhattacharjee et al., 2010).

Quelques études récentes révèlent l'existence d'une promiscuité d'activité des enzymes à domaine Rhd dépendante de la longueur de la boucle catalytique. Ainsi, la thioltransférase d'*Azotobacter vinelandii* présente en plus de son activité thioltransférase une activité phosphatase lorsque sa boucle catalytique est allongée d'un résidu (Forlani *et al.,* 2003*)*. D'autre part, le domaine catalytique des CDC25B et C présente une activité phosphatase mais aussi une activité arséniate réductase (Bhattacharjee *et al*., 2010).

Objectifs

Mon projet consistait à identifier les bases moléculaires à l'origine de la promiscuité d'activité des enzymes à domaine Rhd avec un intérêt particulier pour le rôle de la longueur de la boucle catalytique dans la « sélection » des activités enzymatiques thioltransférase, phosphatase et arséniate réductase décrites. Les modèles d'étude étaient la thioltransférase TSTD1 et le domaine catalytique de la phosphatase CDC25B. Ce choix est fondé sur un alignement de séquences d'enzymes à domaine Rhd généré à partir de la superposition de 14 structures tridimensionnelles dans lequel sont retrouvées majoritairement des enzymes de

type thioltransférase TSTD1 avec une signature Glu/Asp31 et Arg84 (résidu de la boucle catalytique) récemment montrée importante pour l'activité thioltransférase (Résultats de l'équipe non publiés). Est également retrouvé le domaine catalytique de la CDC25B humaine et l'arséniate/antimonate réductase de *Leishmania major* qui présentent tous les deux la signature Glu31/Arg84 mais une boucle catalytique plus longue d'un résidu (CX_5R vs. CX_4R). Dans ces dernières, la présence de cette signature "TSTD1-like" suggère l'existence d'une activité thioltransférase et le fait que la boucle soit plus longue ne devrait pas être un obstacle à l'existence de cette activité, les chaînes latérales des résidus Cys79, Glu31 et Arg84 étant parfaitement superposables.

Dans ce cadre, les objectifs majeurs de mon projet concernaient :

1) L'identification des bases moléculaires responsables de la promiscuité d'activité des enzymes à domaine Rhd en mettant l'accent sur la relation entre la longueur et la séquence de la boucle catalytique et les propriétés catalytiques (thioltransférase, phosphatase et arséniate réductase). Les enzymes TSTD1 et CDC25B ont été utilisées comme modèles d'étude, la signature Glu31/Arg84 connue pour être essentielle à l'activité thioltransférase de TSTD1 étant également présente dans CDC25B.

Par des études de relations structure-fonction, l'objectif était de répondre aux questions suivantes : La CDC25B est-elle capable de catalyser le transfert d'un atome de soufre ? La TSTD1 présente-t-elle des activités phosphatase et arséniate réductase ? Existe-t-il une relation entre la longueur et la séquence des boucles catalytiques et ces activités ? Et qu'en est-il des autres membres de la famille des thioltransférases à domaine Rhd ?

2) La caractérisation de la spécificité de substrat de la thioltransférase humaine MOCS3.

En effet, il a été montré que le domaine Rhd de MOCS3 isolé présente une faible activité thioltransférase en présence de thiosulfate, ce qui suggère que le thiosulfate n'est pas son substrat physiologique. D'autre part, il a été proposé que la L-cystéine désulfurase NFS1 et la 3MST interagissent avec MOCS3, ce qui suggère que MOCS3 pourrait être une thioltransférase impliquée dans le trafic d'atomes de soufre. Cela soulève les questions suivantes : Qu'en est-il des autres petites molécules en tant que substrat donneur pour MOCS3 ? NFS1 et 3MST sont-elles réellement des donneurs de soufre pour MOCS3 ? Qu'en est-il de l'accepteur de soufre ? Le domaine Rhd est-il responsable des spécificités de substrat de MOCS3 ?

Résultats et discussions

Axe 1:

Deux enzymes humaines ont été utilisées comme modèles : une thioltransférase nommée TSTD1 précédemment étudiée dans le groupe pour son activité thioltransférase, et le domaine catalytique de la tyrosine phosphatase CDC25B, ci-après dénommée CDC25Bcd, déjà connu pour ses activités phosphatase et arséniate réductase et donc sa promiscuité. Pour évaluer la relation entre la longueur de la boucle catalytique et les activités, une étude des relations structure-fonction a été réalisée en utilisant différents variants de la boucle :
1) un variant de TSTD1 avec une boucle catalytique CX_5R étendue obtenue par ajout d'un résidu Ser entre les résidus Gly85 et Lys86 (TSTD1+Ser), 2) un variant de TSTD1 dans lequel la boucle catalytique de CDC25Bcd (CEFSSER) a été introduite (appelée EX-MUT-TSTD1), 3) un variant de CDC25Bcd avec une boucle catalytique CX_4R plus courte, c'est-à-dire sans le résidu Ser86 (CDC25BcdΔSer), et 4) un variant de CDC25Bcd présentant la boucle catalytique de TSTD1 (CQMGKR), appelée EX-MUT-CDC25Bcd.

Les différents variants ont été produits sous forme recombinante dans *Escherichia coli*, et purifiés à homogénéité *via* la mise au point de nombreux protocoles. Les activités thioltransférase, phosphatase et arséniate réductase des différents variants ont ensuite été déterminées en utilisant différentes méthodes : l'activité thioltransférase a été testée dans des conditions de cycle catalytique unique afin d'évaluer spécifiquement la capacité de l'enzyme à catalyser le transfert de soufre d'un substrat donneur vers sa Cys catalytique pour former un intermédiaire persulfure ; l'activité phosphatase a été évaluée à l'état stationnaire en présence d'un analogue de substrat, le para-nitrophényle phosphate (pNPP) ; l'activité arséniate réductase a été évaluée à l'état stationnaire en utilisant un système couplé composé de glutarédoxine / glutathion / NADPH / glutathion réductase.

L'ensemble des résultats nous a permis de conclure que :

1- Le CDC25Bcd natif présente une promiscuité d'activité thioltransférase

La forme recombinante purifiée CDC25Bcd présente comme attendue une activité phosphatase mais également une activité thioltransférase (tableau A). Cette dernière est

légèrement plus efficace que celle de la TSTD1 (la thioltransférase de référence) lorsque le 3-mercaptopyruvate (3MP) est utilisé comme substrat donneur de soufre (k_{max}/K_{3MP} 13650 vs 11870 M^{-1}). La paire Gln80/Arg108 de TSTD1, spécifiquement dédiée au transfert de soufre depuis le 3MP, étant conservée dans CDC25Bcd (Glu80/Lys108) (Figure C), l'efficacité catalytique élevée de CDC25Bcd n'est pas surprenante. Bien qu'il soit tentant de discuter du fait que cette activité thioltransférase est 100 fois plus efficace que l'activité native (13650 vs 125 M^{-1}), cela serait toutefois trop spéculatif car l'activité phosphatase a été testée avec un analogue de substrat (le pNPP).

En revanche, aucune activité n'a pu être détectée en présence de thiosulfate comme substrat donneur (jusqu'à 80 mM), mettant en évidence une spécificité stricte pour le 3MP contrairement à ce qui a été déterminé pour la TSTD1 ($k_{max}/K_{Thiosulfate}$ de 2.10^3 $M^{-1}.s^{-1}$). Ce résultat est assez surprenant car la paire d'ions Glu31/Arg84 indispensable à la rupture de la liaison soufre-soufre dans TSTD1 est conservée dans CDC25Bcd (Figure C).

	$CDC25B_{cd}$	**$CDC25B_{cd}$△Ser**	**EX-MUT-$CDC25B_{cd}$**
Phosphatase activity			
k_{cat} (s^{-1})	0.20 ± 0.01	0.007 ± 0.001	No activity
K_M (pNPP) (mM)	1.6 ± 0.2	21 ± 4 [a]	
k_{cat} / K_M ($M^{-1}.s^{-1}$)	125	22	
Sulfurtransferase activity			
k_{max} (s^{-1})	101 ± 6	N.D.	N.D.
K_{3MP} (mM)	7.4 ± 1.2	N.D.	N.D.
k_{max} / K_{3MP} ($M^{-1}.s^{-1}$)	$13.6.10^3$	620 ± 59 [b]	1622 ± 71 [c]
Arsenate reductase activity			
k_{cat} (s^{-1})	0.09 ± 0.02	0.12 ± 0.03	No activity
K_M (arsenate) (mM)	15 ± 12	38 ± 6 [d]	
k_{cat} / K_M ($M^{-1}.s^{-1}$)	5.8	3.1	

Tableau A : Paramètres cinétiques déterminés pour les formes sauvage et mutées de CDC25Bcd
[a] $K_{0,5}$ (n = 2,3 ± 0,7) ; [b, c] k_2 ; [d] $K_{0,5}$ (n = 3,7 ± 0,9).

Ainsi, on pourrait émettre l'hypothèse que le thiosulfate ne peut pas accéder au site actif en raison d'un encombrement stérique (le thiosulfate est plus volumineux que le 3MP), mais cela peut être exclu pour deux raisons : 1) le site actif du CDC25Bcd est réellement

exposé en surface ; 2) une molécule de sulfate occupe le site actif dans la structure RX de CDC25Bcd (Figure C). Par conséquent, ce manque d'activité résulte probablement de la formation d'un complexe Michaelien CDC25Bcd/thiosulfate qui n'est pas compétent pour la catalyse en raison d'un positionnement incorrect de l'atome de soufre distal du thiosulfate par rapport au thiolate de la Cys79 catalytique.

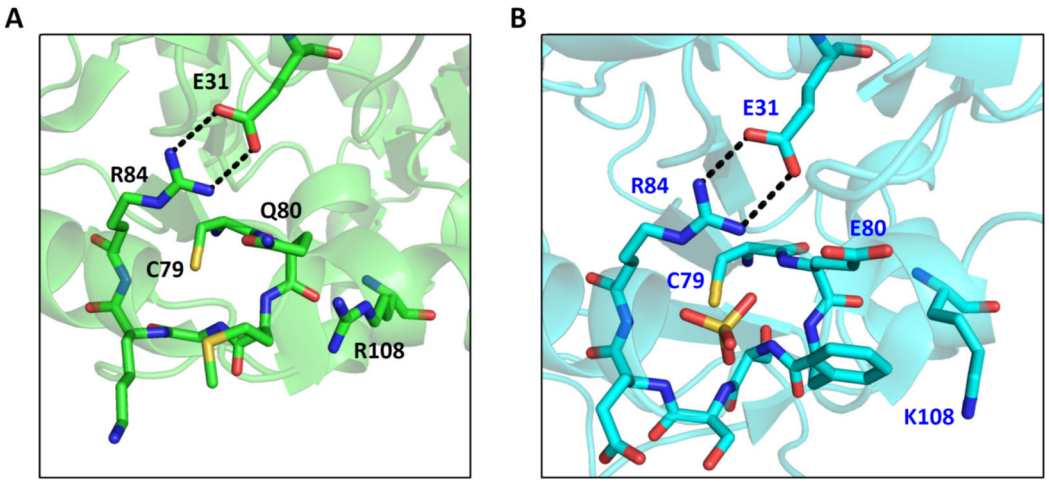

Figure C : Site actif de la TSTD1 (A, PDB 4JGT) et de la CDC25Bcd (B, PDB 1CWT) *Les résidus en position 31, 79, 80, 84 et 108 sont représentés en mode batônnets. L'atome de soufre de la Cys79 catalytique est représenté en jaune, les figures ont été générées avec PyMOL version 2.0.1.*

2- Modifier la boucle catalytique de CDC25Bcd n'améliore pas mais supprime sa promiscuité d'activité

Pour le variant CDC25Bcd△Ser, la réduction de la longueur de la boucle induit une diminution de l'efficacité catalytique de l'activité phosphatase de 5,7 fois et une diminution de l'activité thioltransférase de 22 fois (tableau A). Pour EX-MUT-CDC25Bcd, l'échange de la boucle abolit l'activité phosphatase et diminue de 8,4 fois l'efficacité catalytique de l'activité thioltransférase (Tableau A). Il est intéressant de noter que lorsque l'activité phosphatase est testée dans des conditions d'état stationnaire pour le variant CDC25BcdΔSer, une phase de latence d'environ 10 min est observée en présence de 5 mM de pNPP. Cela signifie que le complexe michaelien initialement formé n'est pas totalement compétent sur le plan catalytique et nécessite des changements de conformation, même mineurs, pour atteindre le régime stationnaire. Cette hypothèse est étayée d'abord par le fait que la liaison du phosphate entraîne un changement de conformation dont la nature reste à définir. La réaction phosphatase nécessite une fixation du groupement phosphate du pNPP par les groupements amides du squelette principal et de la chaîne latérale de l'Arg84 de la boucle

catalytique. On peut donc émettre l'hypothèse que ce mode de liaison est altéré lorsque la longueur de la boucle est réduite, une adaptation conformationnelle qui pourrait être restreinte à cette partie active du site actif est donc nécessaire pour restaurer une liaison productive.

Deuxièmement, l'allure sigmoïdale du profil k_{obs} = f([pNPP]) révèle l'existence d'une coopérativité cinétique, qui peut résulter d'une hystérèse. Brièvement, des transitions conformationnelles doivent se produire au sein du site actif entre les deux étapes de la réaction, avec deux conformations catalytiquement compétentes pour respectivement la première et la deuxième étape. Pour CDC25BcdΔSer, les transitions entre ces deux conformations ne sont pas assez rapides pour être à l'équilibre pendant la catalyse, ce qui conduit à une coopérativité. Sur la base de ce modèle, l'absence de comportement coopératif pour CDC25Bcd peut être expliquée par des transitions beaucoup plus rapides probablement associées à la dynamique de la boucle catalytique.

La situation est clairement différente pour EX-MUT-CDC25Bcd car l'introduction de la boucle catalytique de la TSTD1 abolit totalement l'activité phosphatase. Cet effet radical ne peut pas s'expliquer par la longueur de la boucle, qui est similaire à celle de CDC25Bcd ΔSer, mais plutôt par sa séquence. Compte tenu de la contribution clé de la conformation/dynamique de la boucle dans l'activité phosphatase, ces données suggèrent que la boucle TSTD1 n'est intrinsèquement pas adaptée pour lier le phosphate de manière productive. Comme l'Arg84 est non seulement conservée, mais aussi ancrée par le pont salin avec le Glu31 dans les deux enzymes, les différences proviennent du positionnement des amides du squelette par rapport aux oxygènes du phosphate.

Concernant les conséquences induites par les changements de boucle catalytique sur l'activité arséniate réductase, la réduction de la longueur de la boucle d'un résidu n'a pas d'impact significatif sur les paramètres cinétiques (Tableau A). Cependant, et de manière similaire à ce qui a été observé pour l'activité phosphatase, une coopérativité cinétique est révélée. De plus, l'échange de la boucle catalytique supprime également totalement l'activité. Par conséquent, les conclusions concernant l'activité phosphatase peuvent raisonnablement être étendues à l'activité arséniate réductase, ce qui serait normal étant donné que le phosphate et l'arséniate sont considérés comme des analogues chimiques.

La situation est assez différente lorsque l'on examine les propriétés de transfert de soufre des variants de CDC25Bcd, car EX-MUT-CDC25Bcd reste actif. La diminution modérée

de l'efficacité catalytique observée pour les deux variants est principalement due à un effet K_{3MP}, des concentrations plus élevées de substrat étant nécessaires pour former des complexes enzyme/3MP compétents. Cependant, une fois formés, ces complexes sont parfaitement adaptés à un transfert efficace de soufre comme le montrent les valeurs de constante de vitesse proches de celle déterminée pour CDC25Bcd. Ces données suggèrent que quelle que soit la longueur/séquence de la boucle, la présence d'une paire Glu80/Lys108 ou Gln80/Lys108 respectivement dans CDC25BcdΔSer ou EX-MUT-CDC25Bcd est suffisante pour permettre une catalyse efficace.

3- TSTD1 et les variants de boucle catalytique associés ne présentent pas de promiscuité catalytique

Comme déjà discuté pour CDC25Bcd, l'activité thioltransférase en présence de 3MP dépend de la présence de la paire 80/108, qui est « conservée » pour les deux variants de TSTD1, expliquant les changements mineurs dans l'efficacité catalytique (diminution de 2 à 5 fois de k_{max}/K_{3MP}) (Tableau B). Cependant, par rapport au contexte CDC25Bcd, la principale différence réside dans le fait que la reconnaissance du 3MP est préservée (c'est-à-dire que la saturation est observée) quelle que soit la version de la boucle catalytique. Ceci suggère que le site actif de TSTD1 est intrinsèquement plus adapté pour catalyser cette réaction de transfert de soufre. Cette propriété pourrait dépendre de la dynamique locale de la boucle.

	TSTD1	TSTD1+Ser	EX-MUT-TSTD1
Sulfurtransferase activity			
k_{max} (s^{-1})	95 ± 8	145 ± 44	83 ± 14
K_{3MP} (mM)	8 ± 2	25 ± 14	34 ± 12
k_{max} / K_{3MP} ($M^{-1}.s^{-1}$)	$11.9.10^3$	$5.8.10^3$	$2.4.10^3$
Phosphatase activity			
		Not detectable	
Arsenate reductase activity			
		Not detectable	

Tableau B : Paramètres cinétiques déterminés pour les TSTD1 de type sauvage et mutées.